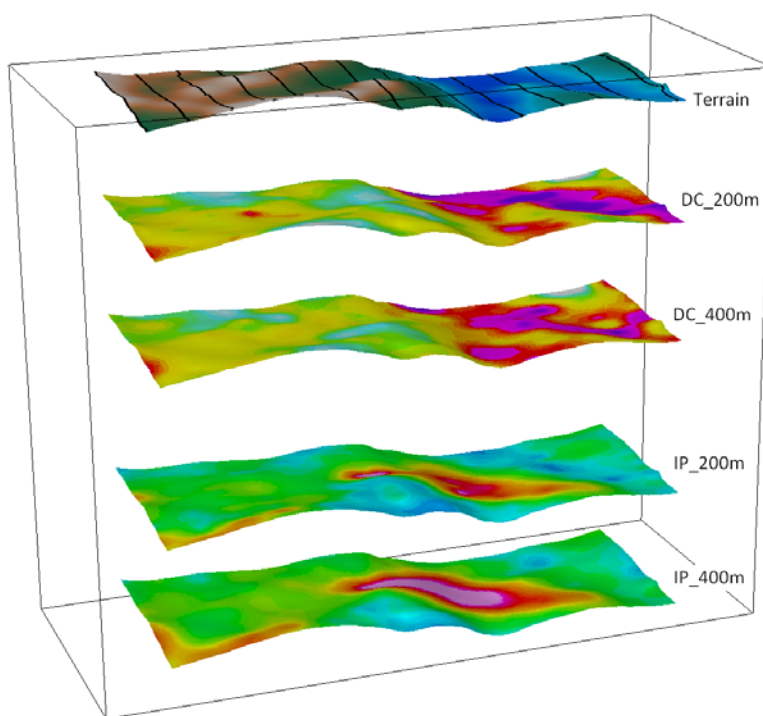


TITAN-24 DC – IP SURVEY
GEOPHYSICAL REPORT
TAD/TORO PROJECT
(WHITEHORSE MINING DISTRICT, YUKON, CANADA)
ON BEHALF OF
DAWSON GOLD CORP.
(BRITISH COLUMBIA, CANADA)



EXECUTIVE SUMMARY

INTRODUCTION

A Titan-24 DCIP survey was undertaken on behalf of Dawson Gold Corp., British Columbia, Canada, from August 18th to September 9th, 2011, over the Tad/Toro Project in Yukon, Canada.

The survey is located approximately 100 km northwest of Carmacks, in the Whitehorse Mining District of Yukon, and includes a grid of 14 north-south lines, evenly spaced at 500m. Each Titan-24 spread was surveyed using a pole-dipole configuration with a dipole size of 100m having a final coverage of 2.4km.

SURVEY OBJECTIVES

The exploration objective of the Titan 24 DCIP survey at Tad/Toro Project was to map and detect gold and silver mineralization related to geology within the Tad/Toro Project for drill targeting, delineation and structural control identification.

RESULTS

The quality of the DCIP data is very good. The data were inverted using the 2D inversion algorithms to produce sections of the resistivity and chargeability distributions of the subsurface.

The analysis and interpretation of the DCIP results allow the identification of several chargeable anomalies, several of which are associated with zones of low resistivity.

A total of 24 anomalies had been identified, among which 9 anomalies (L01-IP1, L01-IP3, L04-IP1, L07-IP1, L08-IP1, L09-IP1, L09-IP2, L10-IP3 and L11-IP1) were classified as 1st priority over the survey area depending on their depth of occurrence and associated DC resistivity and IP chargeability. Anomalies L07-IP1, L08-IP1, L09-IP1, L09-IP2 and L10-IP3 seem to be covering one large zone of mineralization and depict strong IP chargeability, which seems to be extending further deep. L07-IP1 on line L07E (3000E) at station 1450N may be a preferred choice for testing this strong chargeability. Other group of 15 anomalies were classified as 2nd priority targets for drilling survey or for other geophysical survey follow up.

Quantec recommends the complete integration of the Titan-24 results with the known geology, and in particular with the drilling information available in that area to further enhance the interpretation and drill targeting. We also recommend consideration of future follow up over the property with magnetotelluric data in order to better delineate the structural control of mineralization at depth.

TABLE OF CONTENTS

| | |
|--|-----|
| List of Figures | 4 |
| List of Tables..... | 4 |
| 1 Introduction | 5 |
| 1.1 Survey Objectives | 5 |
| 1.2 General Survey Information | 5 |
| 2 Previous Work & Geology | 9 |
| 2.1 Geology of the area | 9 |
| 2.2 Previous Geophysical work in the area | 12 |
| 3 Results and Interpretation | 13 |
| 3.1 Overview of Inversion Procedure..... | 13 |
| 3.1.1 DC Resistivity & Induced Polarization Inversions | 13 |
| 3.2 Discussion of Results | 15 |
| 3.2.1 Cross-section Interpretation | 16 |
| 3.2.2 Discussion on Plan Maps | 34 |
| 4 Conclusions and Recommendations | 38 |
| 5 Statement of Qualifications | 39 |
| 6 Digital Archive | 43 |
| A Production Summary | 45 |
| B Survey Logistics | 47 |
| C DC – IP Pseudo-Sections of Final Processed Data | 55 |
| D Instruments Specifications..... | 111 |
| E Geosoft Sections of the 2D Models | 115 |
| F Geosoft Plan Maps of the 2D Models | 145 |
| G An Introduction to Titan-24 Direct Current (DC) Resistivity and Induced Polarisation (IP) Methods..... | 151 |
| H References..... | 161 |

LIST OF FIGURES

| | |
|--|----|
| Figure 1-1: General Project Location. | 6 |
| Figure 1-2: Surveyed Location Map. | 7 |
| Figure 1-3: Claim map of survey area. | 8 |
| Figure 2-1: General Geology of the Property..... | 10 |
| Figure 2-2: Surveyed Lines Shown over General Geology. | 11 |
| Figure 3-1: Example of DC-IP misfit curves showing relaxation of the model after iteration #40. | 14 |
| Figure 3-2: Interpretation legend with symbols and colour bars. | 16 |
| Figure 3-3: Line L01E (0000E) – DCIP results..... | 17 |
| Figure 3-4: Line L02E (0500E) – DCIP results..... | 19 |
| Figure 3-5: Line L03E (1000E) – DCIP results..... | 20 |
| Figure 3-6: Line L04E (1500E) – DCIP results..... | 22 |
| Figure 3-7: Line L05E (2000E) – DCIP results..... | 23 |
| Figure 3-8: Line L06E (2500E) – DCIP results..... | 24 |
| Figure 3-9: Line L07E (3000E) – DCIP results..... | 25 |
| Figure 3-10: Line L08E (3500E) – DCIP results..... | 26 |
| Figure 3-11: Line L09E (4000E) – DCIP results..... | 27 |
| Figure 3-12: Line L10E (4500E) – DCIP results..... | 28 |
| Figure 3-13: Line L11E (5000E) – DCIP results..... | 30 |
| Figure 3-14: Line L12E (5500E) – DCIP results..... | 31 |
| Figure 3-15: Line L13E (6000E) – DCIP results..... | 32 |
| Figure 3-16: Line L14E (6500E) – DCIP results..... | 33 |
| Figure 3-17: DC resistivity results at 100m (top), 200m (middle) and 400m (bottom). | 35 |
| Figure 3-18: IP chargeability results at 100m (top), 200m (middle) and 400m (bottom). | 36 |

LIST OF TABLES

| | |
|--|----|
| Table 3-1: Summary of IP anomaly over the Tad/Toro Project. | 37 |
|--|----|

1 INTRODUCTION

This report presents the logistics and the results of the analysis of the Titan-24 DC – IPdata acquired from 2011/08/18 to 2011/09/08 over the Tad/Toro Project, on behalf of Dawson Gold Corp..

The first part of this report presents the inversion results, their geophysical interpretation, and some recommendations for future follow-up on the property.

The second part of the report presents the logistics of the survey, including the survey parameters and methodology, and the survey results (data) in digital documents.

1.1 SURVEY OBJECTIVES

The exploration objective of the Titan 24 DCIP survey at Tad/Toro Project was to map and detect gold and silver mineralization related to geology within the Tad/Toro Project for drill targeting, delineation and structural control identification. Titan 24 should enable Dawson Gold Corp. To effectively target its future exploration drilling at the property by:

- Detecting and delineating zones and structures related to the emplacement of sulphide mineralization to depths up to 750 meters.
- Mapping the resistivity and chargeability features related to mineralization, alteration, faults and lithology.

The Titan 24 **Distributed Acquisition System (DAS;** Sheard, 1998) employs a combination of multiplicity of sensors, 24-bit digital sampling, and advanced signal processing. It provides three in-dependent datasets capable of measuring subsurface resistivity's (structure, alteration & lithology) and chargeability (mineralization) to depth.

The DC/IP component of the survey should provide an excellent means of delineating target mineralization within the top 500m to 750m pending geologic and cultural environment.

1.2 GENERAL SURVEY INFORMATION

| | |
|-------------------------------|--|
| Quantec Project No.: | CA00882T |
| Client: | Dawson Gold Corp. |
| Client Address | Suite 350, 580 Hornby Street Vancouver, BC, V6C 3B6 Canada |
| Client representative: | Jason McLaughlin Phone: (604) 687 2471 Email: Jason@dawsongold.com |
| Project Name: | Tad/Toro Project |
| Survey Type: | Titan-24 DC – IP |
| Project Survey Period: | 2011/08/18 to 2011/09/08 |

| | |
|----------------------------------|--------------------------------------|
| General Location: | Approx. 100 km northwest of Carmacks |
| Province | Yukon |
| District | Whitehorse Mining District |
| Nearest Settlement: | Carmacks |
| Datum & Projection: | NAD83/Zone 8 Northern Hemisphere |
| Latitude & Longitude: | Approx. 62°33'40"N, 137°57'30"W |
| UTM position: | Approx. 348000m N, 6940000m W |

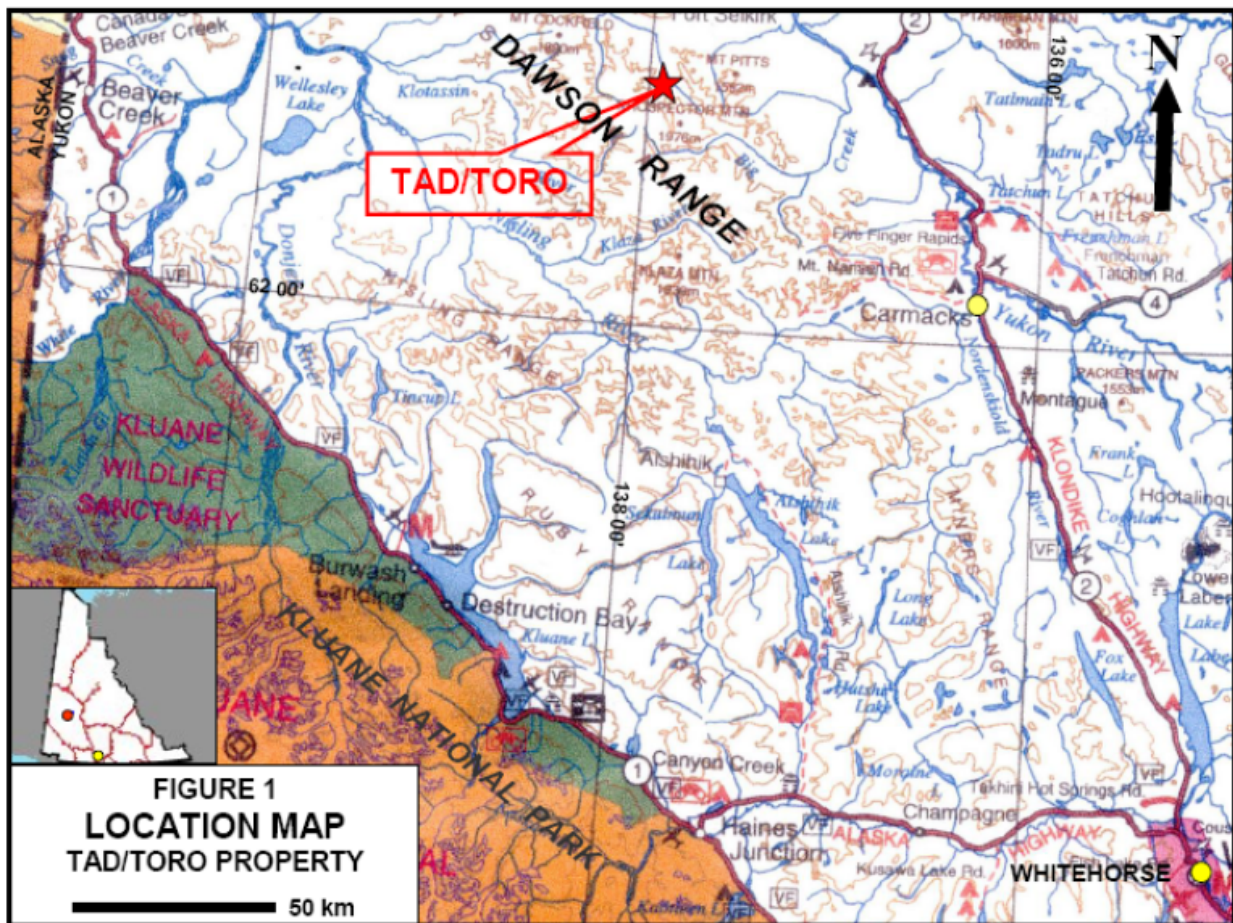


Figure 1-1: General Project Location¹.

¹ Image downloaded from Client Contract, 2011-09-15.

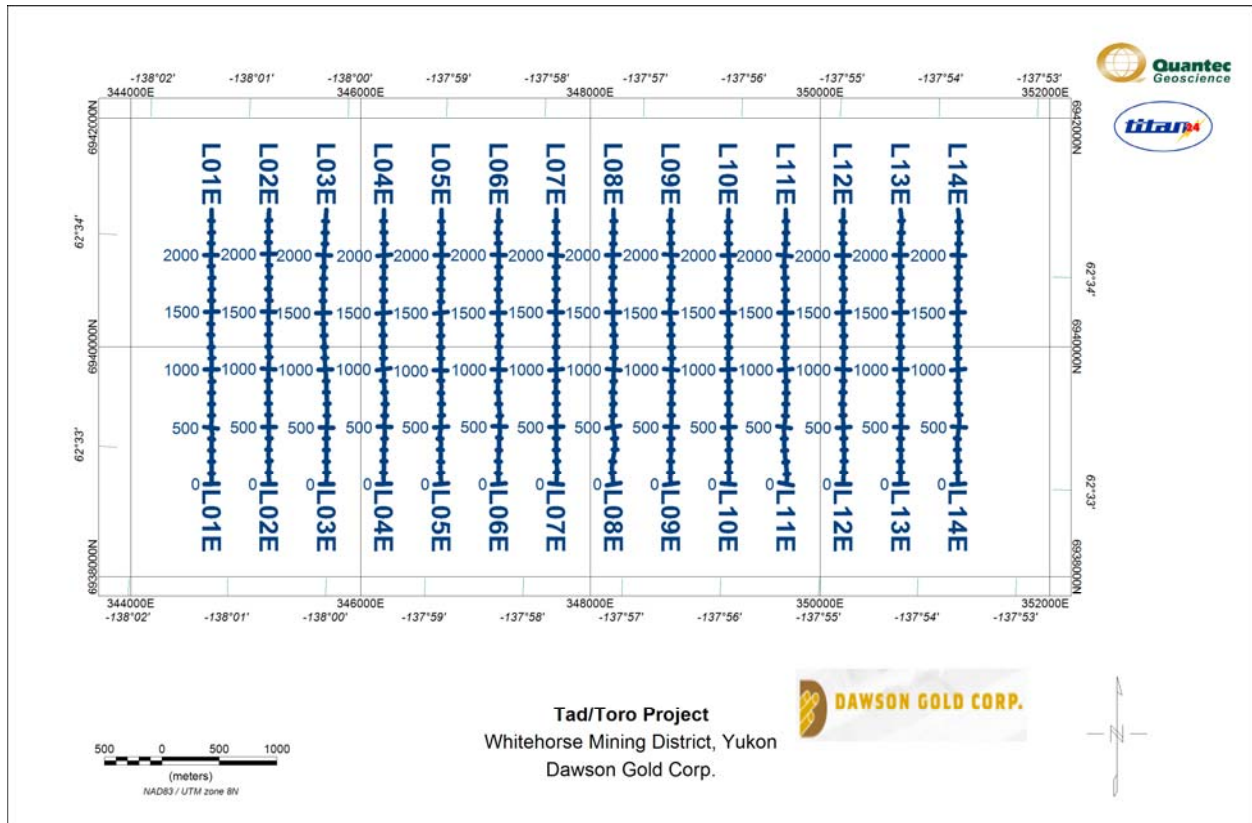


Figure 1-2: Surveyed Location Map.

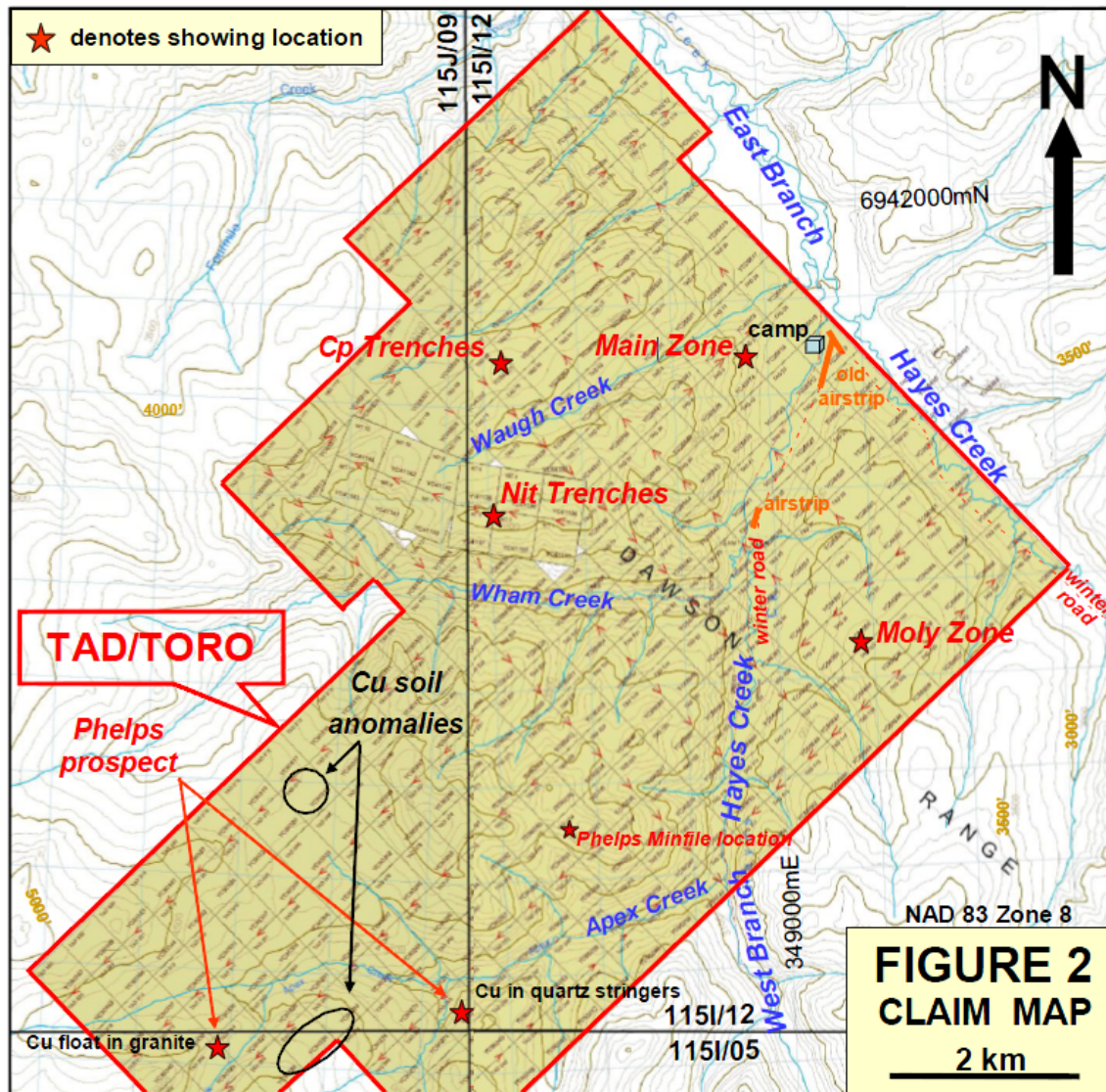


Figure 1-3: Claim map of survey area².

²Image downloaded from Tad/Toro Project Technical Report, 2009/12/20.

2 PREVIOUS WORK & GEOLOGY

2.1 GEOLOGY OF THE AREA³

The Tad/Toro Project is situated within the 100 km long Big Creek portion of the 250 km long Dawson Range Copper-Gold Belt which hosts several deposits and mineralized showings of several deposit models including calc-alkalic porphyry copper-gold±molybdenum, intrusion related gold, associated adjacent epithermal vein and breccia systems and peripheral polymetallic veins.

The Tad/Toro Project is primarily underlain by quartz-hornblende-biotite granitic rocks of the Mid-Cretaceous Dawson Range Batholith (**mKp**) that intrude primarily Devonian-Mississippian meta-igneous and meta-sedimentary rocks of the Yukon-Tanana Terrane (**YTT**) consisting of quartz biotite schist, hornblende schist, gneissic equivalents, quartzite and minor limestone, with a northwest trending foliation. On the property the Dawson Range Batholith includes a biotite-hornblende granodiorite phase (**mKgD**), the Casino granodiorite phase, and a biotite rich leucocratic quartz monzonite to granite phase (**mKfD**), referred to as the Coffee Creek granite phase.

The above units are intruded by quartz feldspar porphyry stocks and dykes of the Late Cretaceous Prospector Mountain Suite (**LKp**), which are known to be associated with gold-copper mineralization within this belt, and are overlain by basalt flows of the Upper Cretaceous Carmacks Group (**uKCv**).

Two phases of the Tad Porphyry have been recognized, a quartz monzonite porphyry and a biotite granite porphyry. Mineralization consists of disseminated pyrite within the Tad Porphyry and narrow sphalerite, galena, and arsenopyrite bearing quartz veins along shear zones. The pyrite mineralization may represent a pyritic halo to a porphyry copper-molybdenum-gold system with associated low grade gold-pyrite-arsenopyrite in sericite-phyllitic alteration zones within the quartz monzonite porphyry and in breccia zones and northerly trending fault zones. Molybdenite occurs within altered potassium feldspar megacrystic quartz monzonite in the Moly Zone in the eastern property area. The zinc-lead veins may represent polymetallic veins outboard of the porphyry system.

A second body of the Prospector Mountain Suite (**LKp**), or the possible extension of the Tad Porphyry, and related north-easterly trending dykes, extend from the Cp trenches across the Nit claims. Aplite dykes were noted cutting medium to coarse grained quartz monzonite in the Nit trenches. A north-north-easterly trending dyke swarm (**LKp**) has been mapped extending to the south towards the Phelps prospect and two small leucocratic stocks were identified in the Phelps area (*Hilker et al., 1970*). The metamorphic and igneous rocks are intruded by mafic dykes and are overlain by basalt flows of the Upper Cretaceous Carmacks Group (**uKCv**) primarily on the north side of Hayes Creek. These weather brown to reddish-brown and vary from olivine-rich to feldspathic.

The north-westerly trending North Big Creek Fault cut across the north-eastern edge of the property following the Hayes Creek. The sub-parallel South Big Creek Fault lies 5 to 6 km to the southwest. A northerly trending extensional fault follows the West Branch of Hayes Creek. This is the same structural environment present on the Nucleus Zone of the Freegold Project of Northern Freegold Resources situated 40 km to the southeast (Technical Report on the Tad/Toro Project, December 2009).

³ Geological information provided by Dawson Gold Corp.; Text and images from the Final Agreement (Contract) document and the Tad/Toro Project Technical Report, 2009/12/20.

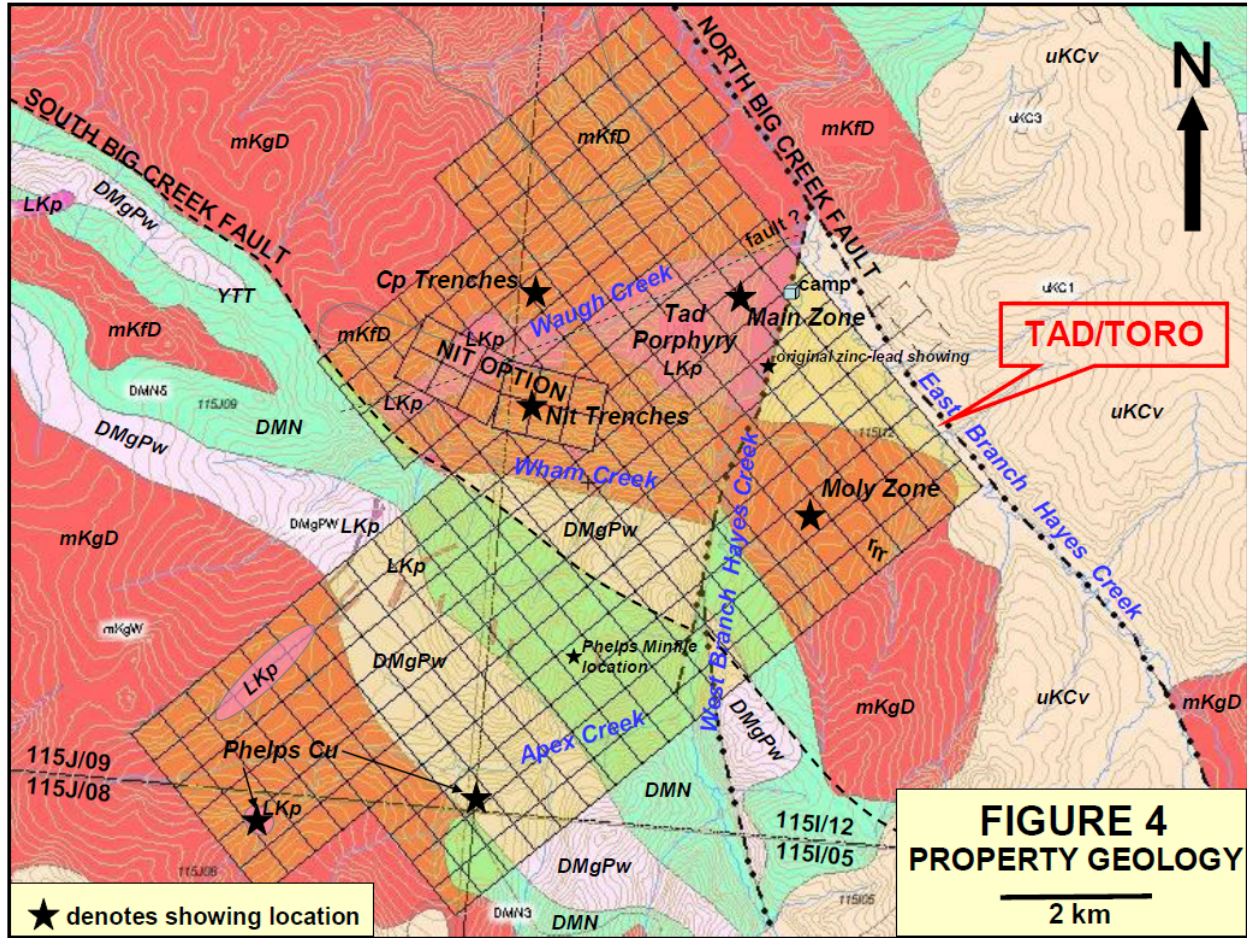


Figure 2-1: General Geology of the Property.

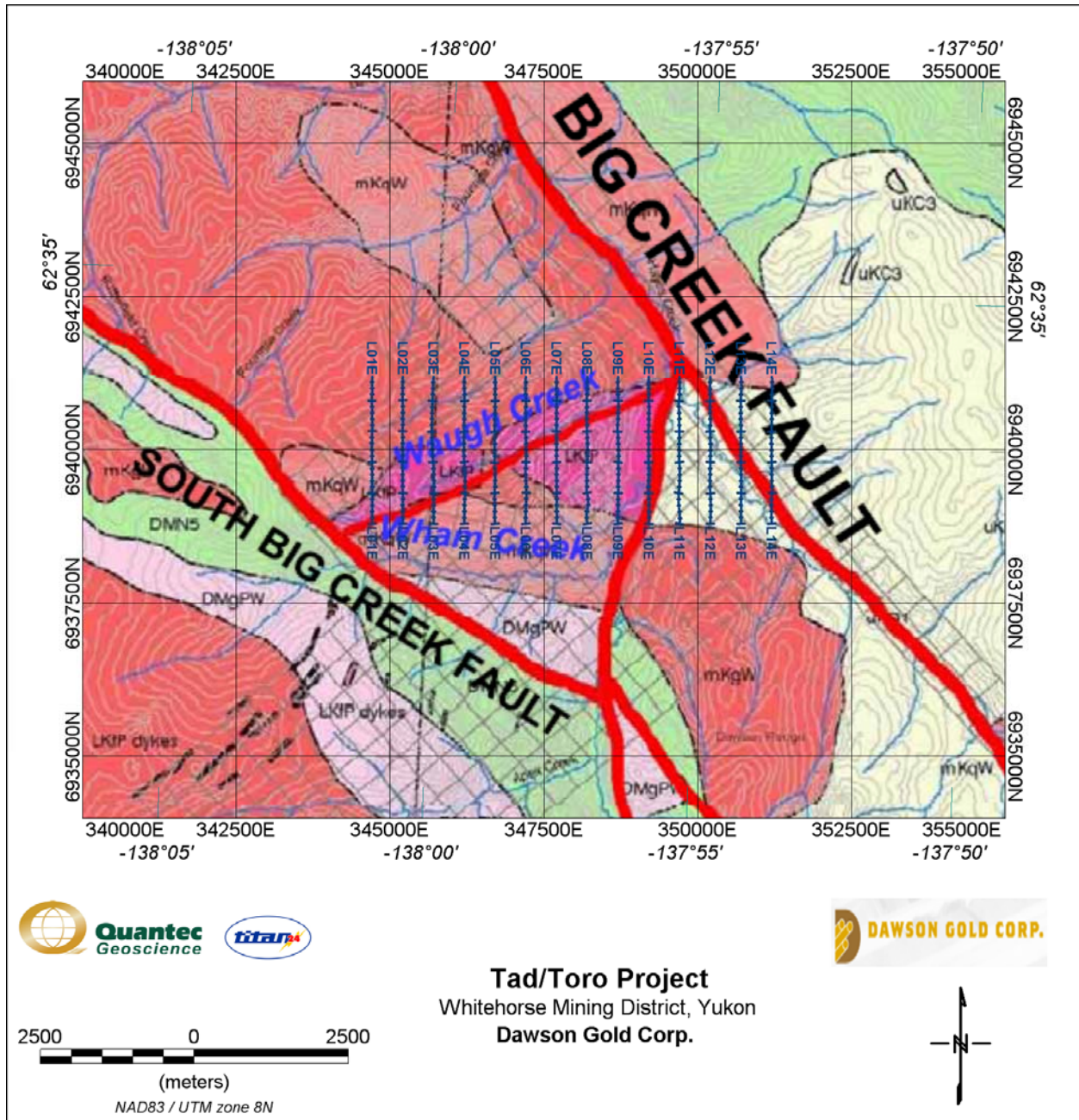


Figure 2-2: Surveyed Lines Shown over General Geology.

2.2 PREVIOUS GEOPHYSICAL WORK IN THE AREA⁴

The Tad/Toro Project area had been explored by a helicopter-borne magnetic and radiometric geophysical survey in 2009. Interpretation of this data identified five porphyry-type and five vein-type target zones. The project area is expected to bear additional prospective targets. The Nit area was identified as a priority exploration target for vein system alteration and permissive zones associated with porphyry dykes and/or quartz monzonite unit. This occurrence was previously reported to comprise three large gold soil geochemical anomalies that have not been adequately tested by trenching or drilling.

Previous drill core from the Main Zone exhibits extreme oxidation with many unsplit oxidized and brecciated sections. A supergene enrichment zone occurs near the top of many of the drill holes in the centre of the mineralized zone. The sulphide minerals are oxidized to a depth of 80m and the gold-bearing oxide zone lies in brecciated and intensely altered quartz monzonite porphyry, below which is a hypogene zone containing up to 10% disseminated pyrite in porphyritic granite with lesser alteration.

⁴ Information extracted from the Tad/Toro Project Technical Report, 2009/12/20 by Dawson Gold Corp.

3 RESULTS AND INTERPRETATION

This section presents the results of the 2D inversion of the Titan-24 data and interpretation in context with the survey objectives and significance to future exploration at Tad/Toro Project.

The Titan-24 system can acquire three types of geophysical data – magnetotelluric (MT), direct current resistivity (DC), and induced polarization (IP).

The MT and DC methods are used to resolve the resistivity distribution of the subsurface by measuring the electric potential (DC) and the variation of natural source electric and magnetic fields (MT). Resistivity can be an indicator of metallic mineralization, but is more often than not controlled by rock porosity and is therefore an indirect indicator of alteration and mineral grain fabric.

In the induced polarization method, electrical capacitance or chargeability of the subsurface is measured. Chargeability is a near-direct indicator of the presence of sulphide mineralization, in both massive and disseminated forms. Chargeable mineralization is most commonly various sulphides and graphite, but also includes clay-type minerals potentially making it a useful tool for base-metals exploration.

For this survey, only the DC-IP component of the Titan24 system had been used. For each line surveyed, the DC-IP utilized a pole-dipole configuration with 100m dipoles with the current injection points located at every 100m between the potential dipoles along the lines. There was no current extension at the end of each profile.

Detailed information on the survey logistics, acquisition parameters and screen capture of the acquired data for the survey are provided in appendices at the end of this report.

The final inversion models are presented graphically in Geosoft plot format along with an interpretation overlay and comments on the most significant results and recommended targets. Scaled sections and plan maps of the DC resistivity and of the chargeability models are also provided at the end of this report.

Detail results, i.e. observed DC-IP data and equivalent calculated responses for each model, are presented on a line per line basis in PowerPoint (PDF) documents delivered in the digital archive (CD/DVD) attached to this report.

3.1 OVERVIEW OF INVERSION PROCEDURE

3.1.1 DC RESISTIVITY & INDUCED POLARIZATION INVERSIONS

DC-IP is an electrical method that uses the injection of current and the measurement of voltage difference along with its rate of decay to determine the subsurface resistivity and chargeability, respectively. Depth of investigation is mainly controlled by the array geometry, but may also be limited by the received signal, which is dependent on transmitted current, and ground resistivity. The chargeability parameter is particularly susceptible to cases with a low signal-to-noise ratio. In its standard configuration ($a=100\text{m}$ / $n=0.5-23.5$) the Titan-24 surveys typically image DC resistivity to depths of 500-750m, and the IP typically images to 500-750m, in sub-vertical tabular geologic settings and up to 50% more for sub-horizontal. The differences in penetration are a function of the relative property contrasts and relative signal-to-noise levels between the two measurements. decreases or increases proportionally to the dipole-size (i.e., 300-500m for 50m dipoles, and 1000-1500m for 200m dipoles). A detailed introduction to DC-IP is given in Telford, et al. (1976).

The primary tool for evaluating the Titan-24 data is through the inversion of the data in two-dimensions

(2D). An inversion model depends not only on the data collected, but also on the associated data errors in the reading and the “model norm”. Inversion models are not unique and may contain “artefacts” from the inversion process. The inversion model may not accurately reflect all of the information apparent in the actual data. Inversion models must be reviewed in context with the observed data, model fit, and with an understanding of the model norm used.

The Titan-24 DC and IP data were inverted to produce cross-sections of the resistivity and chargeability variations along the survey lines. The UBC DCIP2D inversion code (Oldenburg & Li, 1994) was used for the 2D inversion of the DC and IP data.

Potential difference (voltage) and phase values were used as input data in the DC and IP inversions, respectively. DC Resistivity and induced polarization (IP) data are first pre-conditioned; the error of each data point is adjusted for the inversion process using a general error equation similar to:

$$errors\left(\begin{matrix} Vp \\ IP \end{matrix}\right) = A\% \left| \begin{matrix} Vp \\ IP \end{matrix} \right| + B \times \text{Acq_Error}\left(\begin{matrix} Vp \\ IP \end{matrix}\right) + C \text{ (floor)}$$

with the set of parameters $\{A, B, C\}$ adjusted (and large errors data points removed) for each dataset until we achieve convergence with relaxation of the DC or IP models (see example of Model Norm fit curve on Figure 3-1).

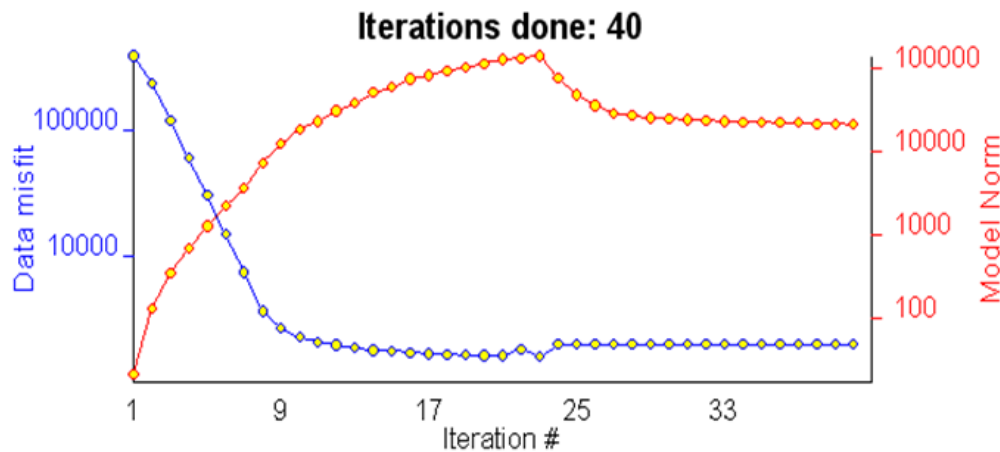


Figure 3-1: Example of DC-IP misfit curves showing relaxation of the model after iteration #40.

Three 2D inversions were carried out along each line.

The DC data was inverted using an unconstrained 2D inversion with a homogenous half-space of average input data as starting model. The DC models are labelled as ‘smDC’.

Two IP inversions are calculated from the same data set and parameters, but they use a different reference model⁵. The first inversion of the IP data uses the previously calculated DC model as the reference model, and is labelled the ‘IP *dcref* model’. The second IP inversion uses a homogeneous half-space resistivity model as the reference model and is labelled ‘IP *hsref* model’ or ‘IP *nullcon*’ model. This model is included to test the validity of chargeability anomalies, and to limit the possibility of inversion artefacts in the IP model due to the use of the DC model as a reference.

The DC and IP inversion use the same mesh. The horizontal mesh was set as 3 cells between electrodes.

⁵ The reference model is used to calculate the sensitivity matrix used at each iteration for the IP inversion.

The vertical mesh was designed with a cell thickness from 10 to 15m for the first hundred's of metres to accommodate the topographic variation along the profile, and then it increases from 20 to 100m with depth. The inversions were generally run for a maximum of 50 iterations, and stop after convergence and relaxation as defined on Figure 3-1.

3.2 DISCUSSION OF RESULTS

This section presents a description of the interpretation results based on the most significant geophysical anomalies prospected as potential targets from the final DC and IP inversion models. The DC resistivity models, and IP (DC referenced) chargeability models are used for presenting the interpretation results. These inversion models were found to produce consistent results along the survey lines and illustrate the resistivity and chargeability distribution of subsurface structures and occurrence of potential mineralized zones in the property. The structural and lithology is interpreted mainly from DC sections, and IP chargeability is considered as a 'direct' indicator of disseminated to massive sulphide mineralization.

Cross-sections of the DC-IP survey, consisting of the DC resistivity and IP chargeability are prepared and interpreted on a line by line basis. Anomalous features are interpreted as structures (i.e. faults, shear, contacts, potential alteration zones, etc.).

Plan maps at depth levels 100m, 200m and 400m are generated for the DC resistivity and IP chargeability.

The presented sections and plan maps use consistent and constant colour bars, which ranges from 100 Ohm-m to 2000 Ohm-m for resistivity and 0 mrad to 30 mrad for chargeability. For resistivity, the cool colours (white) represent high resistivity and the hot colours (red) represent high conductivity, whereas in chargeability, hot (red) represent strong chargeability and cool (blue) represent weak chargeability responses. The interpretation legend and colour bars used in this project are illustrated in Figure 3-2.

The main objective of the survey is to map and to detect gold and silver mineralization related to geology within the Tad/Toro Project for drill targeting, delineation and structural control identification.

A summary of the main zones of anomalous resistivity and chargeability is presented on Table 3-1.

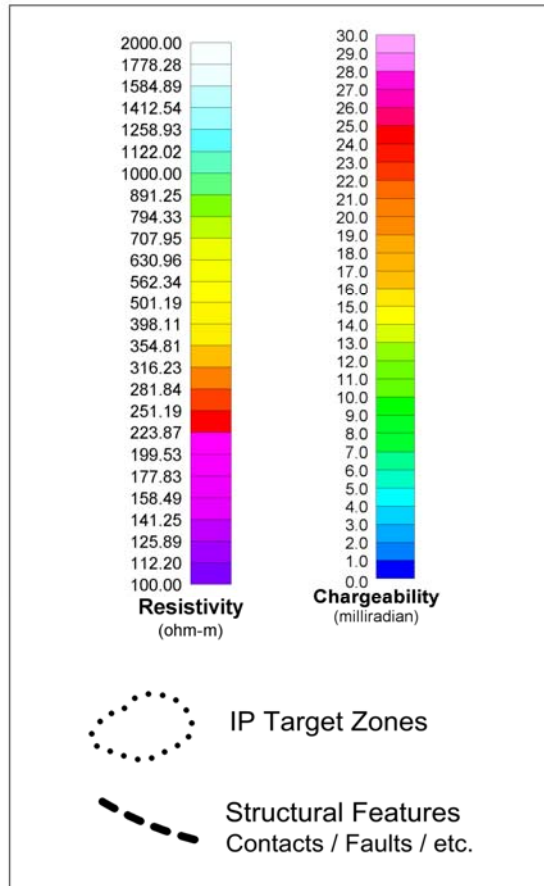


Figure 3-2: Interpretation legend with symbols and colour bars.

3.2.1 CROSS-SECTION INTERPRETATION

The Tad/Toro Project comprises 14 lines spaced at 500m from west to east. Each line spread is oriented south to north with a total length of 2.4 km. The DCIP spread mainly covers the Waugh Creek area between two major northwest southeast trending Fault Systems, namely, South Big Creek Fault and the North Big Creek Fault. All surveyed lines are located at the north-eastern side of South Big Creek Fault. Little evidence could be seen on another north-east trending Fault (marked by Waugh Creek) in the region that cut across majority of the lines, say, L01E to L09E. Some lines show a resistivity variation, which could be correlated with this fault. The region is also believed to be transecting by a north-south trending extensional fault, and line L10E cut across this fault. Eastern most lines L12E to L14E transect the North Big Creek Fault. The region also seems to be influenced by the late Cretaceous Prospector Mountain Suite (**LKp**) intrusions, marked by quartz feldspar porphyry stocks and dykes (Figure 2-1).

It could be possible that the structural influence of these fault systems and contacts between different geologic formations in the region control the overall low resistivity observed in all surveyed lines in the Tad/Toro Project. This survey also helped in resolving some IP chargeability zones for potential test for mineralization targets. The DC referenced IP models are used in this interpretation, where the picked anomalies are also validated with half-space referenced IP models. Following sections illustrate a detailed line by line interpretation of 2D DC and IP inversions.

3.2.1.1 Line L01E (0000E)

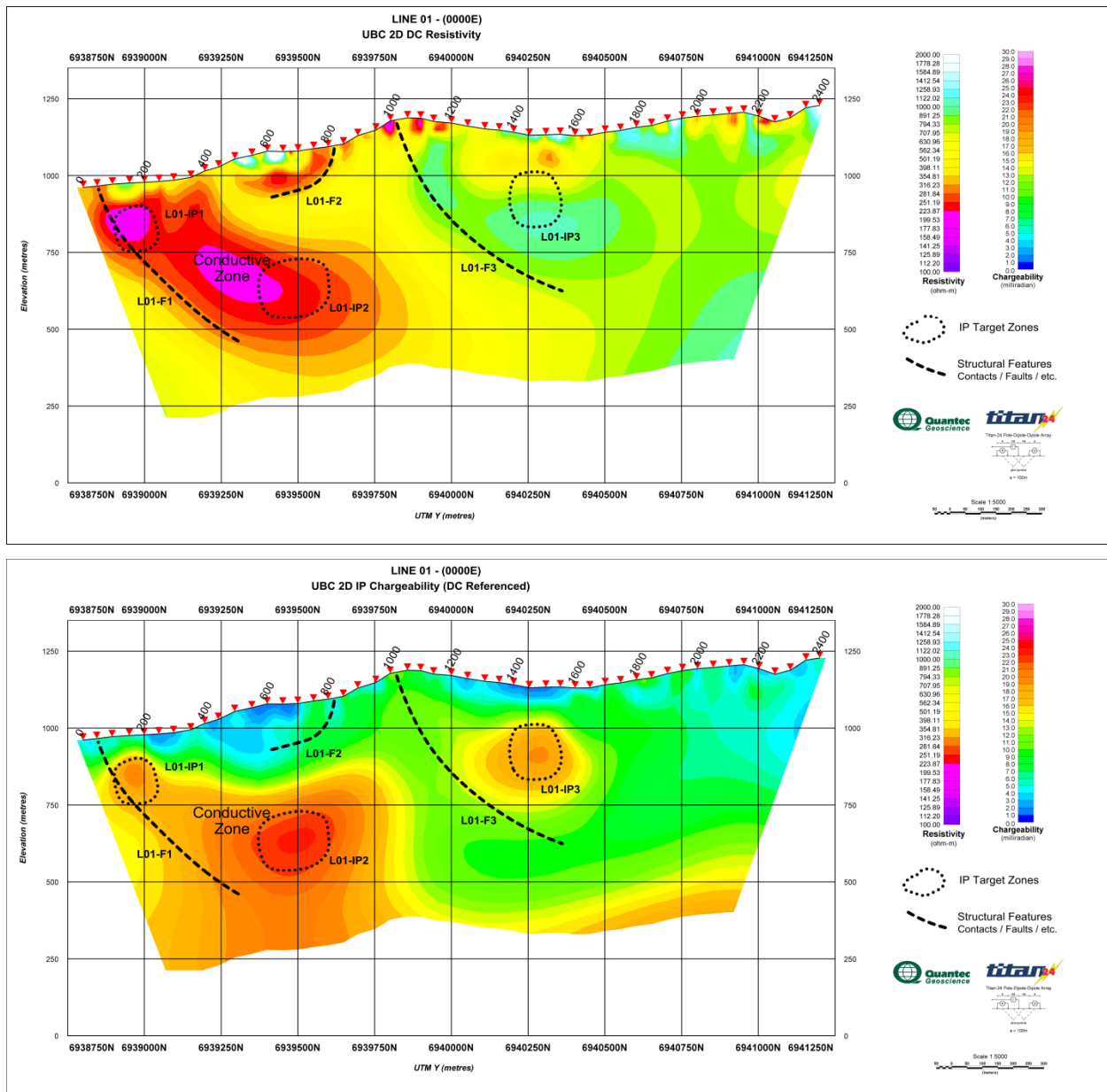


Figure 3-3: Line L01E (0000E) – DCIP results.

The DC inversion model delineates the major lateral resistivity variations in the structure as marked as L01-F1 and L01-F3. The low resistivity signature observed in the southern end of the line, covering stations 0-400N, may be correlated with the possible northeast trending fault in the region. This northward dipping low resistivity structure (L01-F1) may also have influenced by the **Lkp** event in the region. L01-F2 marks a surficial low resistivity zone and L01-F3 defines a lateral resistivity boundary, where the northern half depicts relatively high resistivity structures. This boundary could also be correlated with a variation in the geological formation as evidenced from the geology map.

The IP inversion models resolve three chargeability zones in the cross-section. The low resistivity

structure in the south end of line is associated with two IP anomalies, L01-IP1 below station 150N, and L01-IP2 below station 700N, occurring at depths of about 120m and 420m respectively. The third IP anomaly (L01-IP3) detected below station 1450 at a depth of about 160m is associated with a resistivity gradient. All three IP anomalies exhibit relatively moderate or higher chargeability, suggesting possible mineralization. The shallow anomalies L01-IP1 and L01-IP3 may be potential targets for testing.

3.2.1.2 Line L02E (0500E)

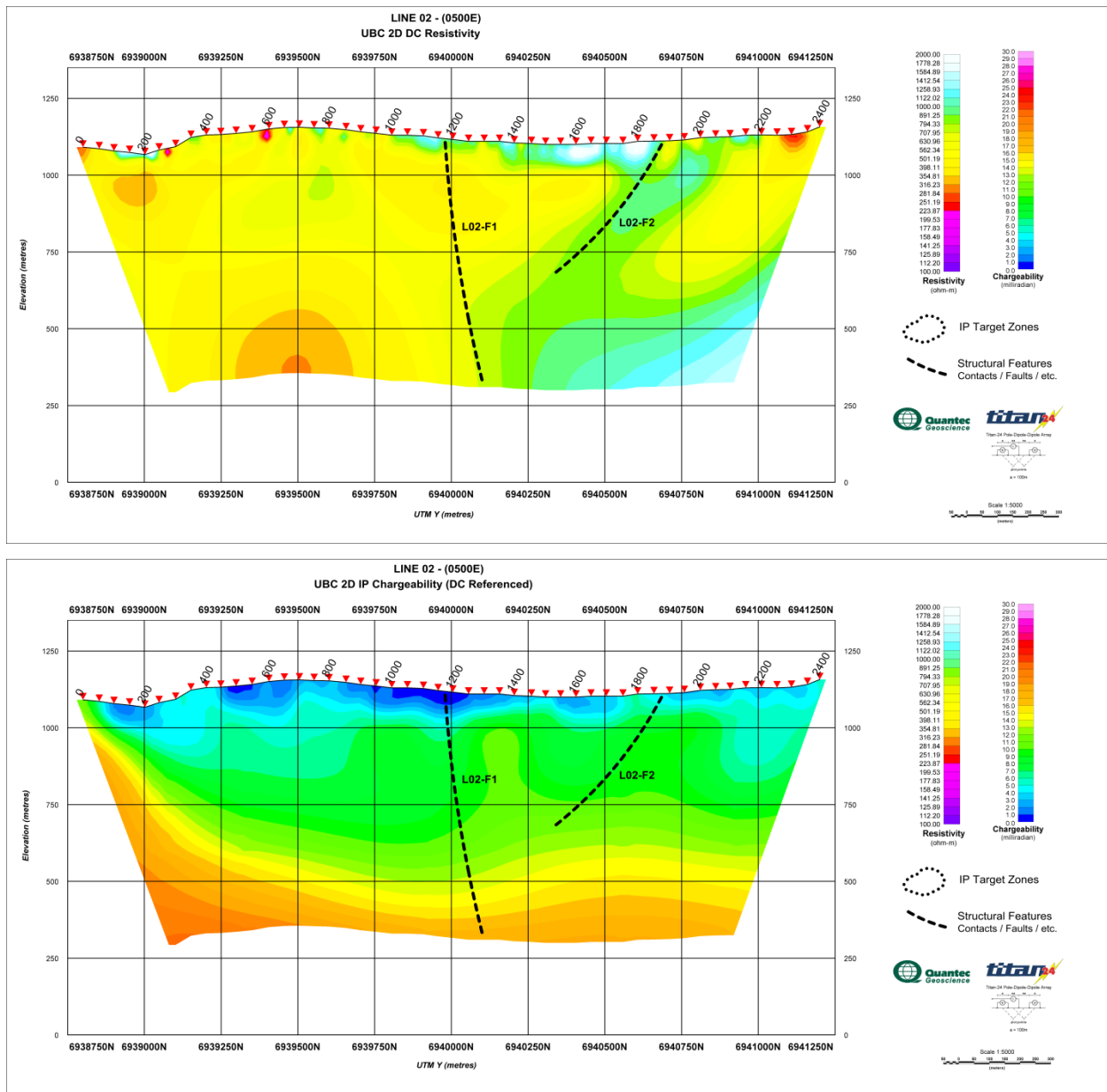


Figure 3-4: Line L02E (0500E) – DCIP results.

Two resistivity boundaries L02-F1 and L02-F2 are demarcated in the DC model for Line L02E. A geological contact seems to be coinciding with the lateral resistivity variation marked by L02-F1 at station 1200N. The northern half of this line shows a more resistive structure, and can be correlated with the general resistivity structures for surveyed lines on either side (L01E and L03E). This high resistivity may be attributed to the bulk rock representation in the region, while the conductive signatures are controlled by other structural/intrusive/alteration events.

No prominent IP anomalies are resolved in this line.

3.2.1.3 Line L03E (0500E)

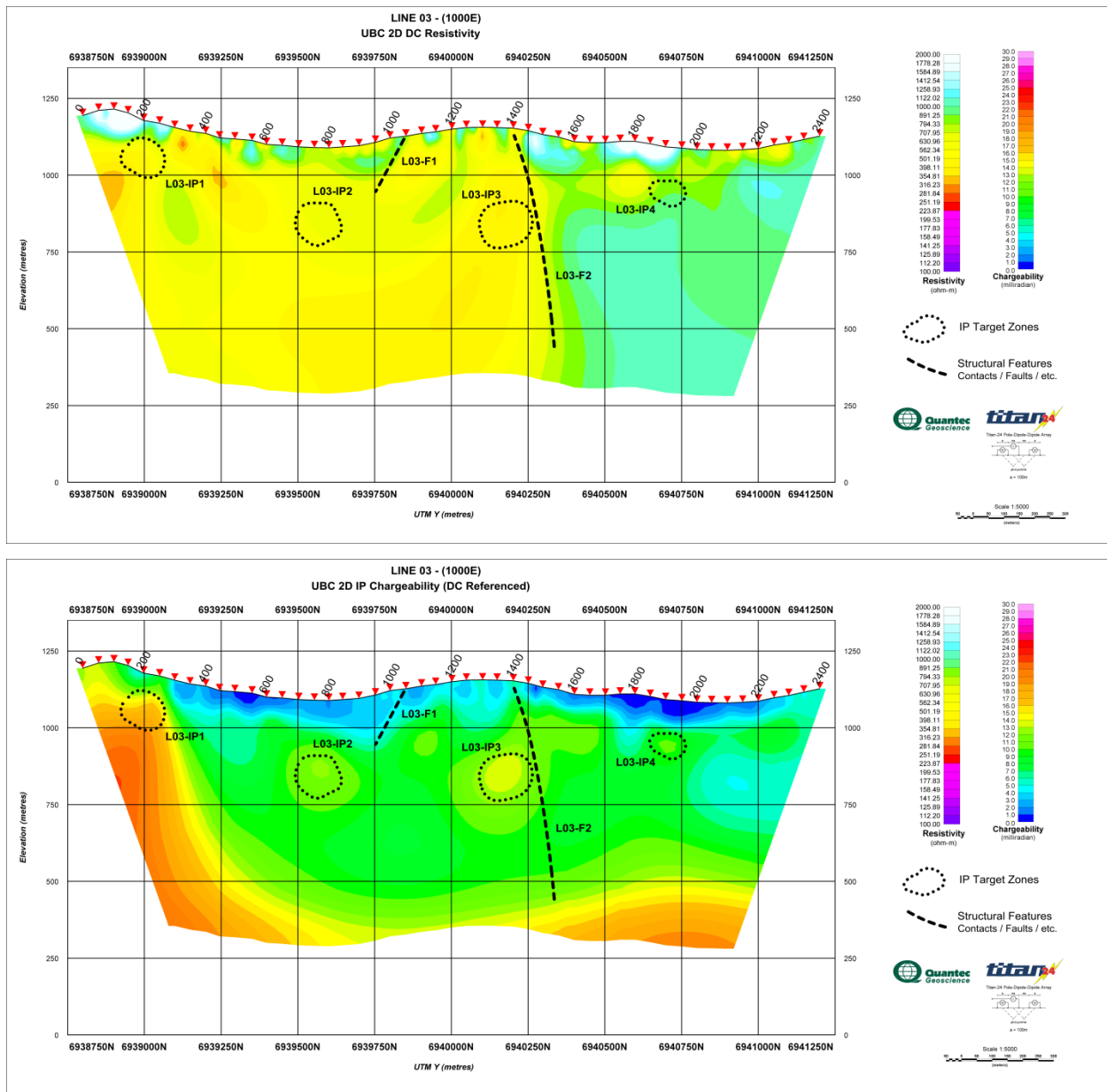


Figure 3-5: Line L03E (1000E) – DCIP results.

DC resistivity cross-section for line L03E shows a clear resistivity boundary around station 1400N, with distinct high resistivity zone towards the east. This may be indicating the structural contact between different geologic formations as evidenced in the geology of the region. Station 1400N is in the vicinity of the geologic boundary marked by LkP units.

Four IP anomalies are detected in line L03E. The anomaly L03-IP1 could be a potential target for testing, for its relatively strong IP chargeability and its shallow occurrence at a depth of about 100m at station 200N. L03-IP2, L03-IP3 and L03-IP4 show relatively moderate IP chargeability, but picked due to its consistent representation in both DC referenced and half-space referenced chargeability models. L03-

IP2 and L03-IP3 occur at stations 750N and 1350N, and at depths of 230m and 300m respectively. L03-IP4 is better defined in the half-space chargeability model and it may also be tested with a low priority, due to its shallow occurrence at depth about 150m below station 1900N.

3.2.1.4 Line L04E (1500E)

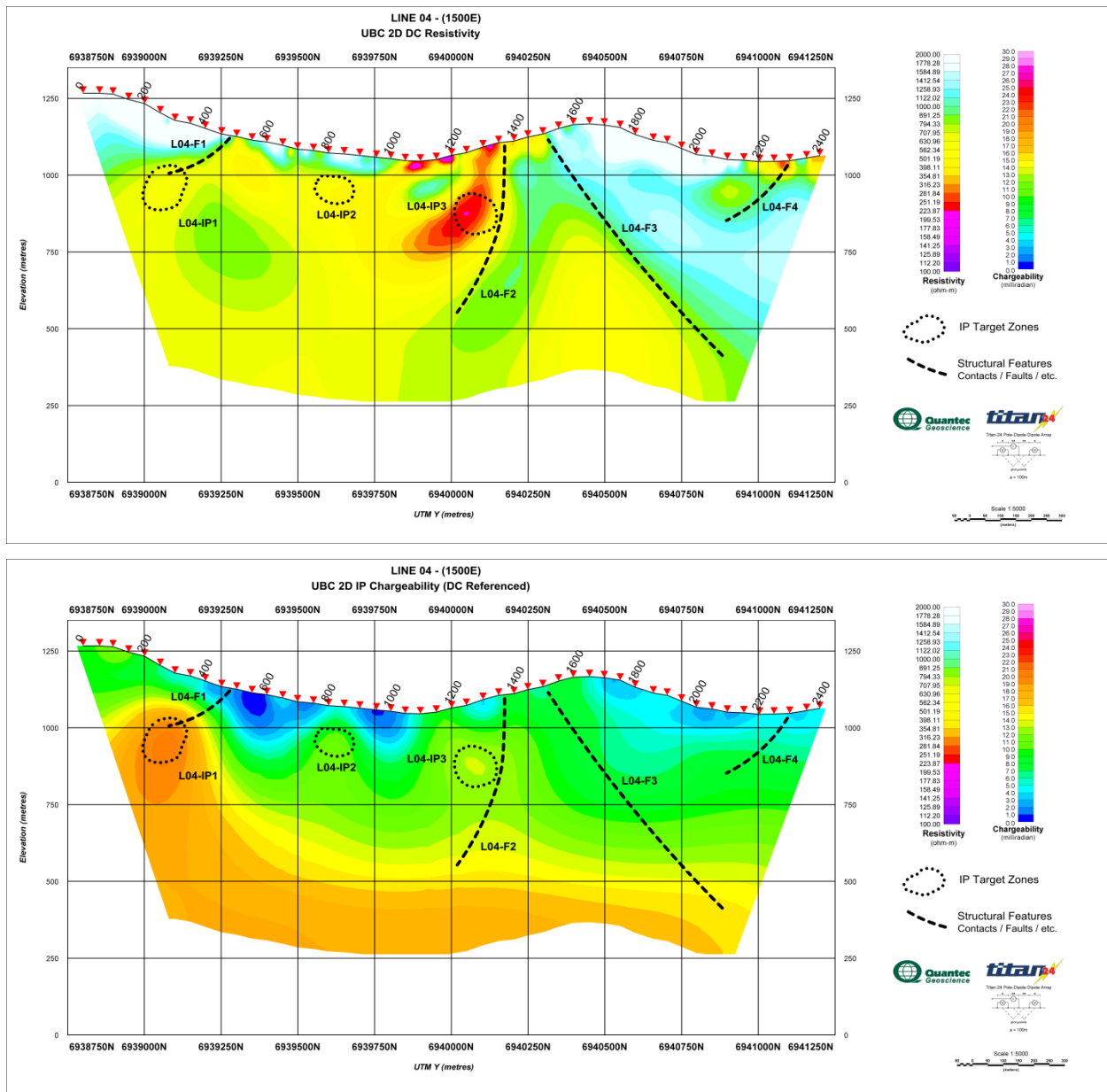


Figure 3-6: Line L04E (1500E) – DCIP results.

The lateral resistivity boundaries observed in previous western lines is also visible in this line L04E, marked as L04-F2 at station 1350N. Another resistivity boundary L04-F3 to further east is marked, just to show a possible resistivity variation due to some sort of alterations within the contact zone.

Three IP anomalies are identified along line L04E. The anomaly L04-IP1 bears relatively strong chargeability and occurs at station 300N at a depth of about 200m. Anomalies L04-IP2 and L04-IP3 have moderate chargeability and picked due to its consistency with half-spaced chargeability models. Both these anomalies occur at stations 800N and 1250N at depths 110m and 175m respectively. Both anomalies L04-IP1 and L04-IP2 may be tested considering their chargeability and depth of occurrence.

3.2.1.5 Line L05E (2000E)

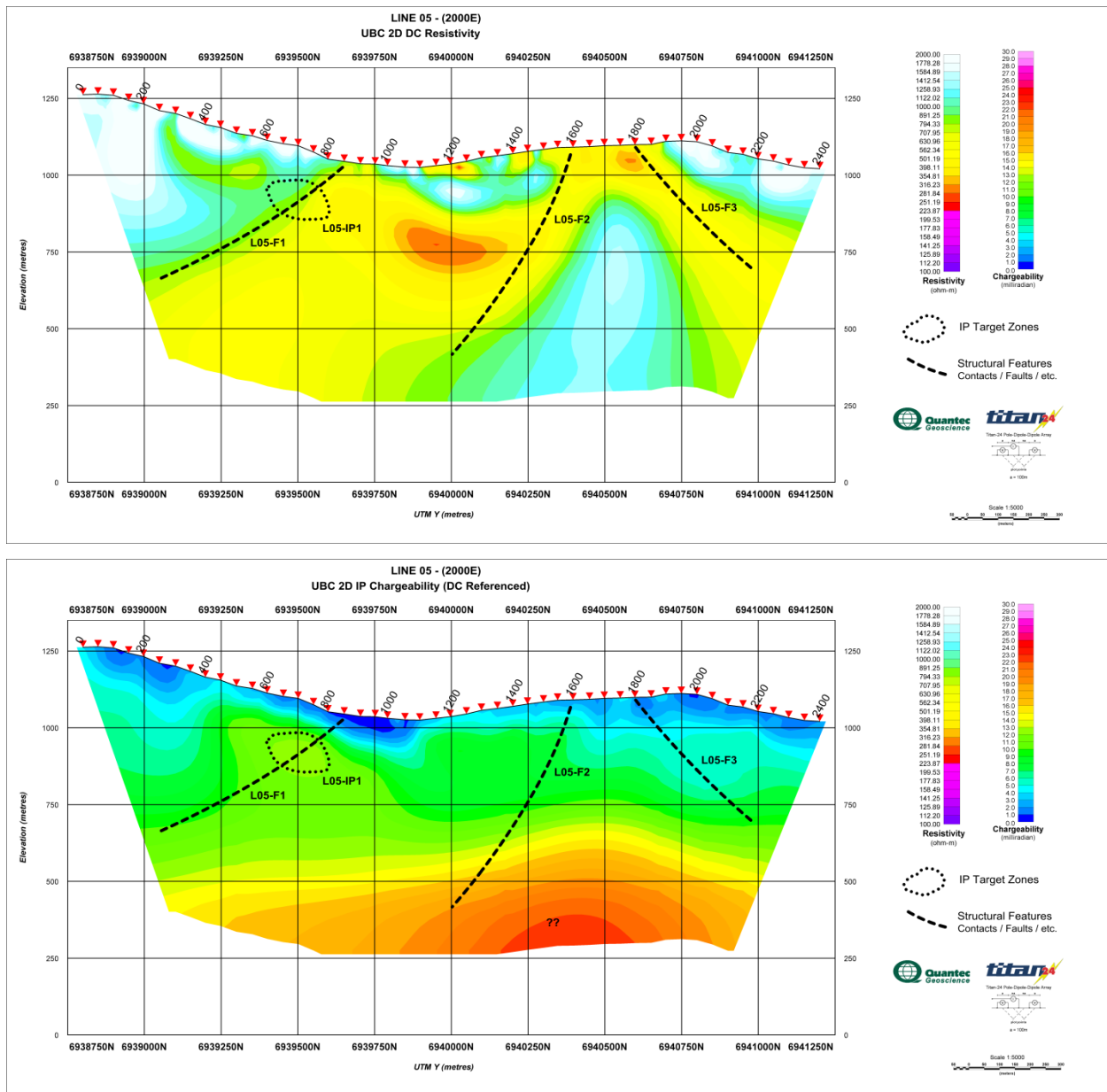


Figure 3-7: Line L05E (2000E) – DCIP results.

Line L05E shows distinct resistivity structures along the DC inversion model. L05-F1, L05-F2 and L05-F3 mark distinct boundaries with high resistivity zones. L05-F2 may be coincident with the geologic boundary as seen in the geology map of the region, where a second Prospectus Mountain suite unit is evident. L05-F3 may be due to some sort of formation contact or suture. A conductive zone is also well demarcated in the DC model between stations 1000N and 1400N at an approximate depth of 250m.

One IP anomaly L05-IP1, with moderate chargeability resolved in both DC and half-spaced models is detected below station 700N at a depth of about 150m. Though not well resolved, this line also depicts the evidence of some deep seated IP anomalies. This may be further explored for possible deep targets.

3.2.1.6 Line L06E (2500E)

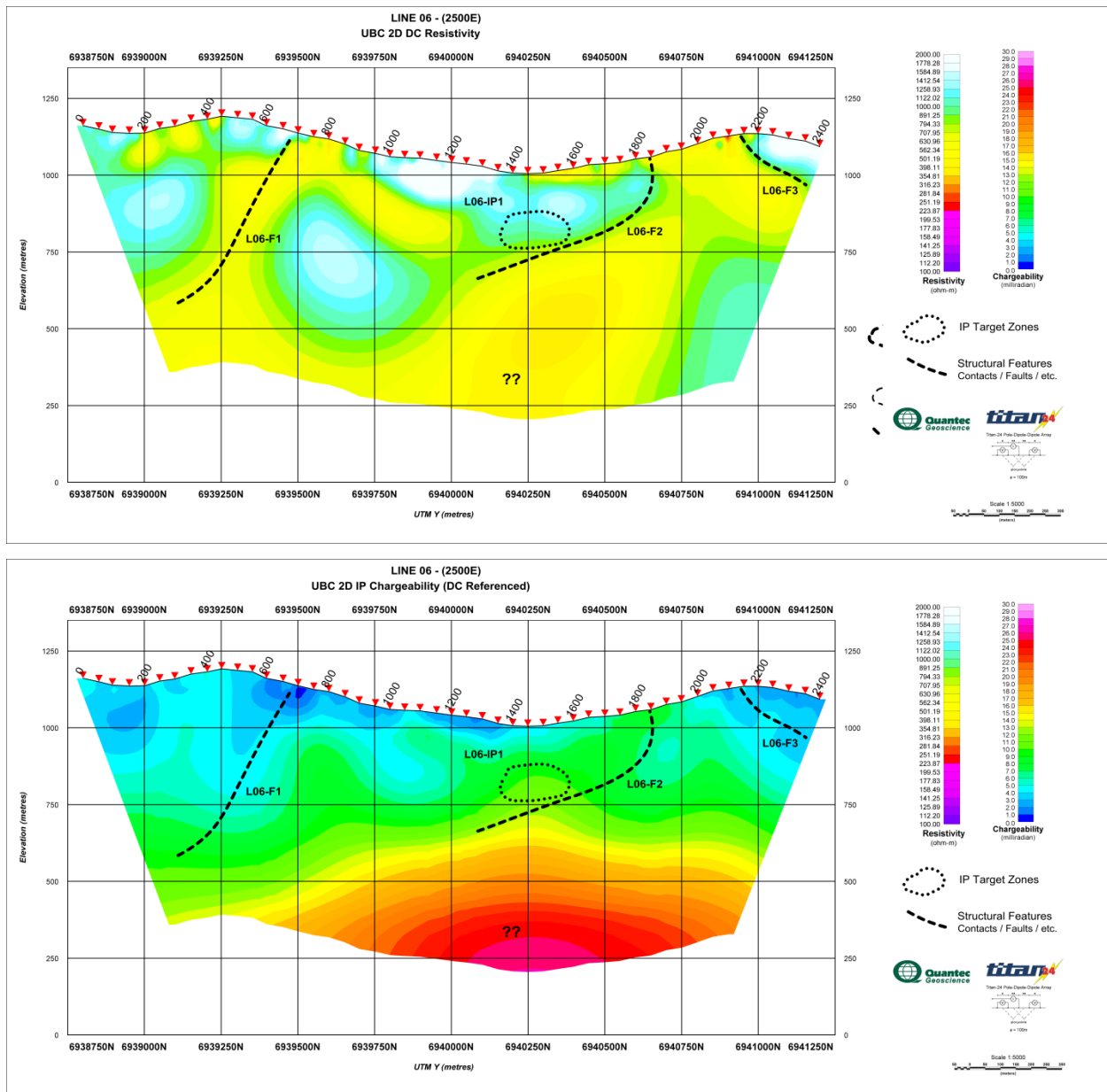


Figure 3-8: Line L06E (2500E) – DCIP results.

The DC model for line L06E more or less depicts a top resistive layer underlain by relatively lower resistivity structures. Three distinct resistivity boundaries are marked as L06-F1 to L06-F3. L06-F1 and L06-F2 may be correlated to the structural contacts evident in the geology of the region.

Only one weak IP anomaly, L06-IP1, is picked in this line at a depth of 200m below station 1450N. The presence of a deep seated IP target may be seen, but cannot be resolved from current model.

3.2.1.7 Line L07E (3000E)

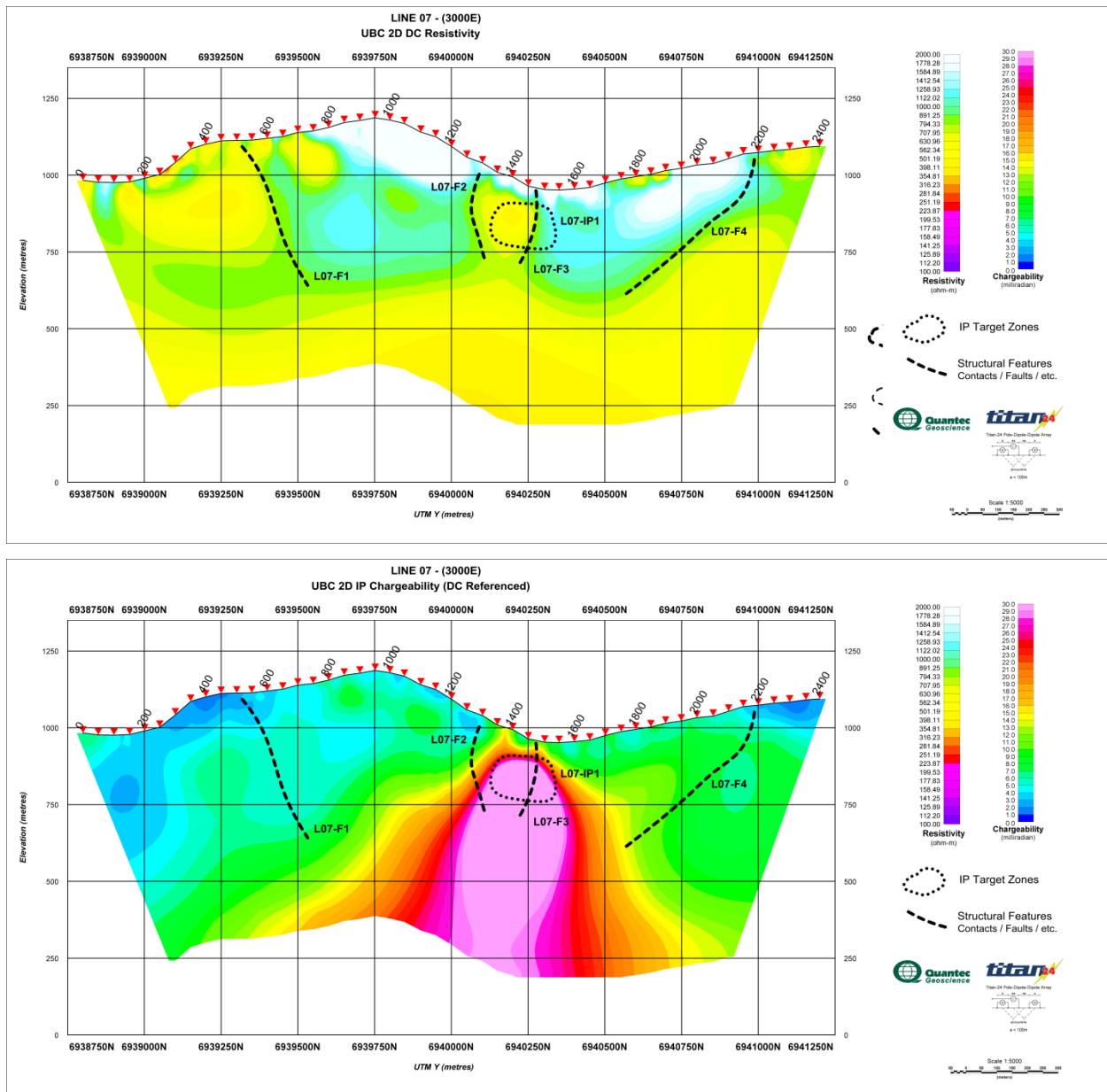


Figure 3-9: Line L07E (3000E) – DCIP results.

Line L07E also exhibits a relatively high resistivity near surface layer followed by a consistent lower resistivity structure below a depth of about 300m. Resistivity boundaries L07-F1 and L07-F4 could be correlated with the visible changes in geologic formations around stations 500N and 2000N respectively. L07-F2 and L07-F3 are marked to note the possible resistivity variation associated with some alteration or mineralization, as supported by strong IP chargeability.

One strong IP chargeability zone, L07-IP1 is located in this line beneath station 1450 at a depth of about 100m. Both DC referenced and half-space referenced chargeability models support this target for a possible test site.

3.2.1.8 Line L08E (3500E)

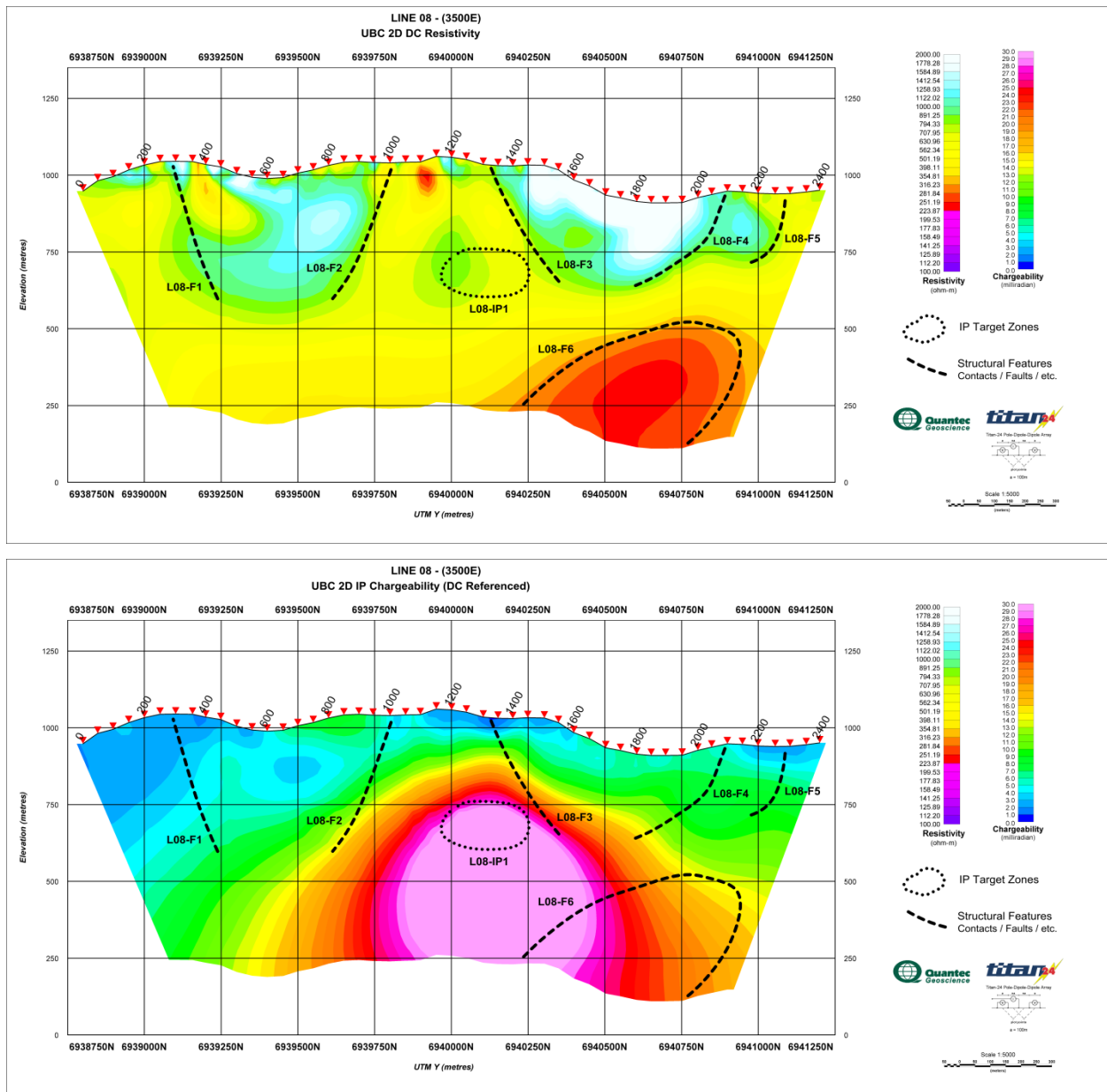


Figure 3-10: Line L08E (3500E) – DCIP results.

Resistivity variation associated with possible geologic contacts are visible along this line. L08-F1 and L08-F4 may be correlated to the visible geologic contacts around stations 300N and 2100N. Other major contacts L08-F2 and L08-F3 may be attributed to any other formational variation or alteration processes as evidenced through strong IP chargeability. A conductive structure, L08-F6, is also evident in this cross section at a depth of about 500m below station 1800N.

One strong IP anomaly is detected in this line at a depth of about 300m below station 1300N. This anomaly L08-IP1 is also resolved in half-space referenced chargeability model and may be tested for possible mineralization.

3.2.1.9 Line L09E (4000E)

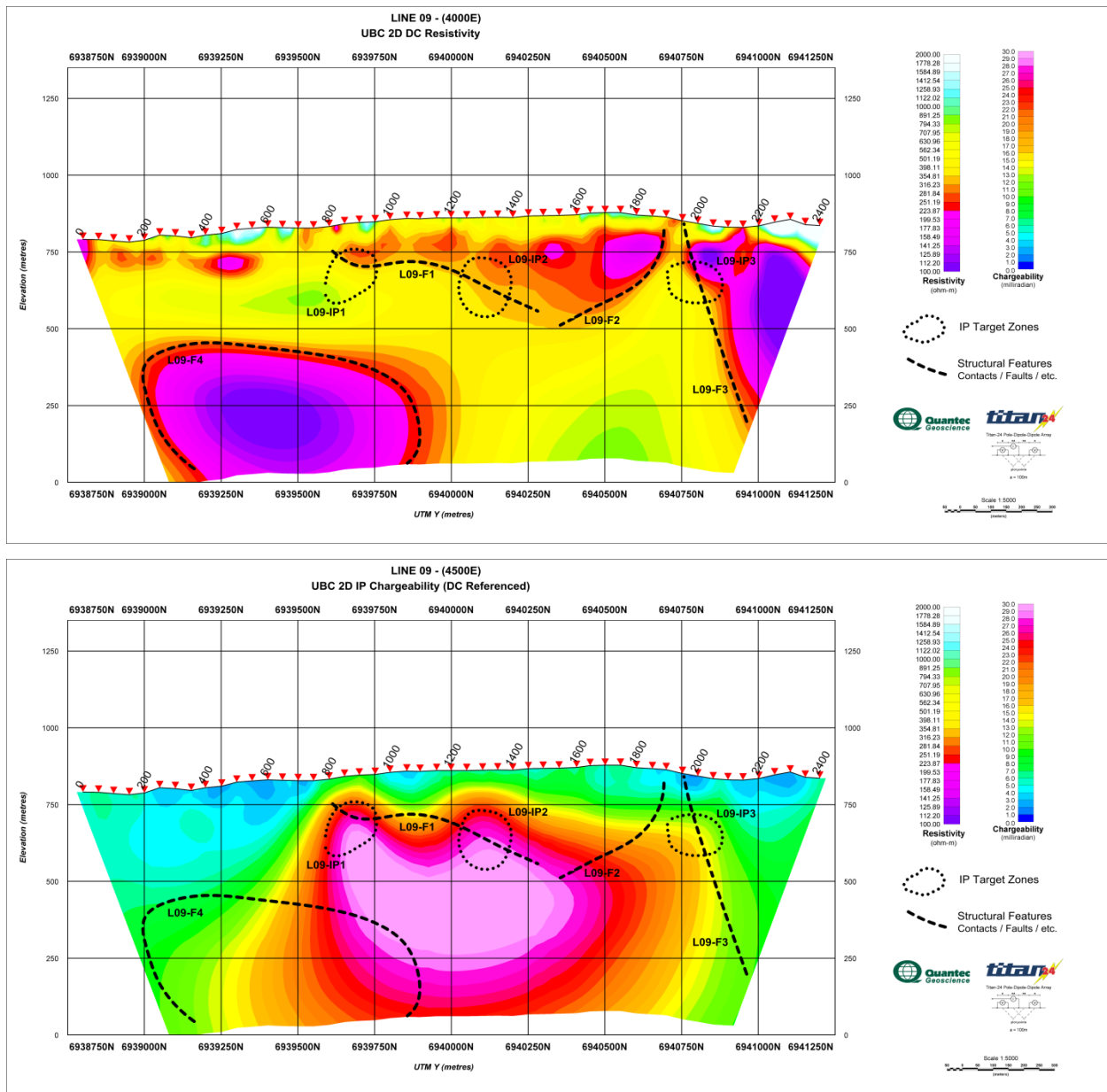


Figure 3-11: Line L09E (4000E) – DCIP results.

DC model for line L09E characterise an overall conductive behaviour. L09-F1 and L09-F2 demarcate the boundaries of conductive shallow subsurface structures, while L09-F3 mark the boundary of a conductive structure extending further deep. The model also delineates another deep seated conductive anomaly extending from station 200N to 1100N at an average depth of about 400m.

Three IP anomalies are detected in this line. L09-IP1 and L09-IP2 are associated with strong chargeability and low resistivity structures, suitable for considering as possible test targets. L09-IP1 occurs at 150m and L09-IP2 occurs at 170m beneath stations 850N and 1300N respectively. L09-IP3 occurs at a depth of 180m below station 1950N and bears a moderate IP chargeability.

3.2.1.10 Line L10E (4500E)

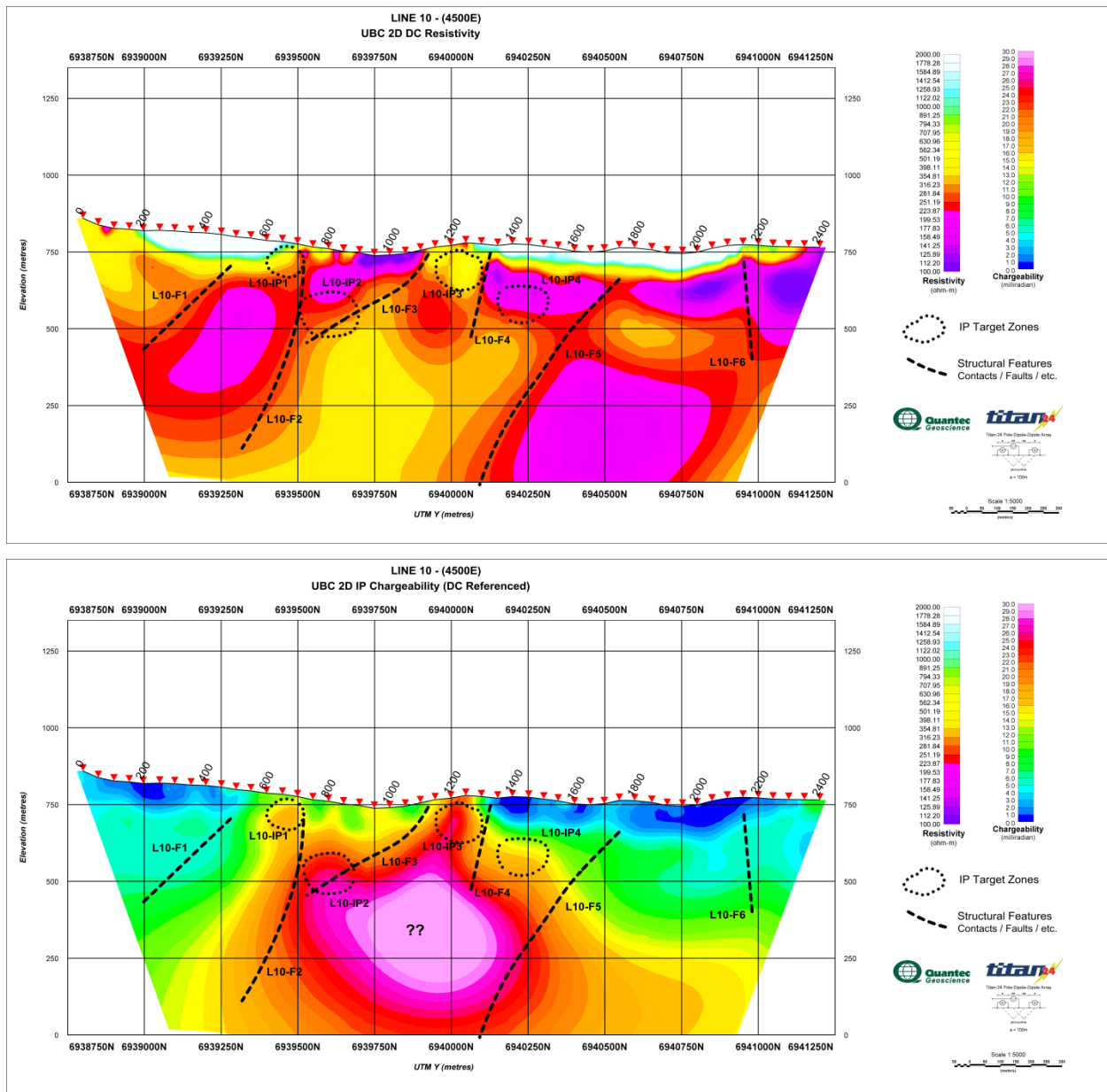


Figure 3-12: Line L10E (4500E) – DCIP results.

This line depicts a very conductive behaviour throughout the section with a thin resistive layer overlying most of the line having a maximum thickness of about 70m. Structures L10-F1 to L10-F6 are drawn to demarcate some prominent resistivity discontinuities. The low resistivity observed all along this cross-section may be controlled by the location of this line along the edge of geologic formations.

A total of four IP anomalies, L10-IP1 to L10-IP4, are noted in this line. L10-IP1 bears a moderate IP chargeability at a depth of about 50m, while L10-IP2 and L10-IP4 bear relatively strong IP chargeability at depths 220m and 170m respectively. Considering their chargeability, associated low resistivity structures and depth of occurrence, one may consider their suitability for target testing. The one strong

IP anomaly to be considered for a priority target test is L10-IP3 due to its strong chargeability and shallow occurrence at a depth of about 70m beneath station 1200N. The strong chargeability observed at the centre of the model may be due to the effects of conductive subsurface or the inversion effects of other shallow chargeabilities. On the other side, the possibility of a massive mineralization could also be tested at a depth of about 350m between stations 1000N and 1200N.

3.2.1.11 Line L11E (5000E)

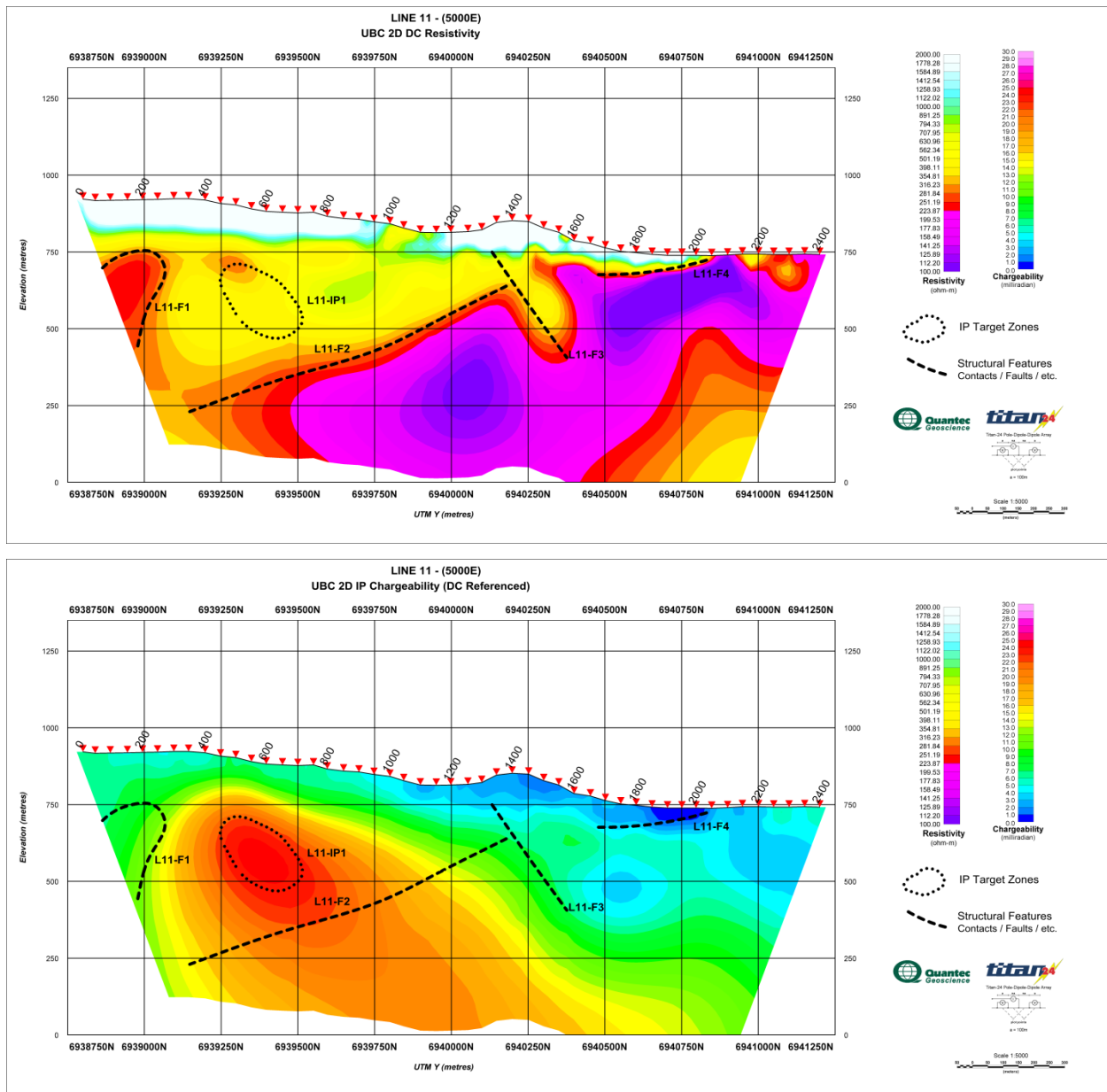


Figure 3-13: Line L11E (5000E) – DCIP results.

As seen in the previous western line L10E, all lines further east exhibit more conductive signatures in the mapped subsurface. A southward dip in the conductive structure is noticed and marked by L11-F2 and L11-F4, with an intermediate discontinuity around station 1400N marked by a contact L11-F3. L11-F1 just highlights another high conductive zone in the DC model.

One IP anomaly, L11-IP1 is detected in this line, which bears relatively high chargeability and size, at a depth of about 250m beneath station 500N. This anomaly is also well resolved in the half-space referenced chargeability model and may be a potential target for testing any viable mineralization associated with this anomaly.

3.2.1.12 Line L12E (5500E)

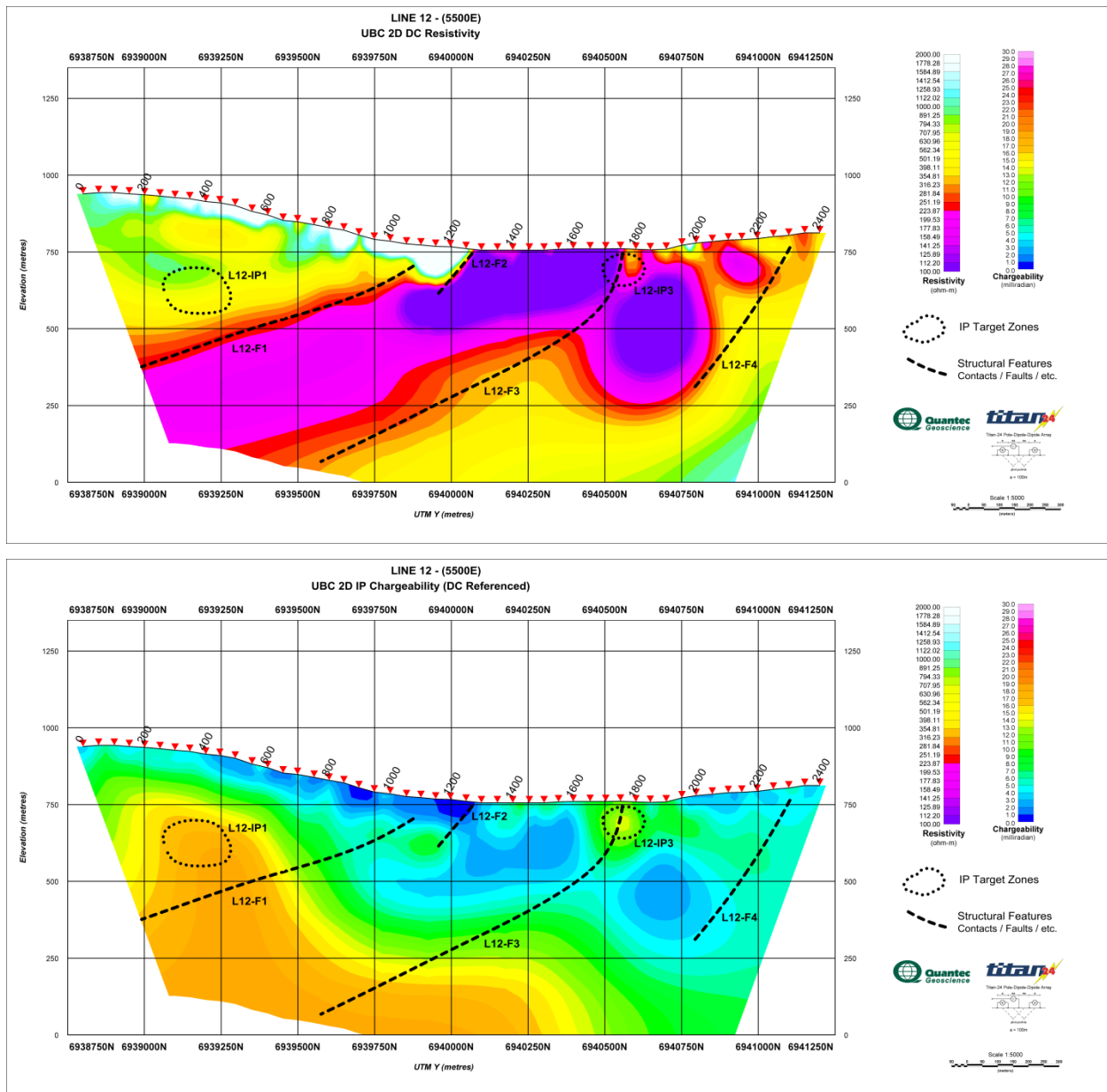


Figure 3-14: Line L12E (5500E) – DCIP results.

Line L12E also shows a southward dipping conductivity structure, which expose beyond station 1300N. Contacts, L12-F1 to L12-F4, are drawn to demarcate the conductive boundaries in the DC model and the available geology doesn't show any prominent features to directly correlate these contacts.

Two IP anomalies are picked along this line at stations 350N and 1750N with their occurrence at depths of about 270m and 75m. Though bearing very moderate chargeability, the anomaly L12-IP2 with 70m could be tested due to its shallow occurrence.

3.2.1.13 Line L13E (6000E)

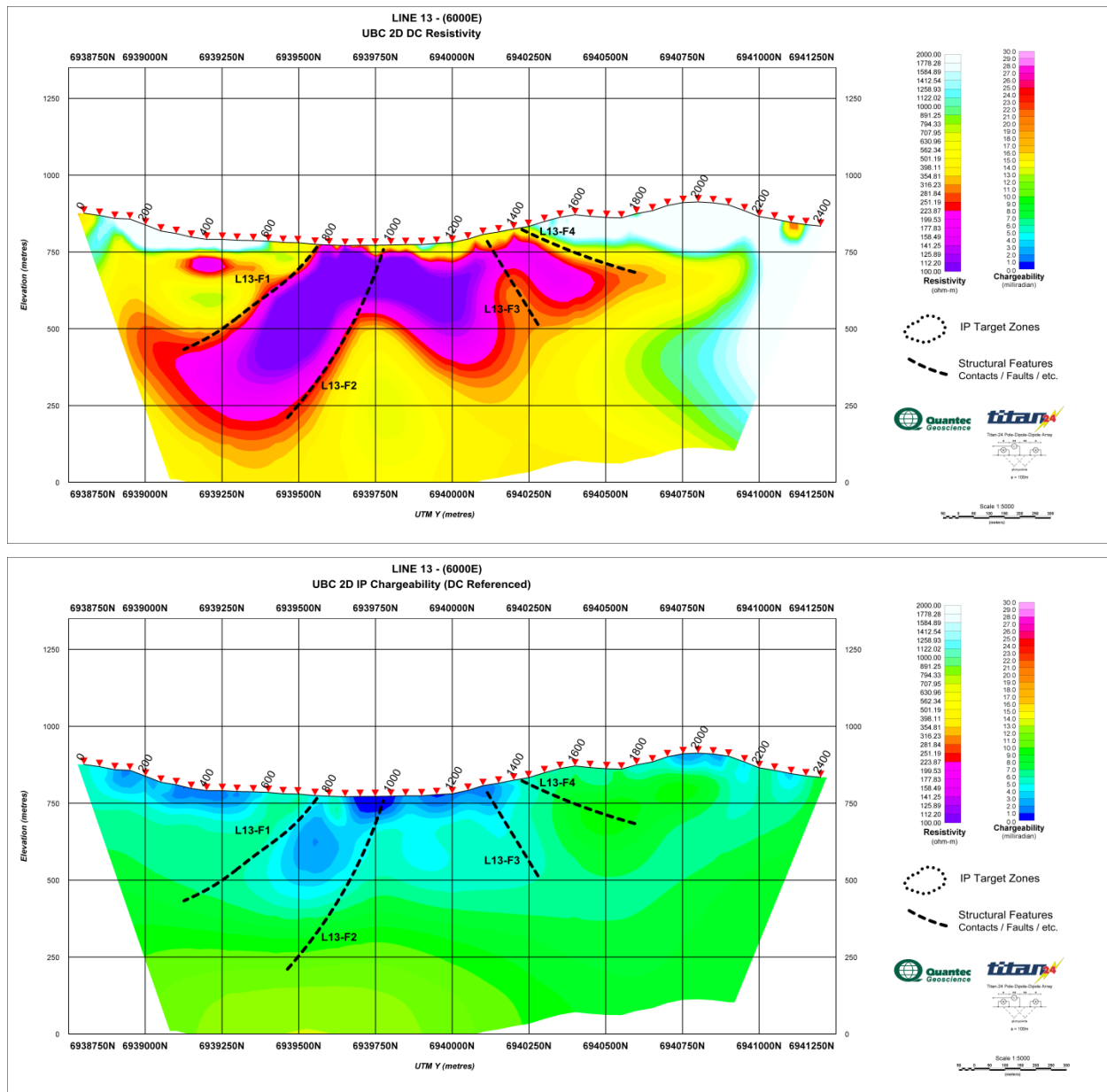


Figure 3-15: Line L13E (6000E) – DCIP results.

Line L13E depicts isolated conductive structures in the DC model. A general southward dip can be observed for this conductive structures, but not seem to extend to the deeper parts of the model beyond about 600m. Also it is possible that the thick conductive top layer impede the depth of investigation in the region.

Noticeable IP anomalies are not identified in line L13E.

3.2.1.14 Line L14E (6500E)

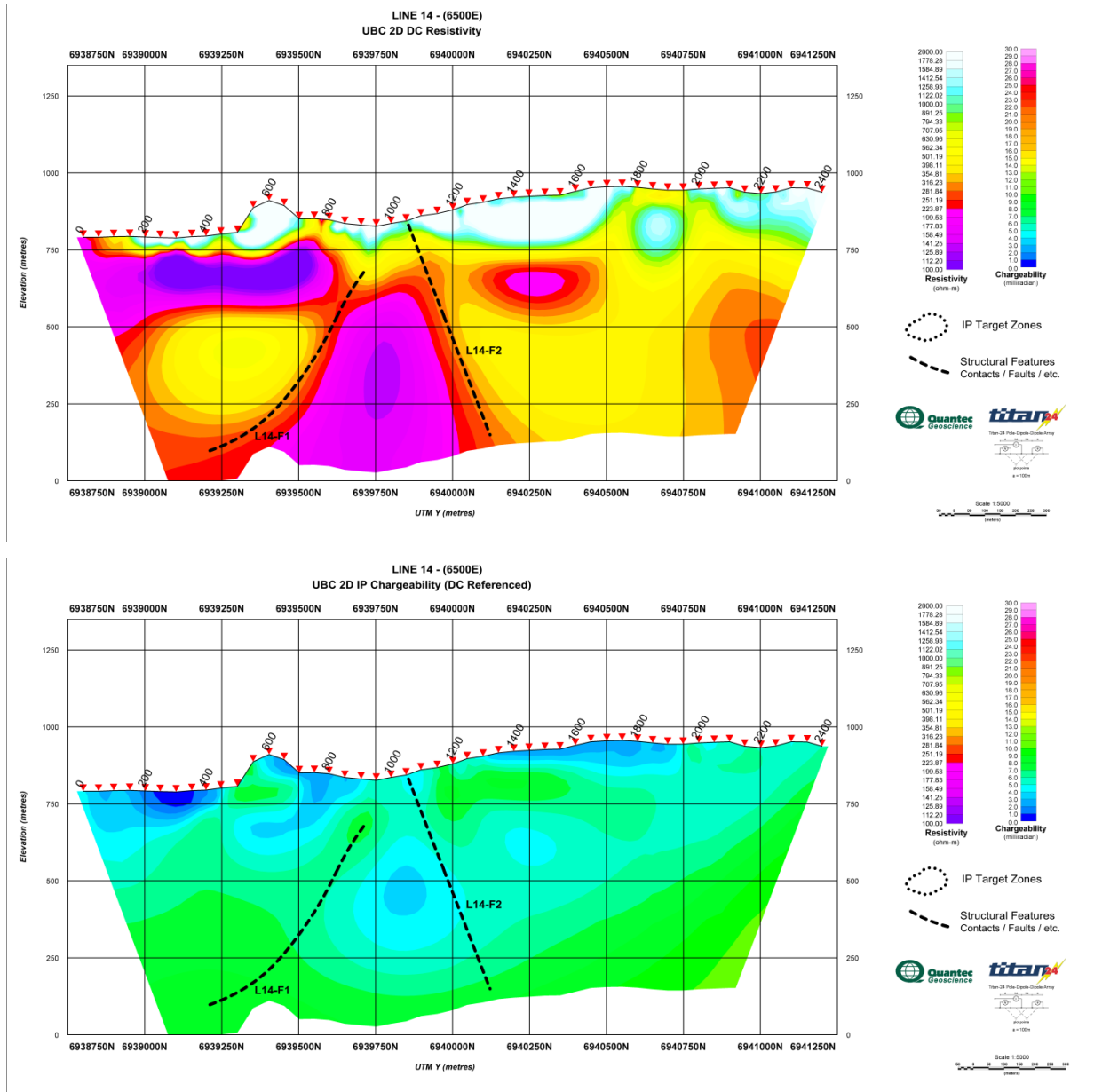


Figure 3-16: Line L14E (6500E) – DCIP results.

The DC model for the eastern most line L14E also depicts very conductive structures in the subsurface. L14-F1 and L14-F2 shows two deeper resistivity boundaries. The model also delineates a near surface layer of relatively higher resistivity extending throughout the section with a gentle northward slope.

No major chargeability is detected along this line.

3.2.2 DISCUSSION ON PLAN MAPS

The DC resistivity and IP chargeability at different depths (plan maps) are used to illustrate different zones of possible mineralization targets. Two zones with consistent chargeability at different depths are demarcated. The 'Zone A' covers southern portions of lines L01E to L04E, and 'Zone B' covers portions of lines from L06E to L12E. Figure 3-17 and Figure 3-18 depict the resistivity variation and IP chargeability at 100m, 200m and 400m depths.

The low resistivity zones are clearly delineated in the DC models. A medium resistivity ranging about 500-1000 Ohm-m is predominant in most of the lines in the west with occasional conductive zones, especially the one visible on line L01E between station 0-200N. Lines L01E to L04E depicts a discontinuity from medium to high resistivity around station 1400N. Further east, lines L05E – L08E shows somewhat layered resistivity features with relatively higher resistivity structures (2000 Ohm-m and higher) overlying medium resistivity structures. All the eastern most lines, L09E – L14E, depict a more conductive behaviour with resistivity around 100 Ohm-m or less. Lateral variation in the resistivity observed along all interpreted cross-sections help to identify different structural features within the survey area.

The prominent structural features as evidenced from available geology are Waugh Creek (Fault?), an extensional fault along West branch of Hayes Creek and the North Big Creek Fault. Though not well defined, some low resistivity and IP chargeability association could be seen with these structural features. For example, Lines L12E, L13E and L14E cut across the North Big Creek Fault and depict very low resistivity signatures. The Waugh Creek Fault diagonally cut across all lines from L01E to L10E and the extensional fault along the West branch Hayes Creek cut across line L10E between stations 500N and 1000N.

The resistivity boundaries marked on the DC resistivity cross-sections resolves the structural contacts on some lines. For example, the structural feature L01-F1 marked along line L01E at station 100N seems to correlate with the Waugh Creek Fault.

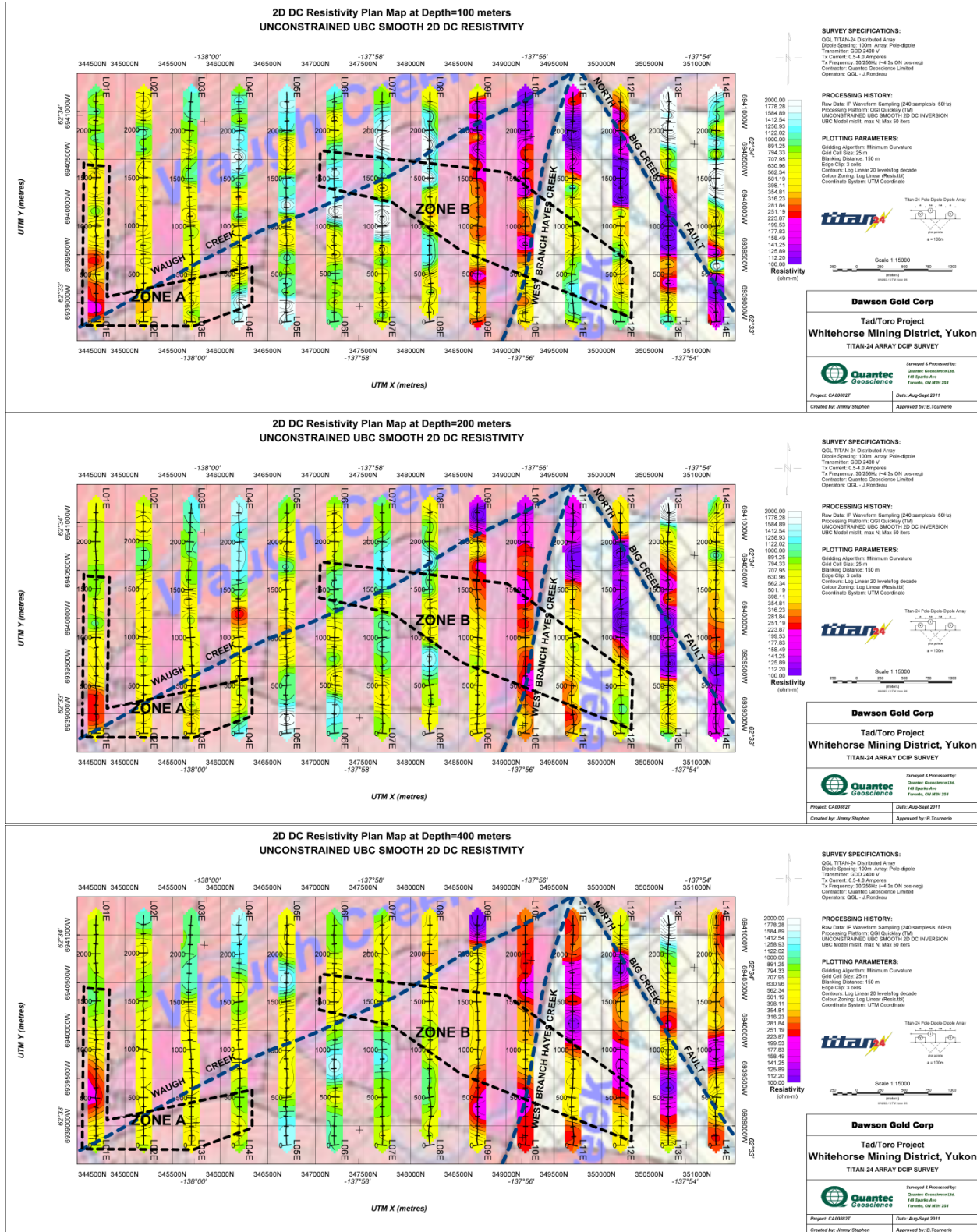


Figure 3-17: DC resistivity results at 100m (top), 200m (middle) and 400m (bottom).

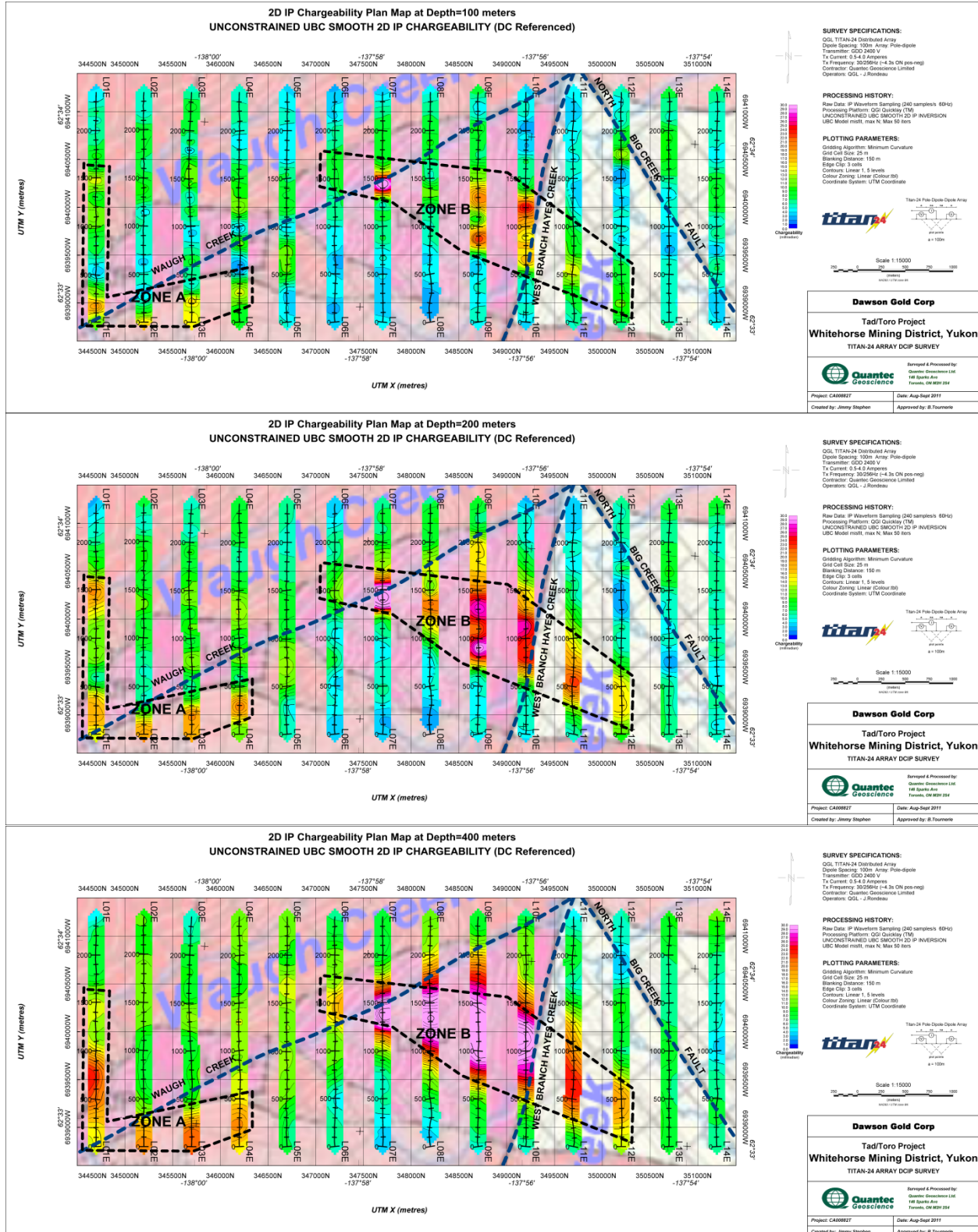


Figure 3-18: IP chargeability results at 100m (top), 200m (middle) and 400m (bottom).

Table 3-1: Summary of IP anomaly over the Tad/Toro Project.

| Line | Station | IP anomaly | Depth (m) | Priority |
|--------------|---------|------------|-----------|----------|
| L01E (0000E) | 150N | L01-IP1 | 120m | I |
| | 700N | L01-IP2 | 420m | II |
| | 1450N | L01-IP3 | 160m | I |
| L03E (1000E) | 200N | L03-IP1 | 100m | II |
| | 750N | L03-IP2 | 230m | II |
| | 1350N | L03-IP3 | 300m | II |
| | 1900N | L03-IP4 | 150m | II |
| L04E (1500E) | 300N | L04-IP1 | 200m | I |
| | 800N | L04-IP2 | 110m | II |
| | 1250N | L04-IP3 | 175m | II |
| L05E (2000E) | 700N | L05-IP1 | 150m | II |
| L06E (2500E) | 1450N | L06-IP1 | 200m | II |
| L07E (3000E) | 1450N | L07-IP1 | 100m | I |
| L08E (3500E) | 1300N | L08-IP1 | 300m | I |
| L09E (4000E) | 850N | L09-IP1 | 150m | I |
| | 1300N | L09-IP2 | 170m | I |
| | 1950N | L09-IP3 | 180m | II |
| L10E (4500E) | 650N | L10-IP1 | 50m | II |
| | 800N | L10-IP2 | 220m | II |
| | 1200N | L10-IP3 | 70m | I |
| | 1450N | L10-IP4 | 170m | II |
| L11E (5000E) | 500N | L11-IP1 | 250m | I |
| L12E (5500E) | 350N | L12-IP1 | 270m | II |
| | 1750N | L12-IP2 | 75m | II |

4 CONCLUSIONS AND RECOMMENDATIONS

This report presents the logistics and results of a Titan-24 DCIP survey undertaken on behalf of Dawson Gold Corp., British Columbia, Canada, from August 18th to September 9th, 2011, over the Tad/Toro Project in Yukon, Canada.

The survey is located approximately 100 km northwest of Carmacks, in the Whitehorse Mining District of Yukon, and includes a grid of 14 north-south lines, evenly spaced at 500m. Each Titan-24 spread was surveyed using a pole-dipole configuration with a dipole size of 100m having a final coverage of 2.4km.

The quality of the DCIP data is very good. The data were inverted using the 2D inversion algorithms to produce sections of the resistivity and chargeability distributions of the subsurface.

The analysis and interpretation of the DCIP results allow the identification of several chargeable anomalies, several of which are associated with zones of low resistivity.

A total of 24 anomalies had been identified, among which 9 anomalies (L01-IP1, L01-IP3, L04-IP1, L07-IP1, L08-IP1, L09-IP1, L09-IP2, L10-IP3 and L11-IP1) were classified as 1st priority over the survey area depending on their depth of occurrence and associated DC resistivity and IP chargeability. Anomalies L07-IP1, L08-IP1, L09-IP1, L09-IP2 and L10-IP3 seem to be covering one large zone of mineralization and depict strong IP chargeability, which seems to be extending further deep. L07-IP1 on line L07E (3000E) at station 1450N may be a preferred choice for testing this strong chargeability. Other group of 15 anomalies were classified as 2nd priority targets for drilling survey or for other geophysical survey follow up.

Quantec recommends the complete integration of the Titan-24 results with the known geology, and in particular with the drilling information available in that area to further enhance the interpretation and drill targeting. We also recommend consideration of future follow up over the property with magnetotelluric data in order to better delineate the structural control of mineralization at depth.

Respectfully Submitted, Toronto, ON, the 26/10/2011,



Benoît Tournier
Quantec Geoscience Ltd

Kevin Killin
Quantec Geoscience Ltd

Jimmy Stephen
Quantec Geoscience Ltd

Darcy McGill
Quantec Geoscience Ltd

5 STATEMENT OF QUALIFICATIONS

BENOÎT TOURNERIE

I, Benoît Tournier, declare that:

I am a Geophysicist with residence in Toronto, Ontario and am presently employed in this capacity with Quantec Geoscience Ltd., Toronto, Ontario;

I obtained a License (equivalent to B.Sc.) in 1989, a DEA (equivalent to M.Sc.) in 1991, and a Doctorate with Honours (equivalent to Ph.D.) in December 1995, in Earth Sciences, option geophysics, from the University of Rennes 1, Rennes, France;

I am a registered geophysicist, since 2008, with license to practice in the Province of Ontario (APGO member # 1609); a registered geoscientist, since 2008 with a license to practice in the Province of Quebec (OGQ #1322); a registered geoscientist, since 2009 with a license to practice in the Province British Columbia (APEG-BC #33786);

I have practiced my profession continuously since April, 1996 in North and South America, in Europe, and in Oceania;

I am a member of the Society of Exploration Geophysicists (SEG), the European Association of Geoscientist and Engineers (EAGE), and the Canadian Exploration Geophysics Society (KEGS);

I have no interest, nor do I expect to receive any interest in the properties or securities of **Dawson Gold Corp.**, its subsidiaries or its joint-venture partners;

I am the Professional Geophysicist responsible for this project and have authored this Geophysical Report.

I have reviewed the survey results and the logistics sections of the report, and can attest that these accurately and faithfully reflect the data acquired on site;

I have reviewed the final processed data, inversions and interpretation results contained in the Geophysical Report.

The statements made in this report represent my professional opinion in consideration of the information available to me at the time of writing this report.

Toronto, Ontario, the 26/10/2011



Benoît Tournier, D. Sc., P.Geo.
Quantec Geoscience Ltd.

JIMMY STEPHEN

I, Jimmy Stephen, declare that:

I am a Geophysicist with residence in Toronto, Ontario and am presently employed in this capacity with Quantec Geoscience Ltd., Toronto, Ontario;

I obtained my Bachelor of Science Degree (B.Sc.), Physics from Mahatma Gandhi University, India in 1994, a Master of Science and Technology Degree (M.Sc.Tech.), Marine Geophysics from Cochin University of Science and Technology, India in 1998, and Doctor of Philosophy (PhD), Geophysics from Swami Ramanand Teerth Marathwada University, India in 2004;

I have practiced my profession continuously since November 1998 in India, Middle East and North America.

I am a member of the Society of Exploration Geophysicists (SEG), and the American Geophysical Union (AGU);

I have no interest, nor do I expect to receive any interest in the properties or securities of **Dawson Gold Corp.**, its subsidiaries or its joint-venture partners;

I undertook the 2D DC-IP inversions and have compiled the final processed data, inversions and interpretation results and have authored this Geophysical Interpretation report.

The statements made in this report represent my professional opinion based on my consideration of the information available to me at the time of writing this report.

Toronto, Ontario, the 26/10/2011

Jimmy Stephen, PhD

Quantec Geoscience Ltd.

KEVIN KILLIN

I, Kevin J. Killin, declare that

I am a Professional Geophysicist with residence in Whitby, Ontario and am presently employed as the Vice President of Interpretation overseeing the interpretation group with Quantec Geoscience Ltd., Toronto, Ontario.

I obtained an Honours Bachelor of Science Degree (HBSc), in Geological Geophysics from the University of Western Ontario in London Ontario, in 1986, including a Geology degree and Geophysics degree.

I am a Professional Geophysicist, with license to practice in the Province of Ontario (APGO member # 0823).

I am a member of the Prospectors and Developers Association of Canada, the Canadian Exploration Geophysics Society (KEGS), and the American Geophysical Union (AGU).

I have no interest, nor do I expect to receive any interest in the properties or securities of **Dawson Gold Corp.**, its subsidiaries or its joint-venture partners;

I am the Professional Geophysicist responsible for supervising the interpretation and reporting of this project and have reviewed this Geophysical dataset. This includes reviewing the survey results, logistics, processing and inversion results contained in the interpretation report.

I can attest that these accurately and faithfully reflect the data acquired on site to the best of my knowledge.

The statements made in this report represent my professional opinion in consideration of the information available to me at the time of writing this report.

Toronto, Ontario, the 26/10/2011

Kevin Killin, H.BSc. P.Geo.

Quantec Geoscience Ltd.

DARCY MCGILL

I, Darcy McGill, declare that:

I am a Geophysicist with residence in Toronto, Ontario and am presently employed in this capacity with Quantec Geoscience Ltd., Toronto, Ontario.

I obtained a Bachelor of Science Degree (B.Sc.), Physics (Geophysics option), from the University of Toronto in Toronto, Ontario in 1995.

I am a Professional Geoscientist (Limited) since 2011 with license to practice in the Province of Ontario (APGO member # 2010).

I am a member of the Canadian Exploration Geophysical Society (KEGS).

I have practiced my profession continuously since June 1995, in North America, South America, Africa, the Middle East, South Asia, and Europe.

I have no interest, nor do I expect to receive any interest in the properties or securities of **Dawson Gold Corp.**, its subsidiaries or its joint-venture partners;

I was the data processor, responsible for the quality control of data acquired throughout the survey.

Toronto, Ontario, the 26/10/2011

Darcy McGill, B. Sc., P. Geo.(Limited)

Quantec Geoscience Ltd.

6 DIGITAL ARCHIVE

The CD or DVD attached to this report contains a copy of all the inversion results, final processed data, including the survey files, the daily processing (and field) notes, and an electronic copy of this report (with all appendices).

General Description of the CD/DVD Structure

| Folder | Sub level 1 | Sub level 2 | Description |
|--------------------------|----------------|-------------|--|
| Contract and Client Info | | | Contract, technical reports, images, and other documents |
| Fields Results | | | Final field results CSV, survey Files, and Processing Notes |
| Presentation of Results | | | Power Points, PDF, and documents presented or emailed to client |
| Geosoft | Base Maps | | Geosoft Files Base maps, location, etc |
| | Interpretation | | Interpretation |
| | Plan Maps | | Plan Maps |
| | Sections | | 2D sections |
| invDCIP | Line ## | data | DC IP inversion raw data and error conditioning |
| | | smDC | DC inversion |
| | | smIP_dceref | IP with DC reference |
| | | smIP_hsref | IP with Half-space reference |

A PRODUCTION SUMMARY

| DATE | FIELD ACTIVITIES AND OBSERVATIONS | LINE SPREAD | LINE START | LINE END | TX START | TX END | Read IP (km) | COMPLETED SPREAD |
|-----------|--|----------------|---------------|-------------|-------------|-----------|-----------------|---------------------|
| 18-Aug-11 | Mob to camp | | | | | | | |
| 19-Aug-11 | Slung gear to grid. | | | | | | | |
| 20-Aug-11 | Infinite and array setup. | | | | | | | |
| 21-Aug-11 | Finish setup of array and infinite. | L01E | 0 | 2400 | 50 | 2350 | | |
| 22-Aug-11 | Survey IP L1E and pickup line. | L01E | 0 | 2400 | 50 | 2350 | 2.4 | 1 |
| 23-Aug-11 | Chopper problems resulted in most of the day needed to sling gear. Read some IP. | L02E | 0 | 2400 | 50 | 2350 | 0.5 | |
| 24-Aug-11 | Finish L2E Setup L3E and start acquisition. | L02E L03E | 0 | 2400 | 50 | 2350 | 1.9 0.2 | 1 |
| 25-Aug-11 | Finish L3E Setup L4E. | L03E L04E | 0 | 2400 | 50 | 2350 | 2.2 | 1 |
| 26-Aug-11 | Noon start due to chopper problems. Read L4E. | L04E | 0 | 2400 | 50 | 2350 | 2.4 | 1 |
| 27-Aug-11 | Setup and read L5E. | L05E | 0 | 2400 | 50 | 2350 | 2.4 | 1 |
| 28-Aug-11 | Setup L6E, no chopper support due to lack of helipads on this line. Survey L6E. | L06E | 0 | 2400 | 50 | 2350 | 2.4 | 1 |
| 29-Aug-11 | Setup and read L7E. | L07E | 0 | 2400 | 50 | 2350 | 2.4 | 1 |
| 30-Aug-11 | Setup L8E. Difficult line, no readings. | L08E | 0 | 2400 | 50 | 2350 | | |
| 31-Aug-11 | Array and infinite problems delay. Read L8E and moved to L9E | L08E | 100 | 2400 | 150 | 2350 | 2.3 | 1 |

QUANTEC GEOSCIENCE LTD

| DATE | FIELD ACTIVITIES AND OBSERVATIONS | LINE SPREAD | LINE START | LINE END | TX START | TX END | Read IP (km) | COMPLETED SPREAD |
|----------|--|----------------|---------------|-------------|-------------|-----------|-----------------|---------------------|
| 1-Sep-11 | Read L9E | L09E | 0 | 2400 | 50 | 2350 | 2.4 | 1 |
| 2-Sep-11 | River crossings and moose breaking infinite delayed setup L10E. Started acquisition. | L10E | 0 | 2400 | 50 | 2350 | 0.5 | |
| 3-Sep-11 | Injury resulted in chopper support. Doghouse move slow. Finish L10E. | L10E | 0 | 2400 | 50 | 2350 | 1.9 | 1 |
| 4-Sep-11 | Finish setup and read L11E. | L11E | 0 | 2400 | 50 | 2350 | 2.4 | 1 |
| 5-Sep-11 | Setup and read L12E. | L12E | 0 | 2400 | 50 | 2350 | 2.4 | 1 |
| 6-Sep-11 | Setup L13E. Infinite was broken. Started acquisition. | L13E | 0 | 2400 | 50 | 2350 | 0.4 | |
| 7-Sep-11 | Finish L13E. Setup and read L14E. | L13E | 0 | 2400 | 50 | 2350 | 2.0 | 1 |
| | | L14E | 0 | 2400 | 50 | 2350 | 2.4 | 1 |
| 8-Sep-11 | Mob out of camp | | | | | | | |
| Total | | | | | | | 33.5 | 14 |

B SURVEY LOGISTICS**B.1 ACCESS**

Base of Operation: Whitehorse Mining District

Mode of Access to Grid: Helicopter, motorcycle

Mode of Access to Lines: By foot

B.2 SURVEY GRID AREA

Established by: Dawson Gold Corp.

Coordinate Reference System: Grid referenced to UTM Coordinates

Datum & Projection: NAD83/ Zones 7N & 8N

Grid Azimuth: 0° True

Magnetic Declination: 22° East

Station Interval: 100 m

Method of Chaining: Metric, slope distance, pickets GPS surveyed

Surveyed Line-start and -end point coordinates.

| Line | Grid Coordinate | | UTM Coordinate Start | | UTM Coordinate End | |
|------|-----------------|-------|----------------------|-----------|--------------------|-----------|
| | Start | End | Easting | Northing | Easting | Northing |
| 1E | 0N | 2400N | 344,700 | 6,938,800 | 344,700 | 6,941,200 |
| 2E | 0N | 2400N | 345,200 | 6,938,800 | 345,200 | 6,941,200 |
| 3E | 0N | 2400N | 345,700 | 6,938,800 | 345,700 | 6,941,200 |
| 4E | 0N | 2400N | 346,200 | 6,938,800 | 346,200 | 6,941,200 |
| 5E | 0N | 2400N | 346,700 | 6,938,800 | 346,700 | 6,941,200 |
| 6E | 0N | 2400N | 347,200 | 6,938,800 | 347,200 | 6,941,200 |
| 7E | 0N | 2400N | 347,700 | 6,938,800 | 347,700 | 6,941,200 |
| 8E | 0N | 2400N | 348,200 | 6,938,800 | 348,200 | 6,941,200 |
| 9E | 0N | 2400N | 348,700 | 6,938,800 | 348,700 | 6,941,200 |
| 10E | 0N | 2400N | 349,200 | 6,938,800 | 349,200 | 6,941,200 |
| 11E | 0N | 2400N | 349,700 | 6,938,800 | 349,700 | 6,941,200 |
| 12E | 0N | 2400N | 350,200 | 6,938,800 | 350,200 | 6,941,200 |
| 13E | 0N | 2400N | 350,700 | 6,938,800 | 350,700 | 6,941,200 |
| 14E | 0N | 2400N | 351,200 | 6,938,800 | 351,200 | 6,941,200 |

B.3 PRODUCTION AND COVERAGE

| | |
|----------------------------------|---|
| Survey Period/days: | August 18 th – September 8 th , 2011 22 days |
| Survey Days (read time): | 16 days |
| Mob/Demob: | 2 days |
| Safety Inductions: | 0 days |
| Weather/Down Days: | 0 days |
| Number of Lines surveyed: | 14 |
| DCIP Survey Coverage: | 33.5 km |

Max and Min Pole (Tx) and Potential (P1-P2) Electrode Position.

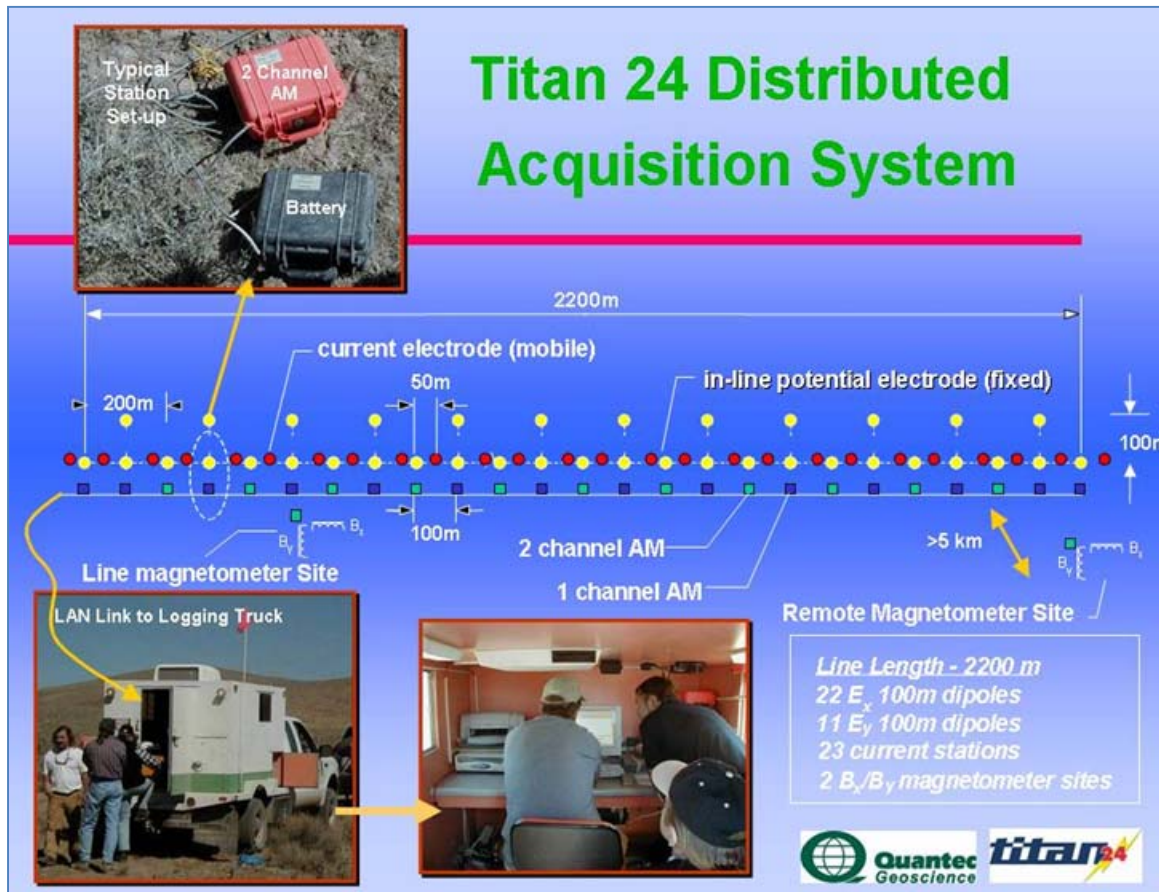
| Line | Setup | Min P1 | Max P2 | Min Tx | Max Tx | Coverage (km) |
|--------------|-------|--------|--------|--------|--------|---------------|
| 1E | | 0 | 2400 | 50 | 2350 | 2.4 |
| 2E | | 0 | 2400 | 50 | 2350 | 2.4 |
| 3E | | 0 | 2400 | 50 | 2350 | 2.4 |
| 4E | | 0 | 2400 | 50 | 2350 | 2.4 |
| 5E | | 0 | 2400 | 50 | 2350 | 2.4 |
| 6E | | 0 | 2400 | 50 | 2350 | 2.4 |
| 7E | | 0 | 2400 | 50 | 2350 | 2.4 |
| 8E | | 0 | 2400 | 50 | 2350 | 2.3 |
| 9E | | 0 | 2400 | 50 | 2350 | 2.4 |
| 10E | | 0 | 2400 | 50 | 2350 | 2.4 |
| 11E | | 0 | 2400 | 50 | 2350 | 2.4 |
| 12E | | 0 | 2400 | 50 | 2350 | 2.4 |
| 13E | | 0 | 2400 | 50 | 2350 | 2.4 |
| 14E | | 0 | 2400 | 50 | 2350 | 2.4 |
| TOTAL | | | | | | 33.5 |

B.4 PERSONNEL

| | |
|------------------------------------|---|
| Project Manager: | Jesse Rondeau |
| Responsible Geophysicist: | Benoit Tournier |
| Data Processing (in field): | Darcy McGill |
| Crew Chief: | Jesse Rondeau |
| IP operator: | Jesse Rondeau/ Patrick Ayukawa |
| Field Technicians: | Dale Hannan Allen Boissoneau Jake Shortt Eric Hotvedt Francis Namox |

B.5 INSTRUMENTATION

| | |
|-------------------------------------|--|
| Receiver System: | Quantec Distributed Array Acquisition System: - 48 channels max. per system (55ch operationally with internal A/D conversion (24bit @120db / dual speed @120-48kHz), and buffer memory (6Mb). 24 x 2-channel Acquisition Modules (AMs) AM data transmission using LAN cabling - 1 Central Recording Units (CRU; 140 Gb data storage) at base |
| Transmitter (DCIP Surveys): | GDD (5kW) with frequency/waveform control, using CRU and Current Monitor (CM) |
| Power Supply (DCIP Surveys): | Honda 6500W generator |
| Transmit Electrodes | 4 x 1.2cm diameter 1 meter long stainless steel rods |
| Receiver Electrodes: | Ground contacts using stainless steel rods |

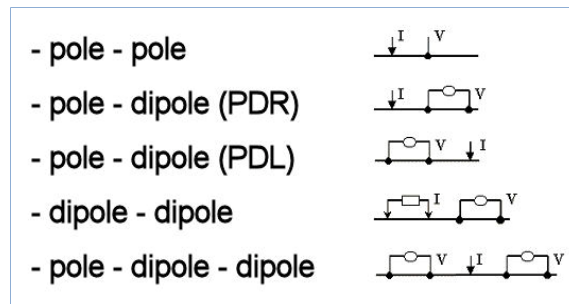


Titan-24 DCIP and MT Schematic Survey Layout.

B.6 DCIP SURVEY SPECIFICATION

B.6.1 GEOMETRY

| | |
|--------------------------------|---|
| Survey Array: | Dipole-Pole-Dipole Array |
| Receiver Configuration: | 23-24 Ex = Continuous In-line voltages, 12-13 Ey = Alternating (2-stations) cross-line voltages ⁶ . |
| Array Length: | 2.4 km |
| Number of Arrays/line: | 1 |
| Dipole length: | Ex = 100 metres |
| Sampling Interval: | Ex = 100 metres |
| Rx-Tx Separation: | N-spacing (Pn-Cn min) ⁷ = 0.5 to 22.5 |
| Infinite Pole Location: | Grid Coordinates: 3357E, 5877N UTM: 347057m E, 6944677m N (NAD83 Zone 8N) |



Common DCIP Survey Layouts.

B.6.2 ACQUISITION & PROCESSING

| | |
|--|--|
| Spectral Domain: | Tx = Frequency-domain square-wave current Rx = Full waveform time-series acquisition Data processing/output in frequency-domain. |
| Spectral Chargeability Model⁸: | Halverson-Wait |
| Transmitter Waveform: | 30/256 Hz square waves at 100% duty cycle (~4sec Pos./Neg.) |
| Transmitter Output Current: | min ~0.66 Amperes to max ~3.73 Amperes |
| Receiver Sampling Speed: | 240 samples/second (24 bit A/D @ 120 db dynamic range) |

⁶ Note: Cross-Line (Ey) voltages obtained for future reference purposes – not presented in cross-sectional plots.

⁷ Current electrodes at midpoints between potential electrodes.

⁸ The Halverson-Wait model chargeability (Halverson et al., 1981) is similar to and improves upon the frequency-domain Cole-Cole model (Pelton et al., 1978) described in the time-domain by Johnson (1984).

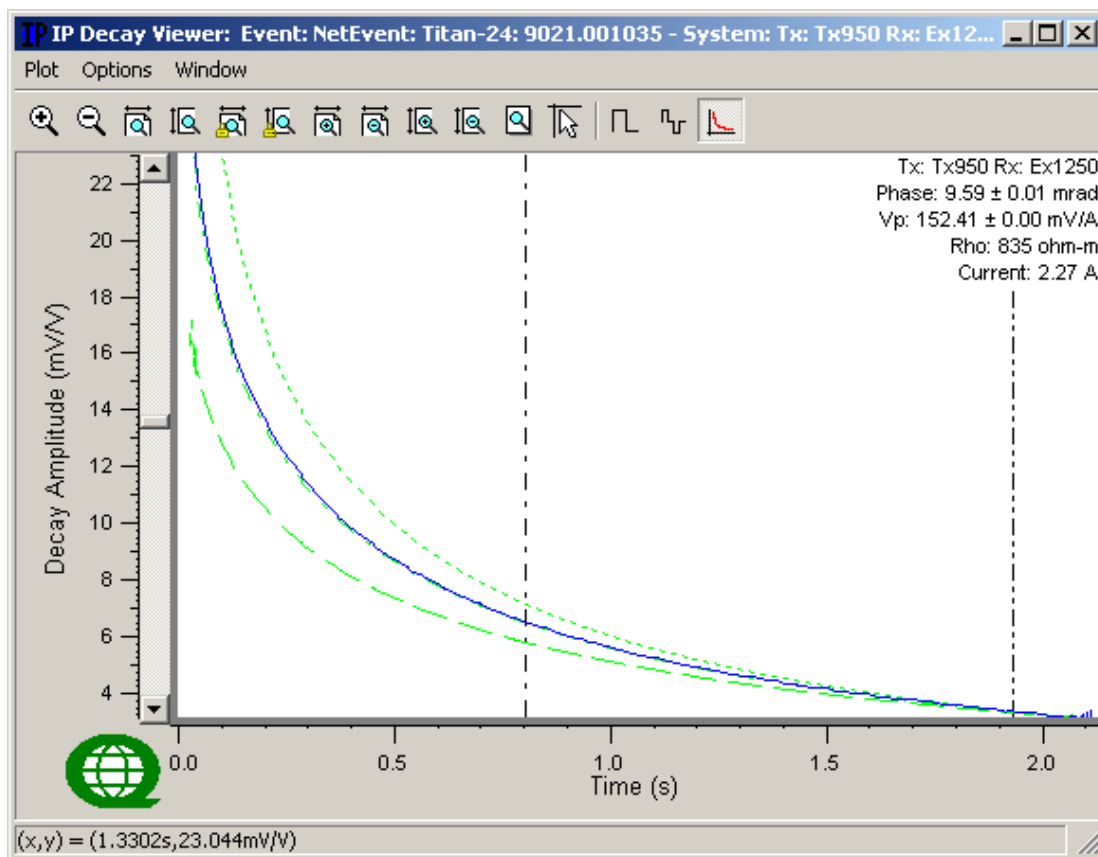
Tx-Rx Synchronization: using current monitor (10 μ sec time-accuracy)
Time-Series Stacking: 20 cycles (full-waveform)
Read Time: approx 3.0 minutes per event
Time-Domain Decay Window:

Integration Start Time: $T_0 = 0.8$ seconds

Integration End Time: $T_F = 1.9$ seconds

Post-Processing: using Quantec proprietary QuickLay v.2.30.14

- 1) Time-series stacking
- 2) Robust statistics
- 3) Current waveform deconvolution
- 4) Digital filtering (60Hz + harmonics)
- 5) Spectral model decay-curve fitting



Spectral Chargeability Model and Calculated Halverson-Wait Decays⁹

⁹ Halverson-Wait (HW) model parameters calculated in frequency domain, with hatched green lines corresponding to theoretical HW decay with spectral r-factors of 0.1, 1.0 (default) & 10, k-factor of 0.2 (default).

B.6.3 DATA PRESENTATION**Accuracy and Repeatability**

Measured Data average error (from CSV files)
using Halverson-Wait model calculation:
Voltage Errors 0.0000175mV/V (average)
Phase Errors 96.6% less than 1.0 mrad

Pseudo-Section Plots:

In-line¹⁰ DC Resistivity and IP Chargeability
pseudo sections, posted, contoured (equal area zoning)
and plotted in ground units using QuickLay viewer.

Raw Data (digital):

(external Hard Drive)
Raw Event Log File Folders (eg. Eventxxxx.dat).
Also contains AU.txt and Event.log files which contain
information on the location and time of the event in
QuickLay digital format
(Raw data output to Matlab format upon request).

Processed Data (digital):

DC/IP Data in ASCII CSV (comma delimited) file format
from QuickLay, containing final processed voltage and
phase data.

CSV File Format:

| | |
|--------------|--|
| Line 1: | Column headings |
| Column 1 | Event name/number (e.g., Eventxxxx) |
| Column 2: | Transmitter site ID (e.g., Tx150) |
| Column 3: | Receiver site ID (e.g., Rx150) |
| Column 4-11: | C1-C2/P1-P2 positions in X and Y (m) |
| Column 12: | Current (Amperes) |
| Column 13: | Current error (Amperes) |
| Column 14: | Normalized voltage (Volts/Ampere) |
| Column 15: | Voltage error (Volts/Ampere) |
| Column 16: | Phase (milliradians) |
| Column 17: | Phase error (milliradians) |
| Column 18: | Apparent resistivity (Ohm-m) ¹¹ |

B.6.4 DATA QA/QC COMMENTS

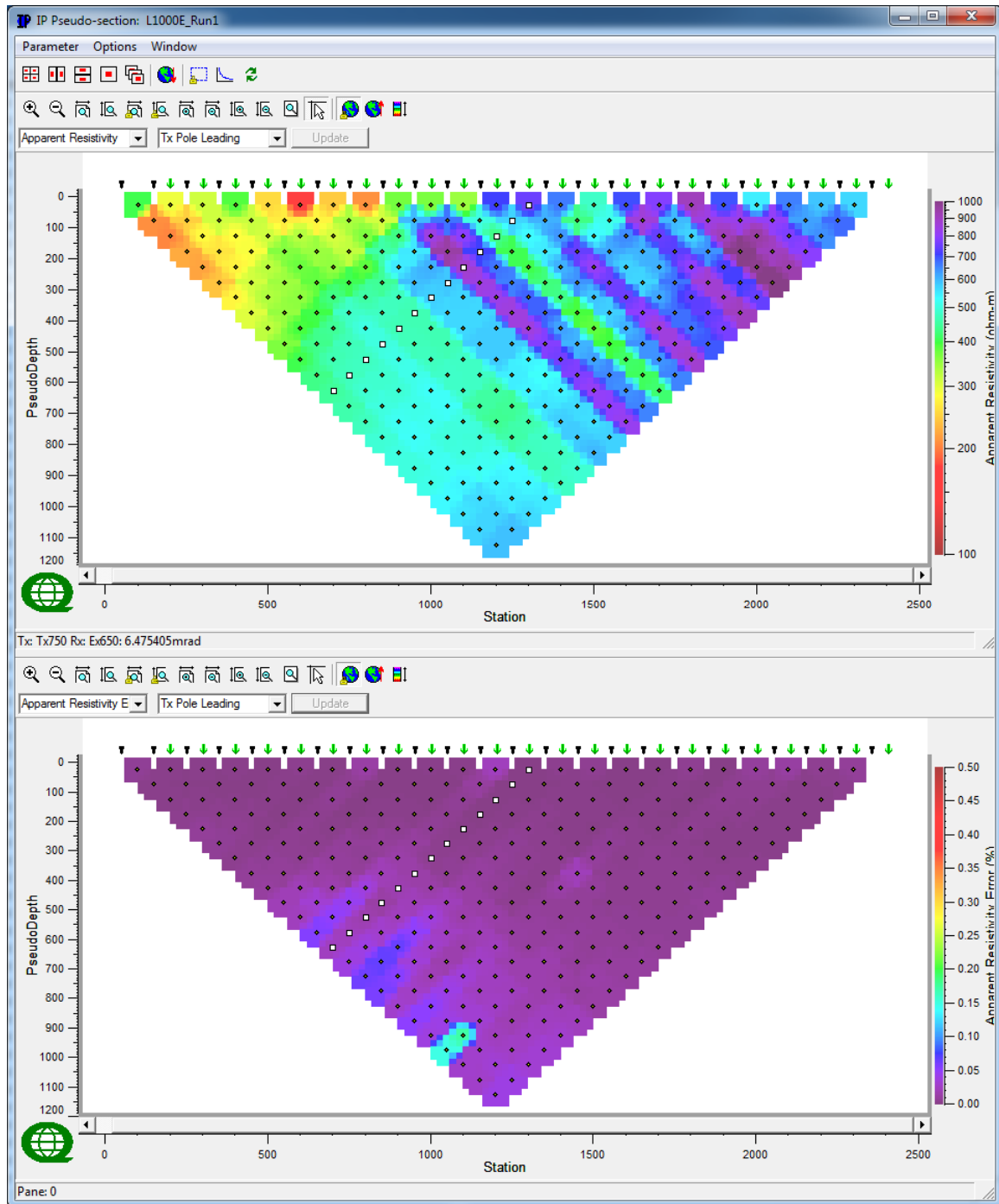
Pseudo sections for all the lines generally look good with minimal errors observed.

¹⁰ Cross-line (Ey) values not shown for presentation purposes.

¹¹ Apparent resistivity's are calculated in 2D space using the 4 electrodes general array configuration (as per XY electrode positioning in columns 4-11 of CSV file) – not based on pole-dipole calculations (K. Nurse, QGL, pers. comm., 07-2004).

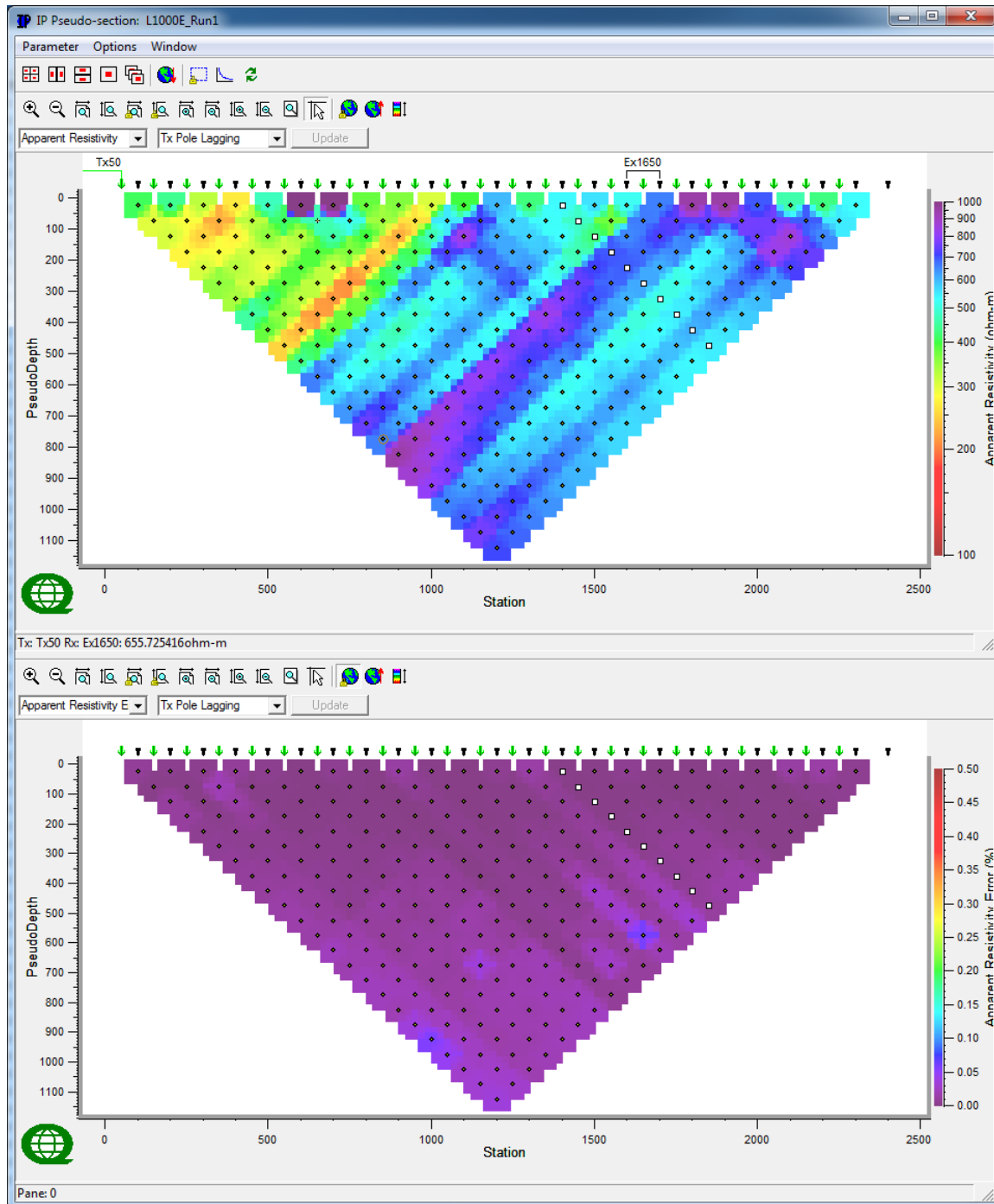
C DC – IP PSEUDO-SECTIONS OF FINAL PROCESSED DATA

C.1 LINE 1E



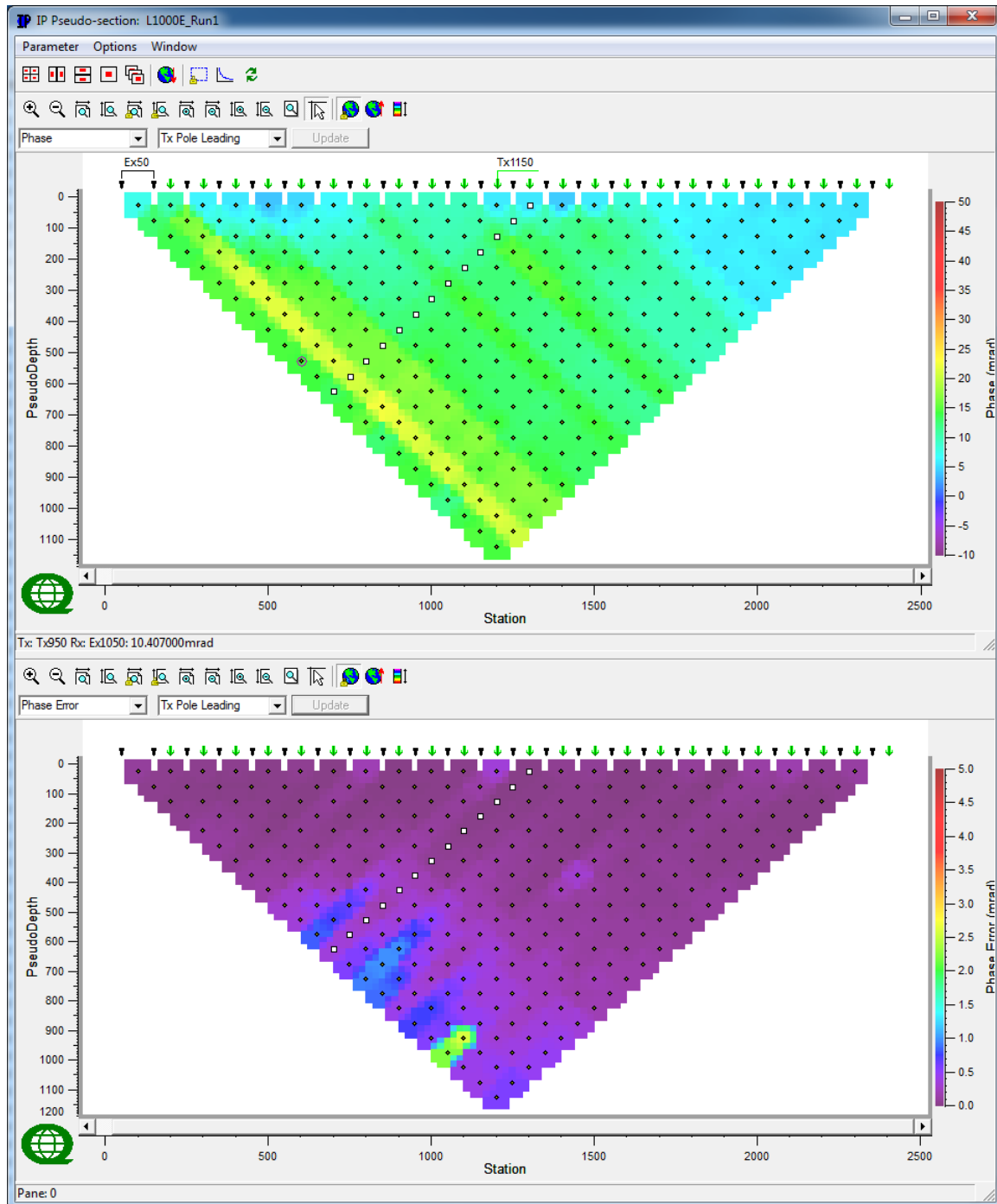
Line 1E – Observed Apparent Resistivity Raw Data (Ohm.m) & Voltage Errors (%) -Tx Pole Leading.

□ Tx with more than one event



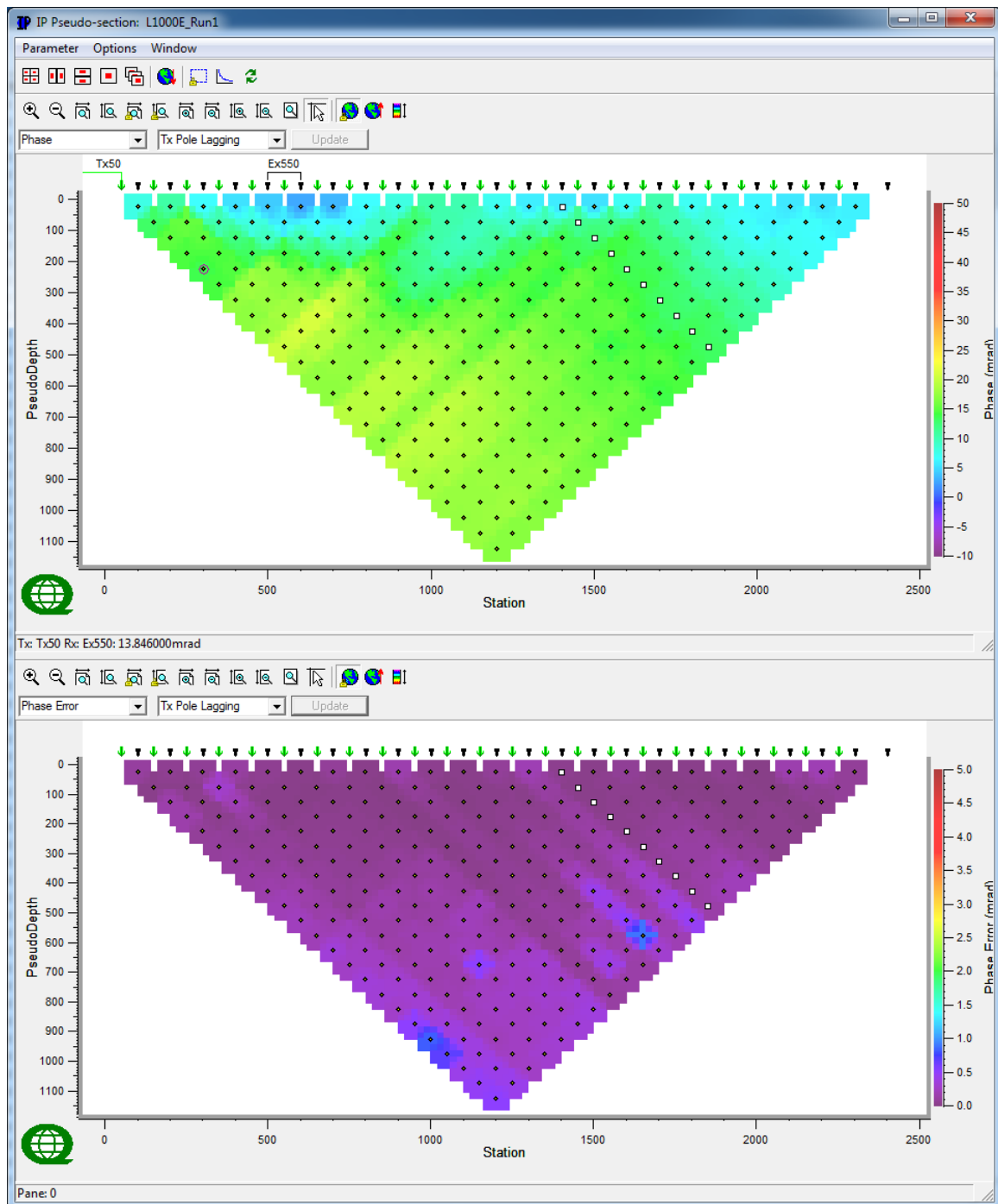
Line 1E – Observed Apparent Resistivity Raw Data (Ohm.m) & Voltage Errors (%) -Tx Pole Lagging.

□ Tx with more than one event



Line 1E – Observed IP Raw Data (mrad) & IP Errors (mrads)-Tx Pole Leading.

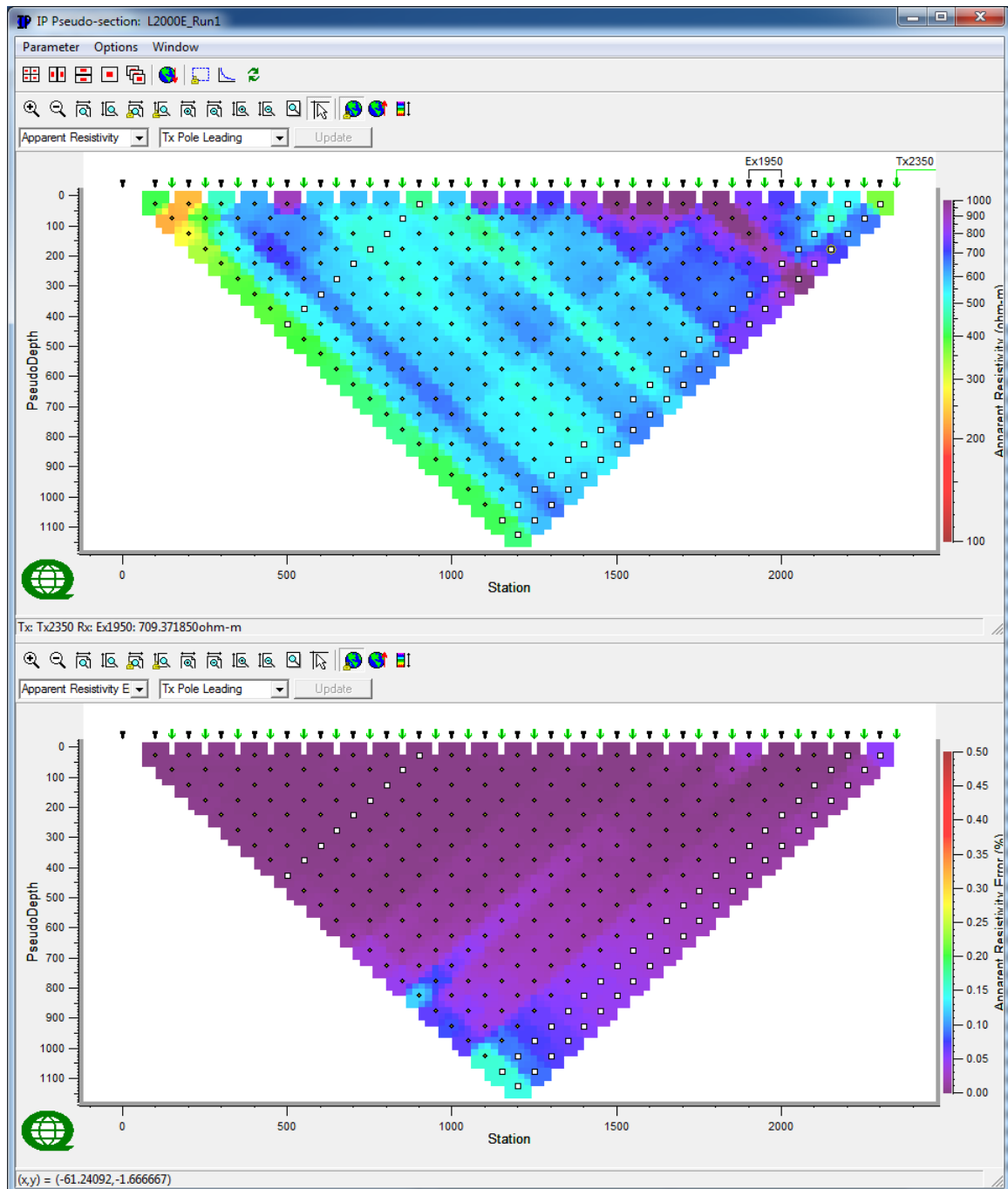
□ Tx with more than one event



Line 1E – Observed IP Raw Data (mrad) & IP Errors (mrads)-Tx Pole Lagging.

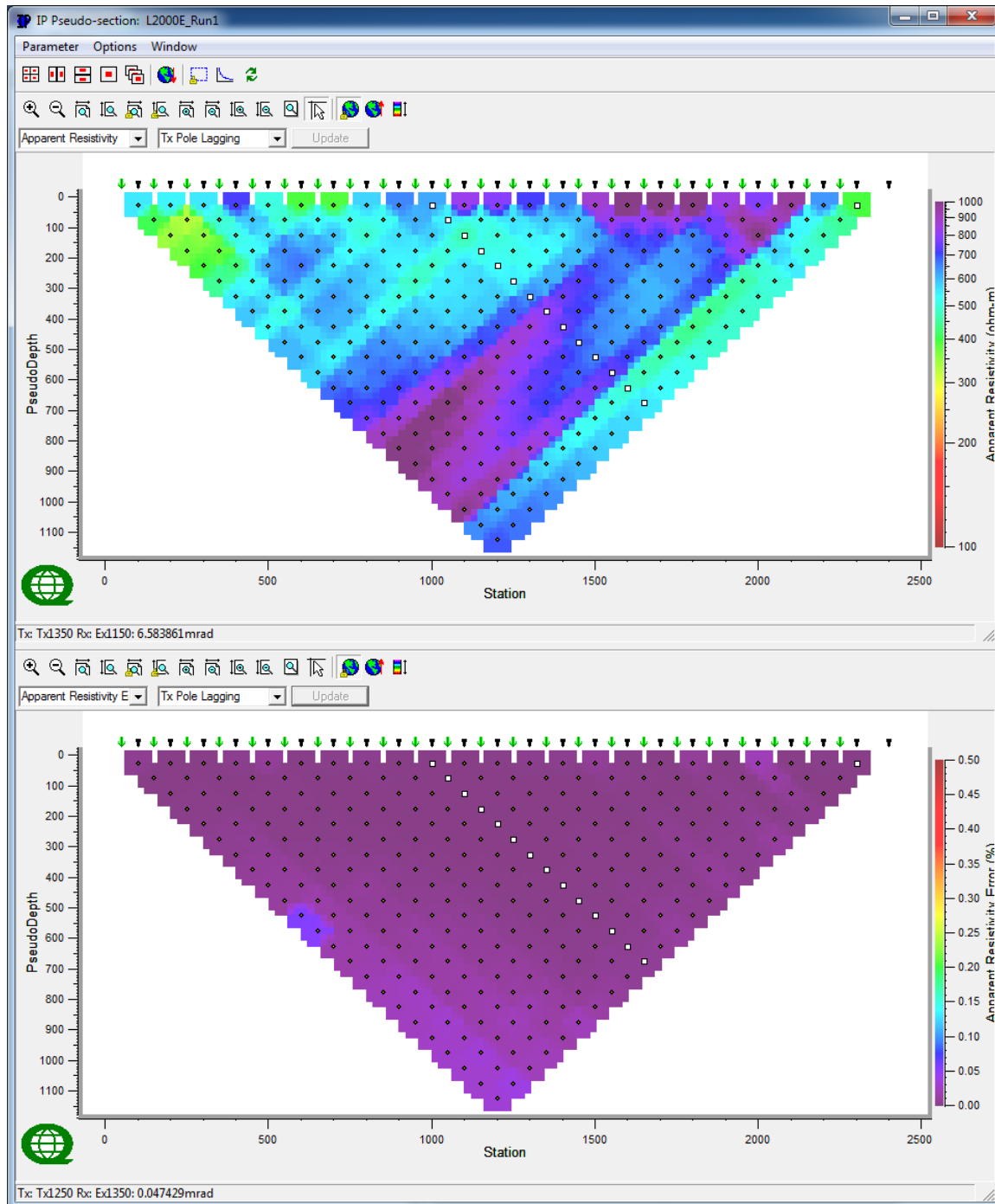
□ Tx with more than one event

C.2 LINE 2E



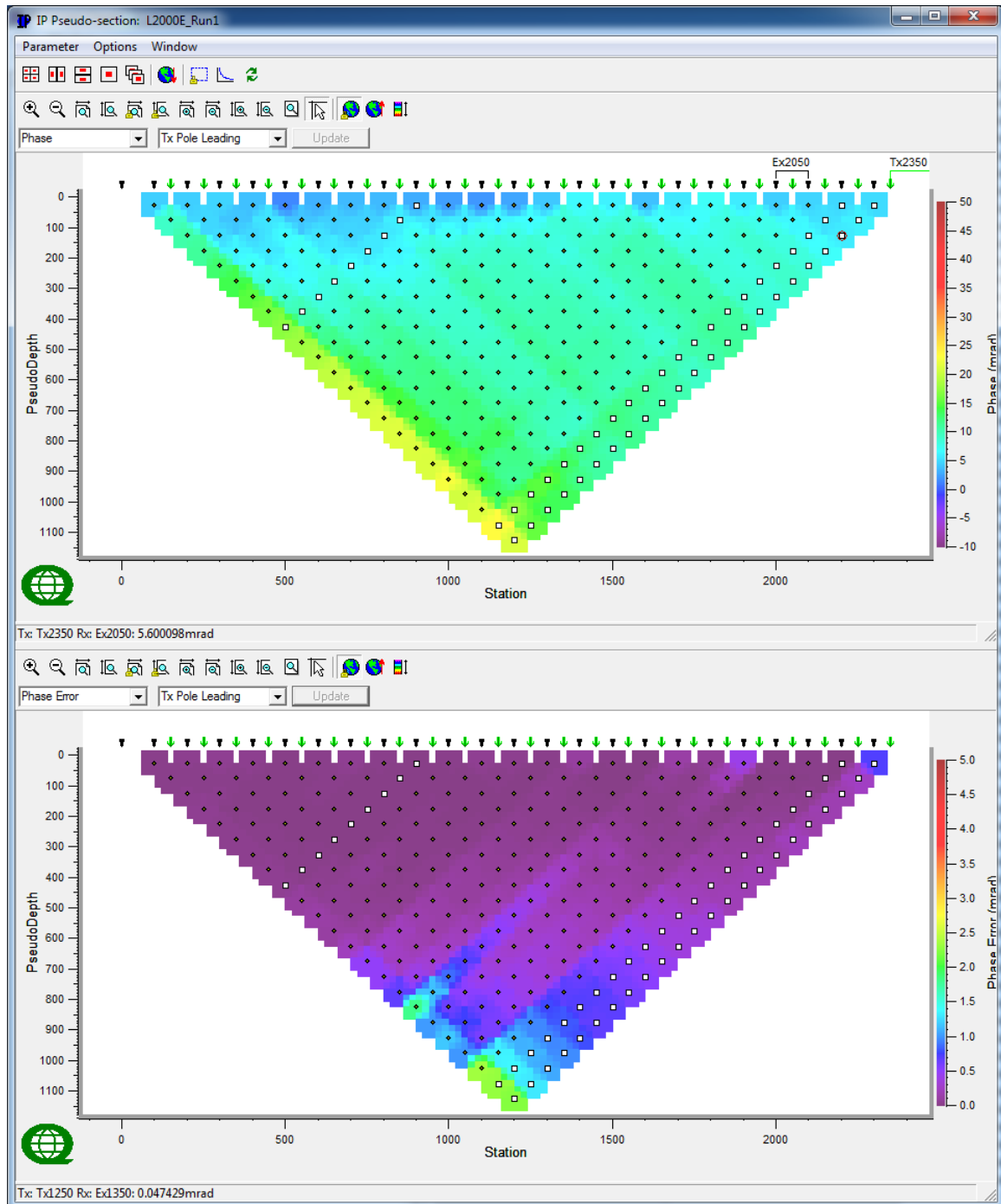
Line 2E – Observed Apparent Resistivity Raw Data (Ohm.m) & Voltage Errors (%) -Tx Pole Leading.

□ Tx with more than one event



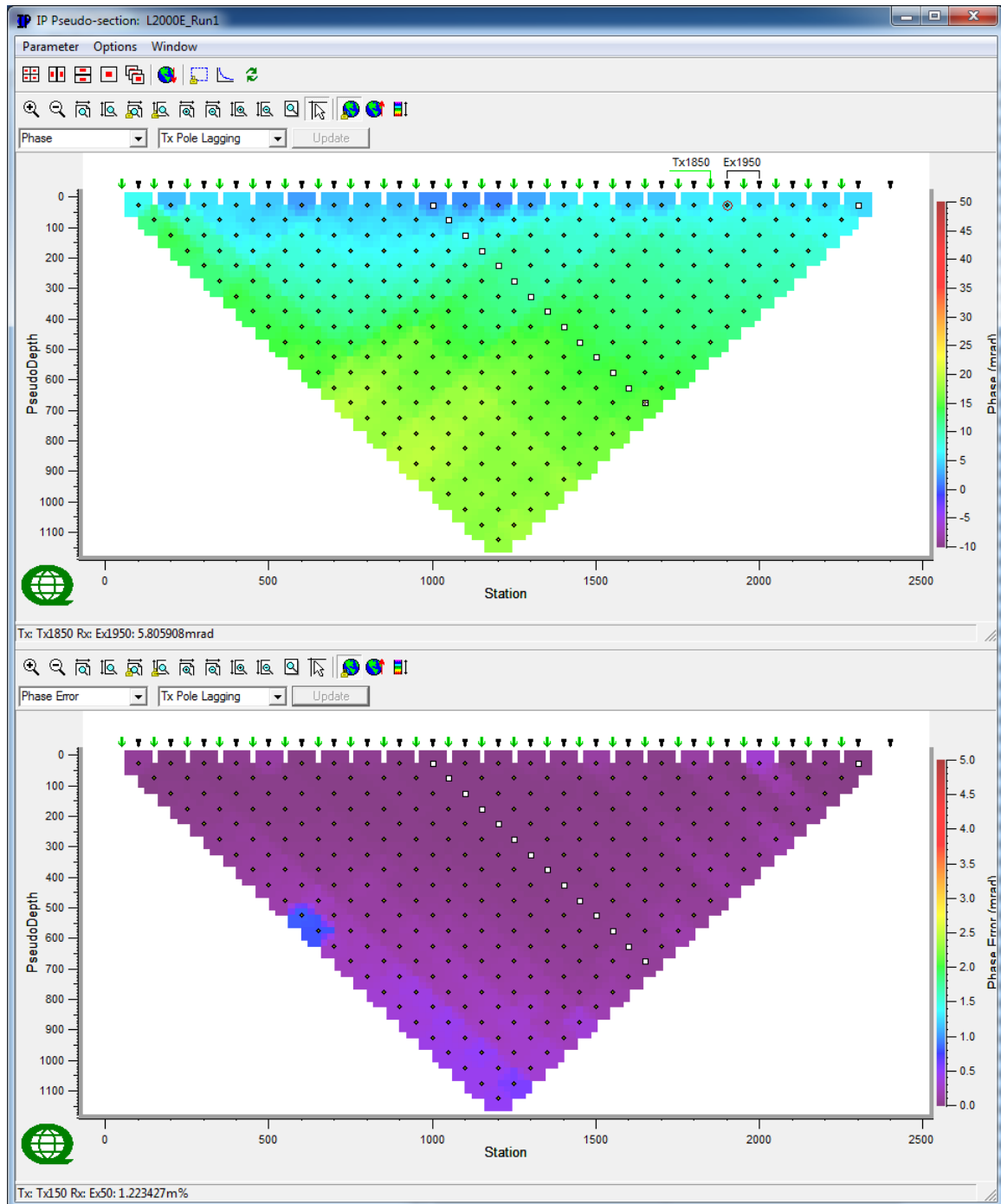
Line 2E – Observed Apparent Resistivity Raw Data (Ohm.m) & Voltage Errors (%) -Tx Pole Lagging.

□ Tx with more than one event



Line 2E – Observed IP Raw Data (mrad) & IP Errors (mrad)-Tx Pole Leading.

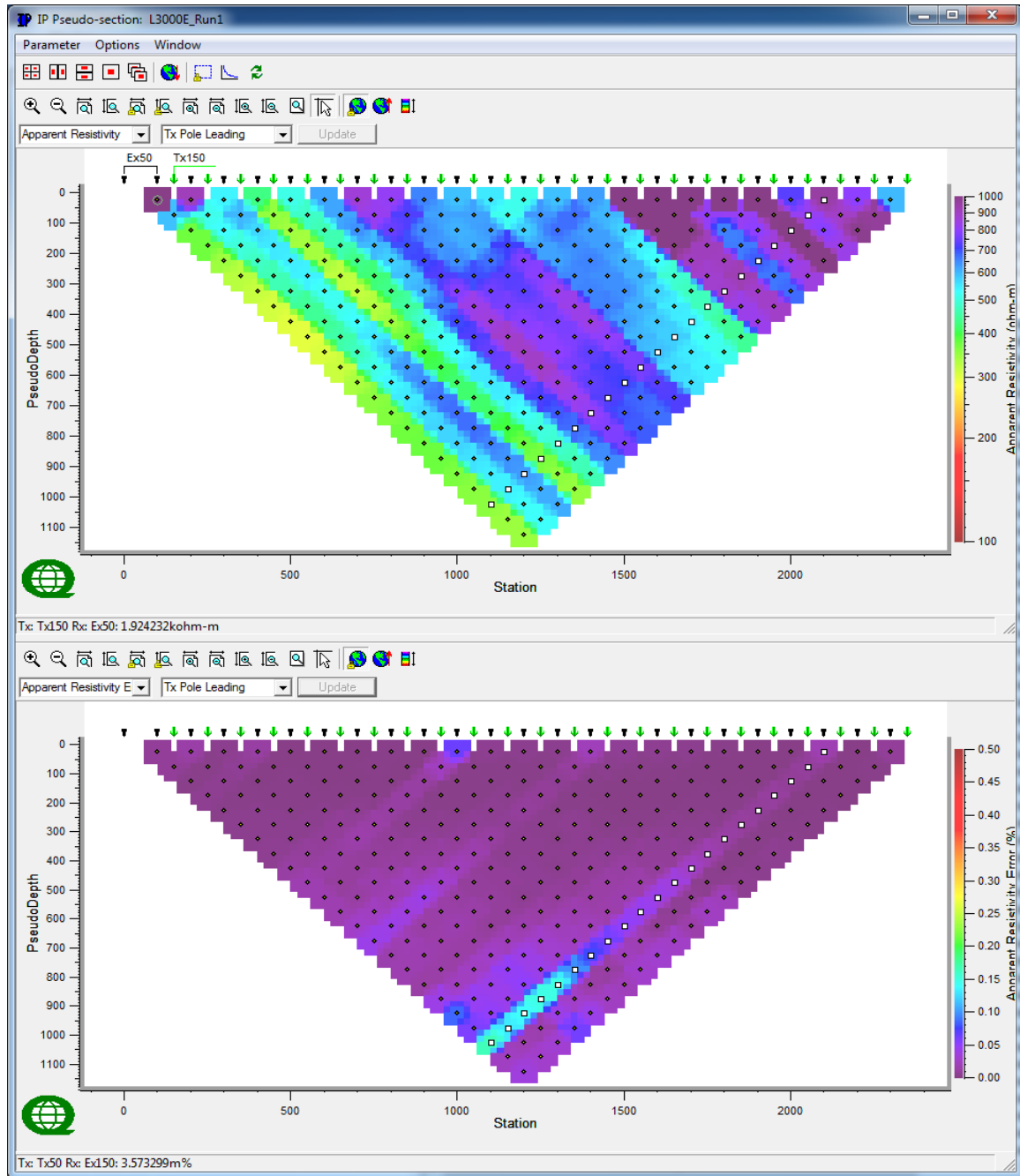
□ Tx with more than one event



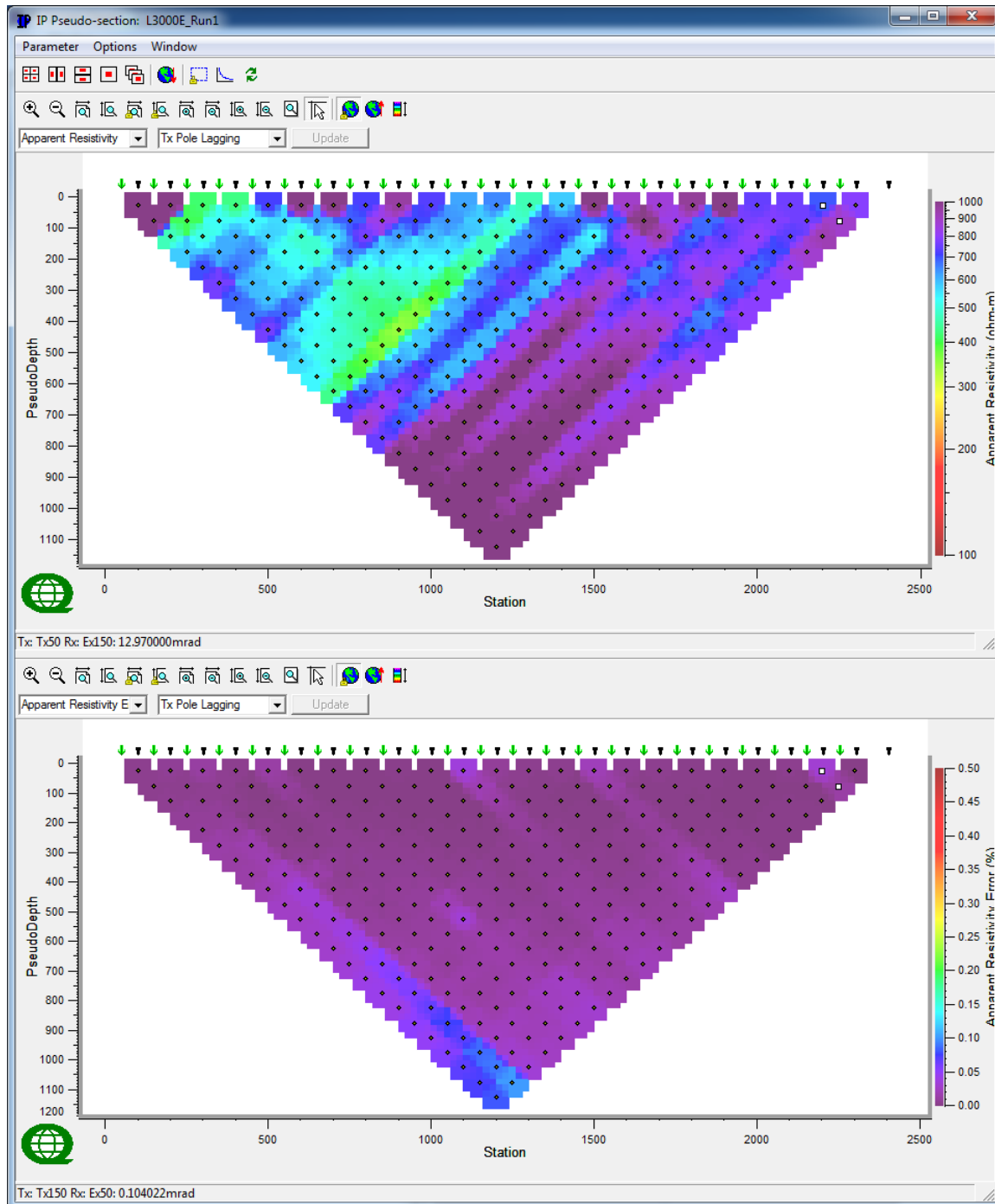
Line 2E – Observed IP Raw Data (mrad) & IP Errors (mrads)-Tx Pole Lagging.

□ Tx with more than one event

C.3 LINE 3E

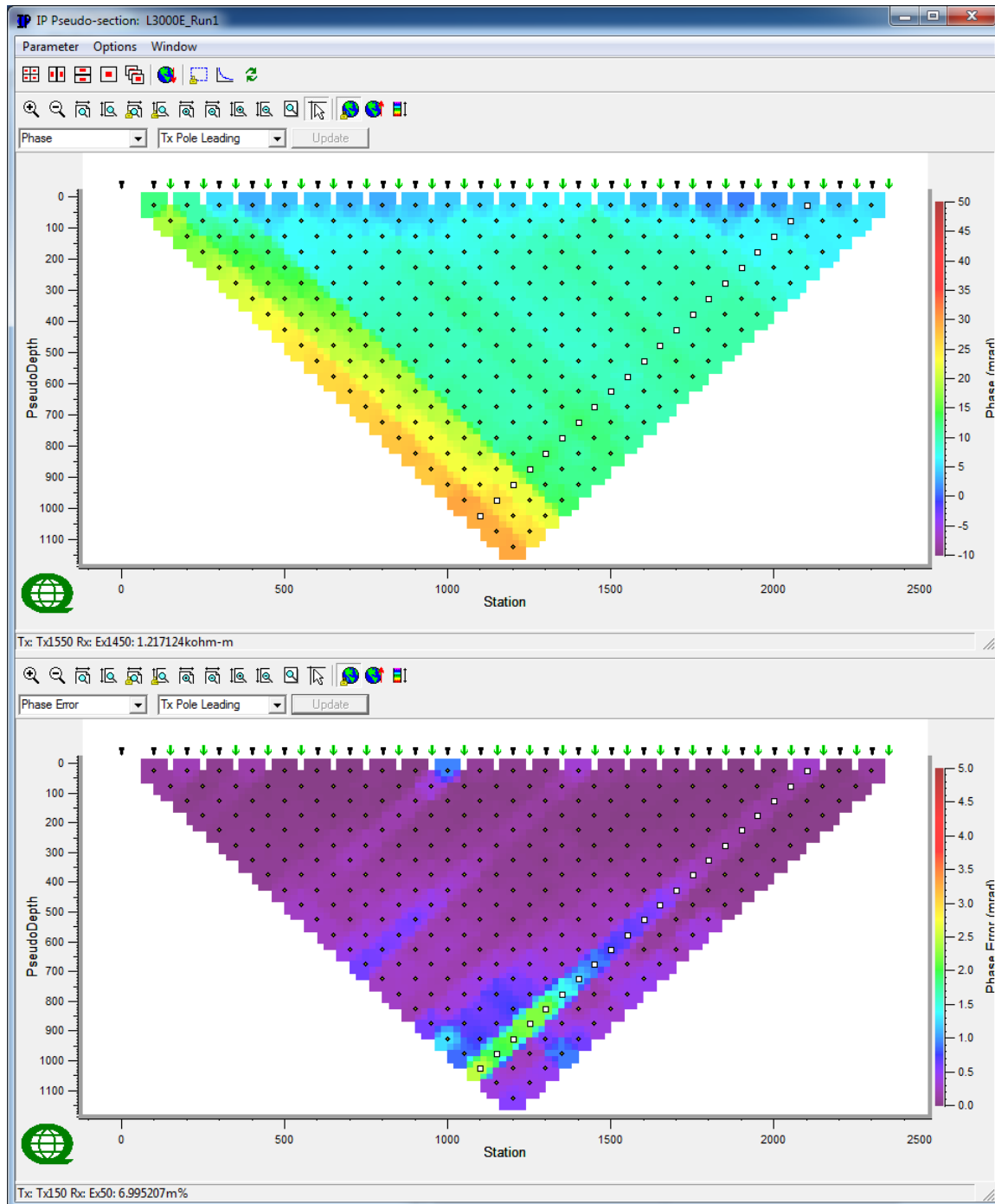


□ Tx with more than one event



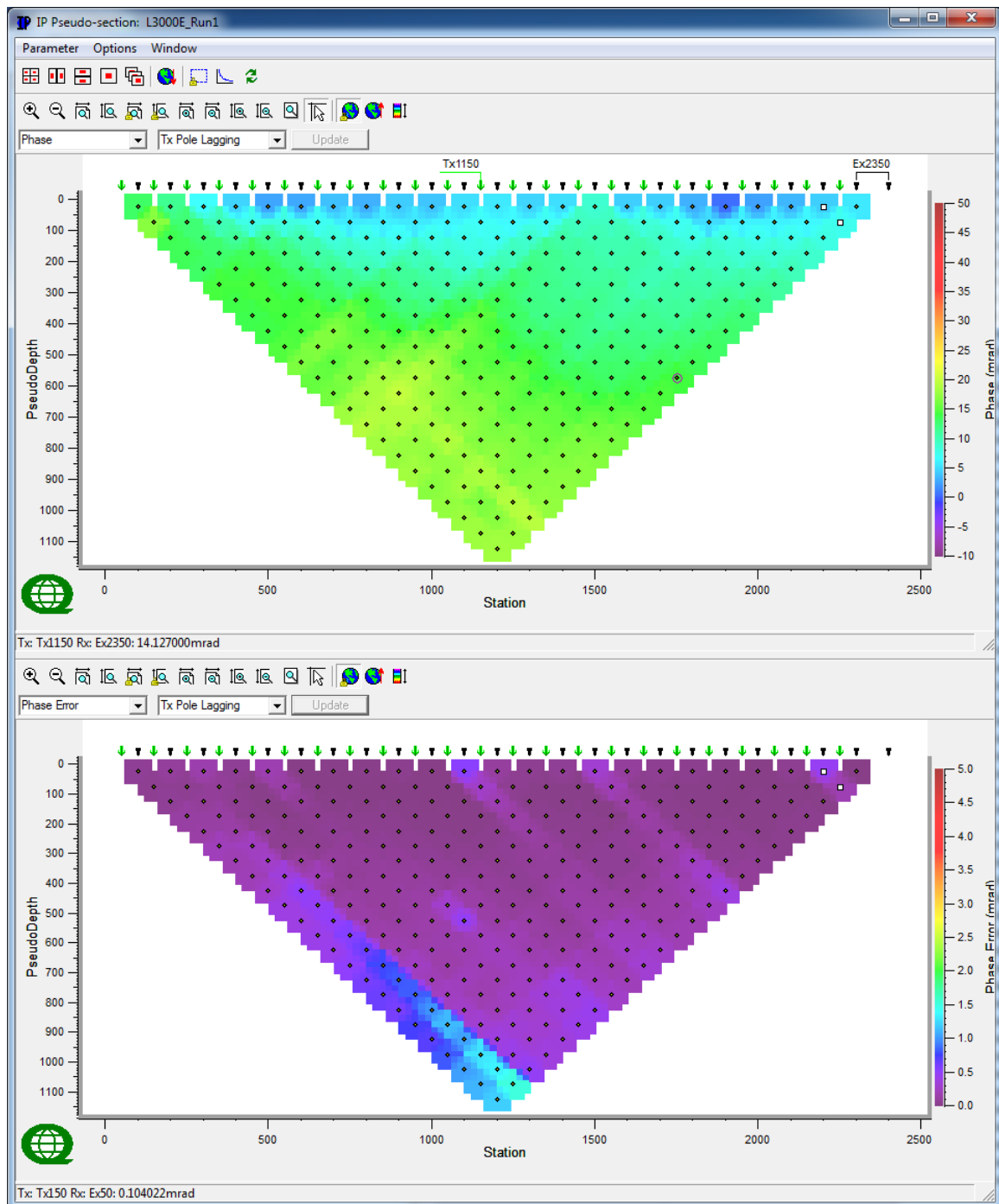
Line 3E – Observed Apparent Resistivity Raw Data (Ohm.m) & Voltage Errors (%) -Tx Pole Lagging.

□ Tx with more than one event



Line 3E – Observed IP Raw Data (mrad) & IP Errors (mrads)-Tx Pole Leading.

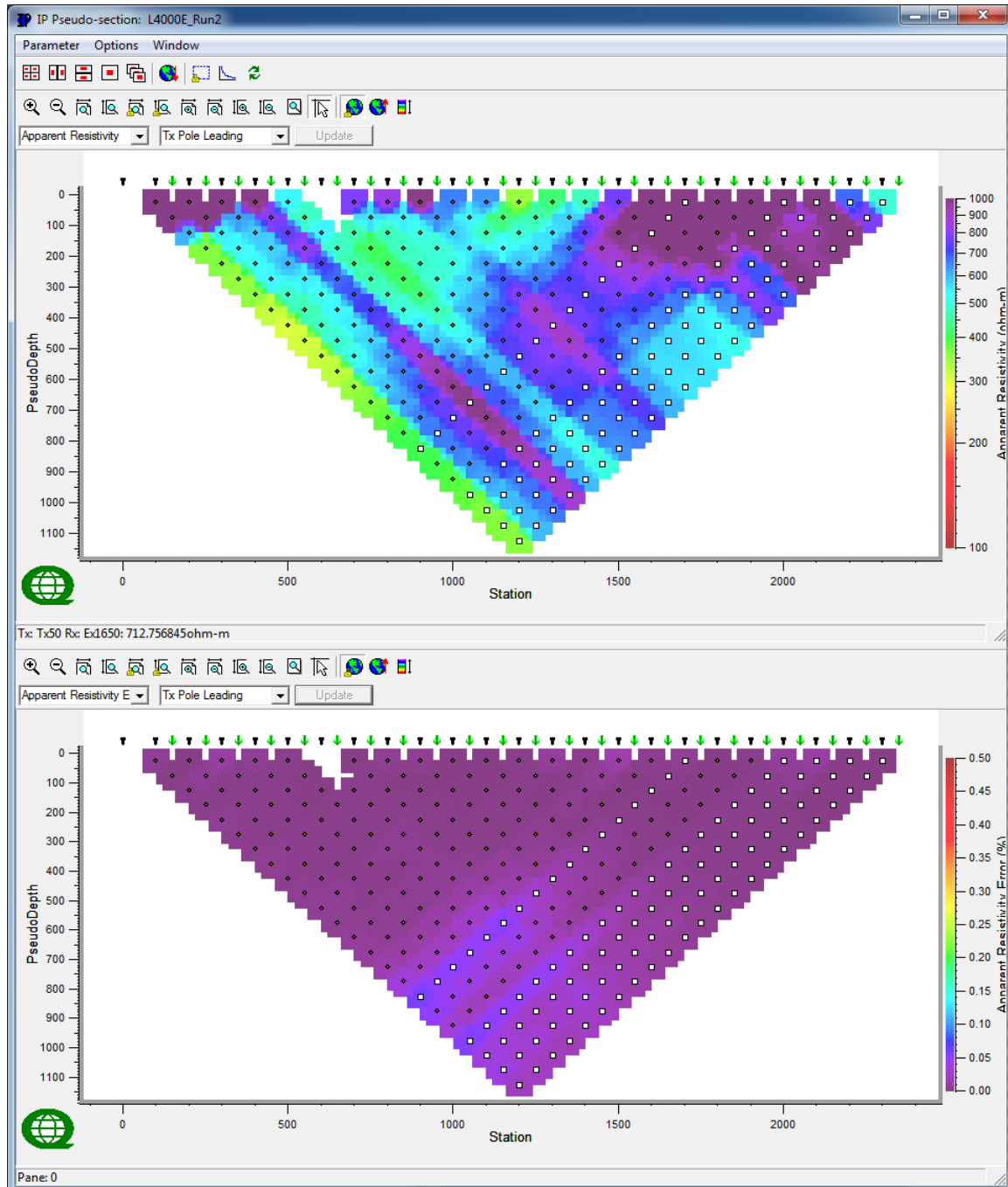
□ Tx with more than one event



Line 3E – Observed IP Raw Data (mrad) & IP Errors (mrads)-Tx Pole Lagging.

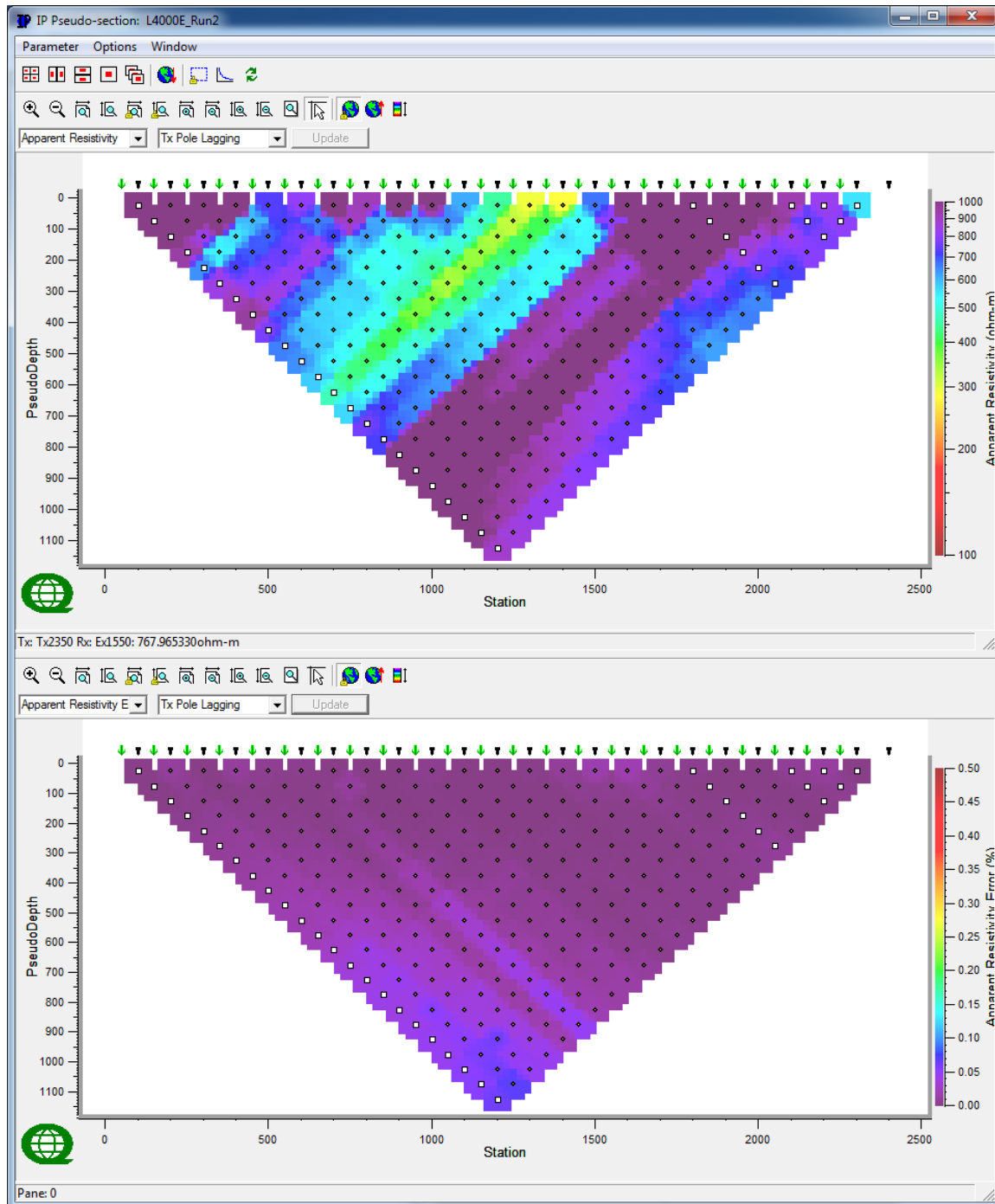
- ☐ Tx with more than one event

C.4 LINE 4E



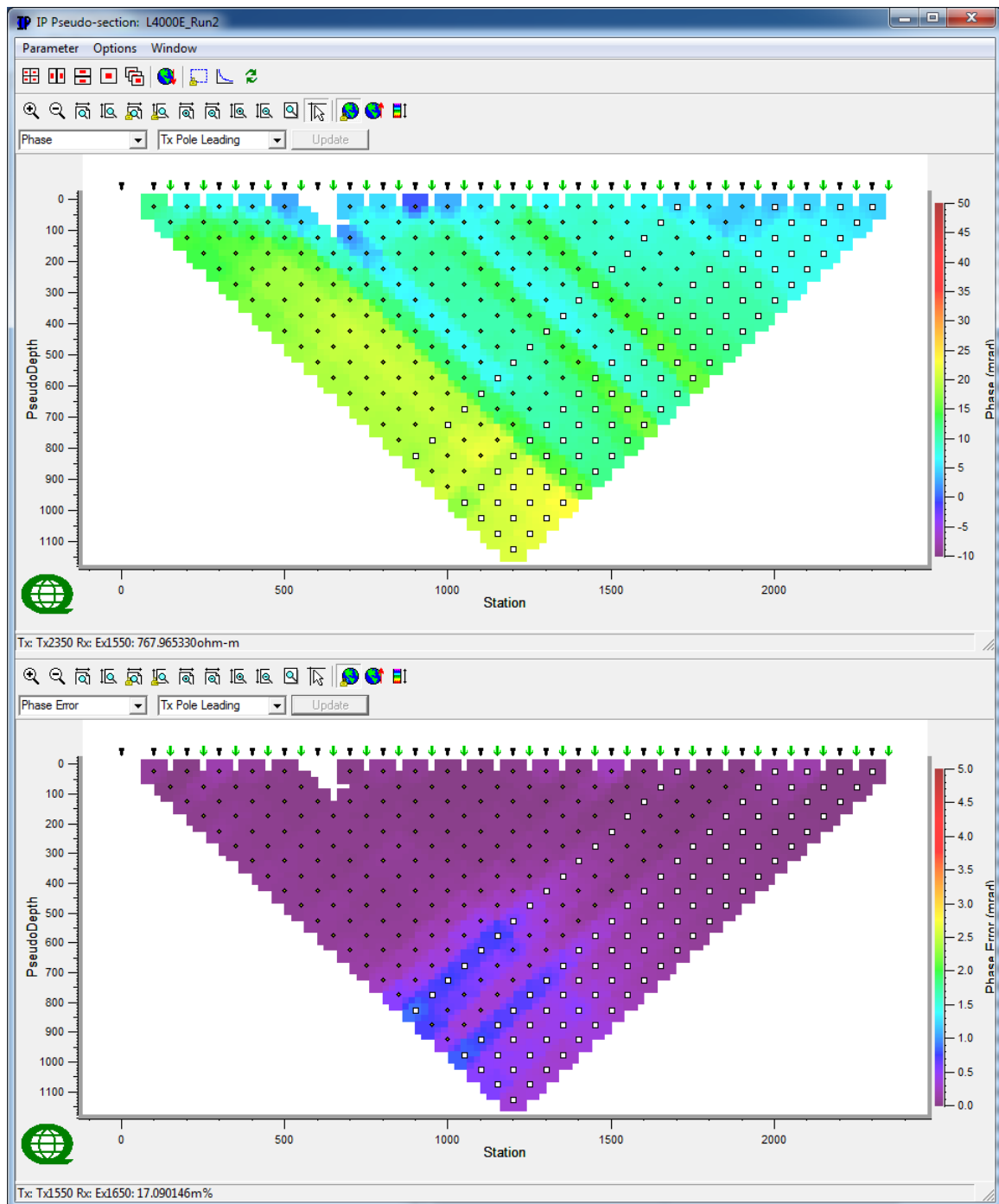
Line 4E – Observed Apparent Resistivity Raw Data (Ohm.m) & Voltage Errors (%) -Tx Pole Leading.

□ Tx with more than one event



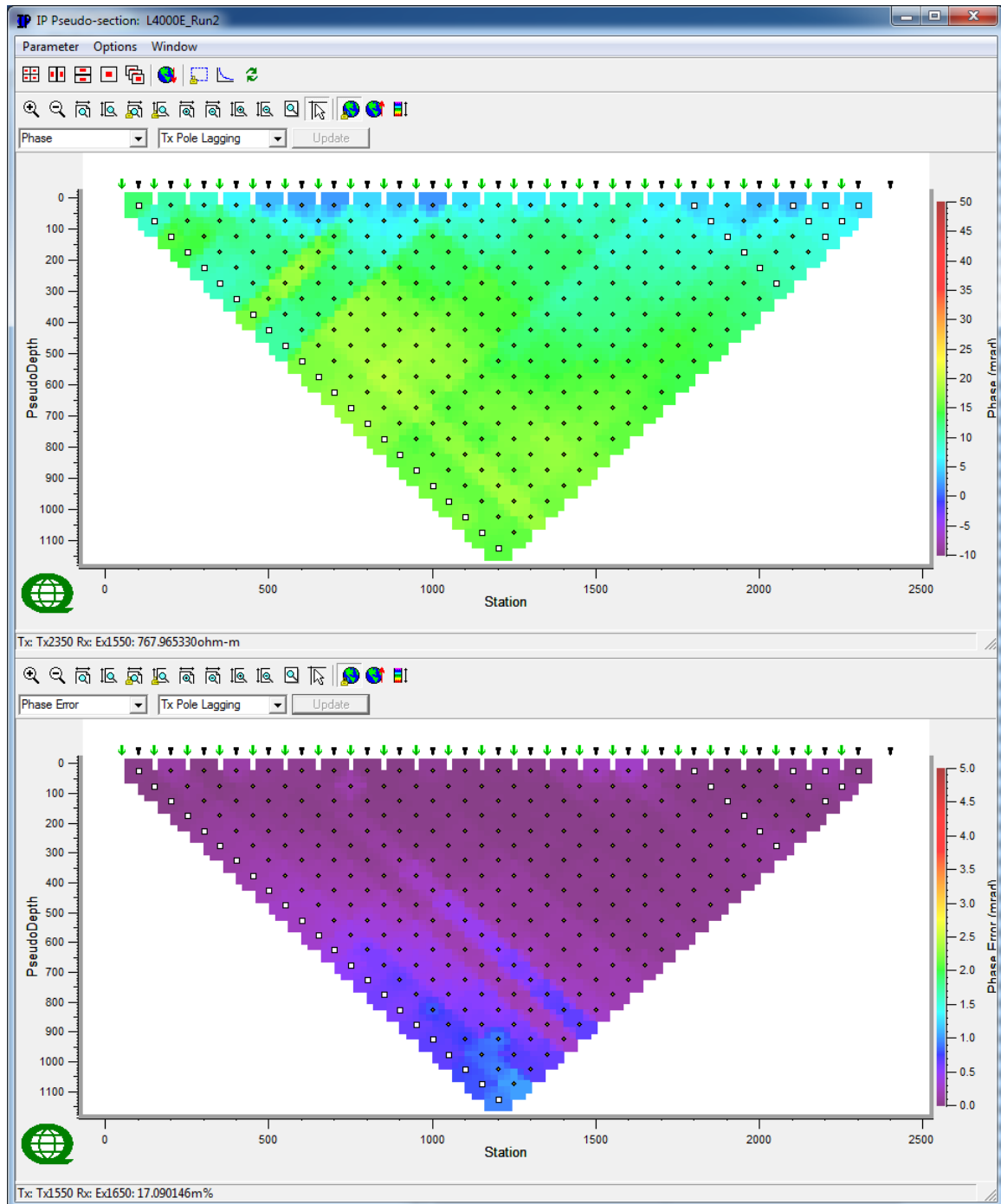
Line 4E – Observed Apparent Resistivity Raw Data (Ohm.m) & Voltage Errors (%) -Tx Pole Lagging.

□ Tx with more than one event



Line 4E – Observed IP Raw Data (mrad) & IP Errors (mrads)-Tx Pole Leading.

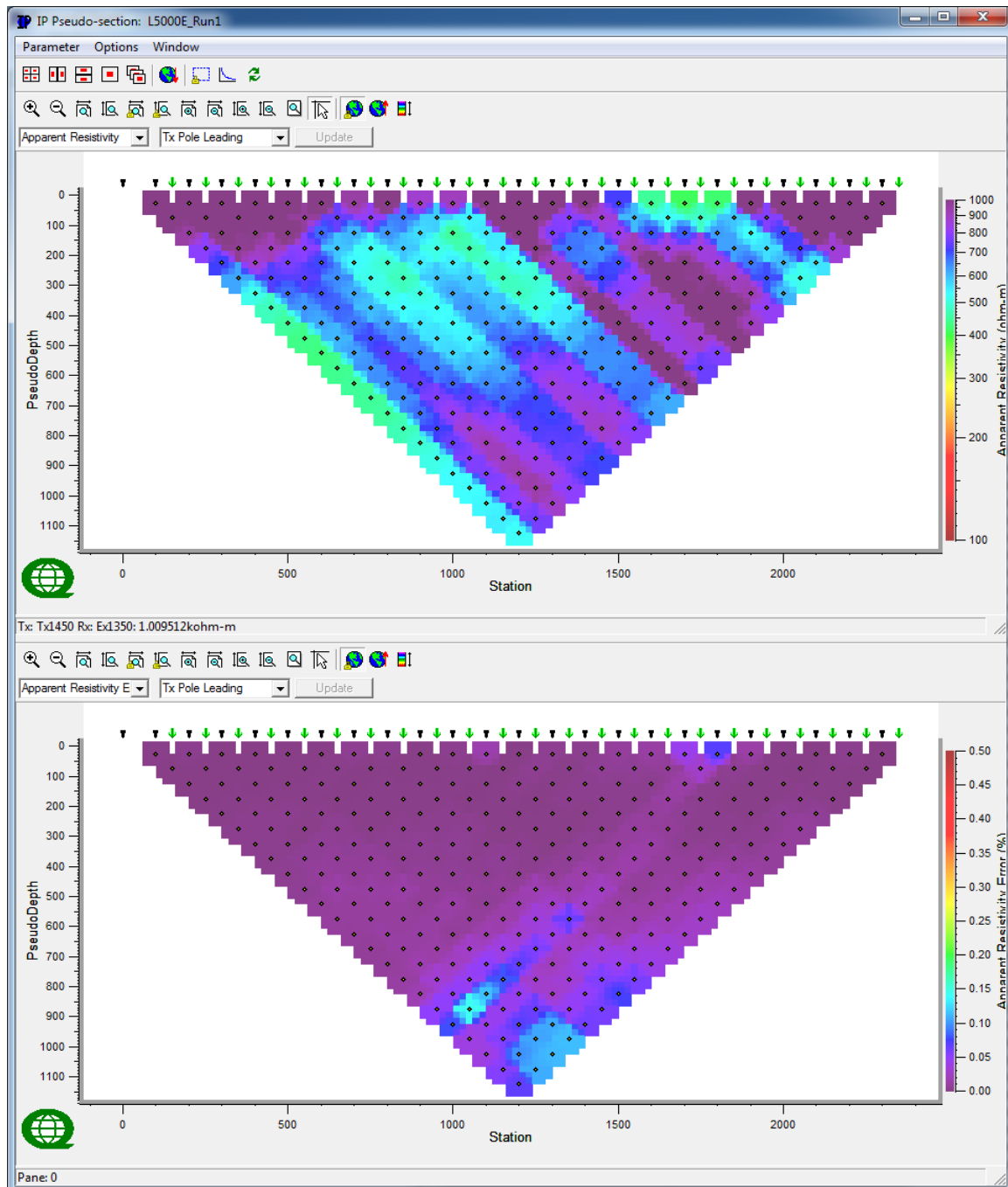
□ Tx with more than one event



Line 4E – Observed IP Raw Data (mrad) & IP Errors (mrads)-Tx Pole Lagging.

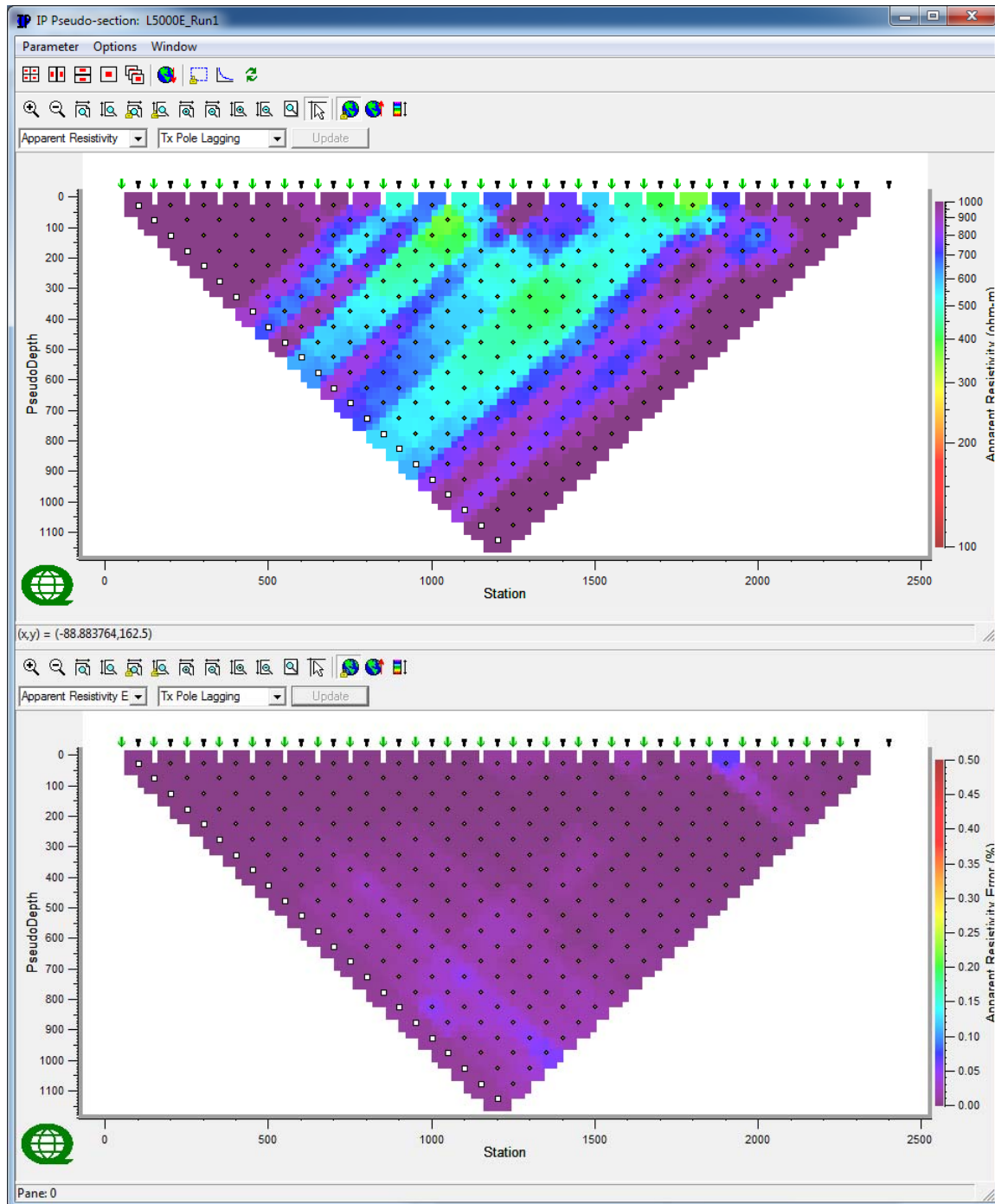
□ Tx with more than one event

C.5 LINE 5E



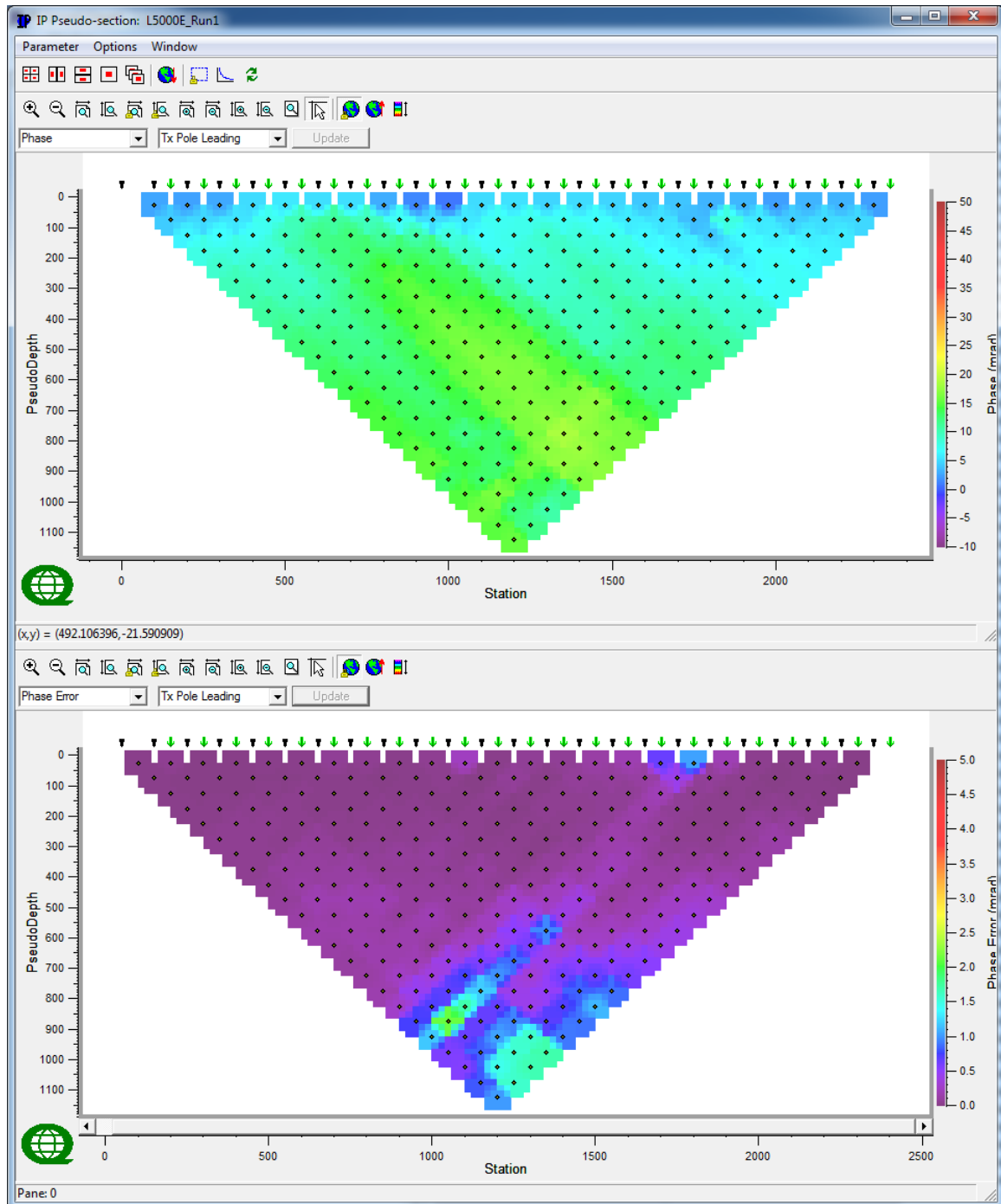
Line 5E – Observed Apparent Resistivity Raw Data (Ohm.m) & Voltage Errors (%) -Tx Pole Leading.

☐ Tx with more than one event



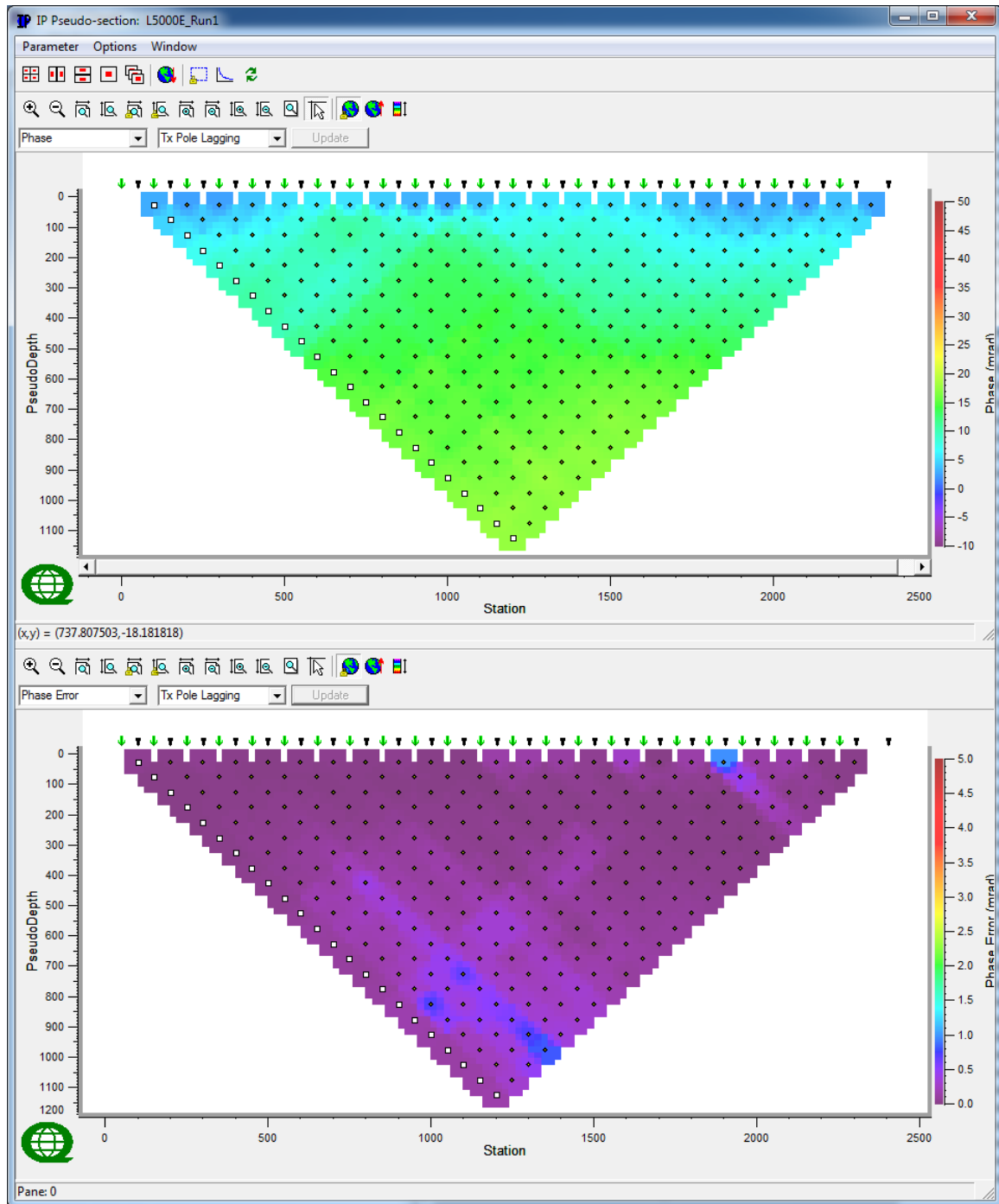
Line 5E – Observed Apparent Resistivity Raw Data (Ohm.m) & Voltage Errors (%) -Tx Pole Lagging.

□ Tx with more than one event



Line 5E – Observed IP Raw Data (mrad) & IP Errors (mrads)-Tx Pole Leading.

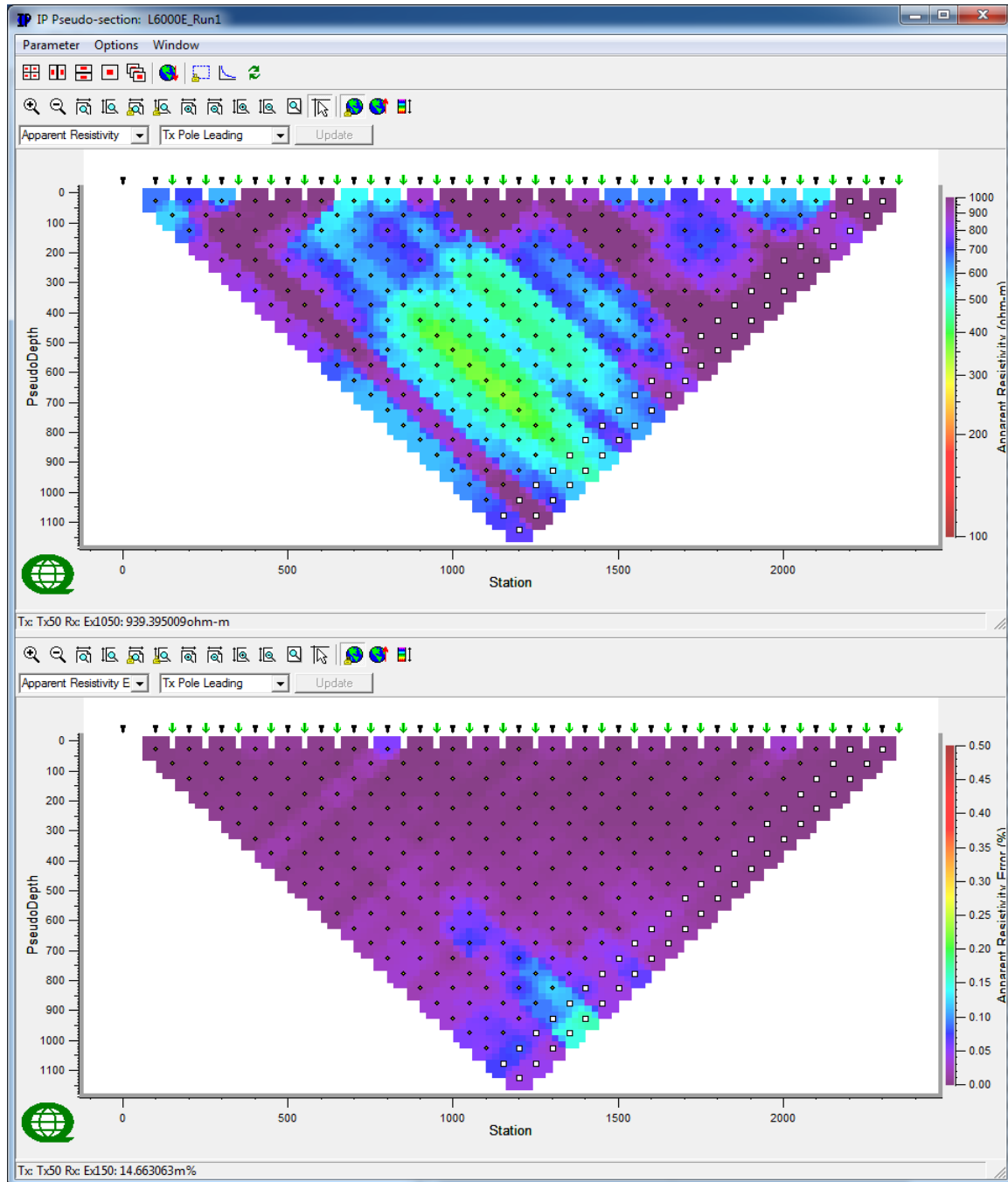
☐ Tx with more than one event



Line 5E – Observed IP Raw Data (mrad) & IP Errors (mrads)-Tx Pole Lagging.

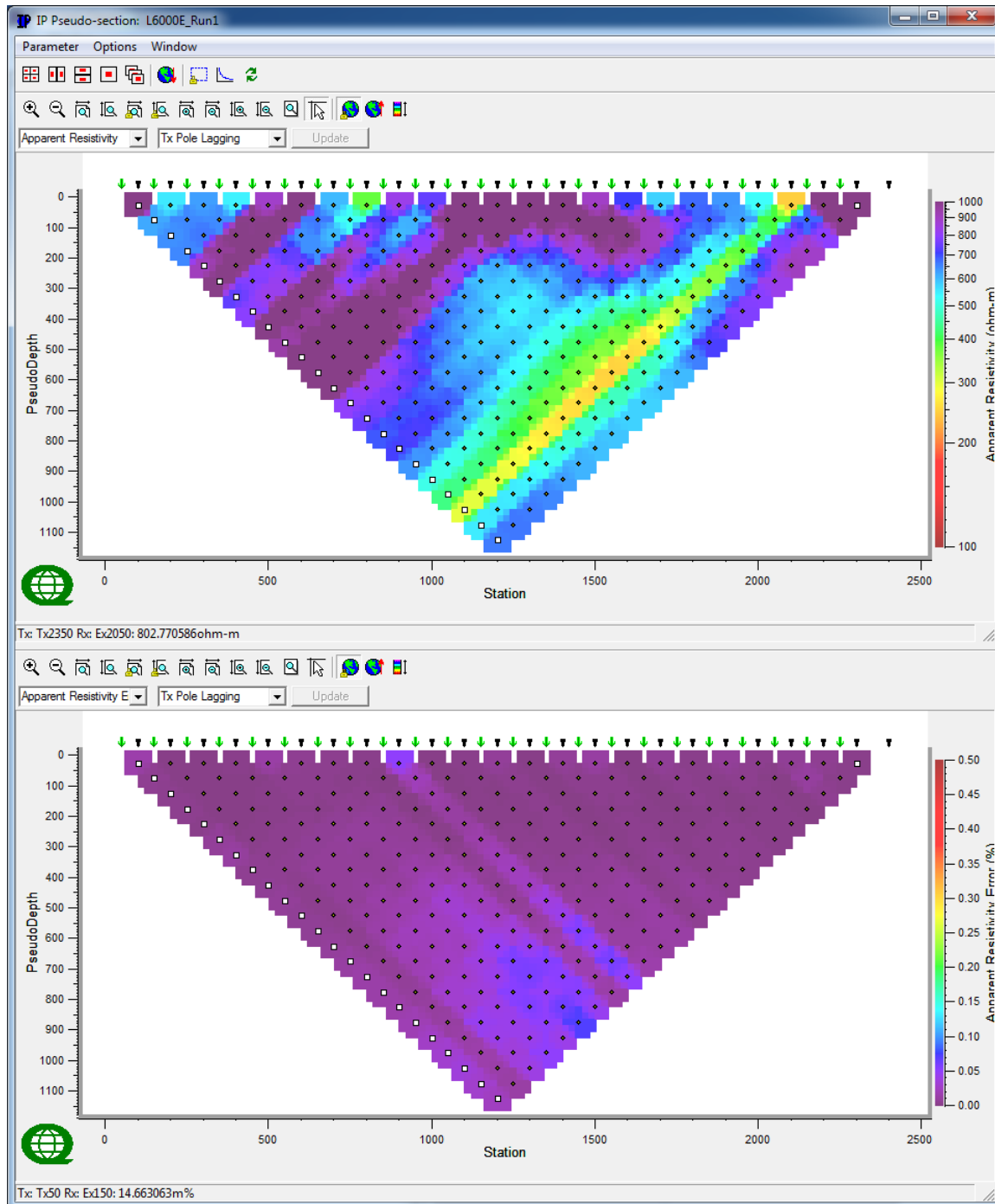
□ Tx with more than one event

C.6 LINE 6E



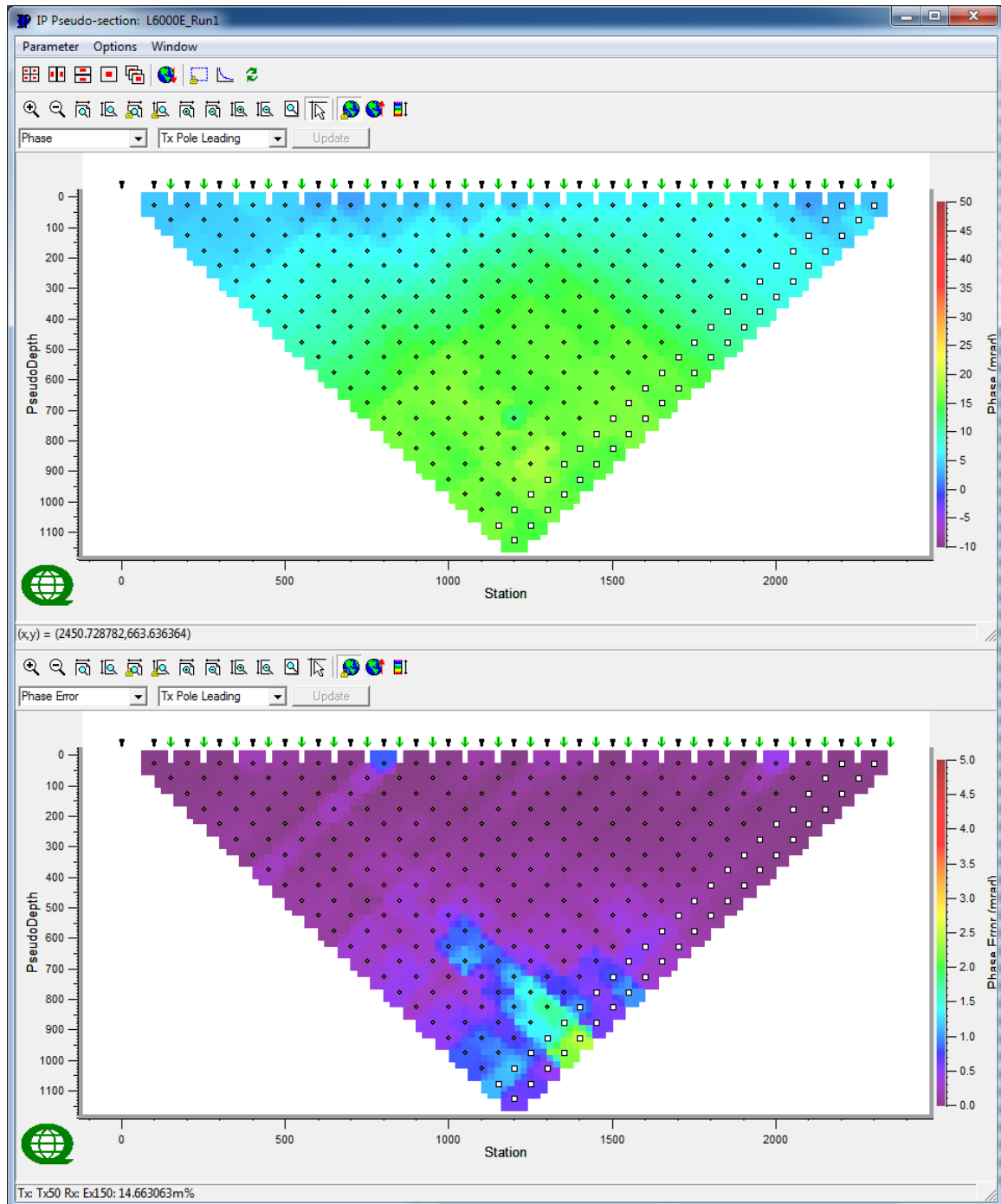
Line 6E – Observed Apparent Resistivity Raw Data (Ohm.m) & Voltage Errors (%) -Tx Pole Leading.

□ Tx with more than one event



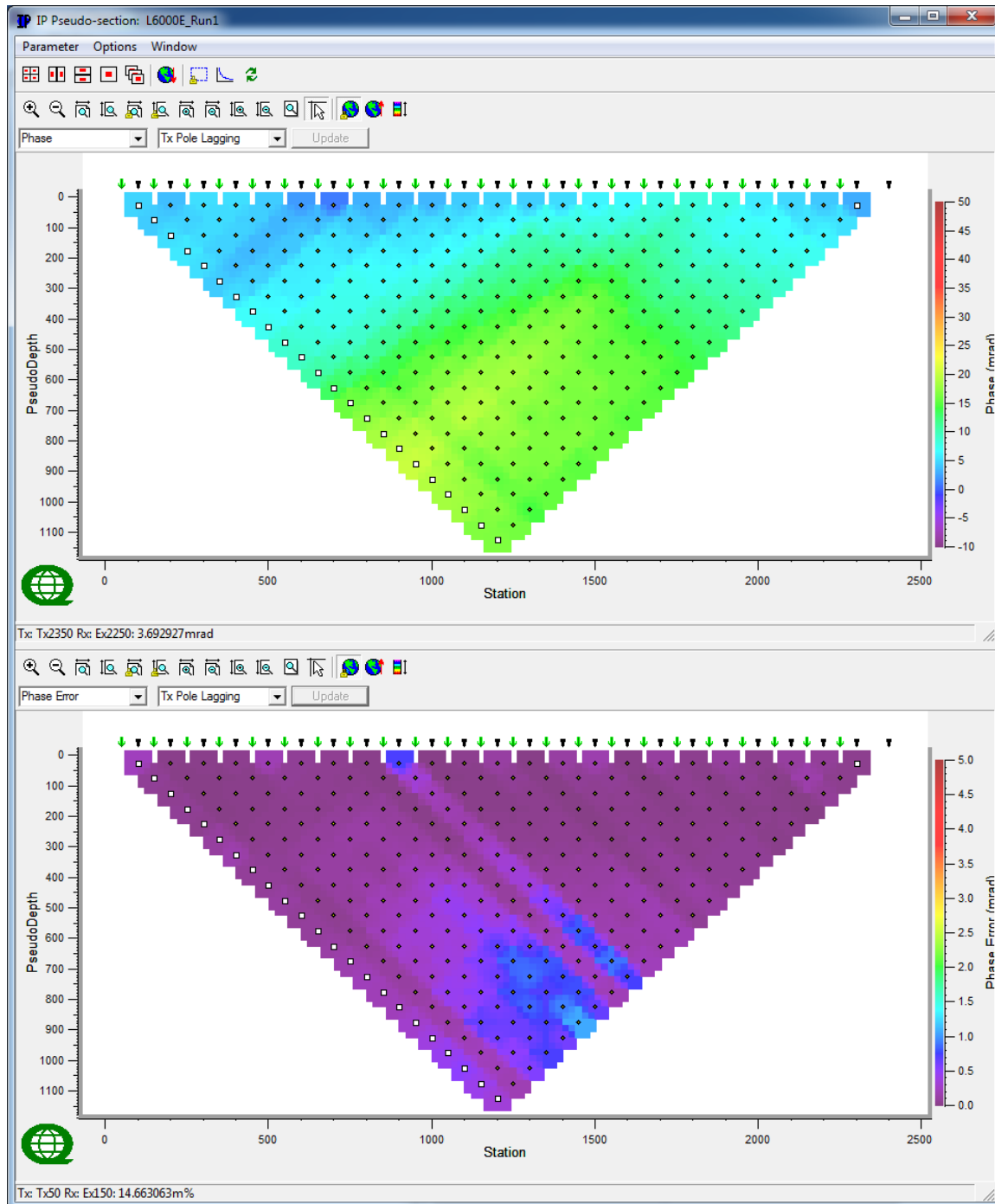
Line 6E – Observed Apparent Resistivity Raw Data (Ohm.m) & Voltage Errors (%) -Tx Pole Lagging.

□ Tx with more than one event



Line 6E – Observed IP Raw Data (mrad) & IP Errors (mrad)-Tx Pole Leading.

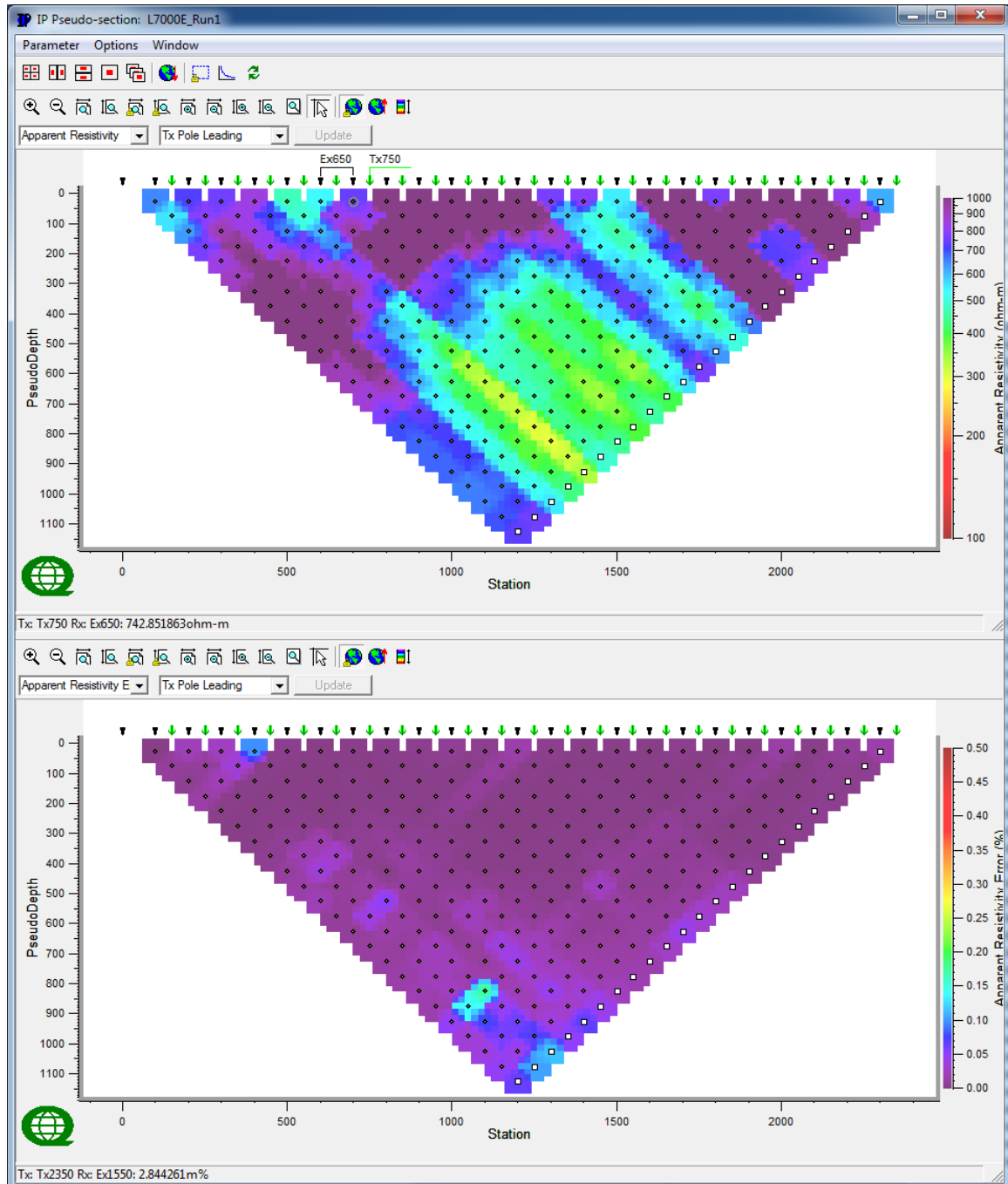
□ Tx with more than one event



Line 6E – Observed IP Raw Data (mrad) & IP Errors (mrads)-Tx Pole Lagging.

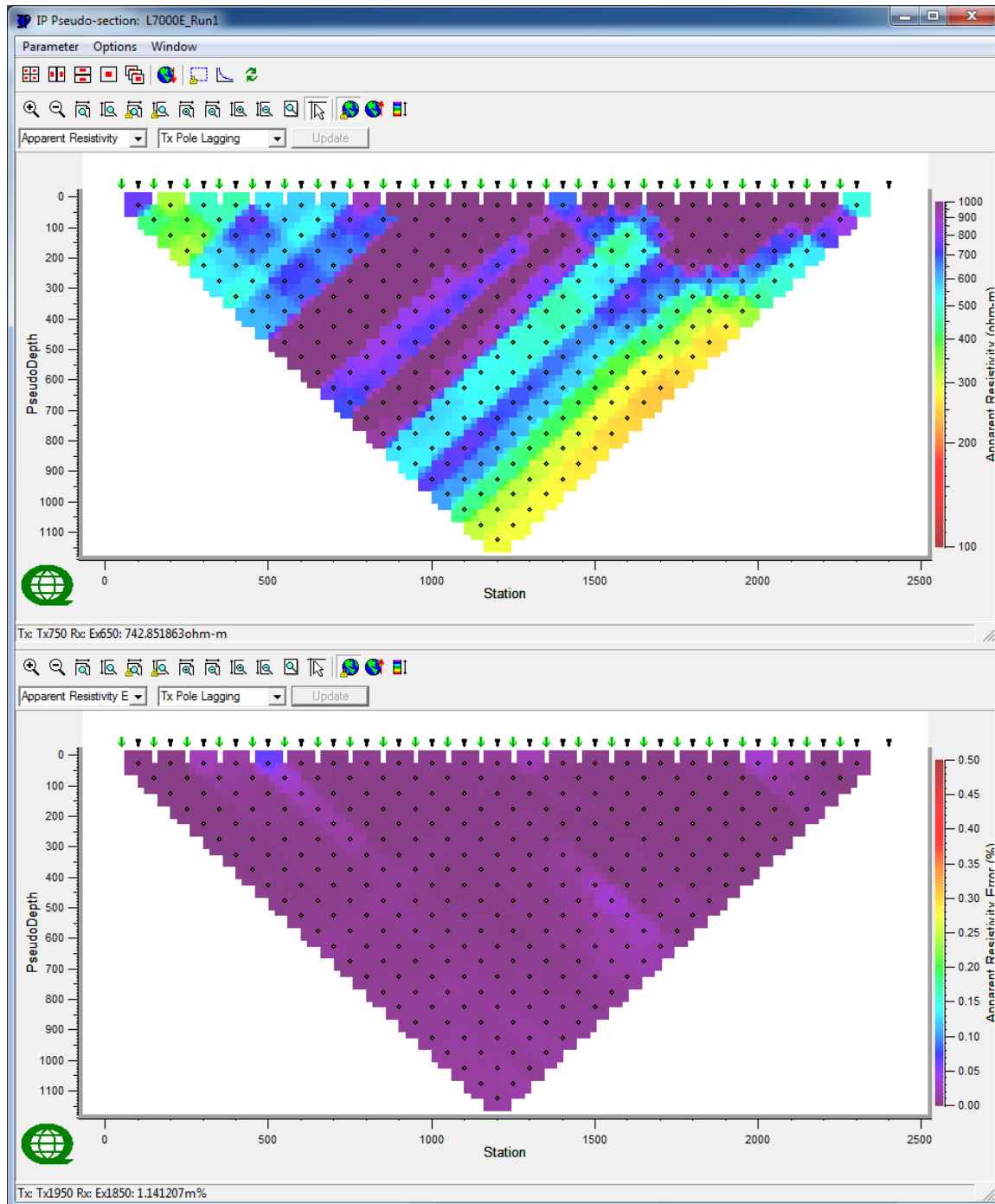
□ Tx with more than one event

C.7 LINE 7E



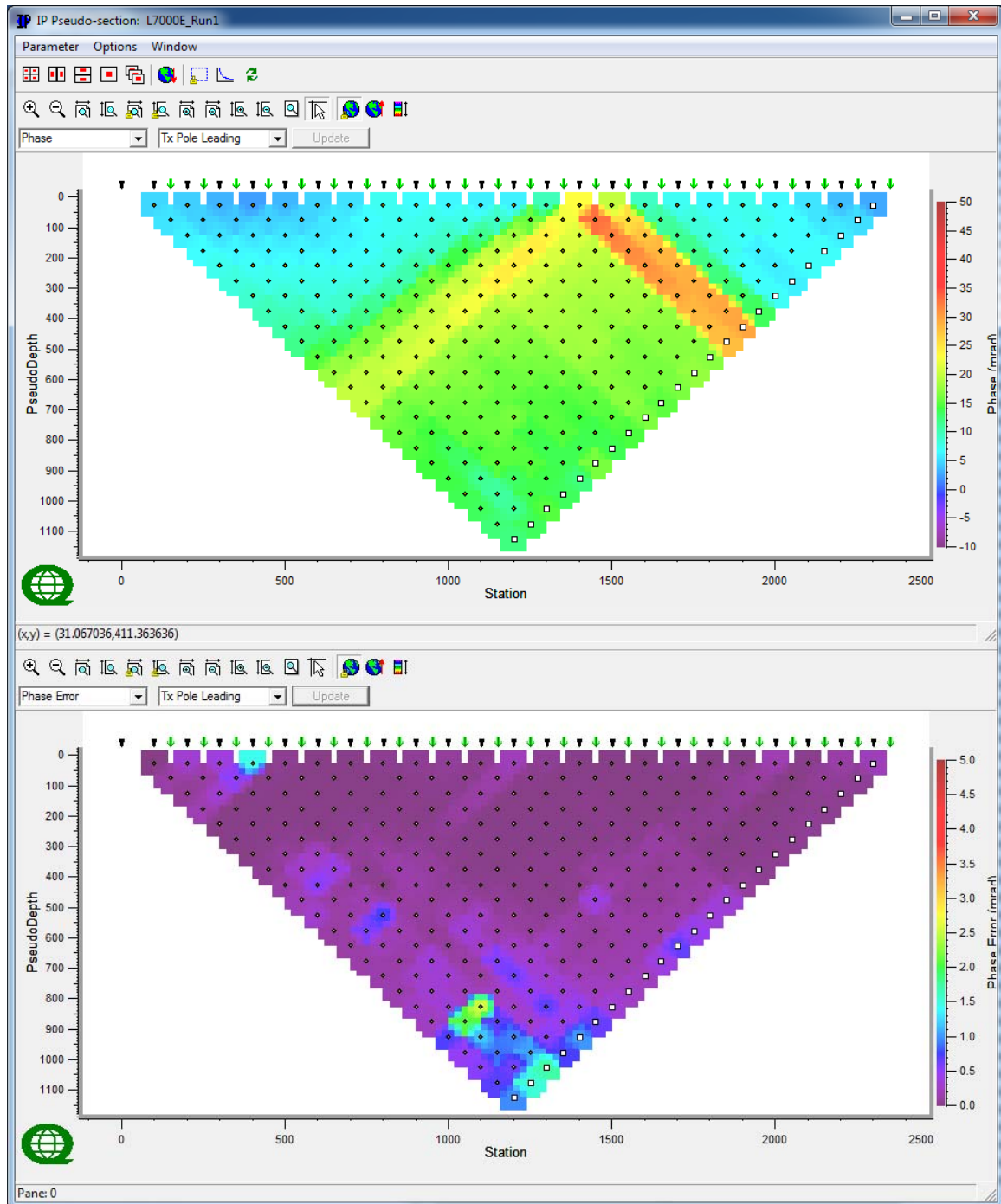
Line 7E – Observed Apparent Resistivity Raw Data (Ohm.m) & Voltage Errors (%) -Tx Pole Leading.

□ Tx with more than one event



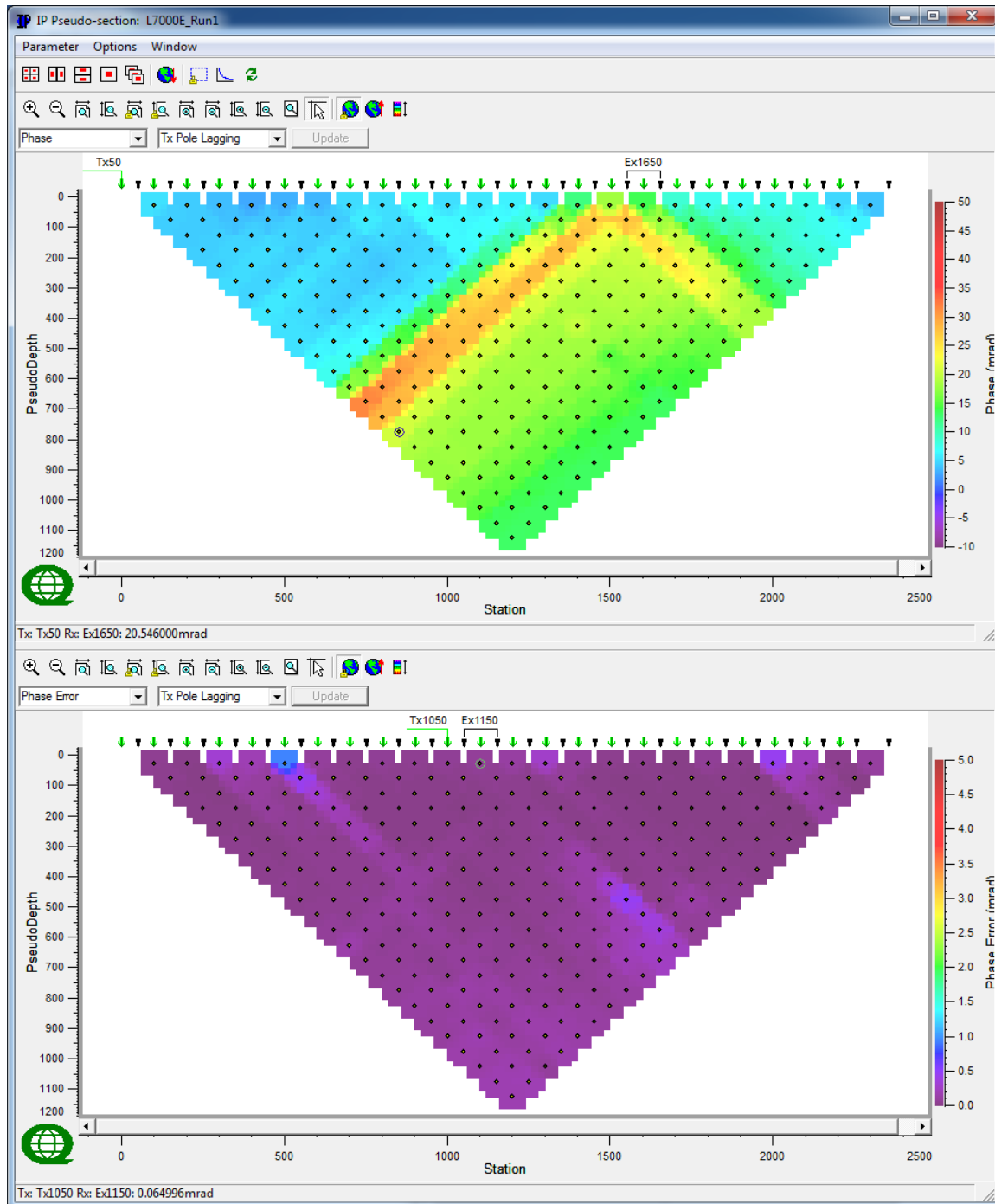
Line 7E – Observed Apparent Resistivity Raw Data (Ohm.m) & Voltage Errors (%) -Tx Pole Lagging.

☐ Tx with more than one event



Line 7E – Observed IP Raw Data (mrad) & IP Errors (mrads)-Tx Pole Leading.

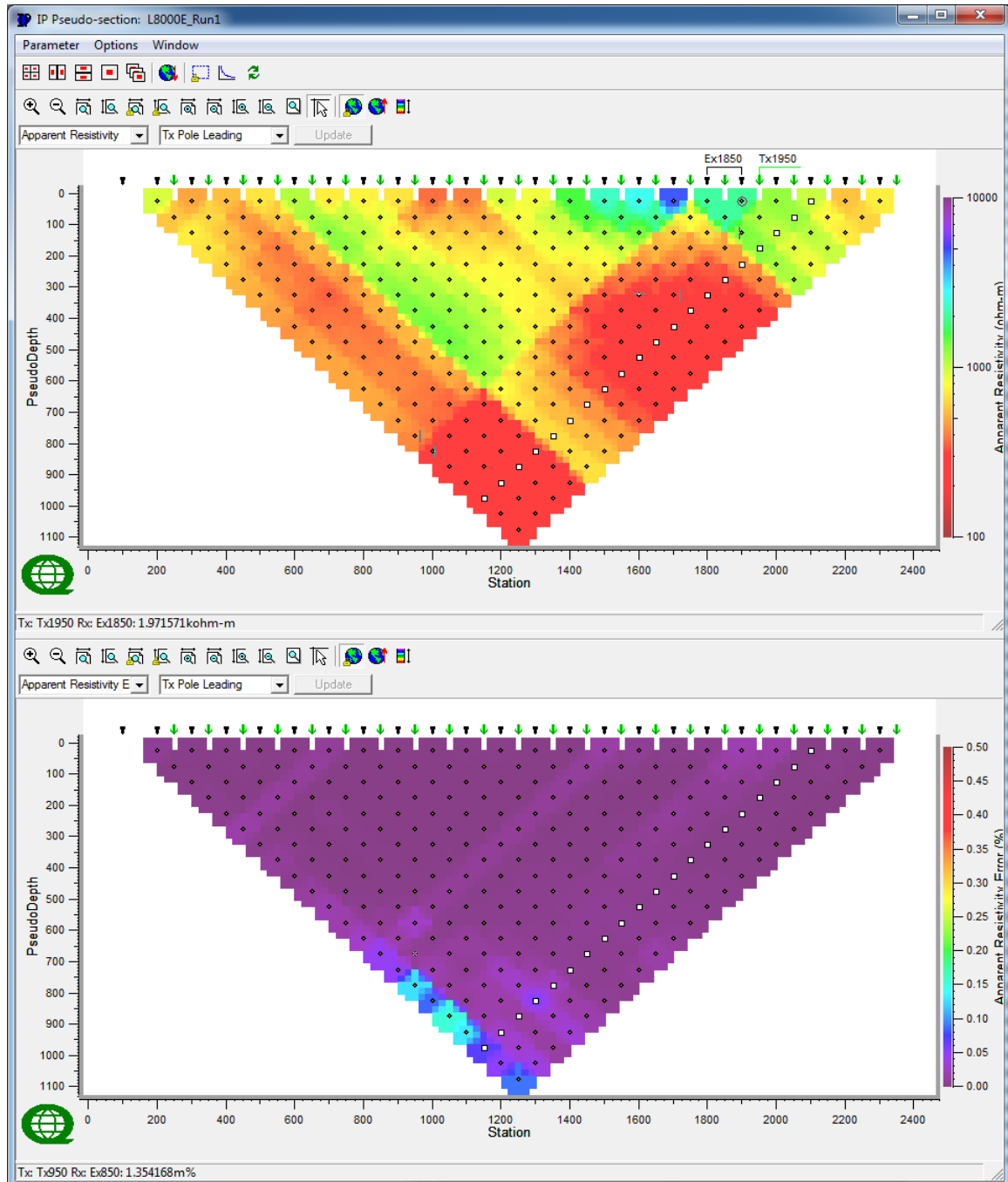
□ Tx with more than one event



Line 7E – Observed IP Raw Data (mrad) & IP Errors (mrad)-Tx Pole Lagging.

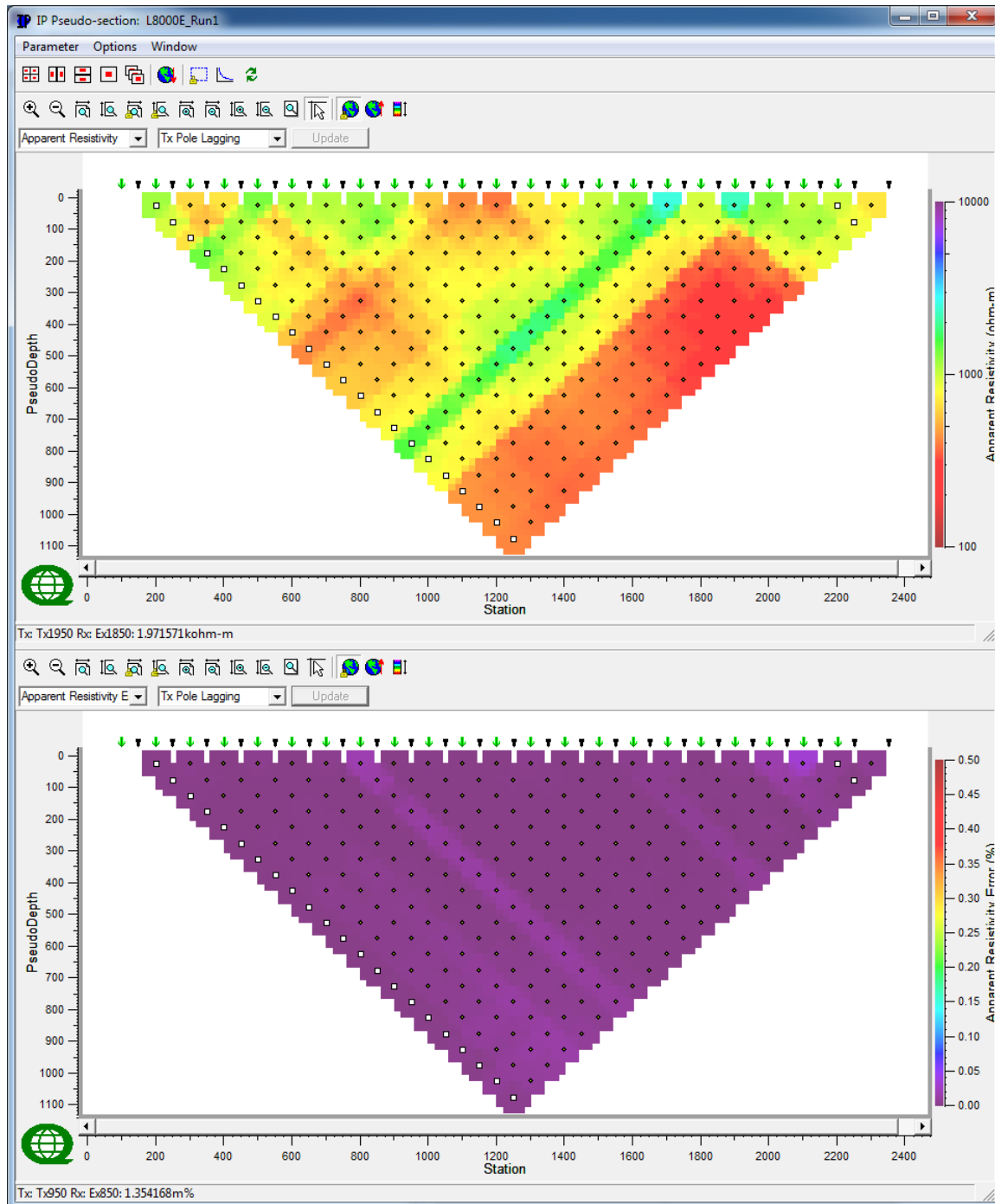
☐ Tx with more than one event

C.8 LINE 8E



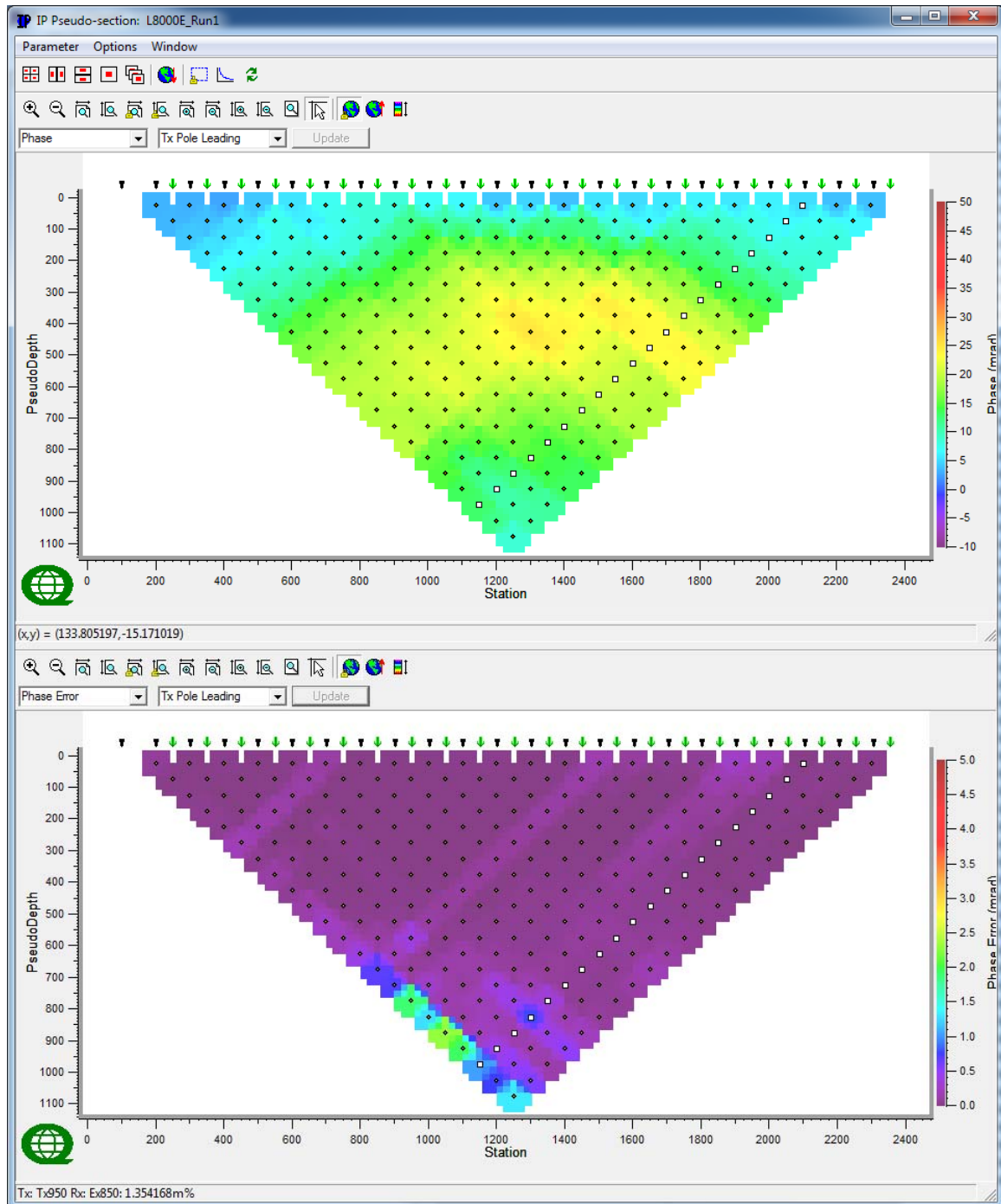
Line 8E – Observed Apparent Resistivity Raw Data (Ohm.m) & Voltage Errors (%) -Tx Pole Leading.

□ Tx with more than one event



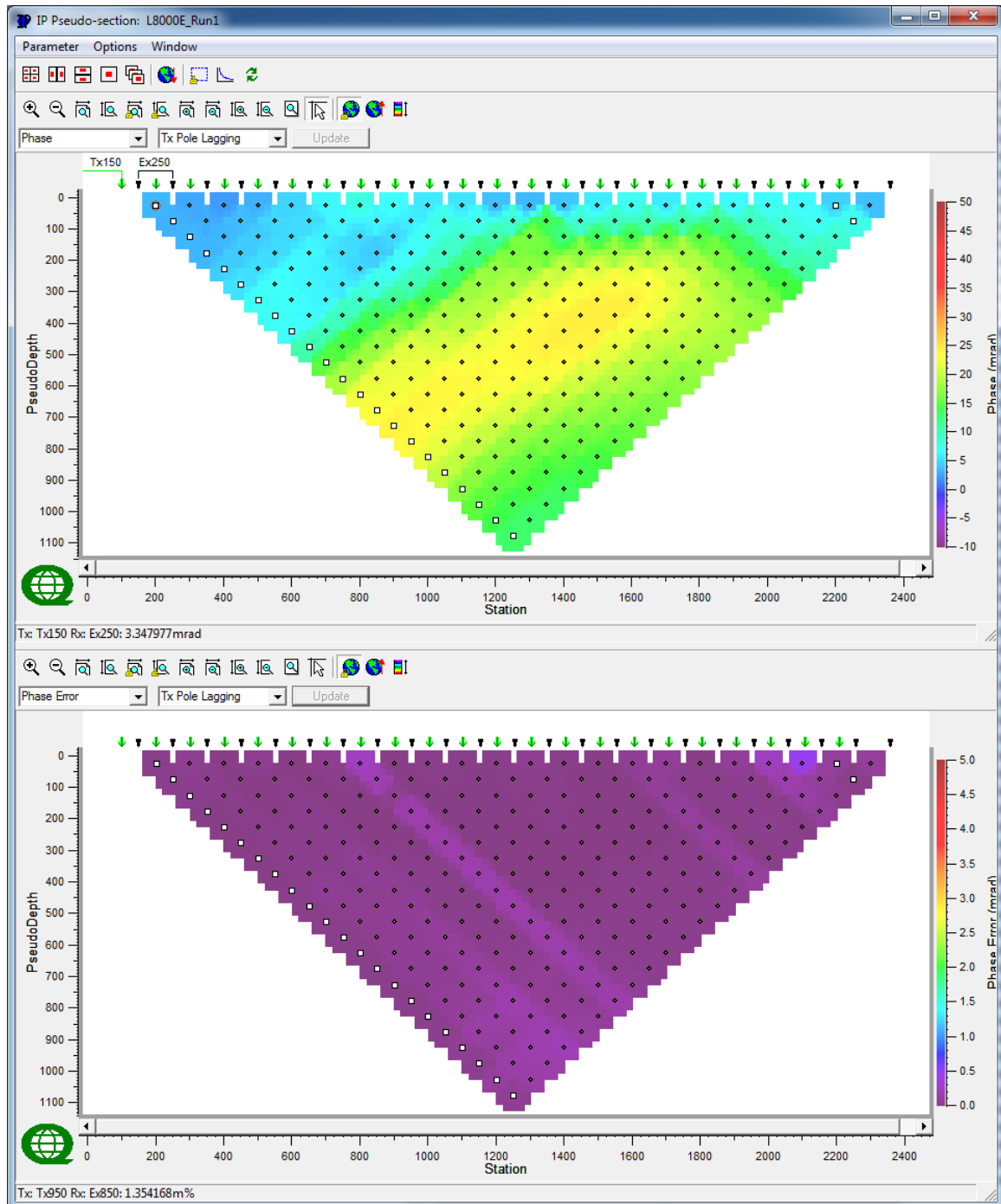
Line 8E – Observed Apparent Resistivity Raw Data (Ohm.m) & Voltage Errors (%) -Tx Pole Lagging.

□ Tx with more than one event



Line 8E – Observed IP Raw Data (mrad) & IP Errors (mrads)-Tx Pole Leading.

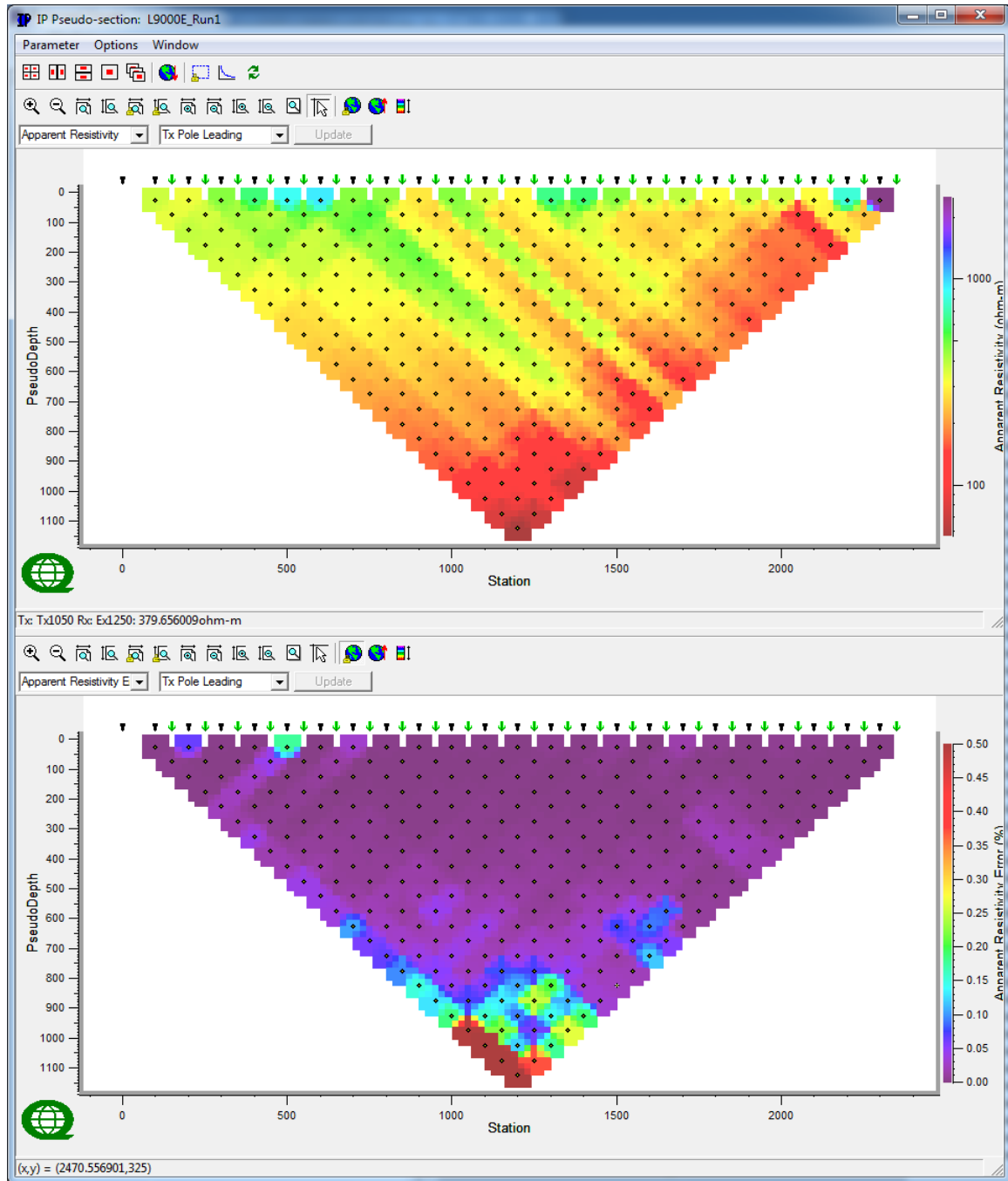
□ Tx with more than one event



Line 8E – Observed IP Raw Data (mrad) & IP Errors (mrads)-Tx Pole Lagging.

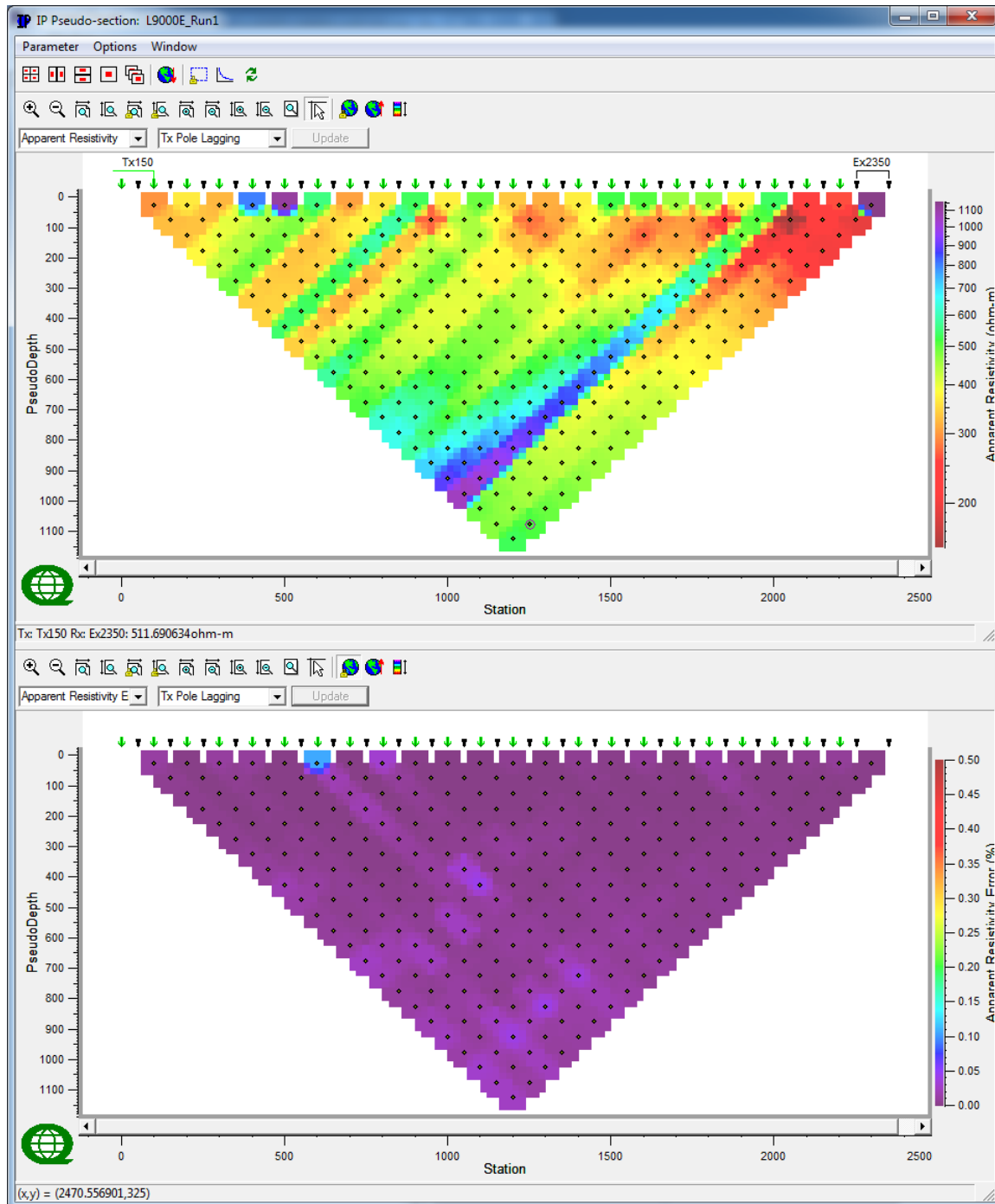
□ Tx with more than one event

C.9 LINE 9E



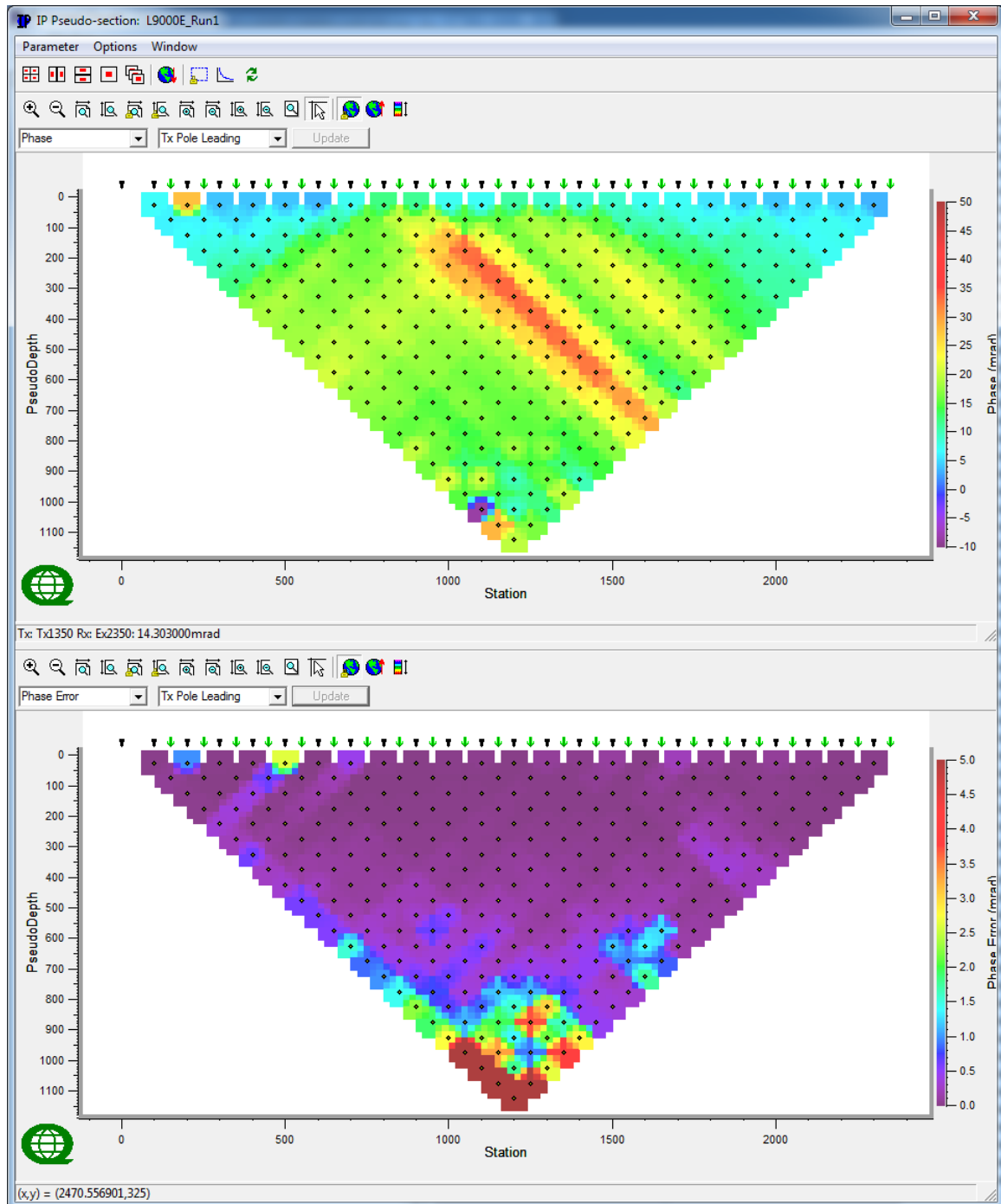
Line 9E – Observed Apparent Resistivity Raw Data (Ohm.m) & Voltage Errors (%) -Tx Pole Leading.

□ Tx with more than one event



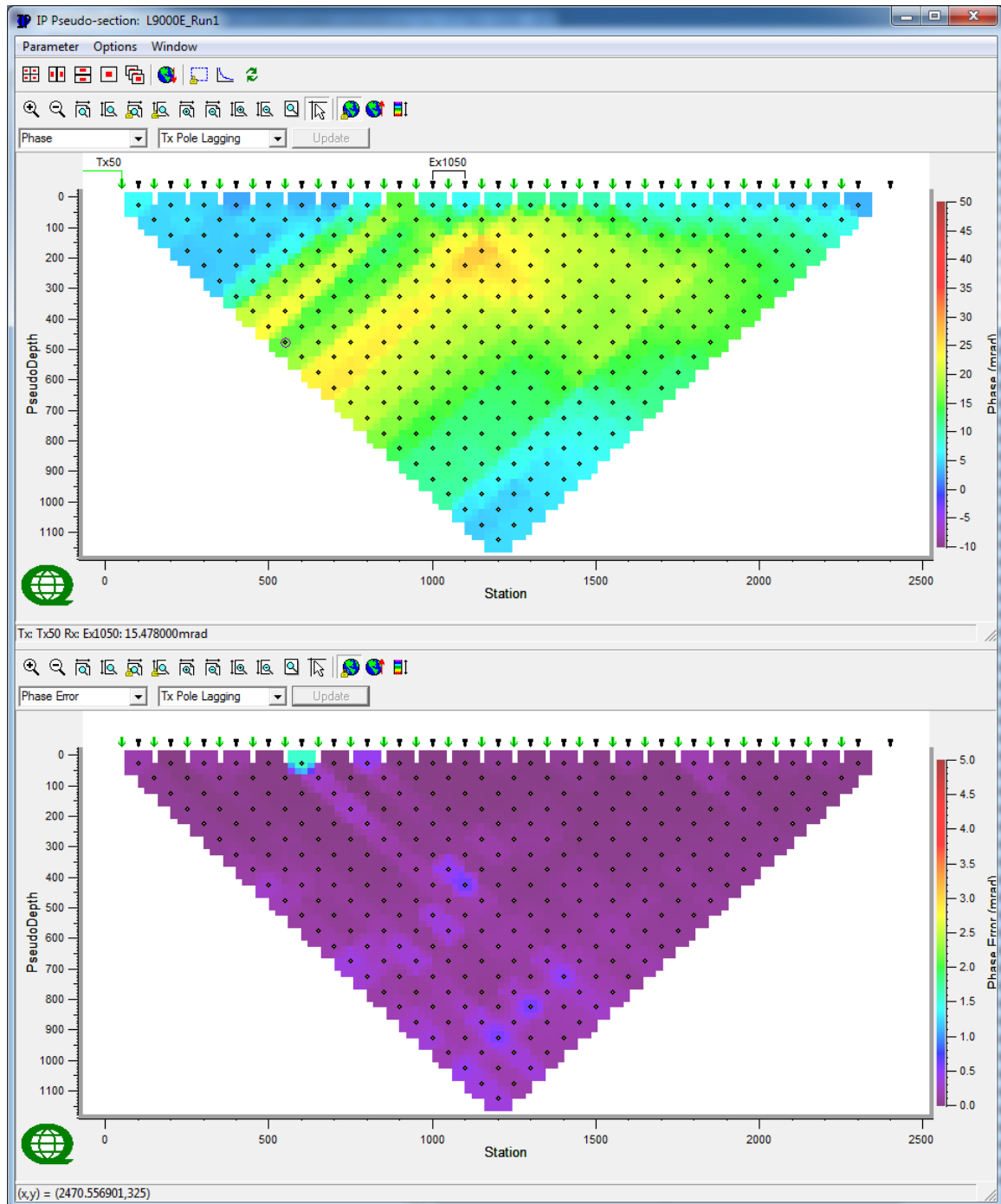
Line 9E – Observed Apparent Resistivity Raw Data (Ohm.m) & Voltage Errors (%) -Tx Pole Lagging.

☐ Tx with more than one event



Line 9E – Observed IP Raw Data (mrad) & IP Errors (mrads)-Tx Pole Leading.

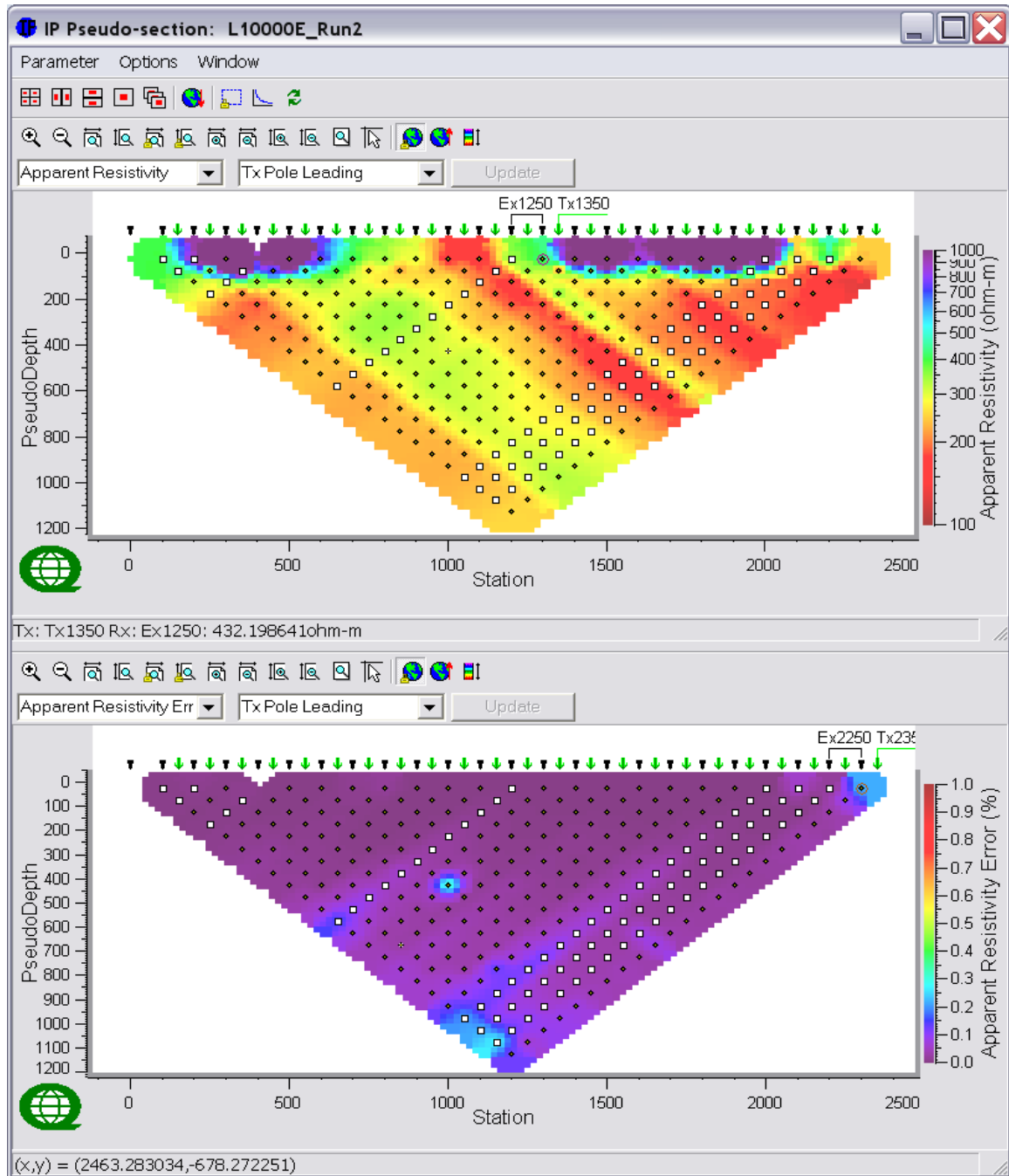
□ Tx with more than one event



Line 9E – Observed IP Raw Data (mrad) & IP Errors (mrads)-Tx Pole Lagging.

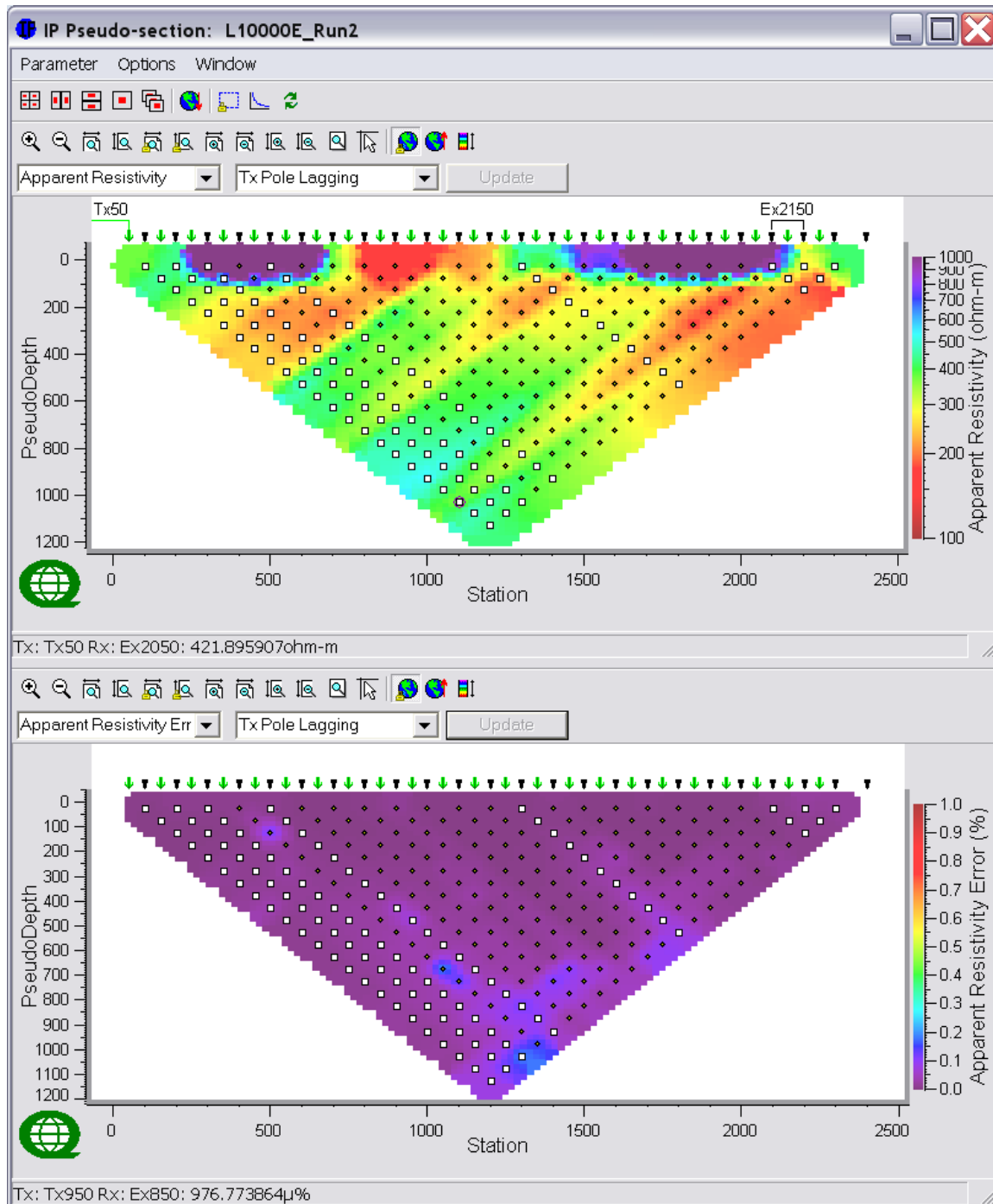
☐ Tx with more than one event

C.10 LINE 10E



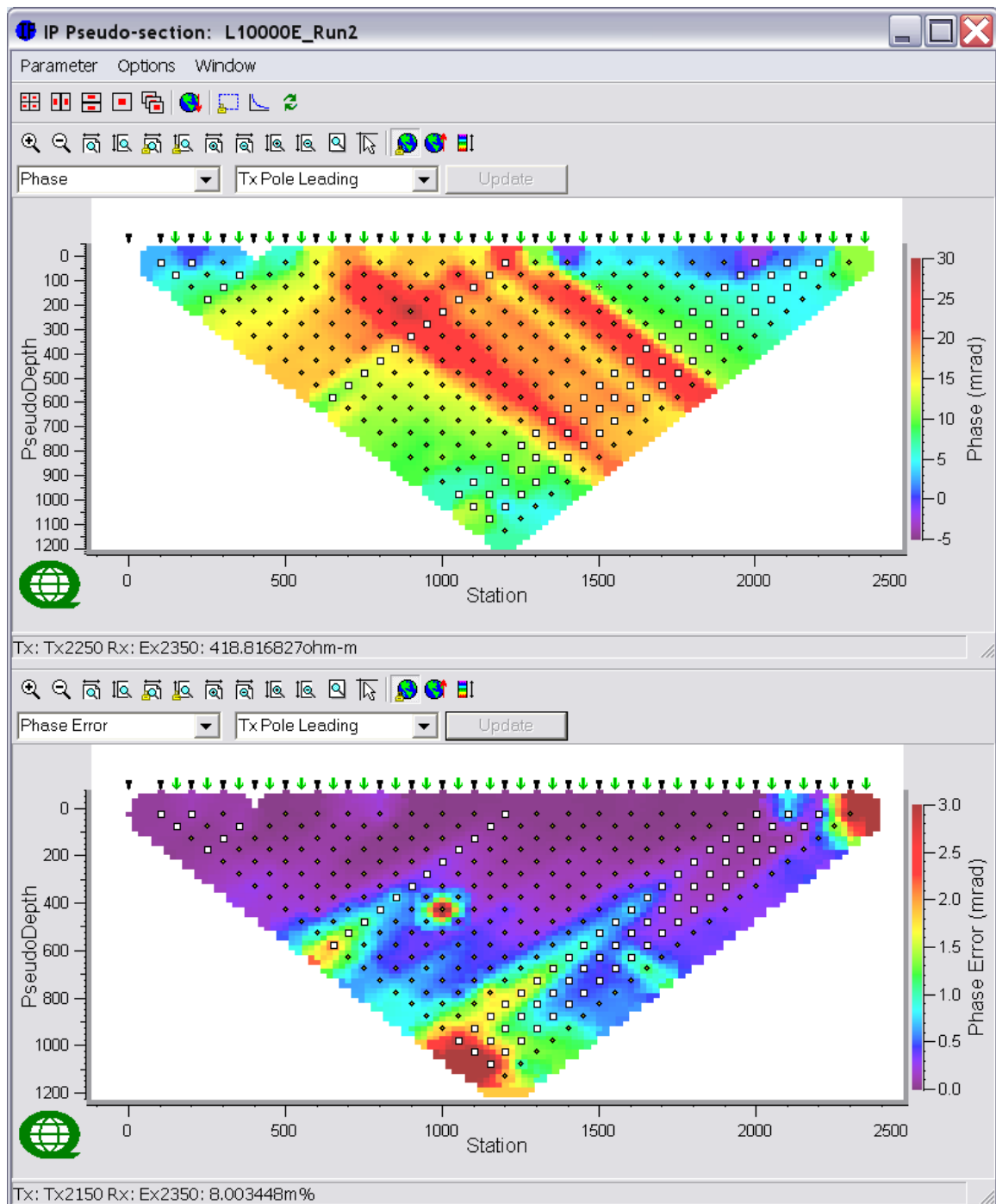
Line 10E – Observed Apparent Resistivity Raw Data (Ohm.m) & Voltage Errors (%) -Tx Pole Leading.

□ Tx with more than one event



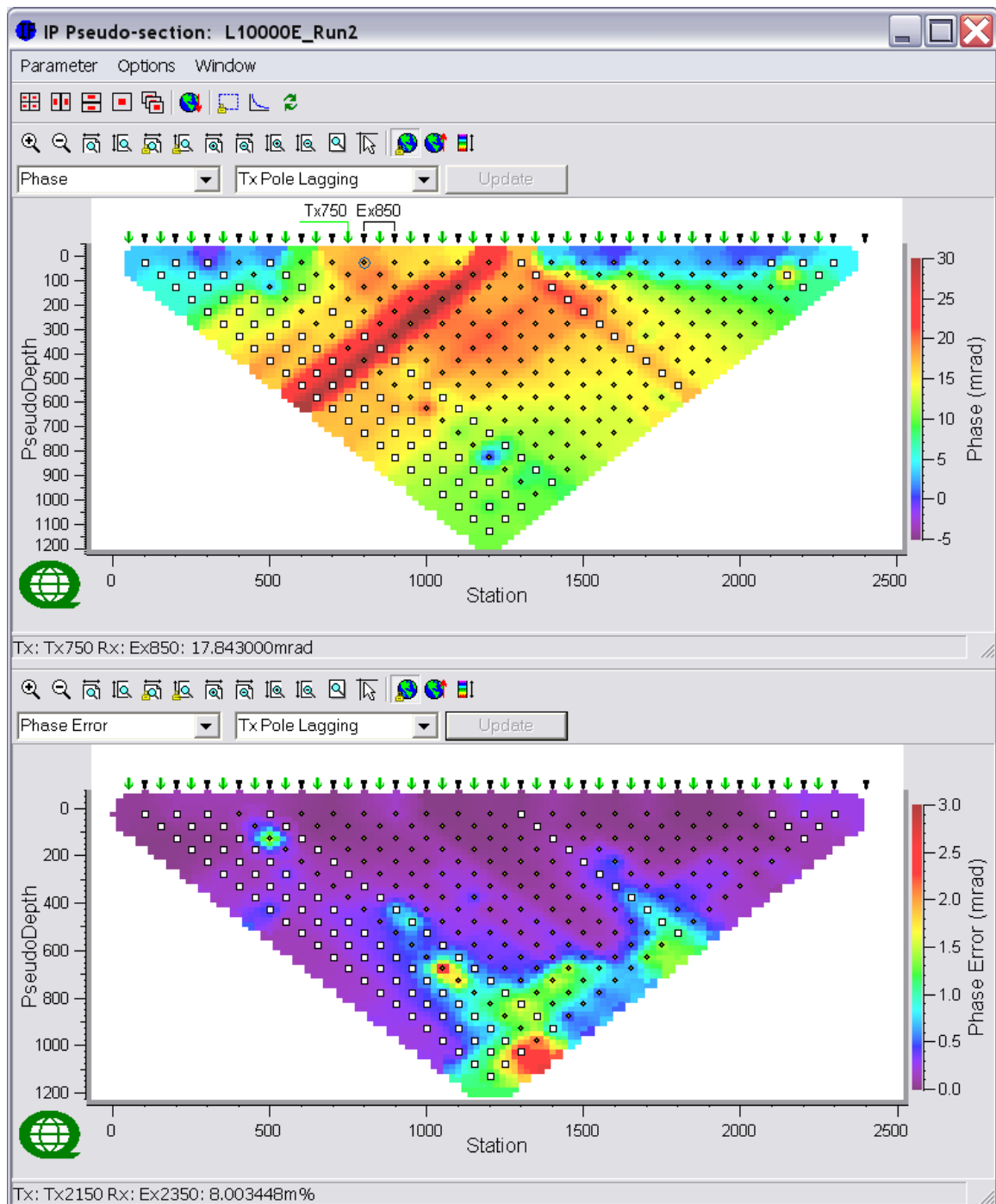
Line 10E – Observed Apparent Resistivity Raw Data (Ohm.m) & Voltage Errors (%) -Tx Pole Lagging.

□ Tx with more than one event



Line 10E – Observed IP Raw Data (mrad) & IP Errors (mrads)-Tx Pole Leading.

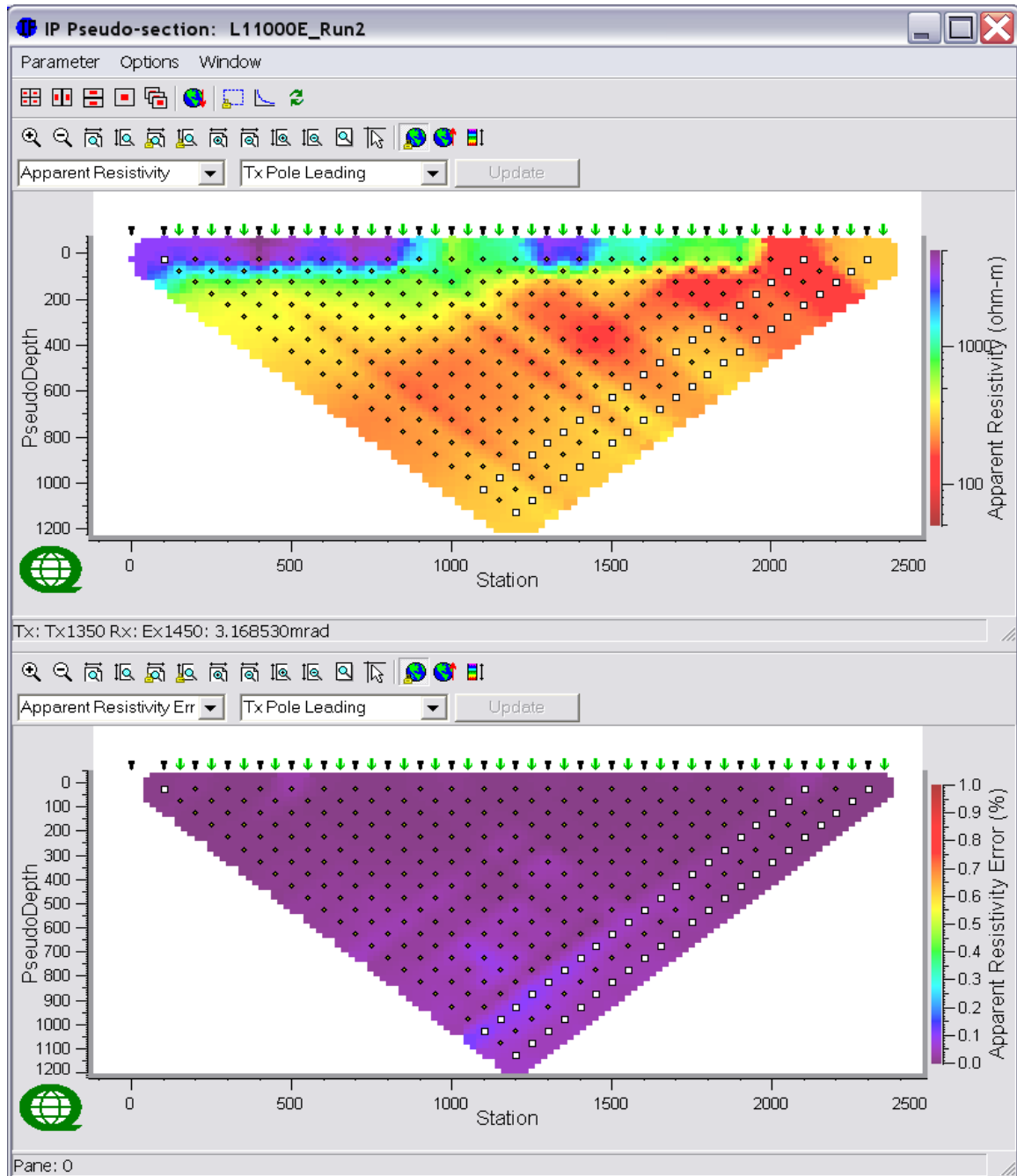
☐ Tx with more than one event



Line 10E – Observed IP Raw Data (mrad) & IP Errors (mrads)-Tx Pole Lagging.

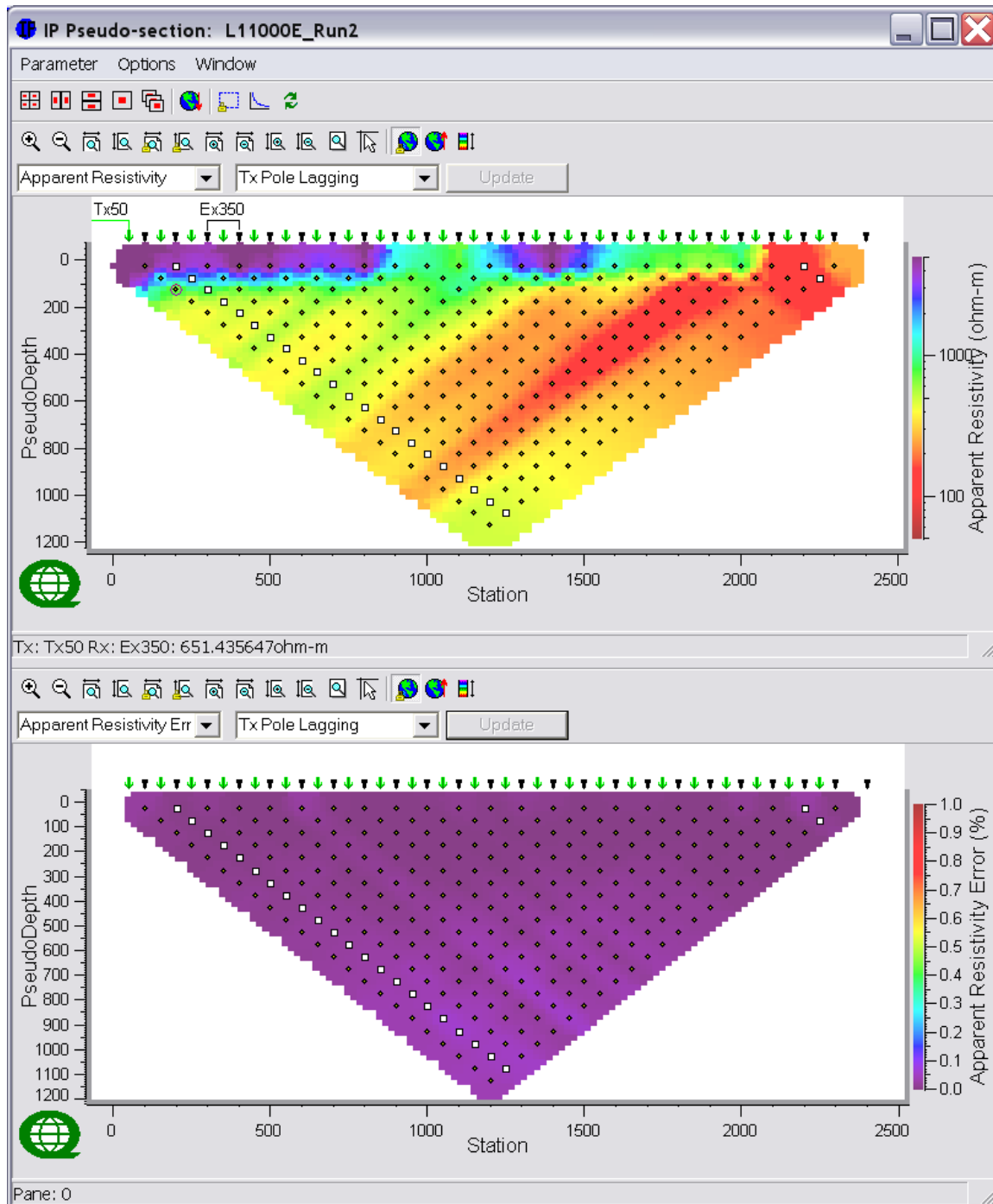
□ Tx with more than one event

C.11 LINE 11E



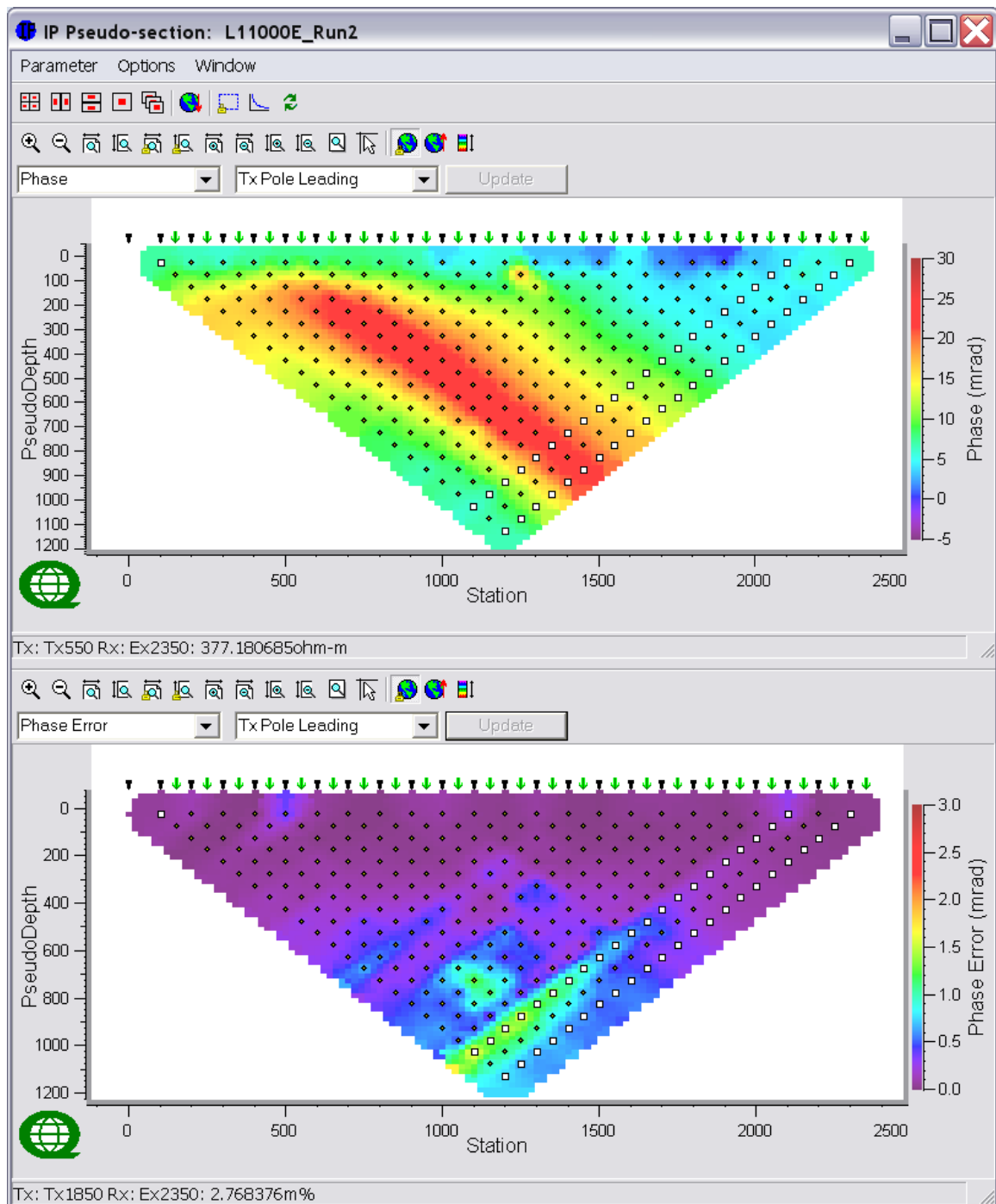
Line 11E – Observed Apparent Resistivity Raw Data (Ohm.m) & Voltage Errors (%) -Tx Pole Leading.

□ Tx with more than one event



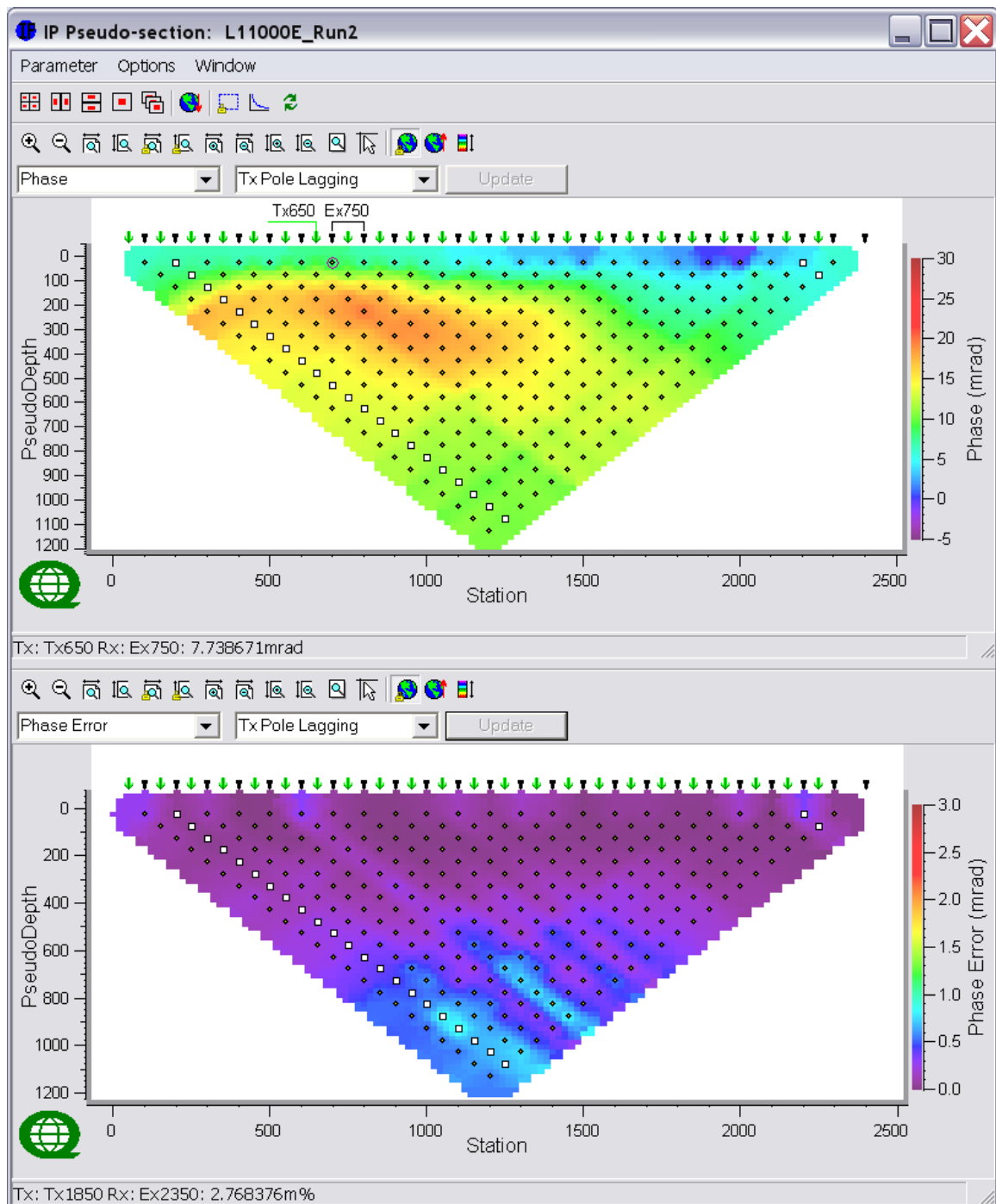
Line 11E – Observed Apparent Resistivity Raw Data (Ohm.m) & Voltage Errors (%) -Tx Pole Lagging.

□ Tx with more than one event



Line 11E – Observed IP Raw Data (mrad) & IP Errors (mrads)-Tx Pole Leading.

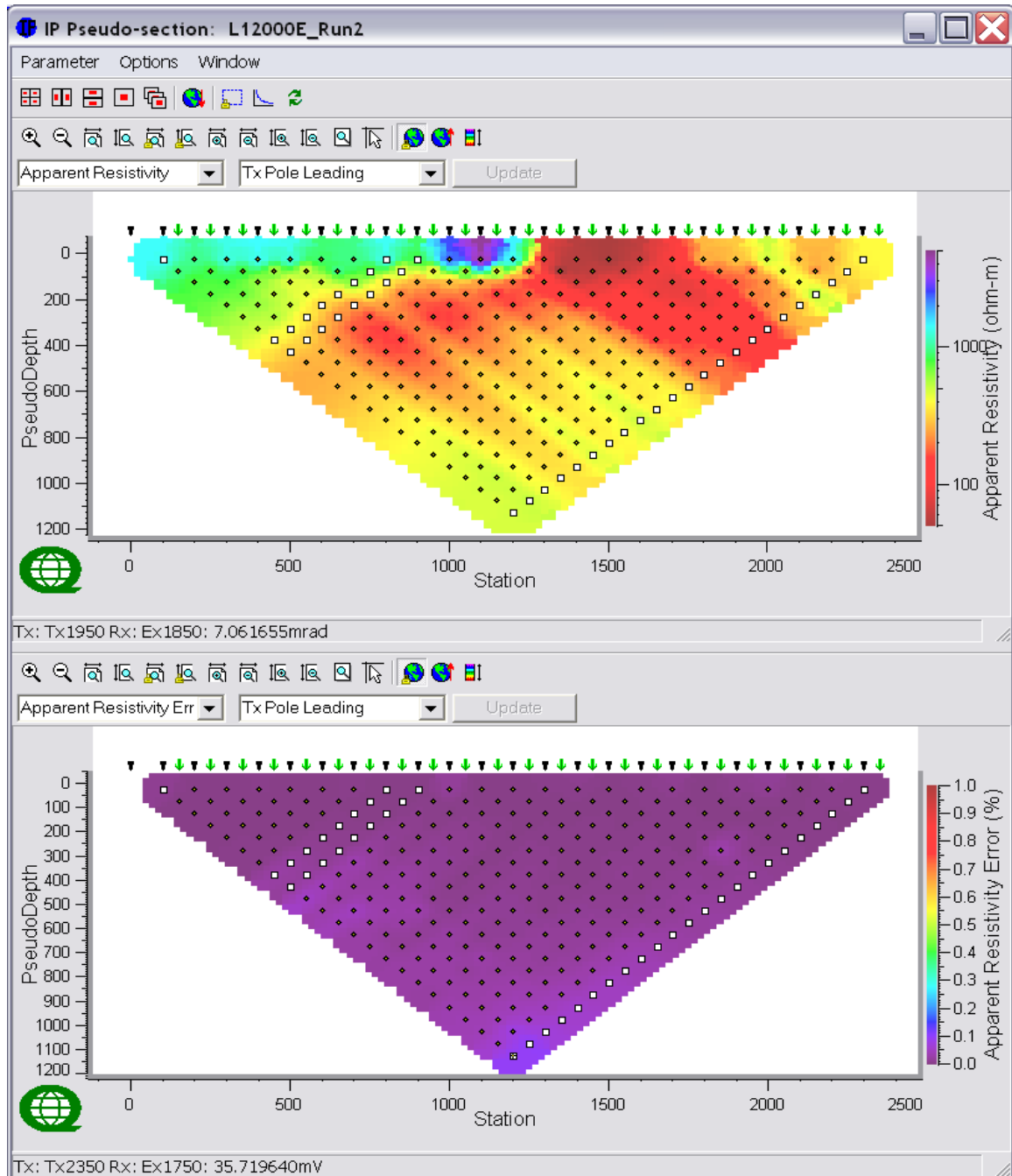
□ Tx with more than one event



Line 11E – Observed IP Raw Data (mrad) & IP Errors (mrads)-Tx Pole Lagging.

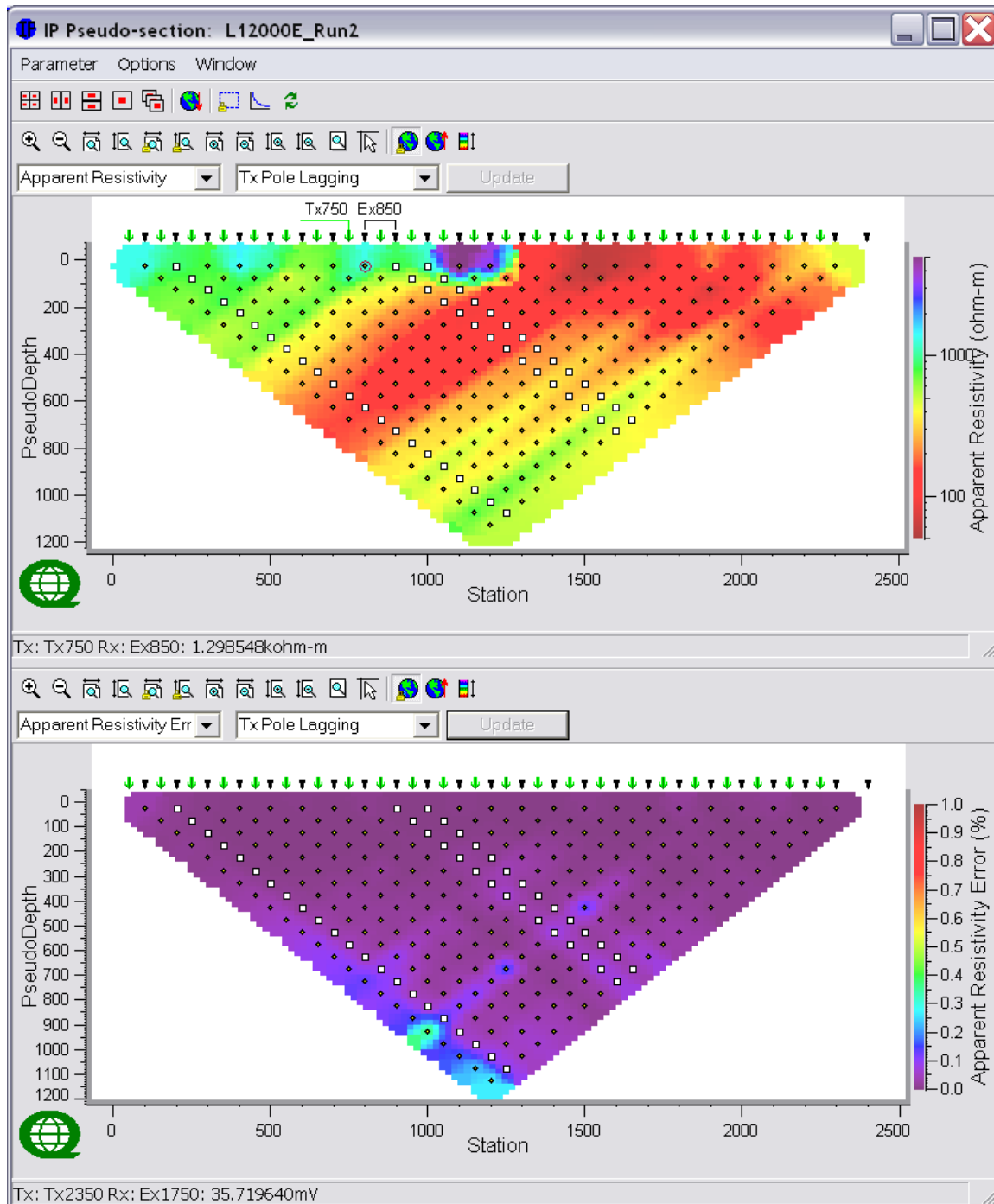
□ Tx with more than one event

C.12 LINE 12E



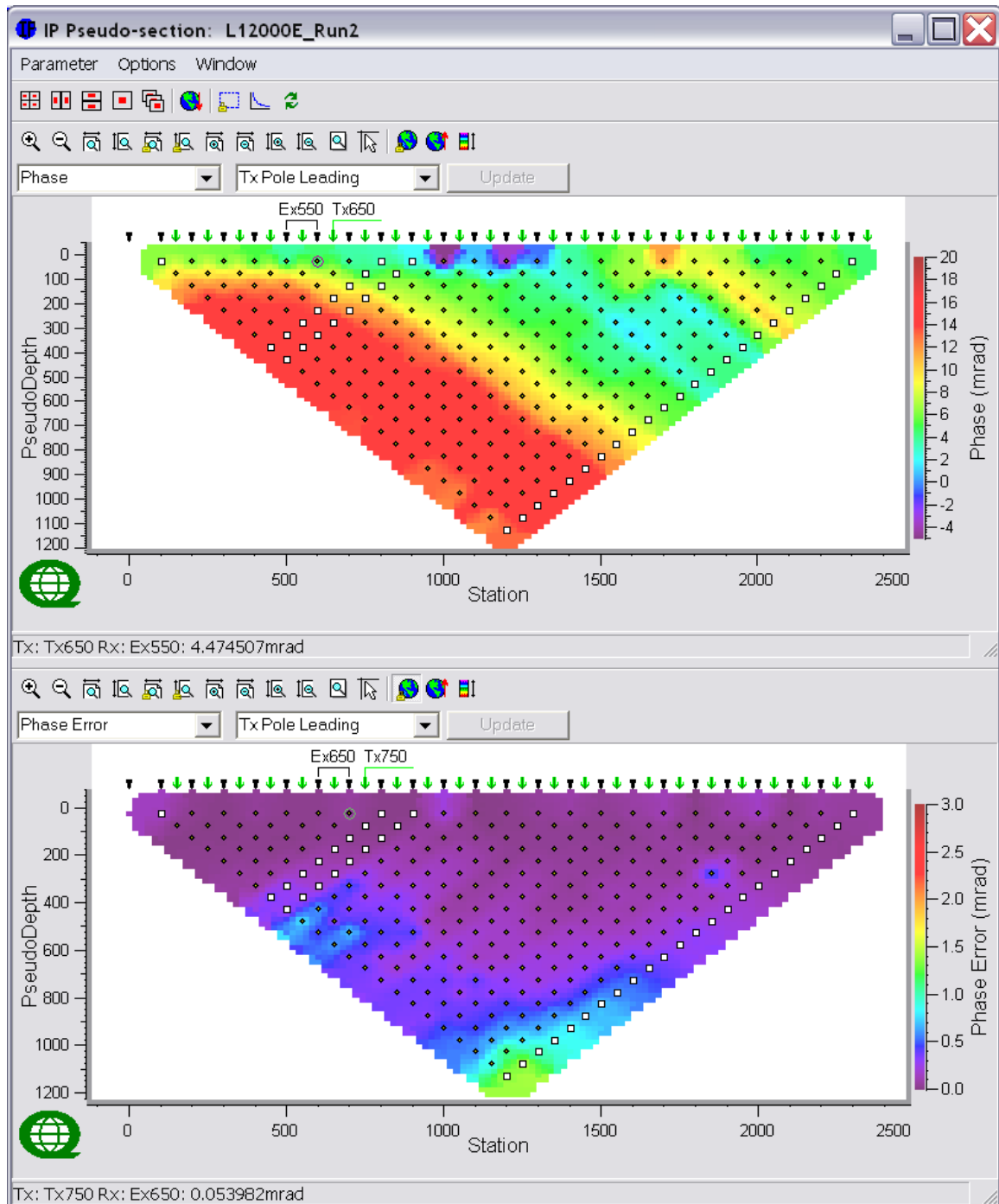
Line 12E – Observed Apparent Resistivity Raw Data (Ohm.m) & Voltage Errors (%) -Tx Pole Leading.

□ Tx with more than one event



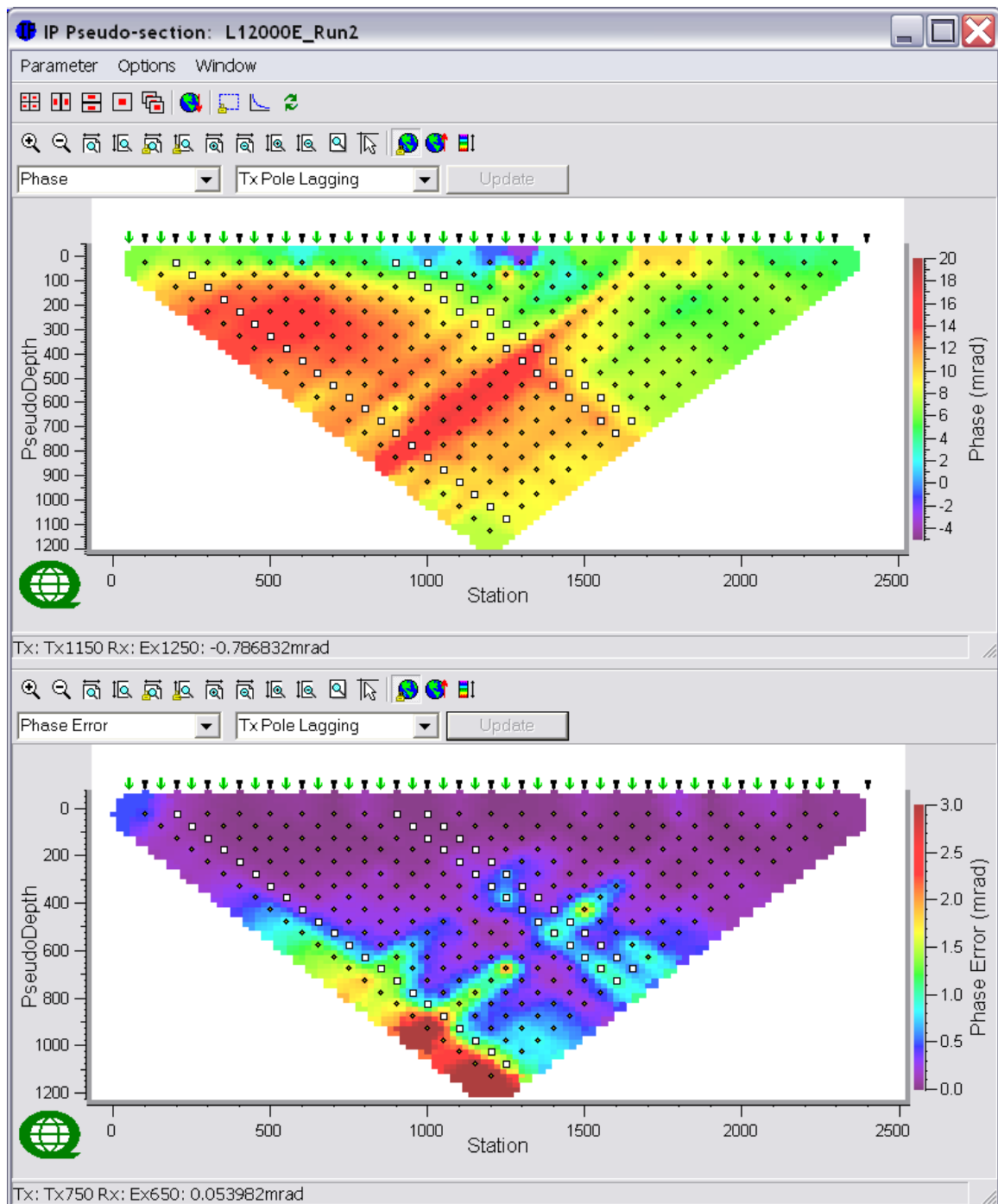
Line 12E – Observed Apparent Resistivity Raw Data (Ohm.m) & Voltage Errors (%) -Tx Pole Lagging.

□ Tx with more than one event



Line 12E – Observed IP Raw Data (mrad) & IP Errors (mrads)-Tx Pole Leading.

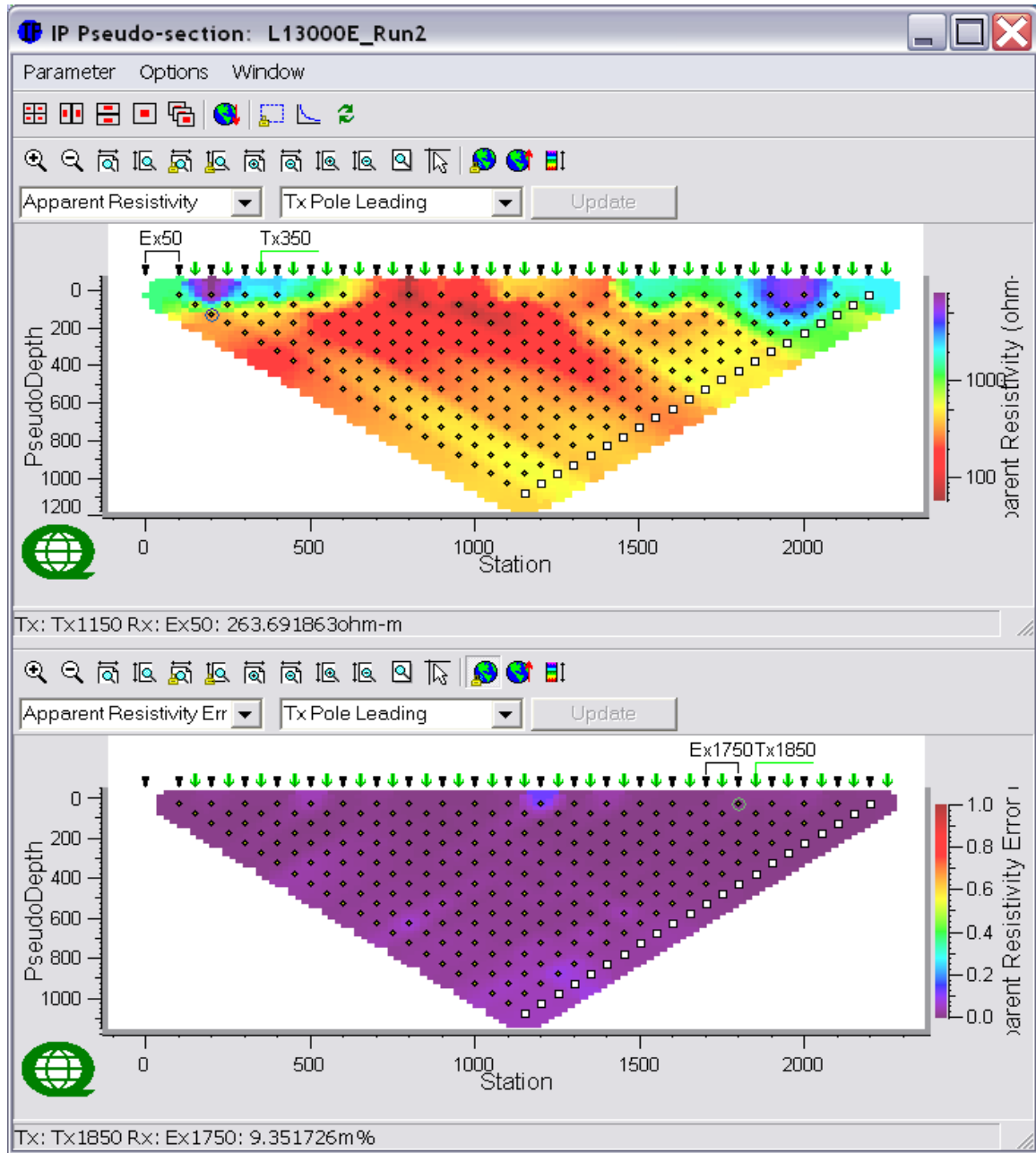
□ Tx with more than one event



Line 12E – Observed IP Raw Data (mrad) & IP Errors (mrads)-Tx Pole Lagging.

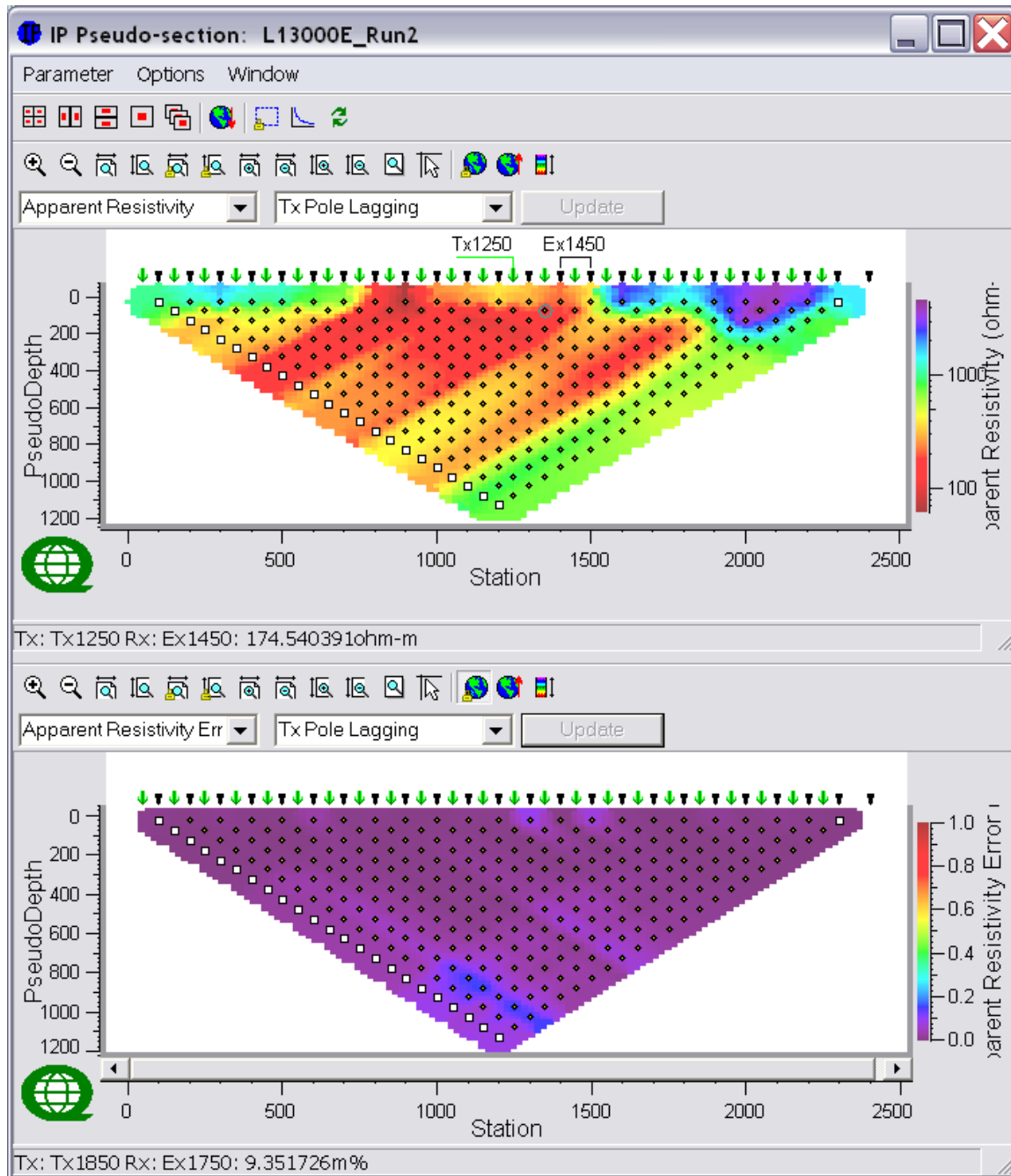
□ Tx with more than one event

C.13 LINE 13E



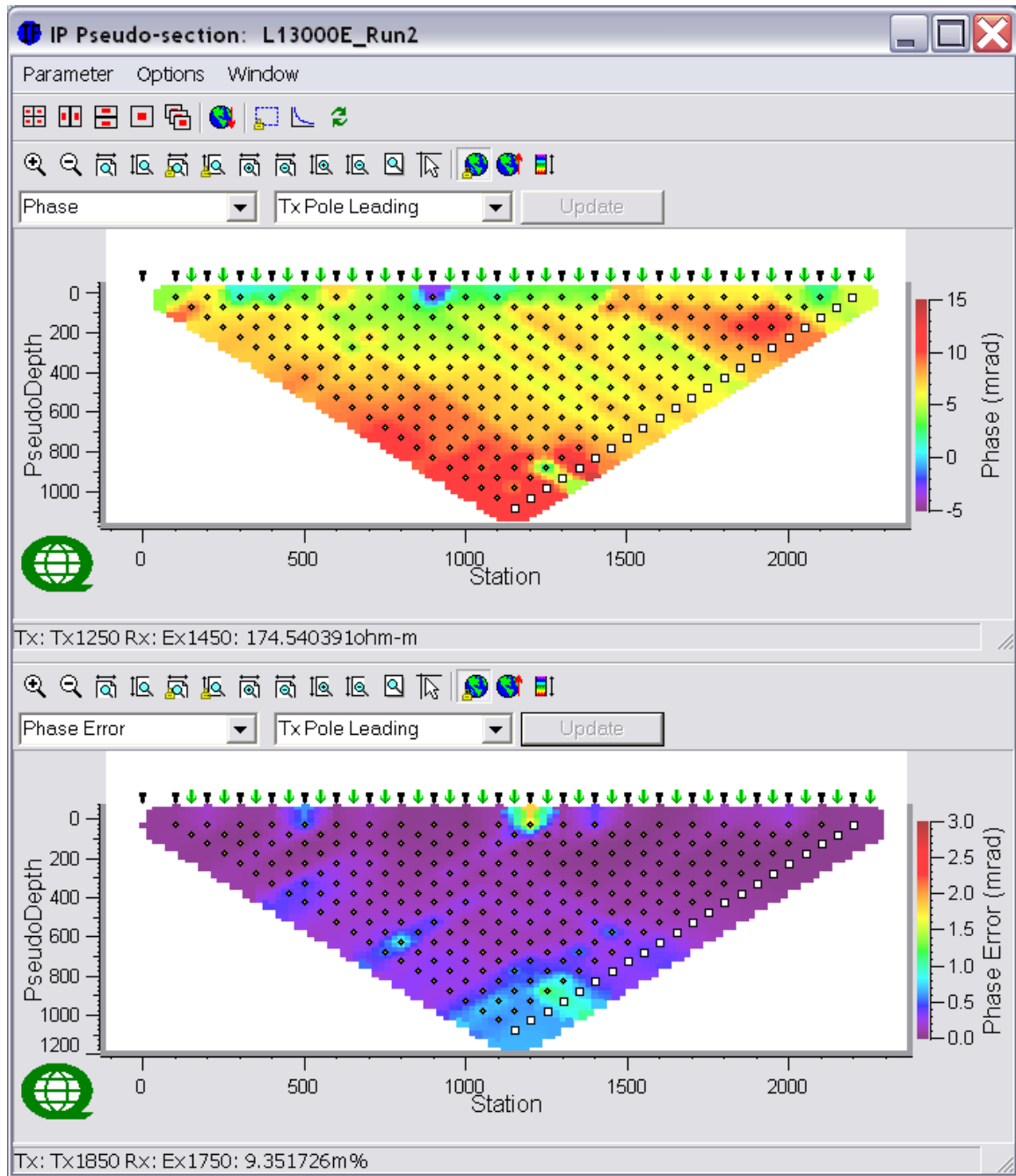
Line 13E – Observed Apparent Resistivity Raw Data (Ohm.m) & Voltage Errors (%) -Tx Pole Leading.

□ Tx with more than one event



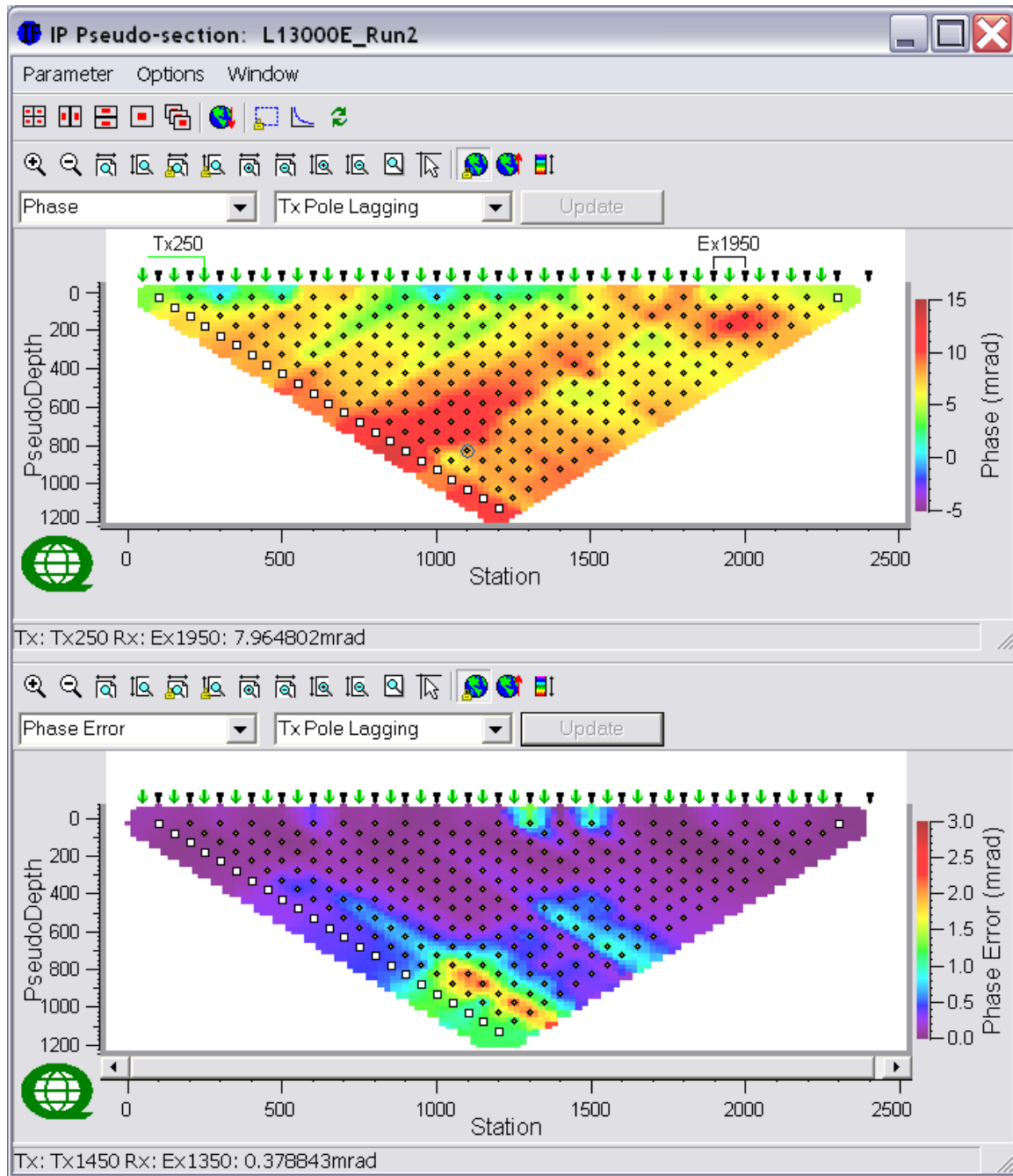
Line 13E – Observed Apparent Resistivity Raw Data (Ohm.m) & Voltage Errors (%) -Tx Pole Lagging.

□ Tx with more than one event



Line 13E – Observed IP Raw Data (mrad) & IP Errors (mrads)-Tx Pole Leading.

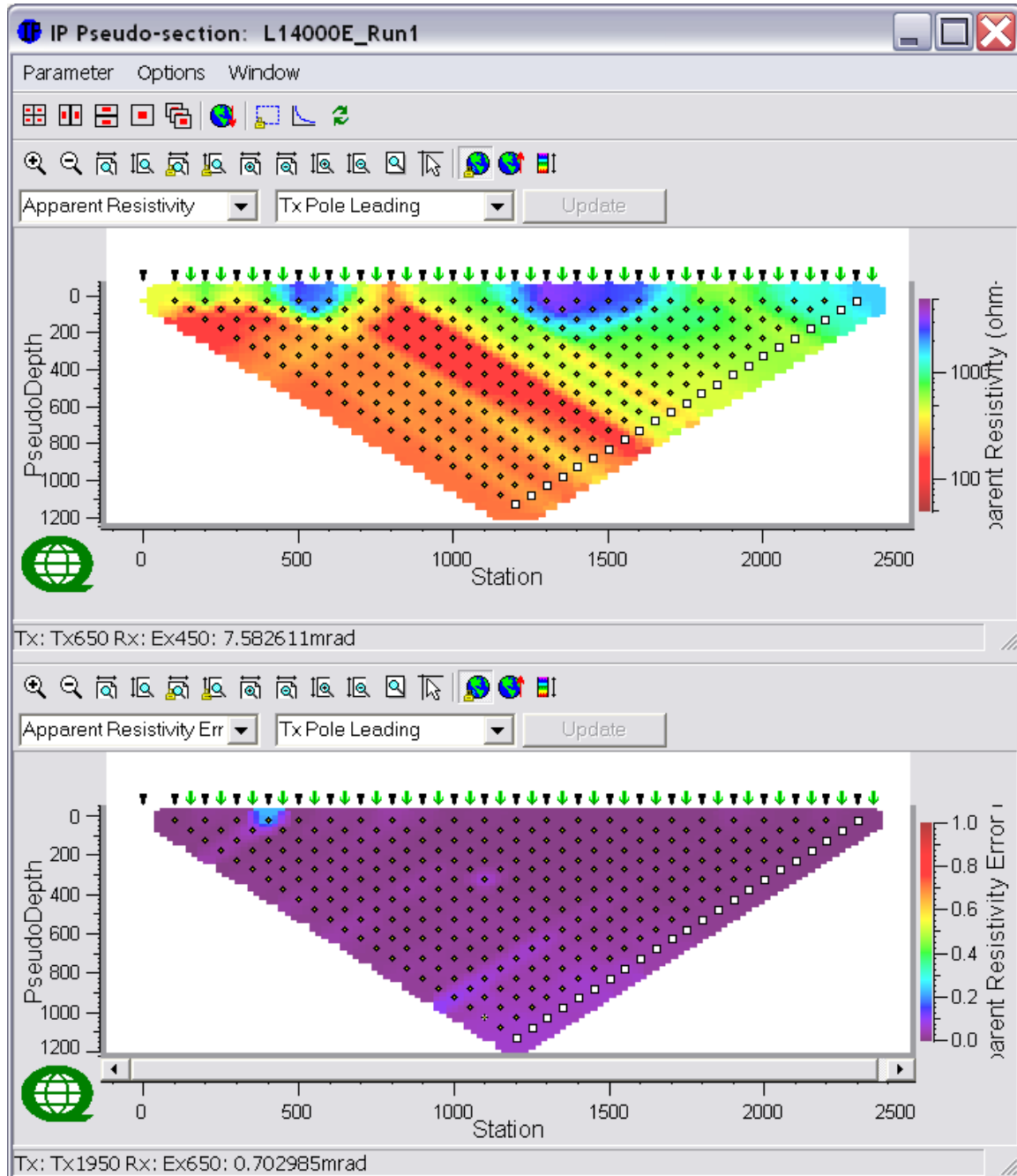
□ Tx with more than one event



Line 13E – Observed IP Raw Data (mrad) & IP Errors (mrads)-Tx Pole Lagging.

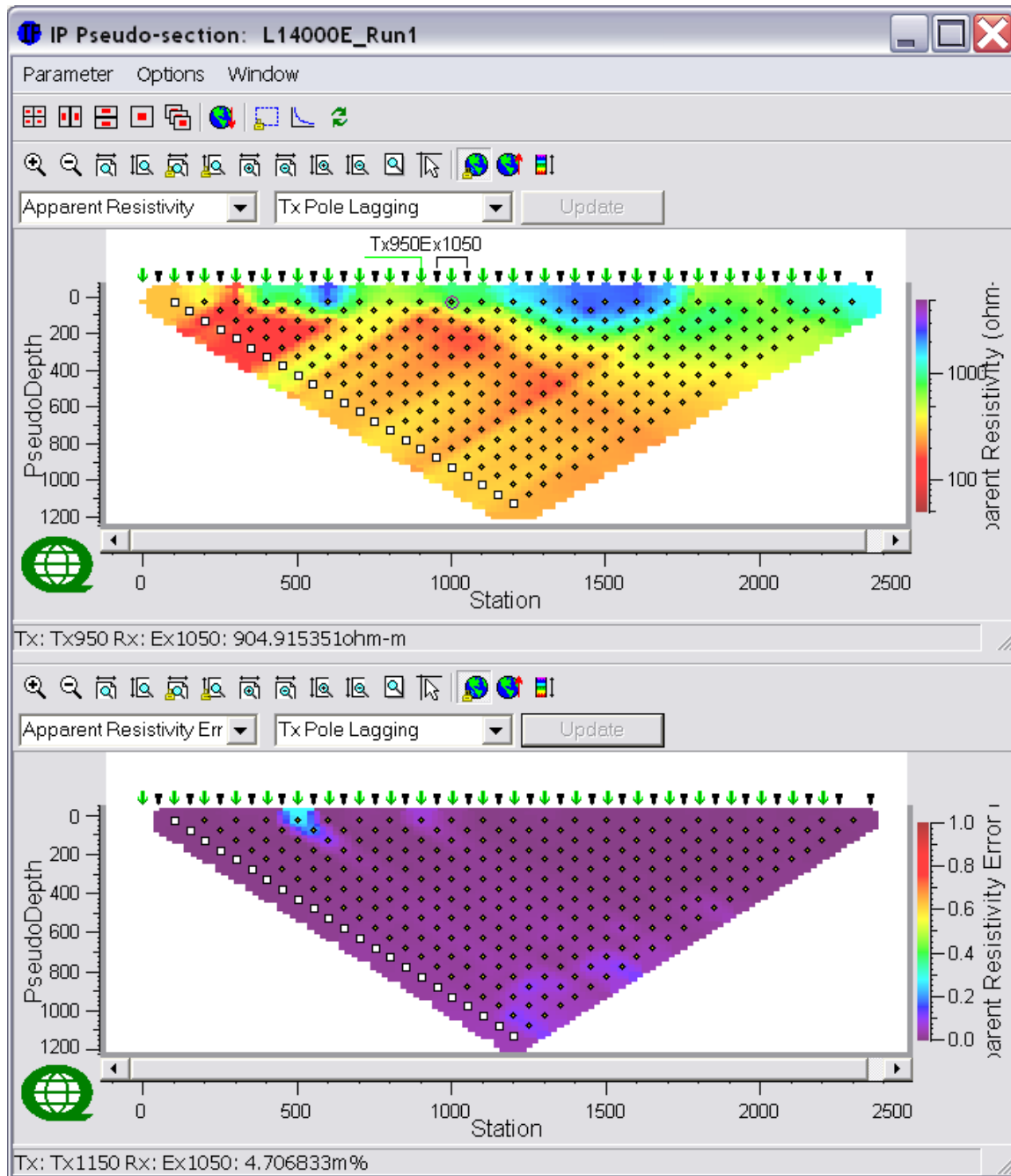
□ Tx with more than one event

C.14 LINE 14E



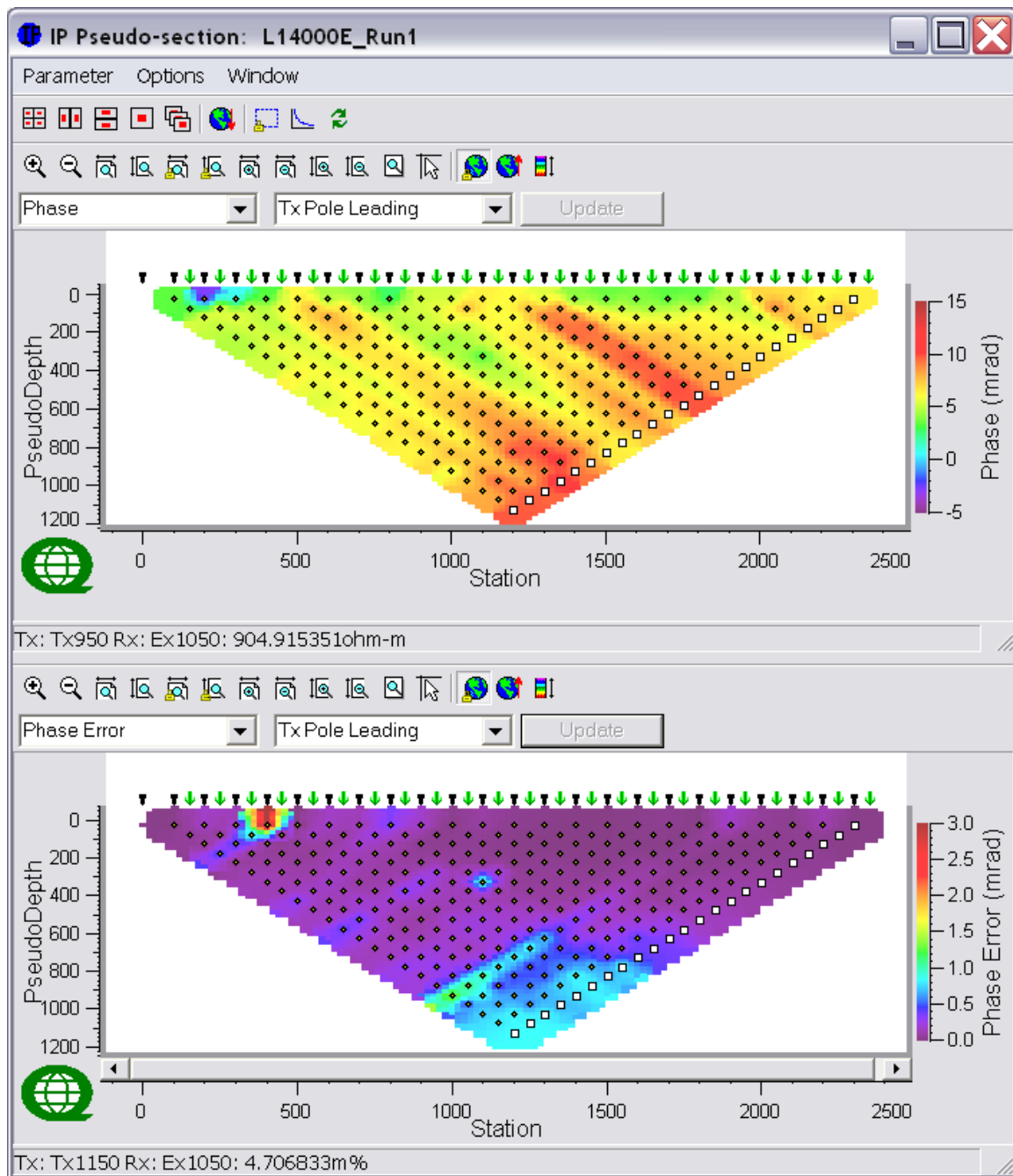
Line 14E – Observed Apparent Resistivity Raw Data (Ohm.m) & Voltage Errors (%) -Tx Pole Leading.

☐ Tx with more than one event



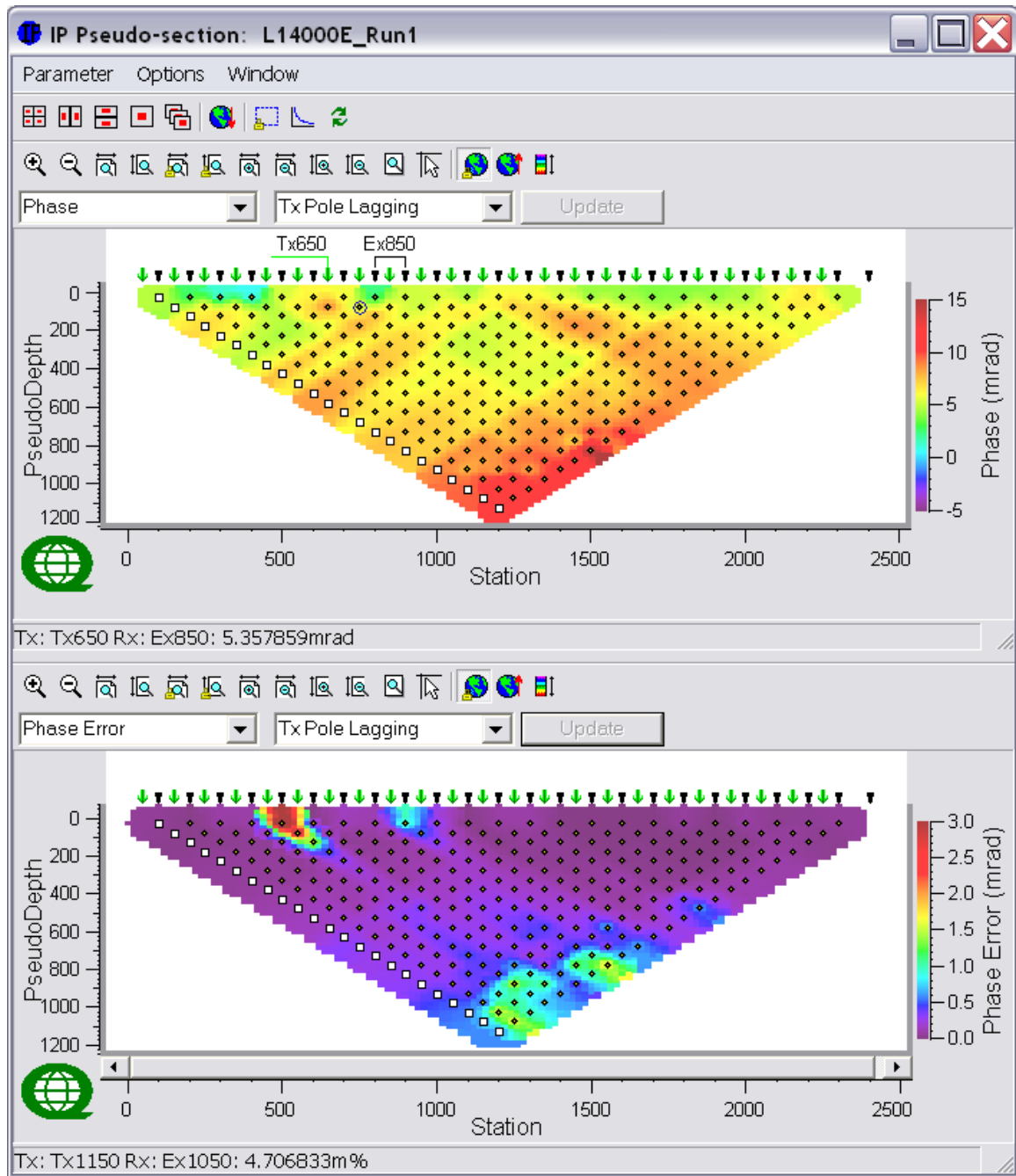
Line 14E – Observed Apparent Resistivity Raw Data (Ohm.m) & Voltage Errors (%) -Tx Pole Lagging.

□ Tx with more than one event



Line 14E – Observed IP Raw Data (mrad) & IP Errors (mrads)-Tx Pole Leading.

☐ Tx with more than one event



Line 14E – Observed IP Raw Data (mrad) & IP Errors (mrads)-Tx Pole Lagging.

□ Tx with more than one event

D INSTRUMENTS SPECIFICATIONS

D.1 REF TEK – 120 DATA ACQUISITION SYSTEM

Refraction Technology Inc. – Plano, Texas

Specifications:

| Specification | Description |
|-----------------------------|---|
| Physical | |
| Size: | 267 x 248 x 184 mm 10.5 x 9.75 x 7.25 in. |
| Weight: | 3.7kg 305 g 8 lbs (2-Channels maximum weight)) |
| Temperature: | -40°C to 60°C operating range. |
| Environmental: | Operates in 1m of water without leaking for 48 hours. Airtight to 1.0 psi. |
| Shock: | Remains operational after 1m drop (any corner) onto cement floor. |
| Connectors | |
| Line A & Line B: | A pair of identical 10 pin U77/U style connectors. Each connector provides 3 pairs of lines (+): A (+)/B (-) Receive telemetry data and/or commands C (+)/D (-) Transmit telemetry data and/or commands E (+)/F (-) Sync |
| Power: | PT07A12-8S style connector. Provides input +12 VDC supplied from battery. |
| Sensor: | PU283/U style connector. Provides for a direct connection from the AM to the sensor. |
| Power Requirements | |
| Battery: | Two 12 volt lead acid battery (7 Ah). |
| Signal Input | |
| Input Impedance: | 10 megohms, 330pF, differential |
| Broadband Dynamic Range: | 130dB (noise power ratio test @ 125 sample per second [sps]) |
| ADC Type: | Delta-sigma modulation |
| Sample Rate: | Multiple 50 to 48,000 |
| Gain Settings: | Four – programmable for 1, 4, 16 and 64. |

| Specification | Description | | | | |
|----------------------------|--|-----------------------|----------|----------------------|----------|
| Sensor Input Signal Range: | Gain | 24-Bit High Speed A/D | | 24-Bit Low Speed A/D | |
| | | Actual | Reported | Actual | Reported |
| | 1 | 1.192μV | 78.12mV | 1.907μV | 125.0mV |
| | 4 | 298.0nV | 19.53mV | 476.8nV | 31.25mV |
| | 16 | 74.51nV | 4.883mV | 119.2nV | 7.812mV |
| | 64 | 18.63nV | 1.221mV | 29.80nV | 1.953mV |
| Data Storage | | | | | |
| Data Size: | 32-bit two's compliment. | | | | |
| Base Memory: | 128K EPROM 6.5Mb SRAM | | | | |
| Base Capacity: | Better than 1.5 million samples or approximately 3 hours 10 minutes continuous data @ 125 sps. | | | | |
| AM Telemetry | | | | | |
| Protocol: | Full duplex synchronous data link control (SDLC). | | | | |
| Error Correction: | Packet acknowledge with modulo 8 sliding window. | | | | |
| Speed | 3.072Mb/second | | | | |
| Encoding: | Bi-phase pulse = 1, missing pulse = 0 | | | | |
| Line Impedance: | 100 Ohm | | | | |
| Synchronization | | | | | |
| Timing: | Each AM on-line is timed and synchronized for simultaneous sampling within + 1.50 μsecond. | | | | |
| Protection | | | | | |
| Electrical Protection: | Line A and Line B signals circuits are protect by: - A surge arrestor located on the RT514 board (SS1-14). - A line isolation transformer located on the RT514 board (T1-6) with over-voltage diodes (D1-4) on both sides of each secondary windings | | | | |
| State-of-Health | | | | | |
| Information Provided: | The AM reports information on battery status, clock setting, gain setting, calibration mode and the communications link. | | | | |

Acquisition Parameters

Acquisition parameters include the sample rate, transmitter frequency and number of samples desired. The operator can also determine whether the AMs calibration signal is activated during data collection.

In typical use, the acquisition parameters are set according to the specific application configuration and event type. For each event type, several recording sessions are made, each at a different transmitter frequency and sample rate. The recording period is set based on event type and transmitter frequency.

The listing below shows several examples of event type, typical transmitter frequency (Hz), sample rates (with applicable ADC resolution) and the corresponding number of samples (record period).

| Event Type | Transmit Frequency | Sample Rate | ADC Resolution | Number of Sample |
|----------------------|--------------------|-------------|----------------|------------------|
| Geophysical Response | 375 Hz | 48,000 | 24 | 124,032 |
| Gain Test | 375 | 48,000 | 24 | 65,536 |
| Geophysical Response | 75 | 9,600 | 24 | 130,176 |
| Gain Test | 75 | 9,600 | 24 | 65,536 |
| Geophysical Response | 25/8 | 3,200 | 24 | 139,264 |
| Gain Test | 25/8 | 3,200 | 24 | 32,768 |
| Sensor Impedance | N/A | 1,600 | 24 | 8,704 |
| Ambient Noise | N/A | 1,600 | 24 | 8,192 |
| Geophysical Response | 25/128 | 800 | 24 | 147,456 |
| Gain Test | 25/128 | 800 | 24 | 16,384 |
| Geophysical Response | 25/2048 | 100 | 24 | 212,992 |
| Gain Test | 25/256 | 100 | 24 | 4,096 |
| Gain Test | N/A | 50 | 24 | 4,096 |
| Geophysical Response | N/A | 50 | 24 | 65,536 |

Sensor Calibration

The AM can source a 12.5Hz, 50 μ A signal to the sensor input for measuring the source impedance of the attached sensor. The user can also specify frequency in amplitude of calibration signal.

Telemetry Cable

The telemetry cable is a *Category V* specification cable and is supplied by the customer.

Sample Rates

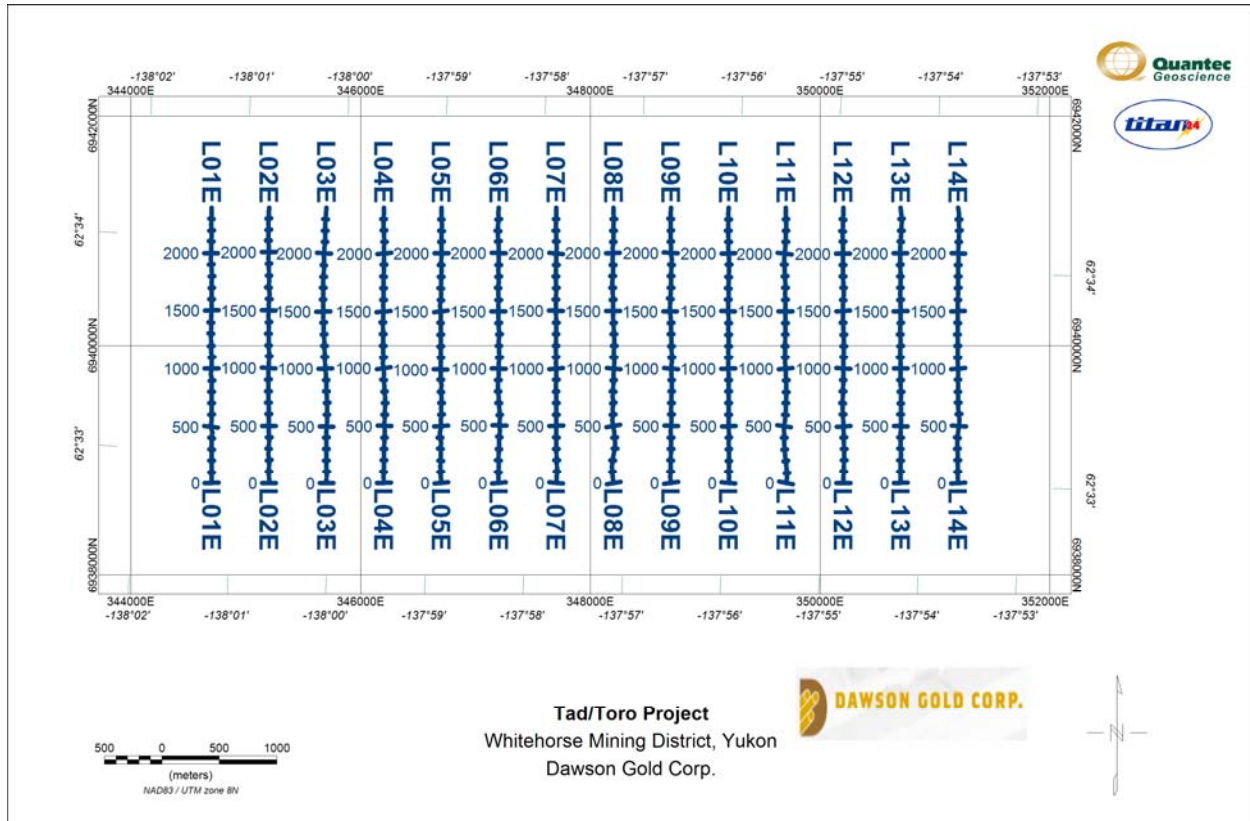
The following table shows all available sample rates, based on a 12.288 Mhz oscillator. A 24-bit resolution ADC is used for sample rates 48000 through 4800 and a 24-bit resolution ADC is used for

sample rates 3200 and below. The correct ADC is selected automatically by the AM, based on the sample rate.

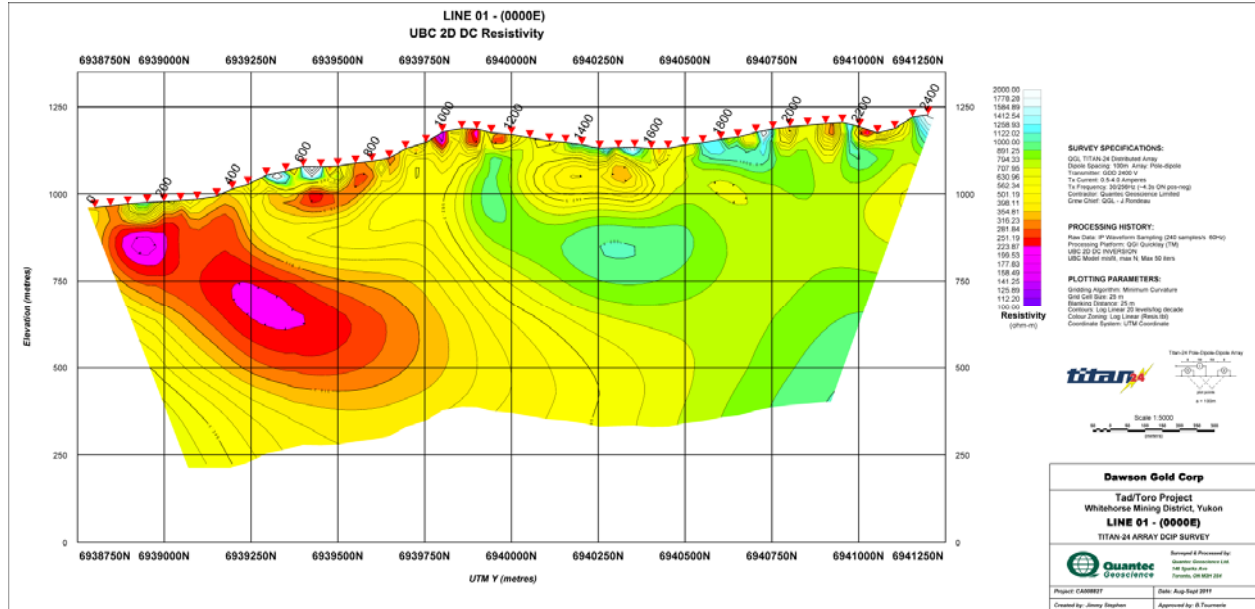
Typically, different sample rates and transmitter frequencies are used in 50 Hz and 60 Hz power environments to minimize AC power effects on the data. In the table, the shaded areas indicate the sample rates typically used in a 60 Hz power environment. A few rates are typically used in both environments.

| Sample Rate | Power Line |
|-------------|------------|
| 48000 | 50 & 60 |
| 24000 | 50 & 60 |
| 19200 | 60 |
| 16000 | 50 |
| 12000 | 50 & 60 |
| 9600 | 50 & 60 |
| 6400 | 50 |
| 4800 | 60 |
| 3200 | 50 |
| 1920 | 60 |
| 1600 | 50 |
| 960 | 60 |
| 800 | 50 |
| 480 | 60 |
| 400 | 50 |
| 240 | 60 |
| 200 | 50 |
| 120 | 60 |
| 100 | 50 |
| 60 | 60 |
| 50 | 50 |
| 60/2 | 60 |
| 50/2 | 50 |
| 60/4 | 60 |
| 50/4 | 50 |
| 60/8 | 60 |
| 50/8 | 50 |
| 60/16 | 60 |
| 50/16 | 50 |
| 60/32 | 60 |
| 50/32 | 50 |

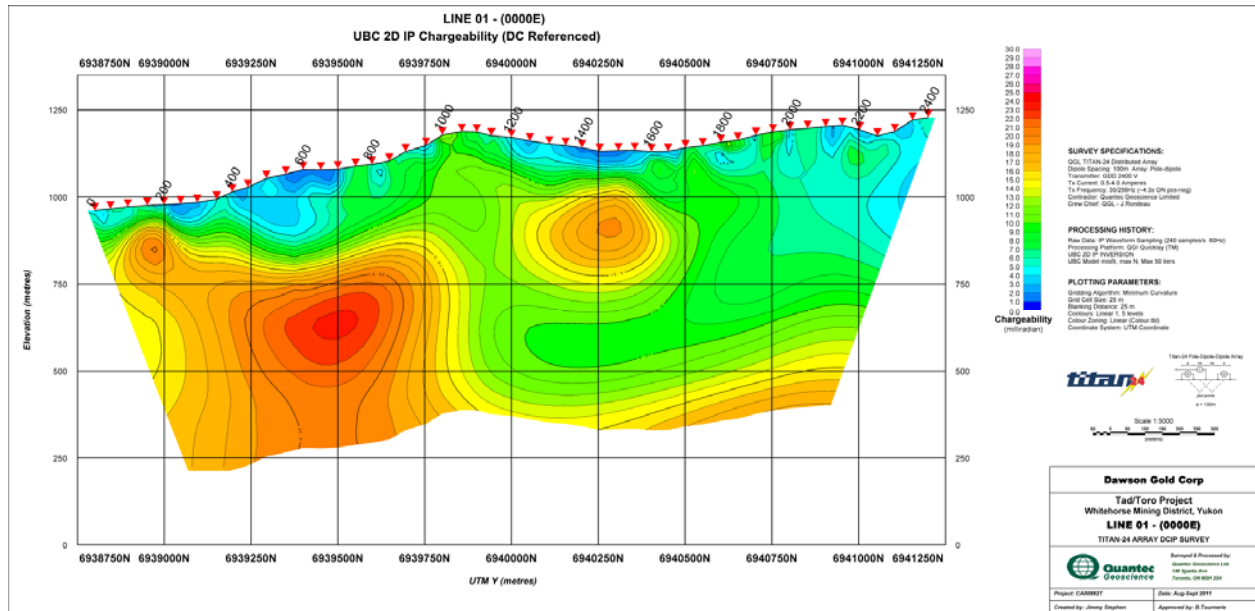
E GEOSOFTECTIONS OF THE 2D MODELS



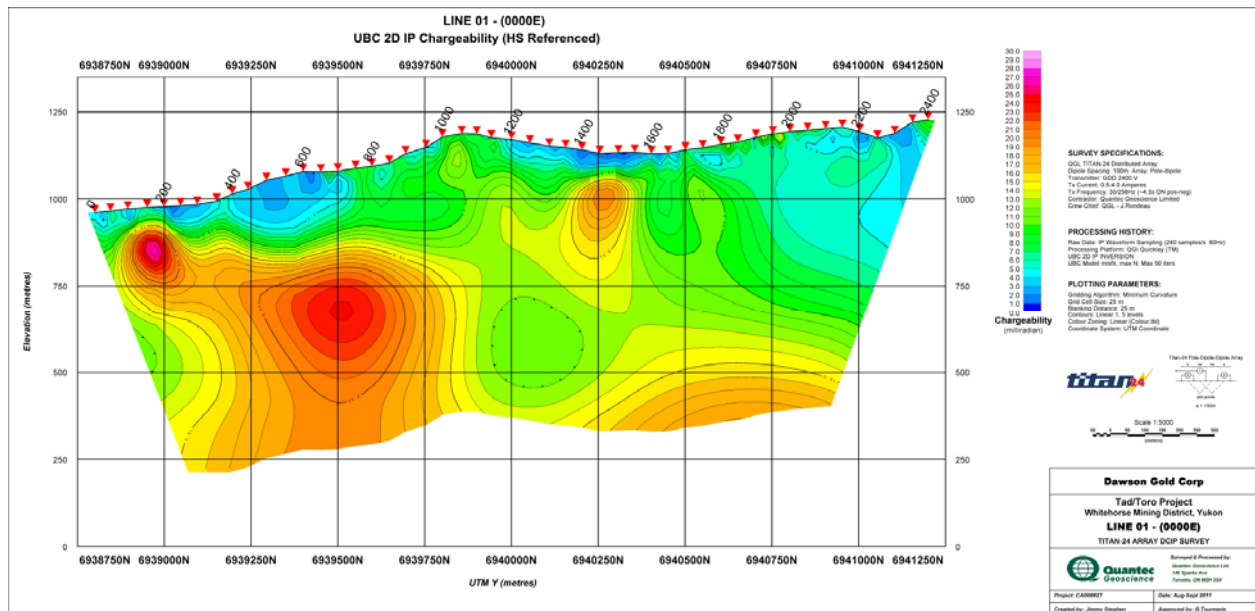
E.1 LINE 01E (0000E)



Line 01E –DC Resistivity 2D Model

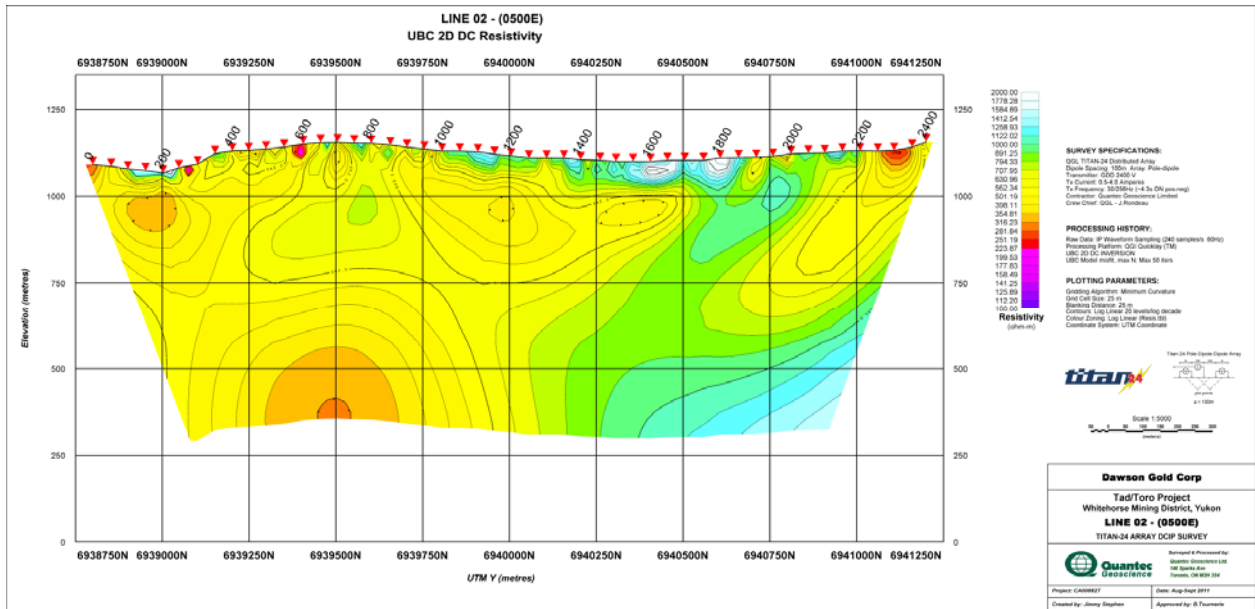


Line 01E –IP Chargeability 2D Model (using DC model as reference)

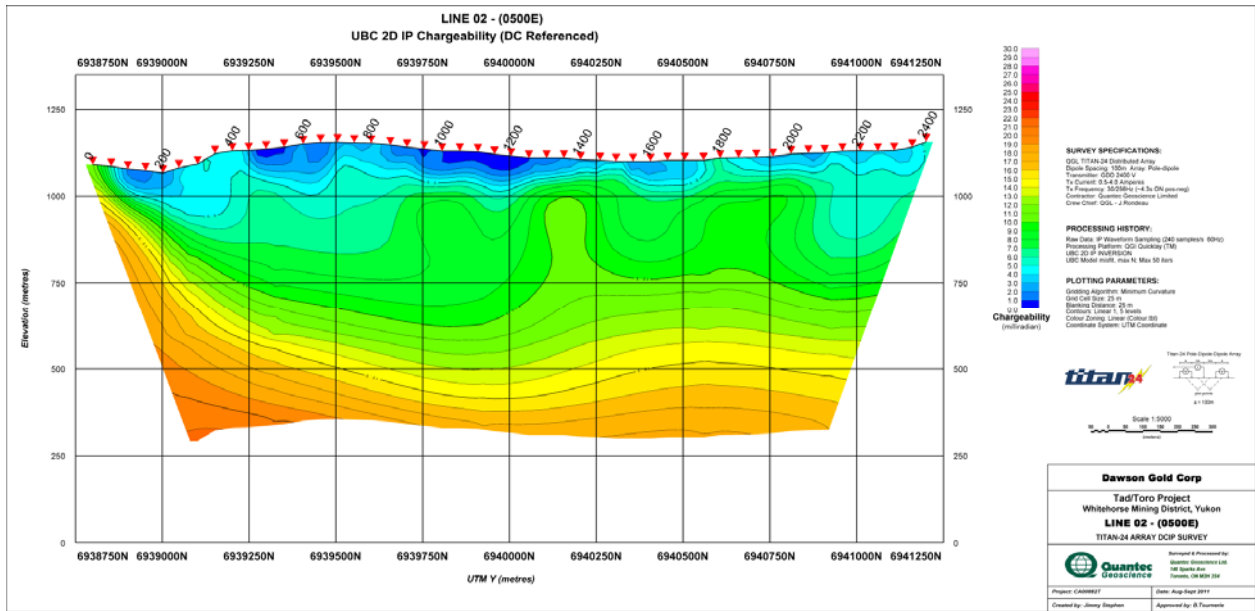


Line 01E –IP Chargeability 2D Model (using Half Space model as reference)

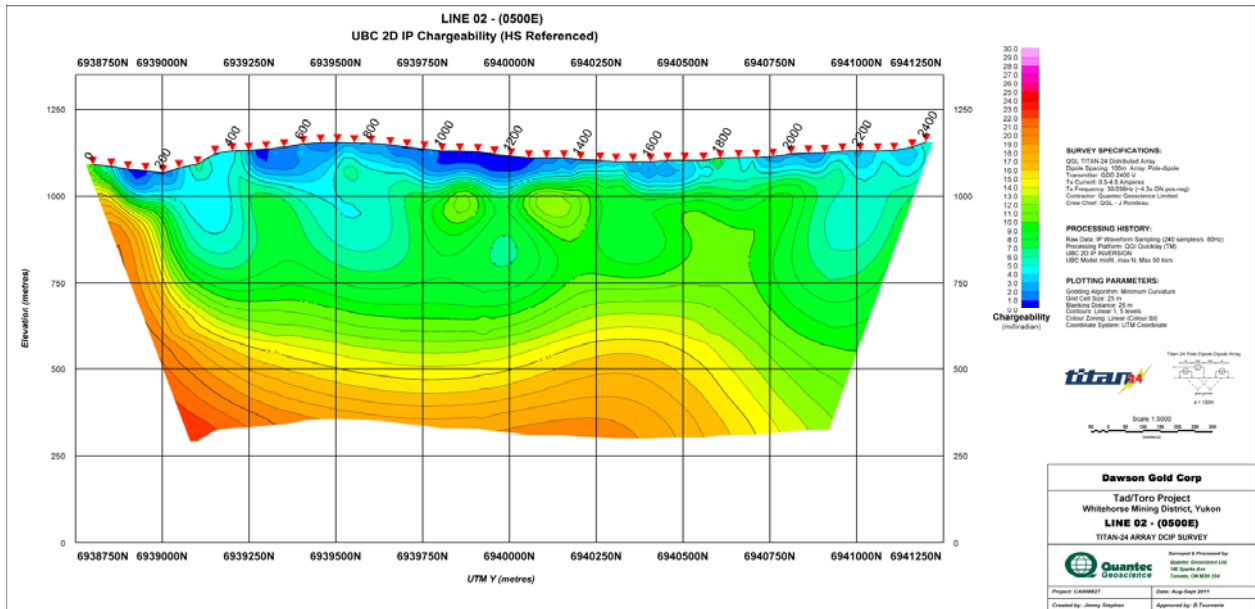
E.2 LINE 02E (0500E)



Line 02E –DC Resistivity 2D Model

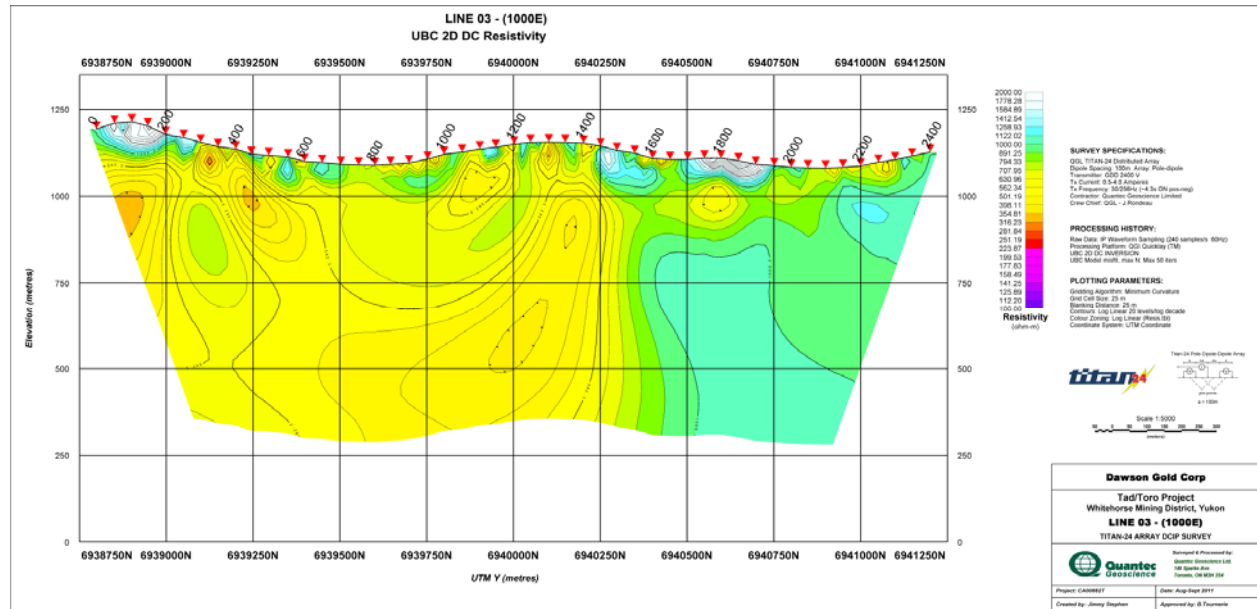


Line 02E –IP Chargeability 2D Model (using DC model as reference)

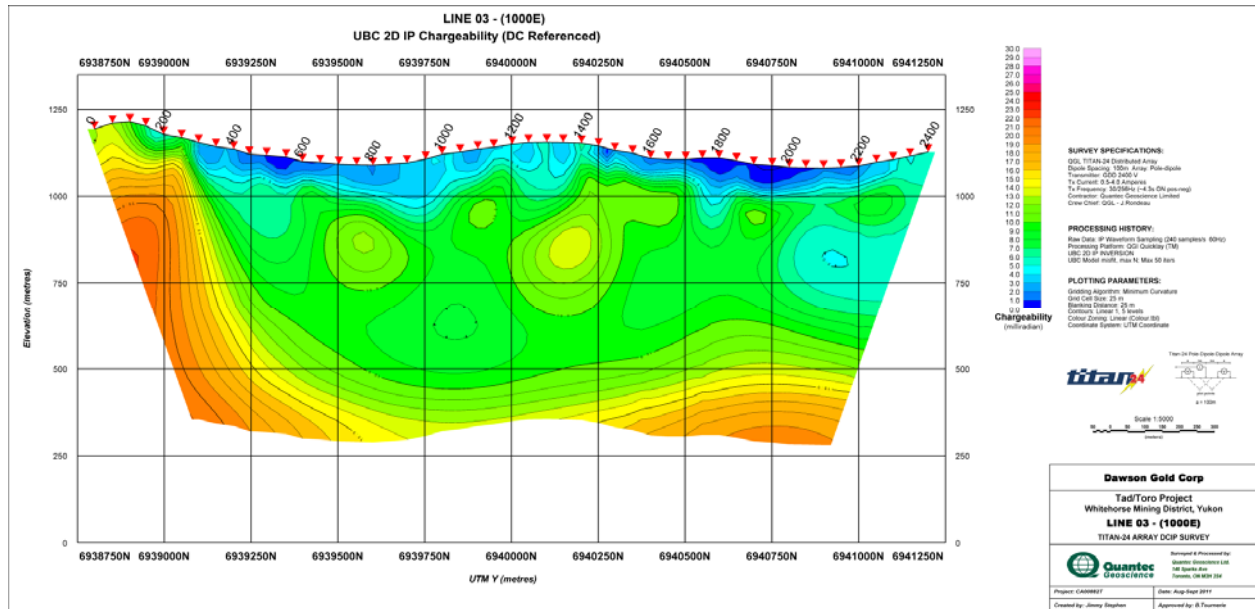


Line 02E –IP Chargeability 2D Model (using Half Space model as reference)

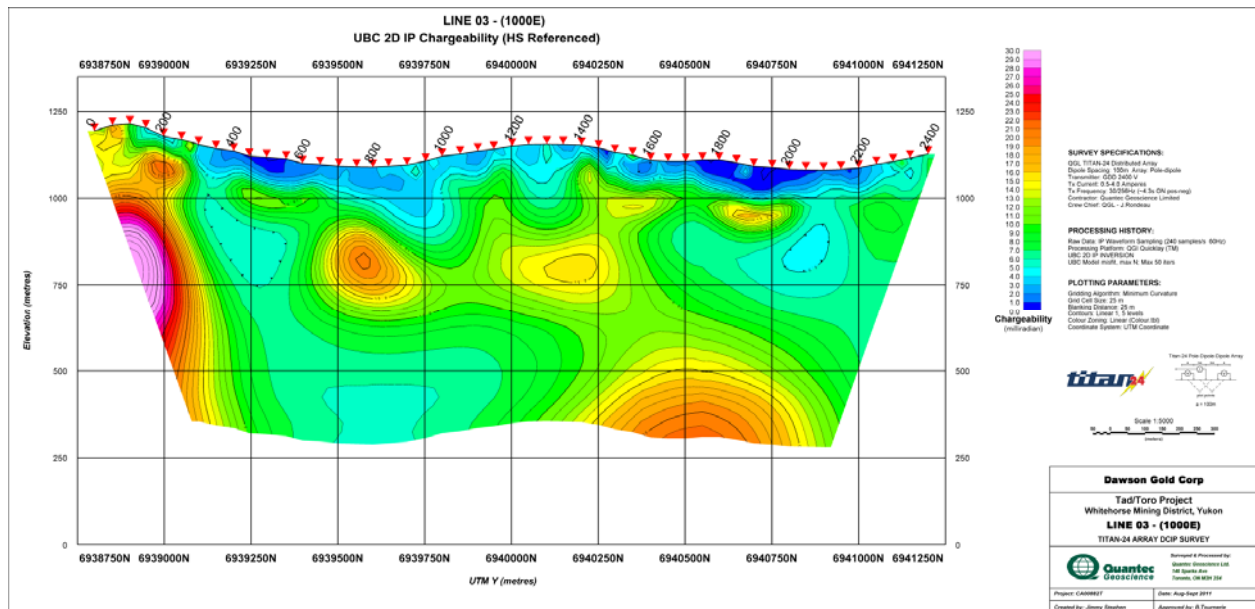
E.3 LINE 03E (1000E)



Line 03E –DC Resistivity 2D Model

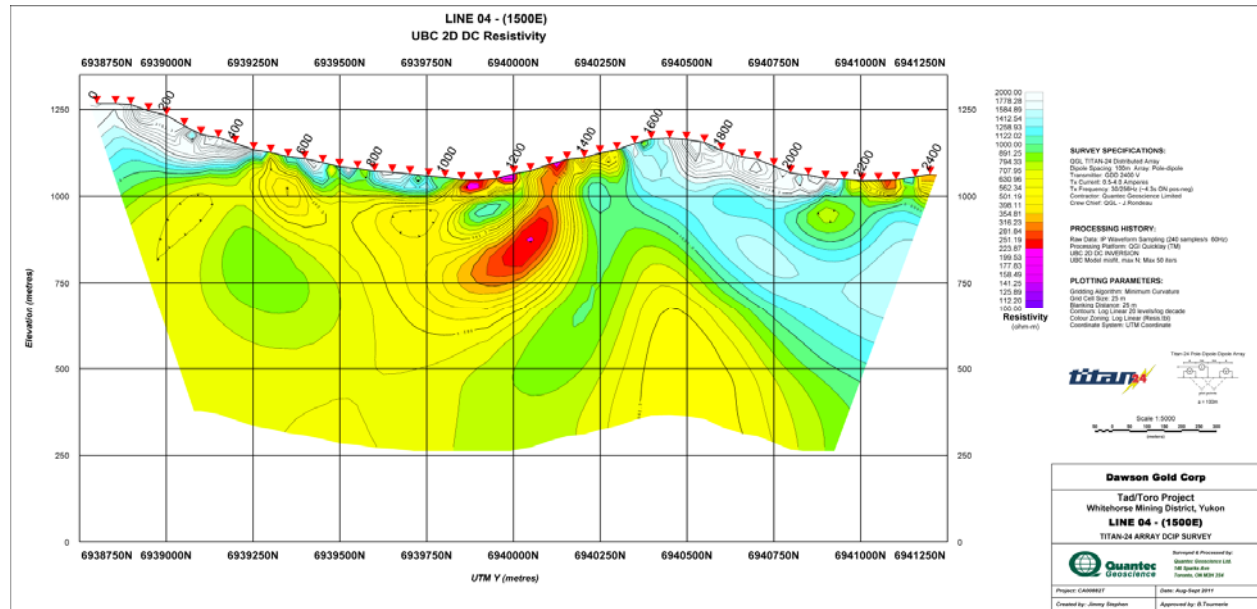


Line 03E –IP Chargeability 2D Model (using DC model as reference)

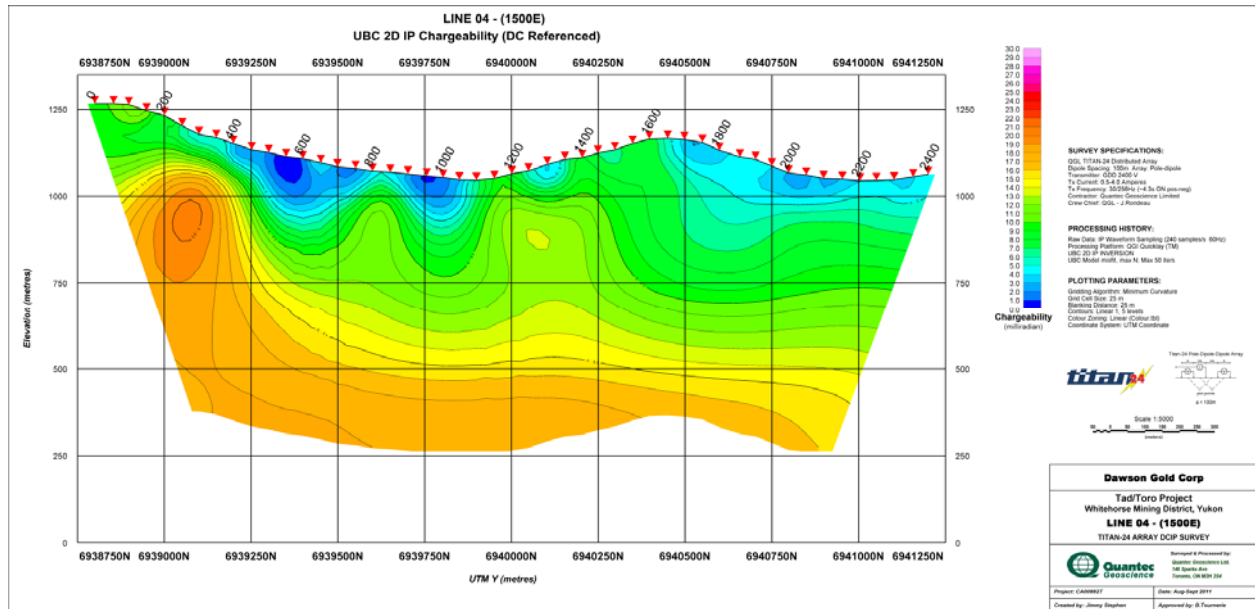


Line 03E –IP Chargeability 2D Model (using Half Space model as reference)

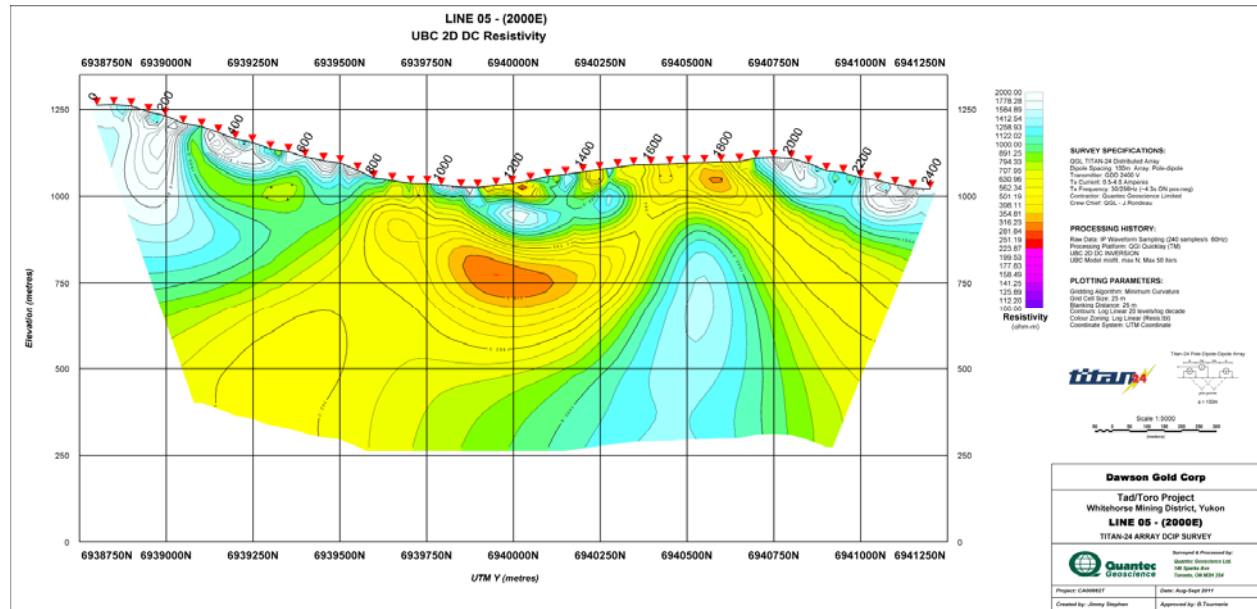
E.4 LINE 04E (1500E)



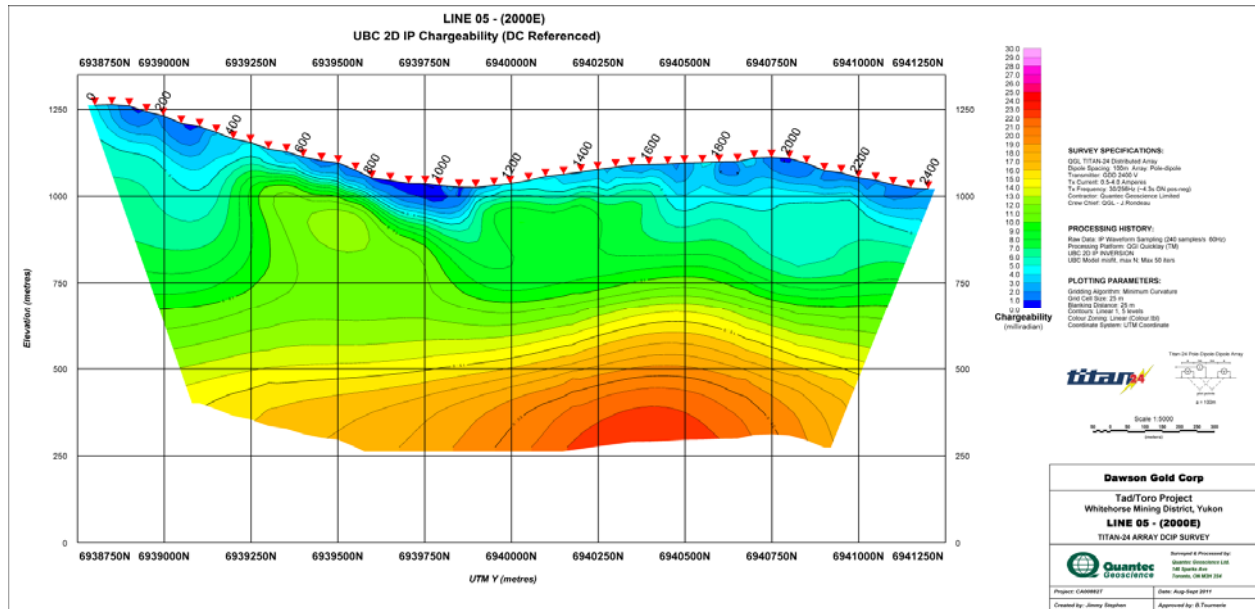
Line 04E –DC Resistivity 2D Model



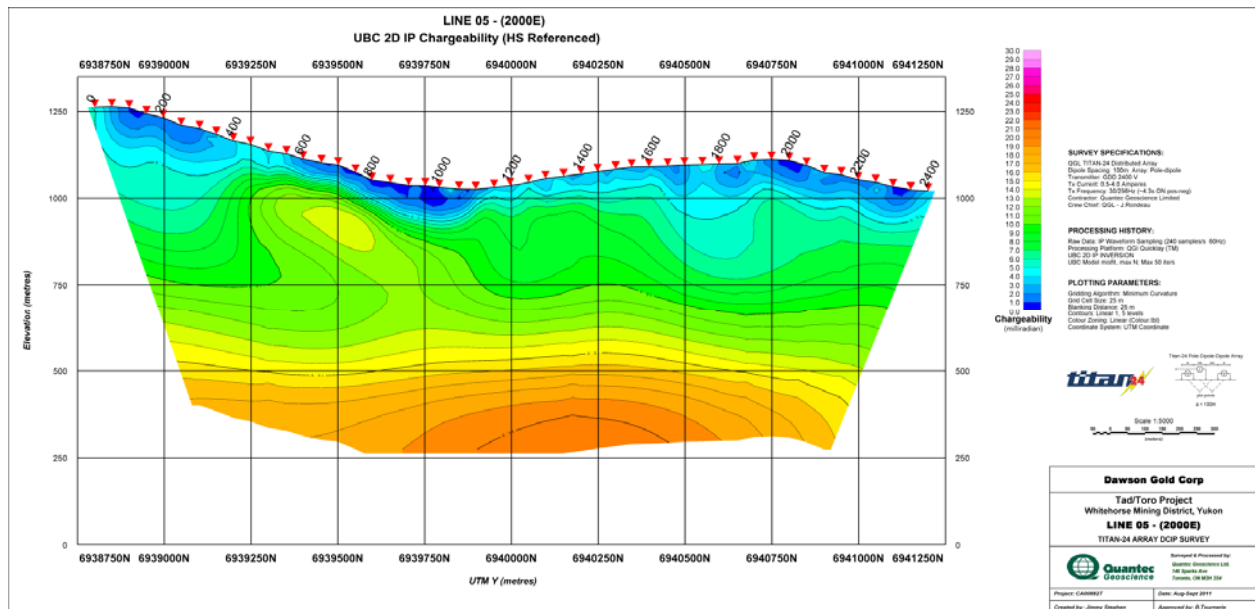
E.5 LINE 05E (2000E)



Line 05E –DC Resistivity 2D Model

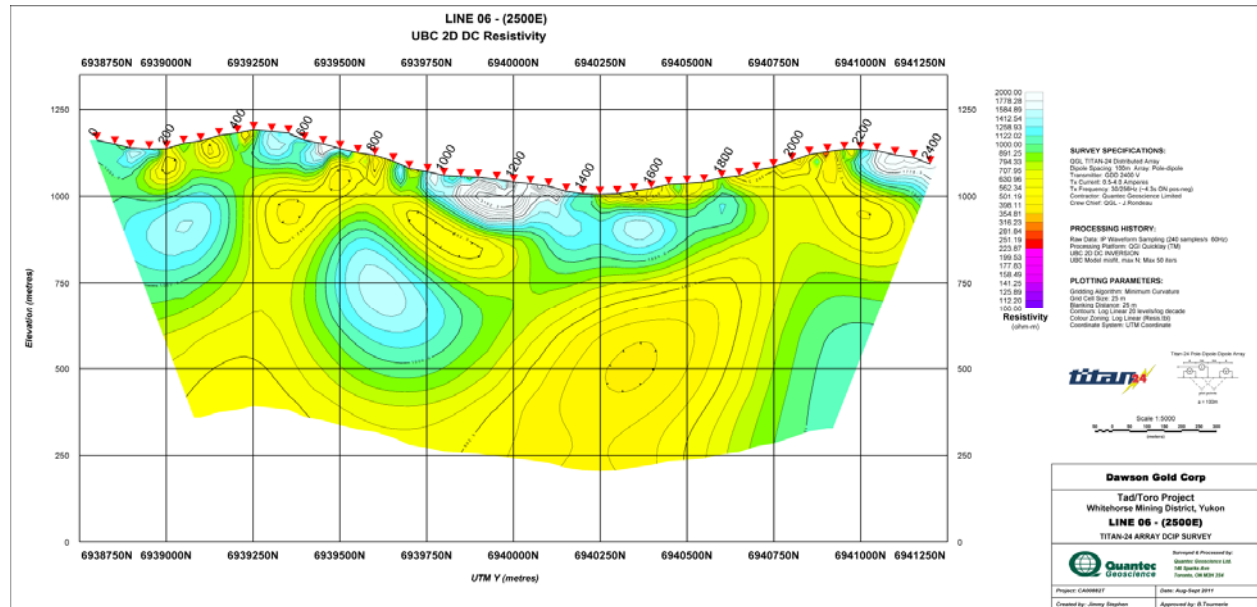


Line 05E –IP Chargeability 2D Model (using DC model as reference)

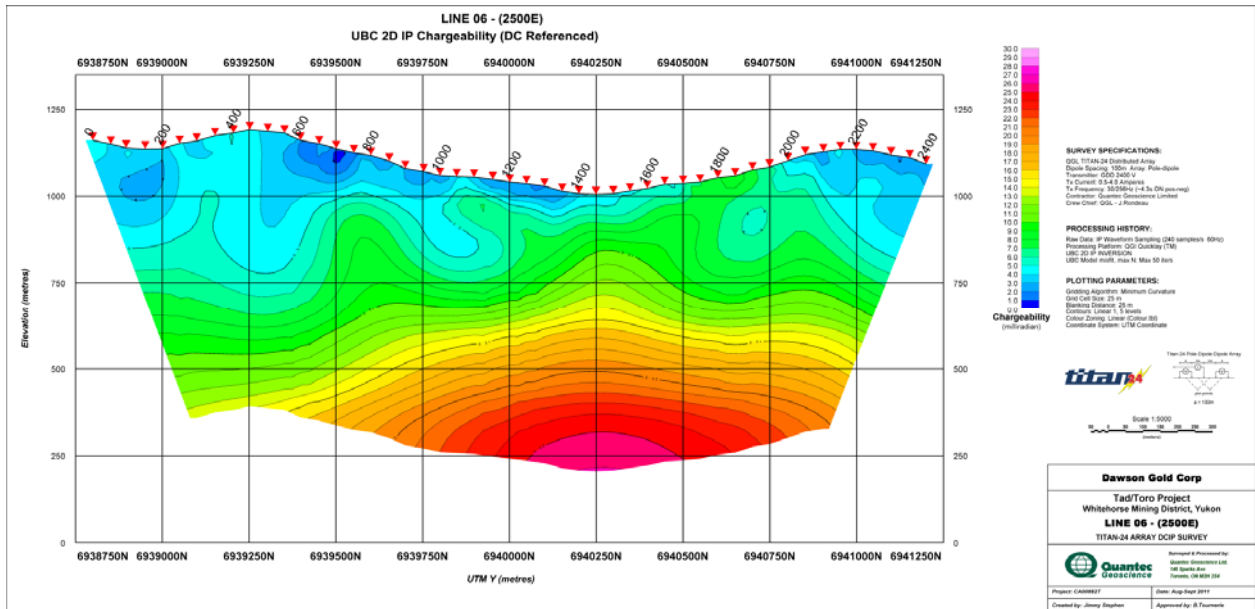


Line 05E –IP Chargeability 2D Model (using Half Space model as reference)

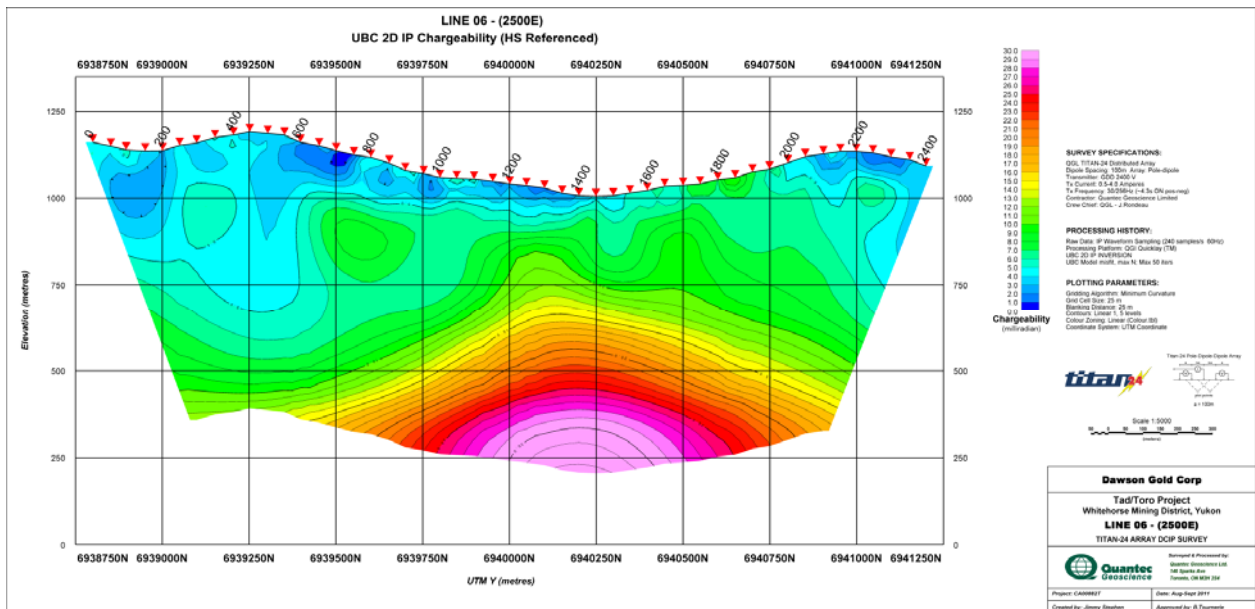
E.6 LINE 06E (2500E)



Line 06E –DC Resistivity 2D Model

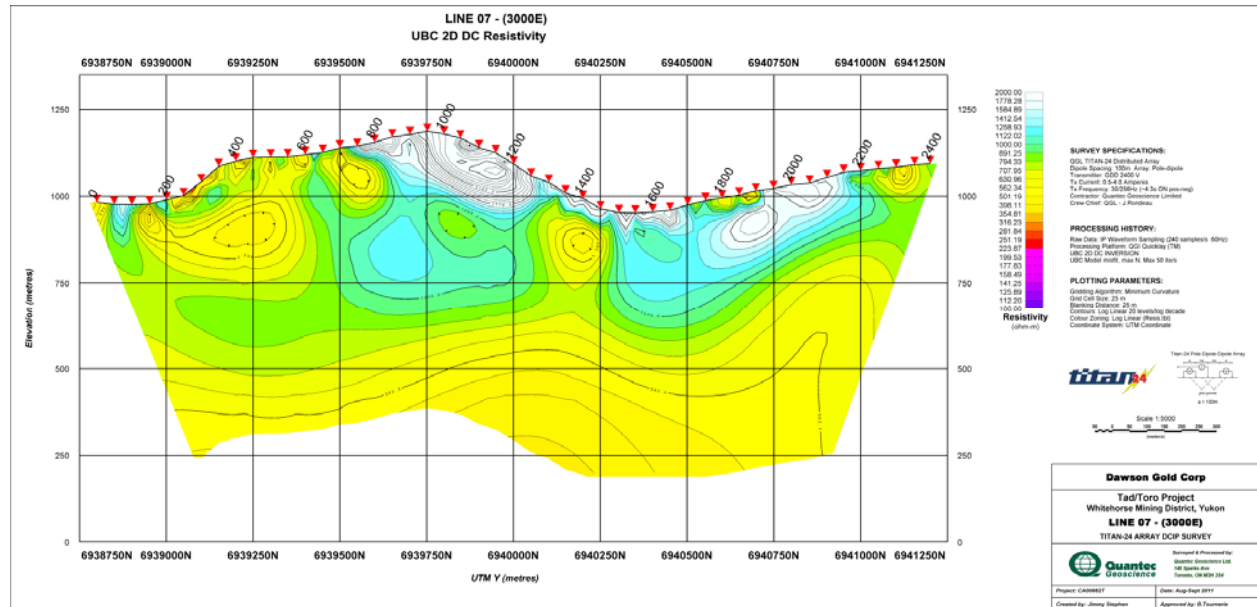


Line 06E –IP Chargeability 2D Model (using DC model as reference)

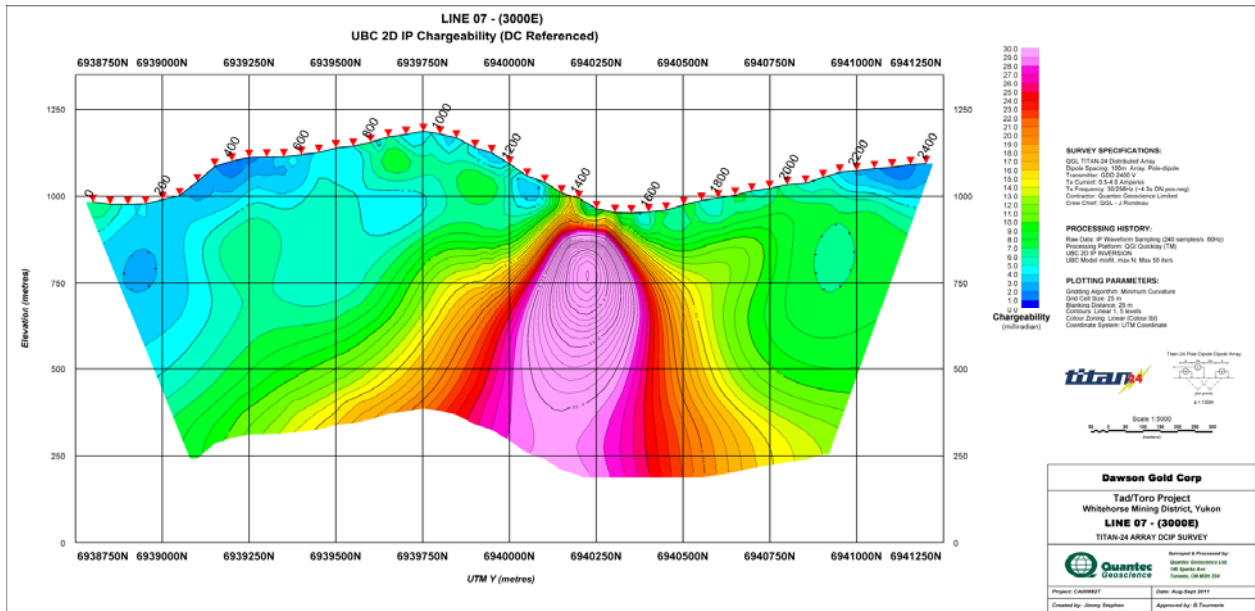


Line 06E –IP Chargeability 2D Model (using Half Space model as reference)

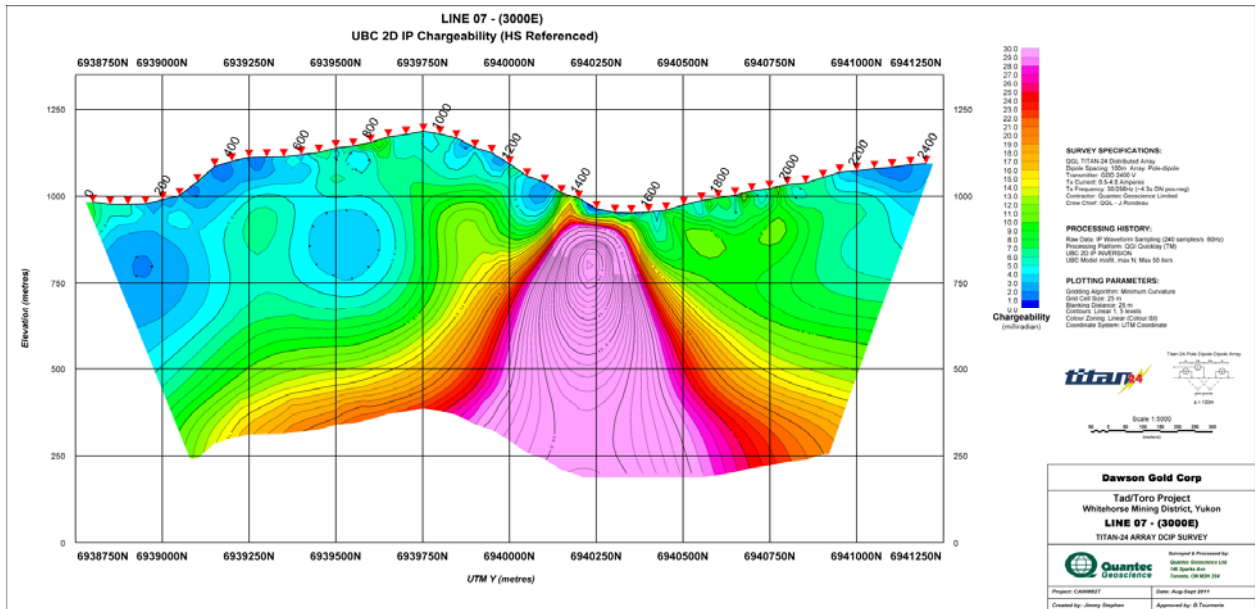
E.7 LINE 07E (3000E)



Line 07E –DC Resistivity 2D Model

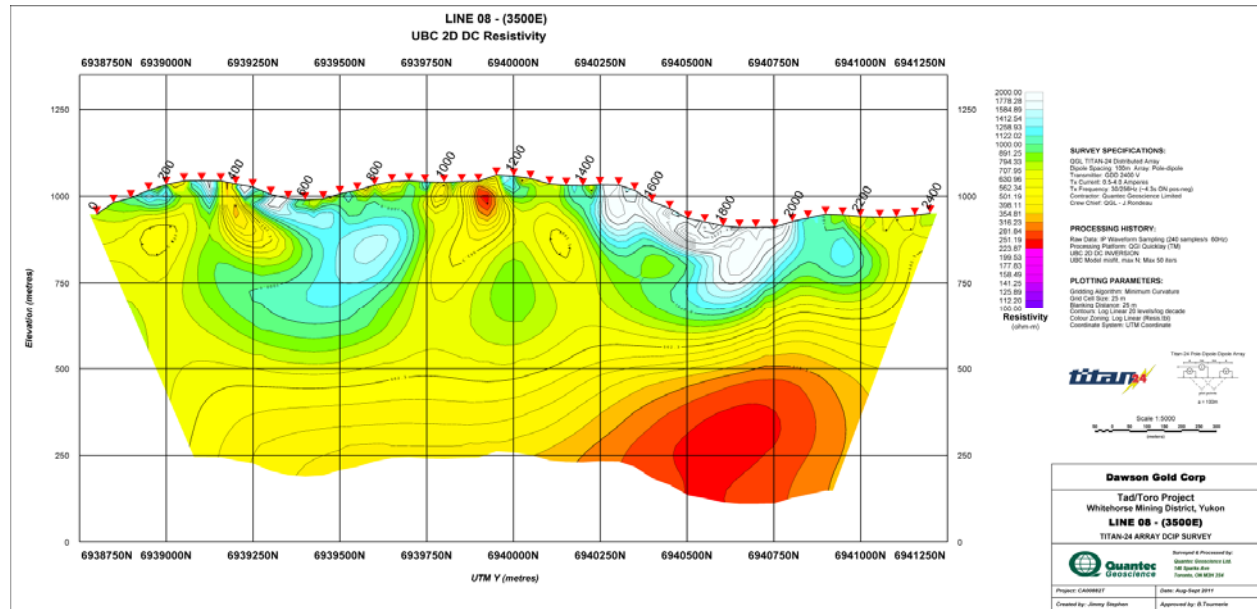


Line 07E –IP Chargeability 2D Model (using DC model as reference)

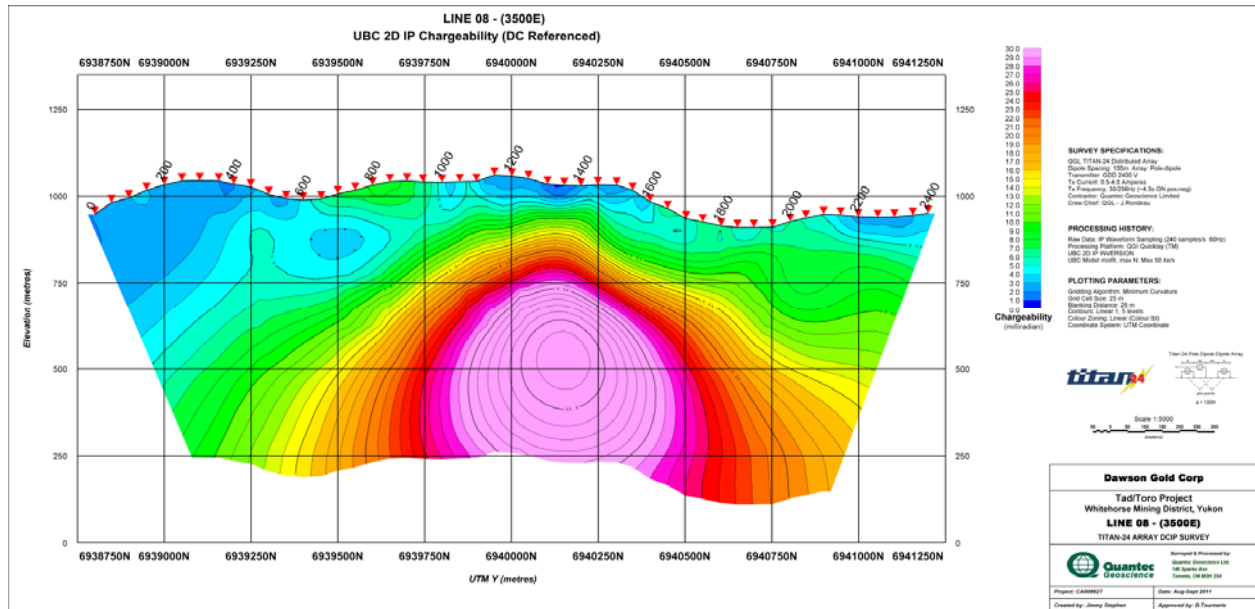


Line 07E –IP Chargeability 2D Model (using Half Space model as reference)

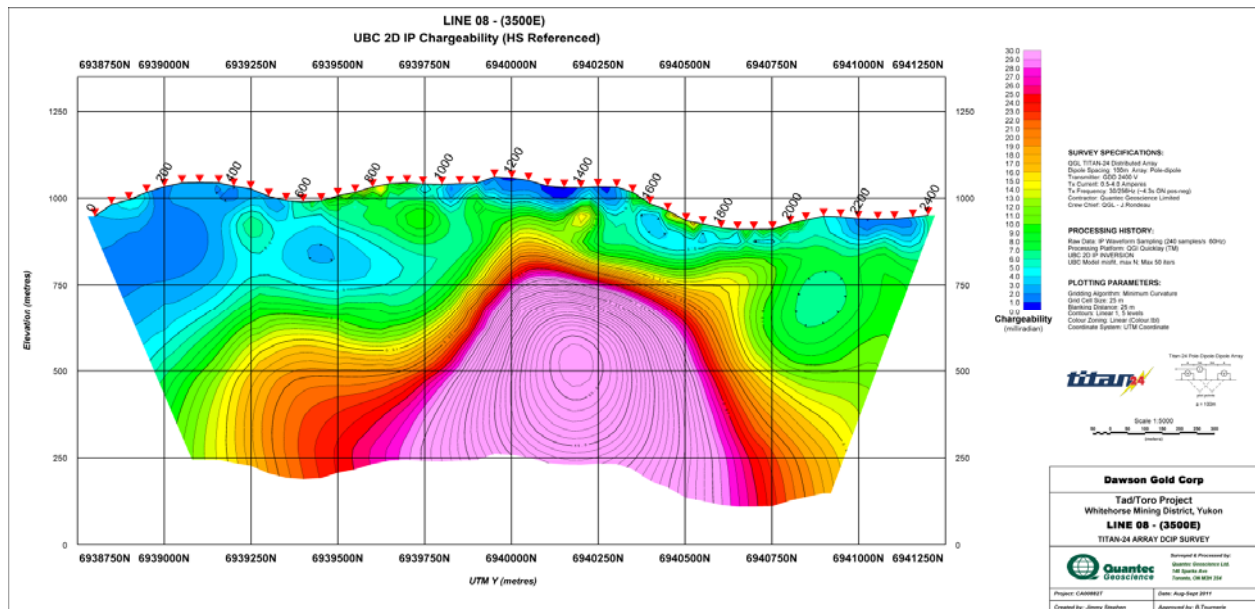
E.8 LINE 08E (3500E)



Line 08E –DC Resistivity 2D Model

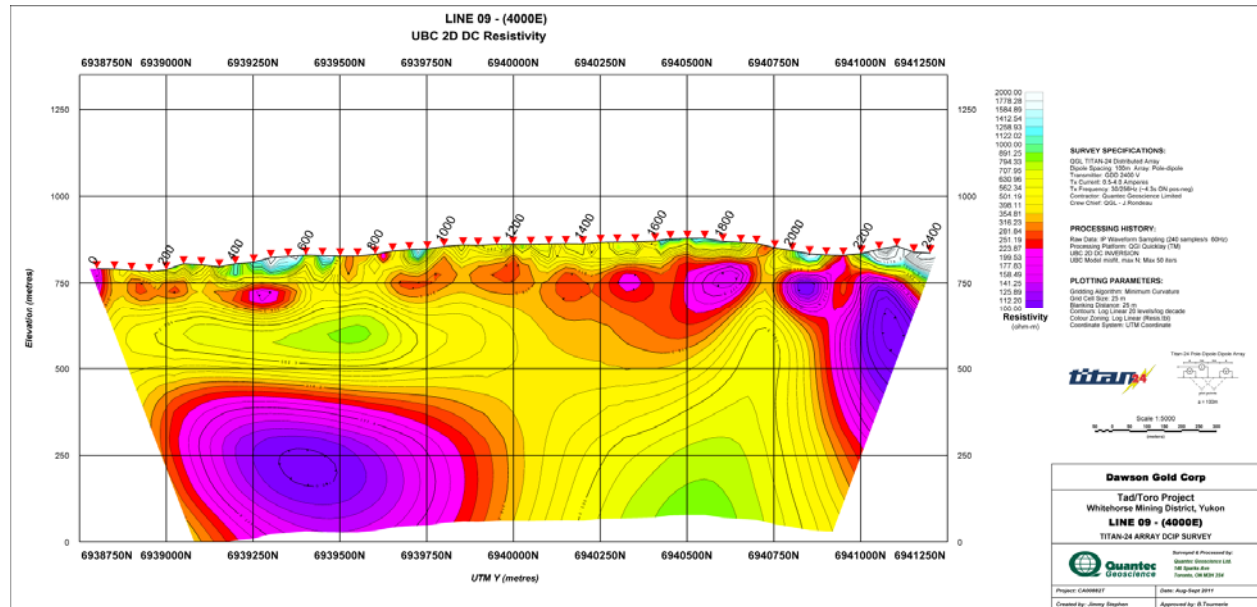


Line 08E –IP Chargeability 2D Model (using DC model as reference)

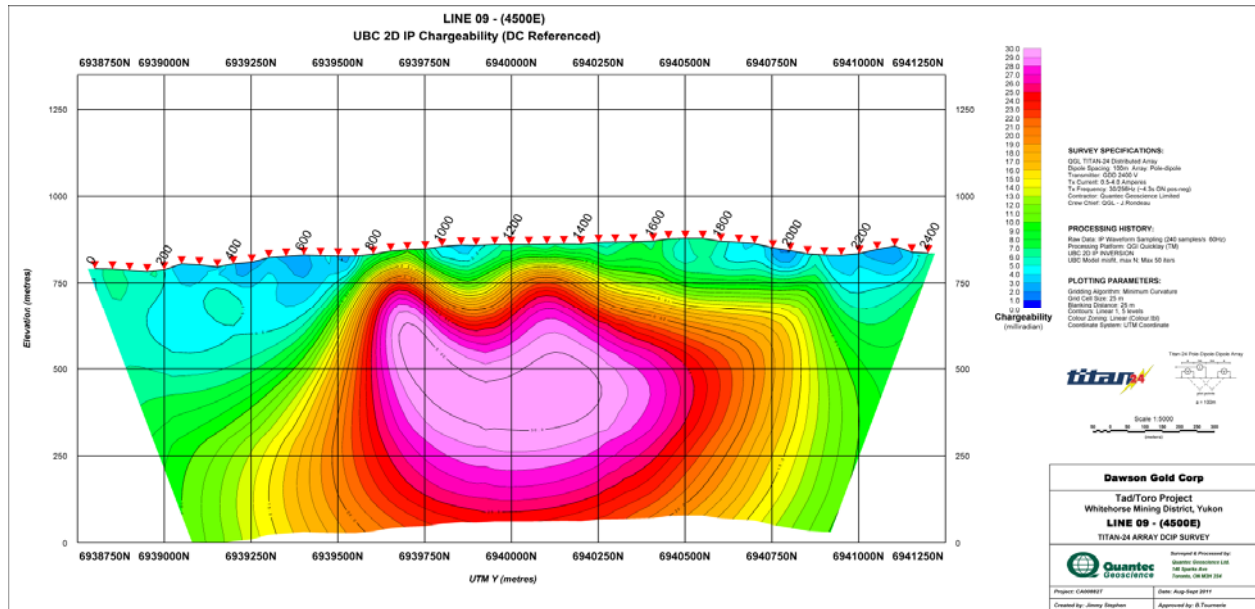


Line 08E –IP Chargeability 2D Model (using Half Space model as reference)

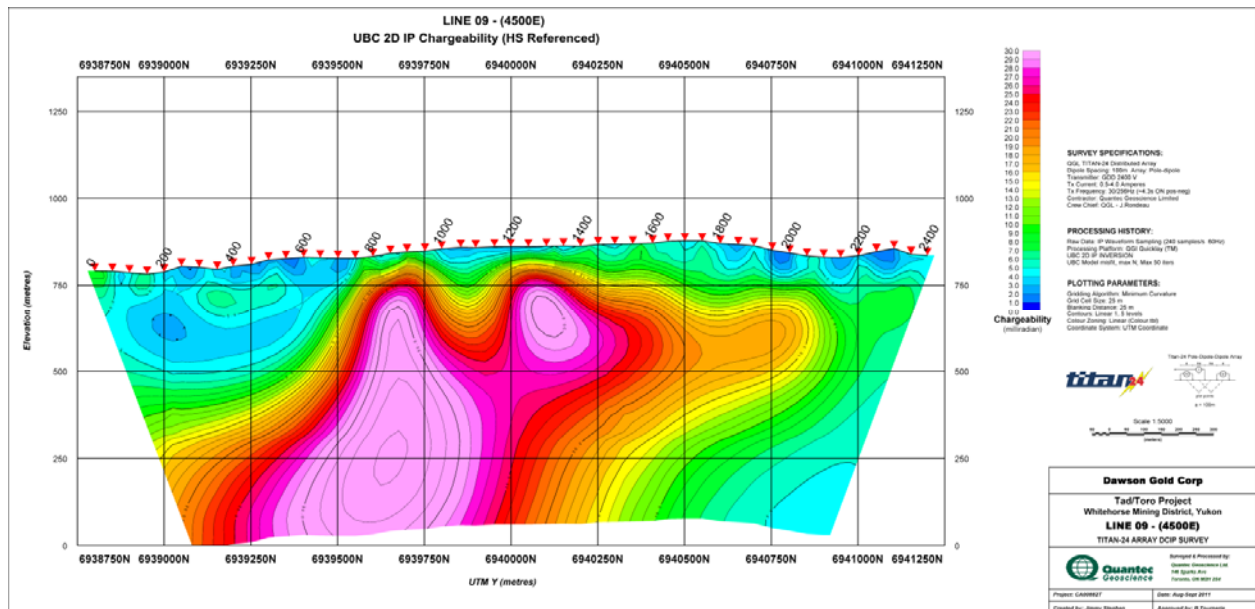
E.9 LINE 09E (4000E)



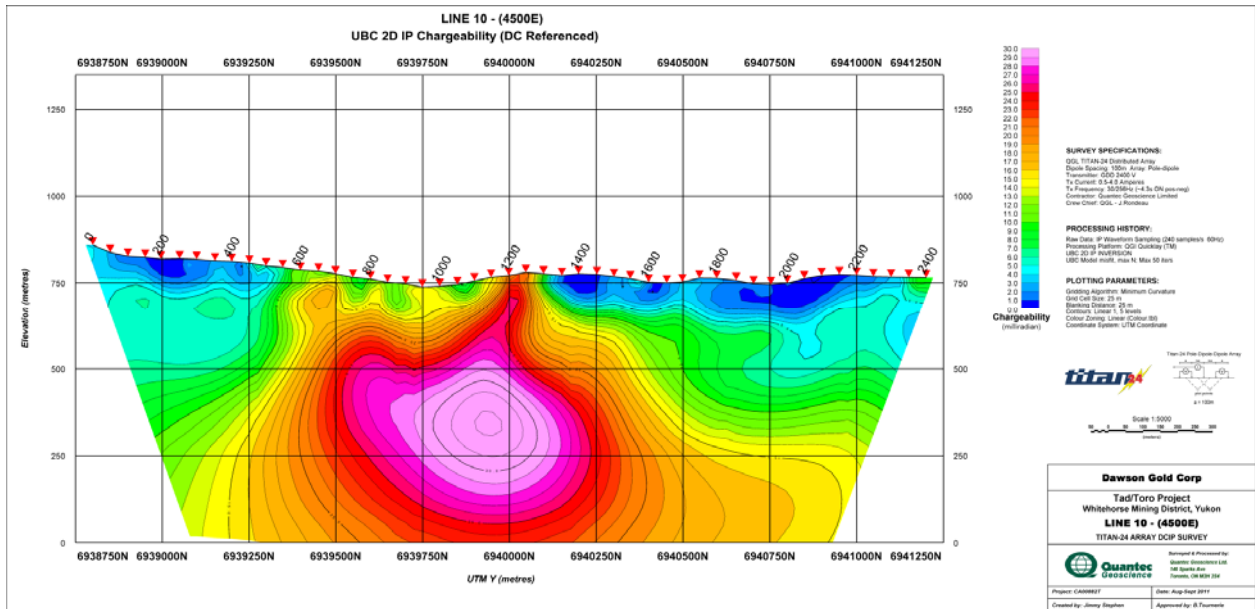
Line 09E –DC Resistivity 2D Model



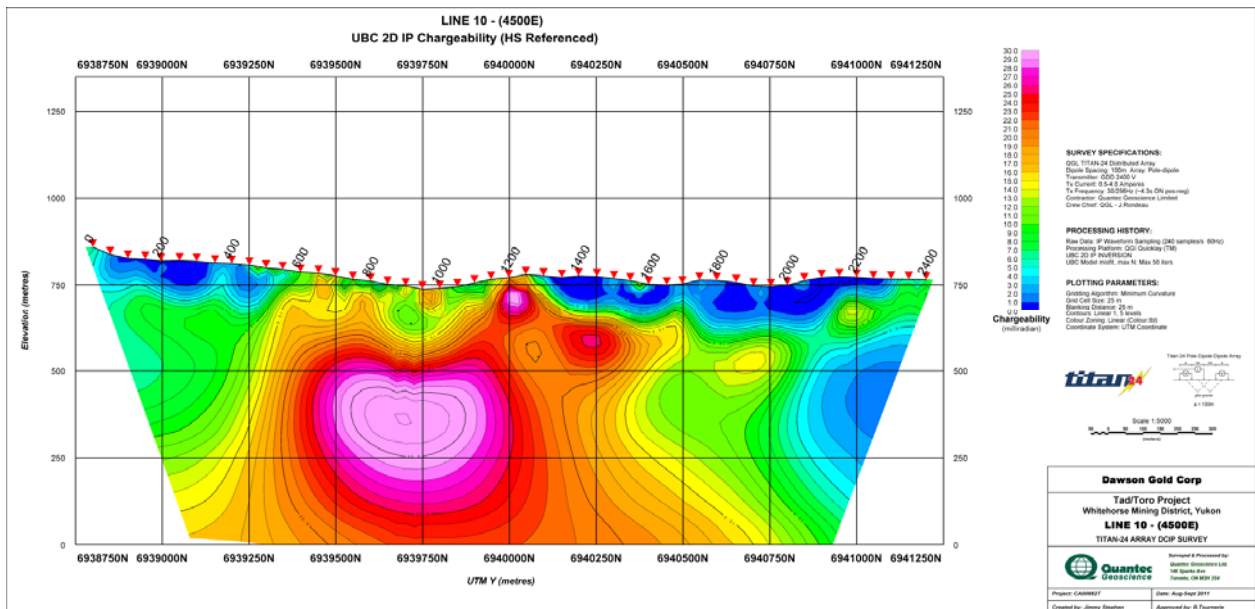
Line 09E –IP Chargeability 2D Model (using DC model as reference)



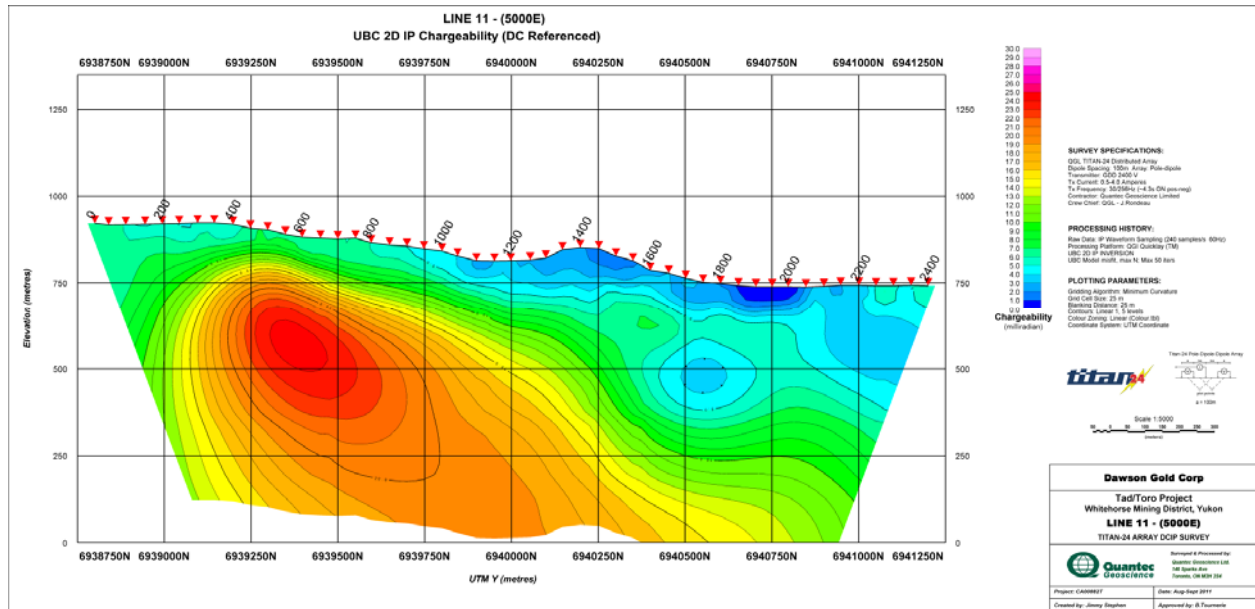
Line 09E –IP Chargeability 2D Model (using Half Space model as reference)



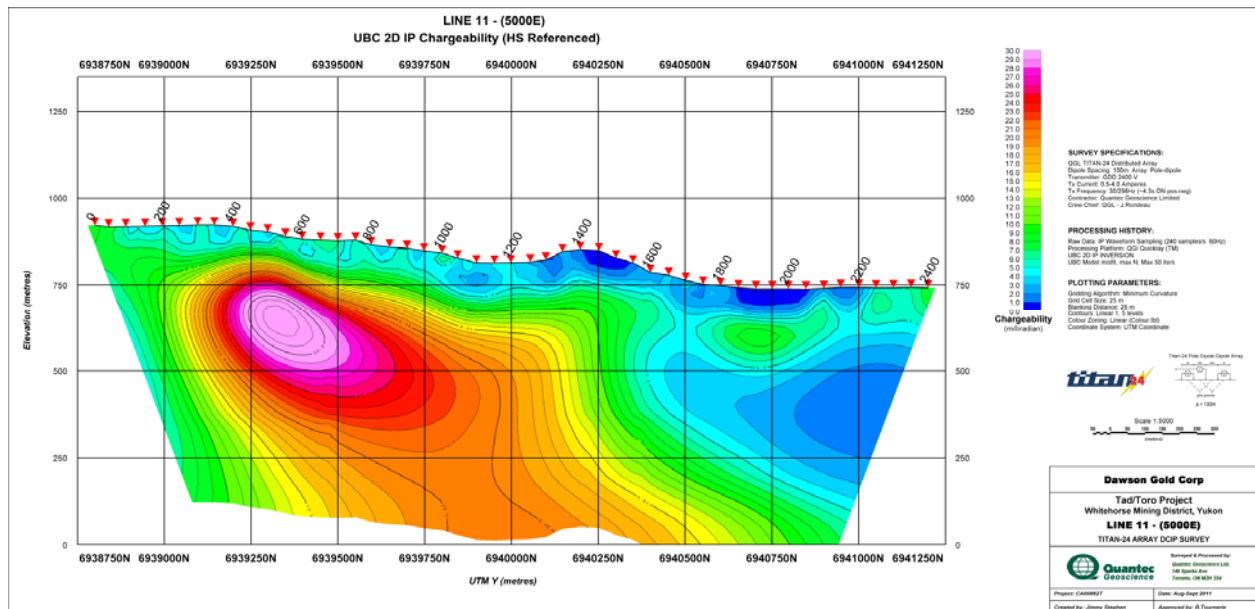
Line 10E –IP Chargeability 2D Model (using DC model as reference)



Line 10E –IP Chargeability 2D Model (using Half Space model as reference)

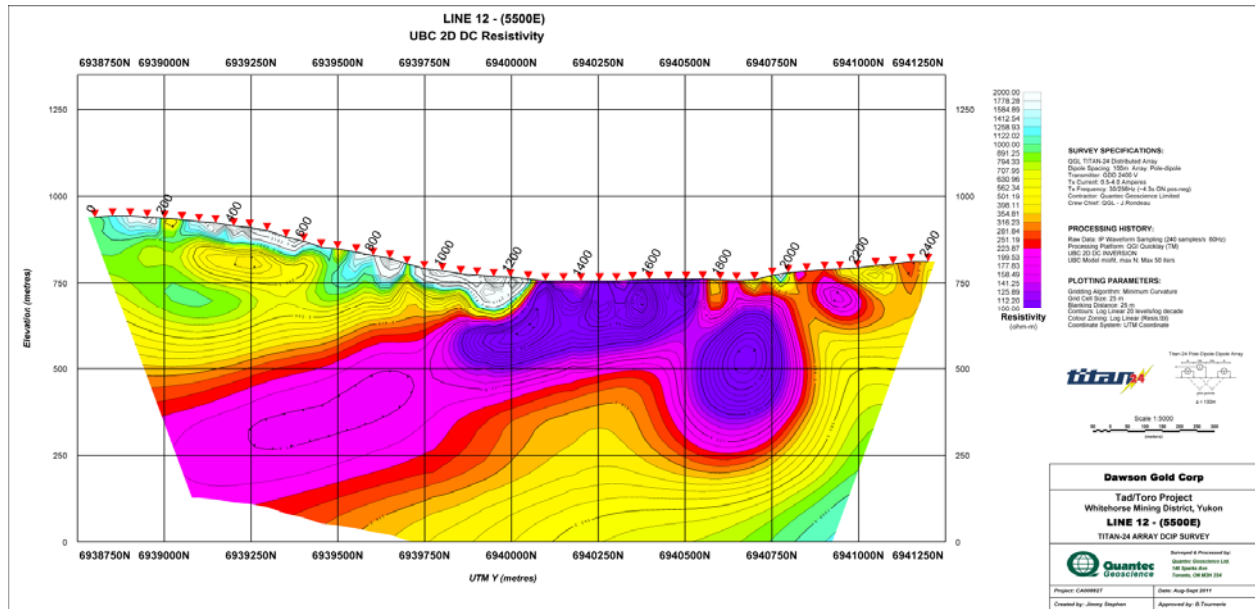


Line 11E –IP Chargeability 2D Model (using DC model as reference)

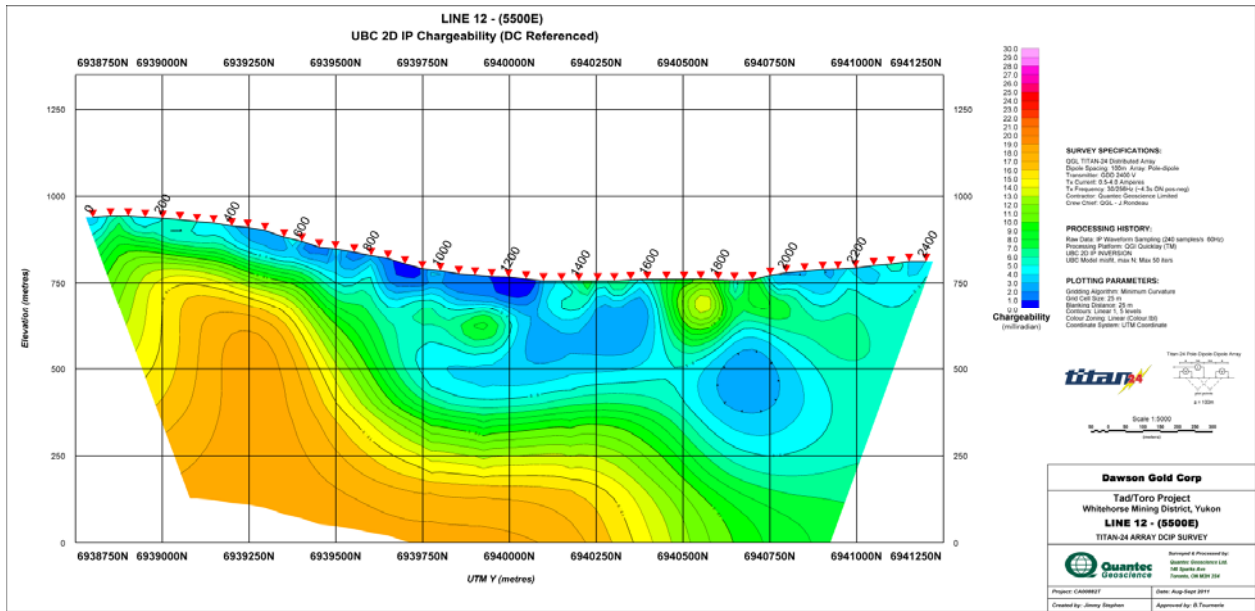


Line 11E –IP Chargeability 2D Model (using Half Space model as reference)

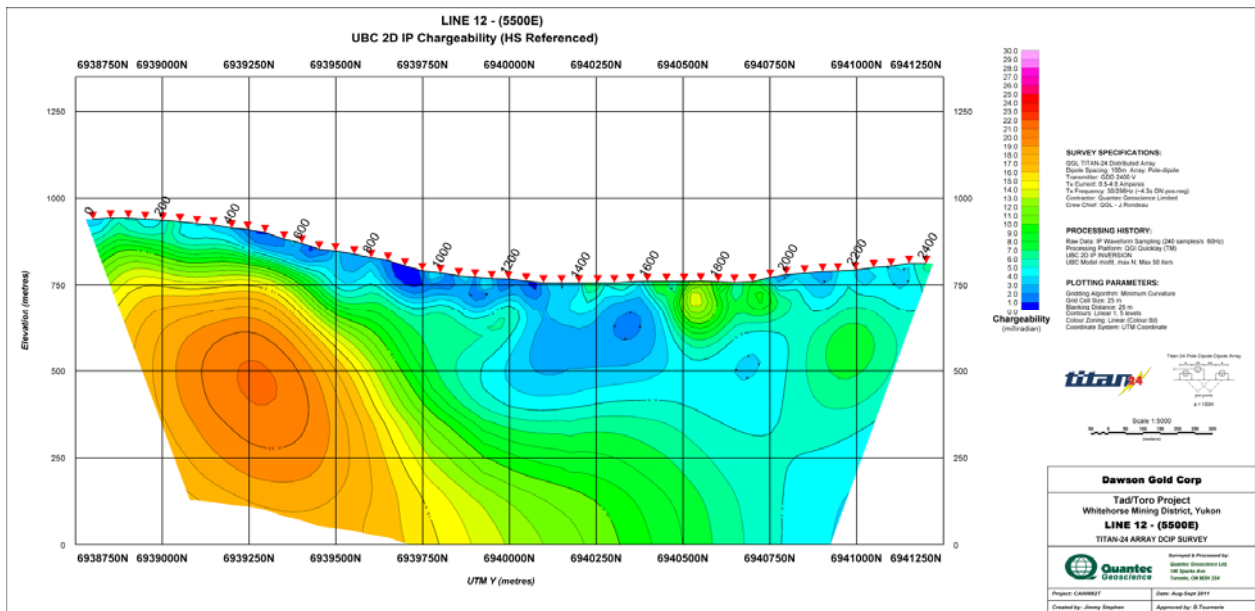
E.12 LINE 12E (5500E)



Line 12E –DC Resistivity 2D Model

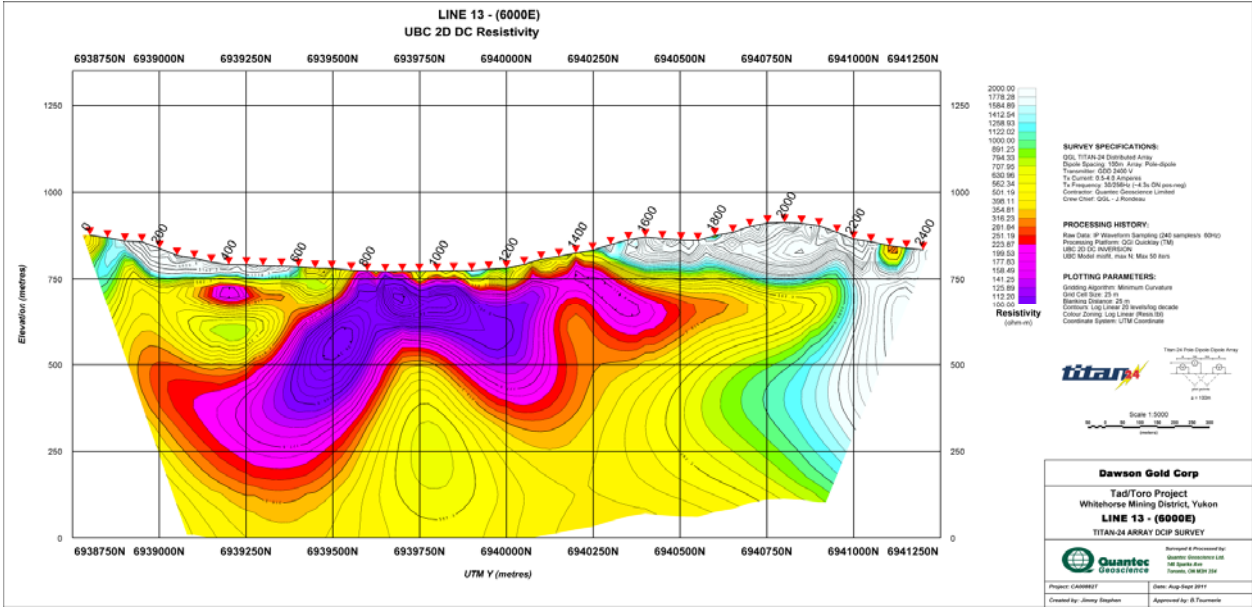


Line 12E –IP Chargeability 2D Model (using DC model as reference)

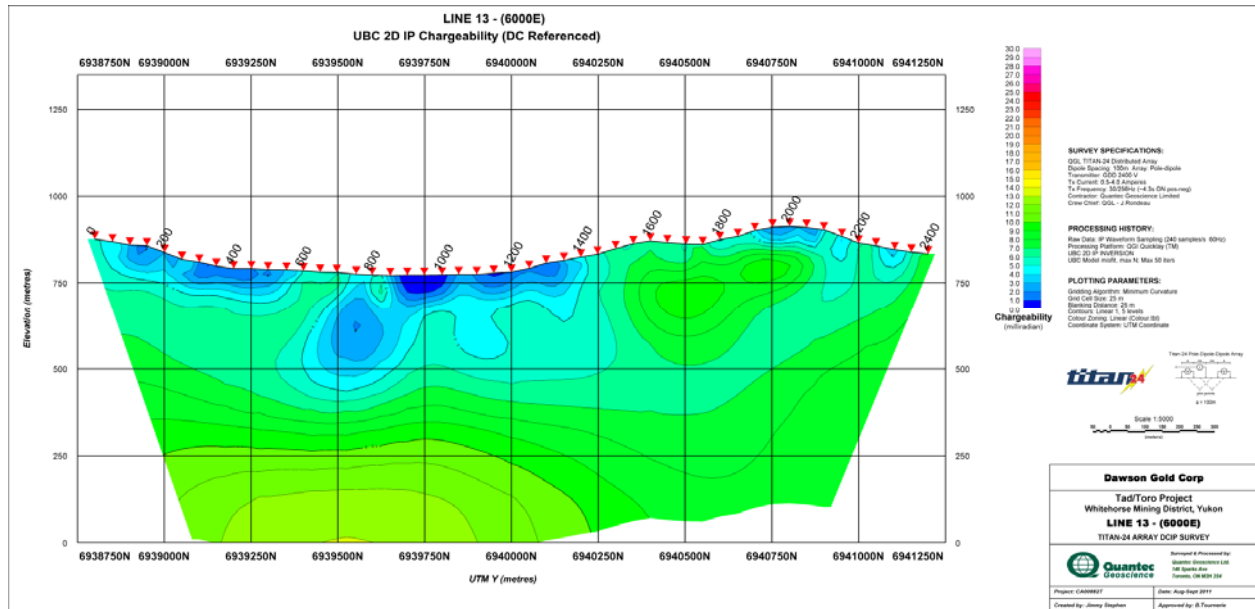


Line 12E –IP Chargeability 2D Model (using Half Space model as reference)

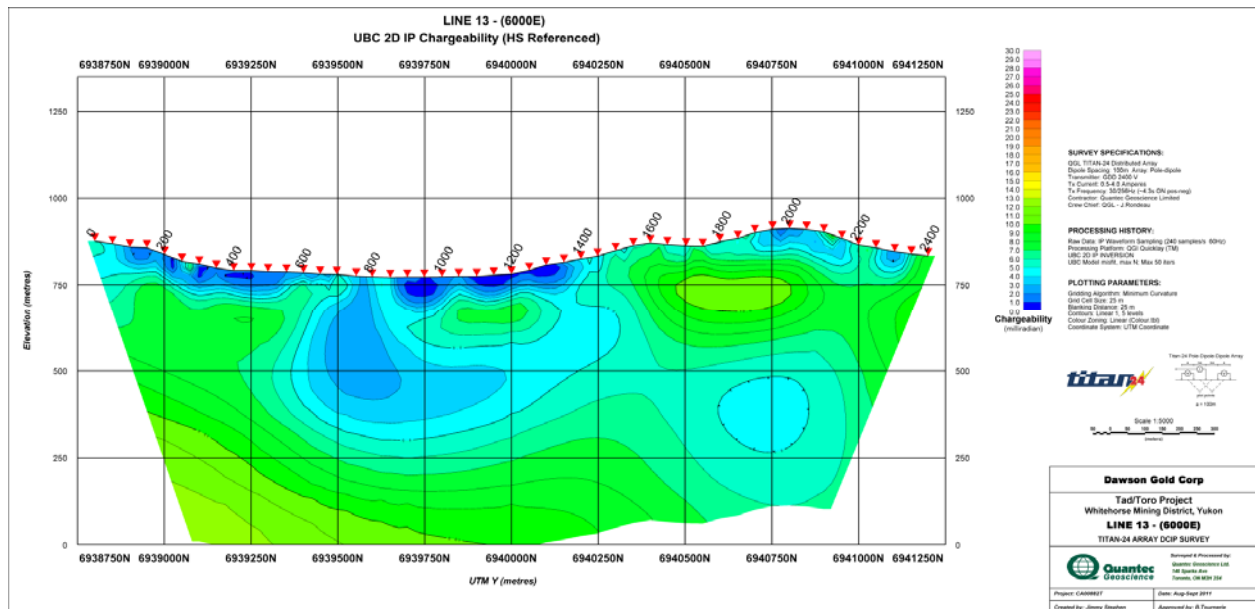
E.13 LINE 13E (6000E)



Line 13E –DC Resistivity 2D Model

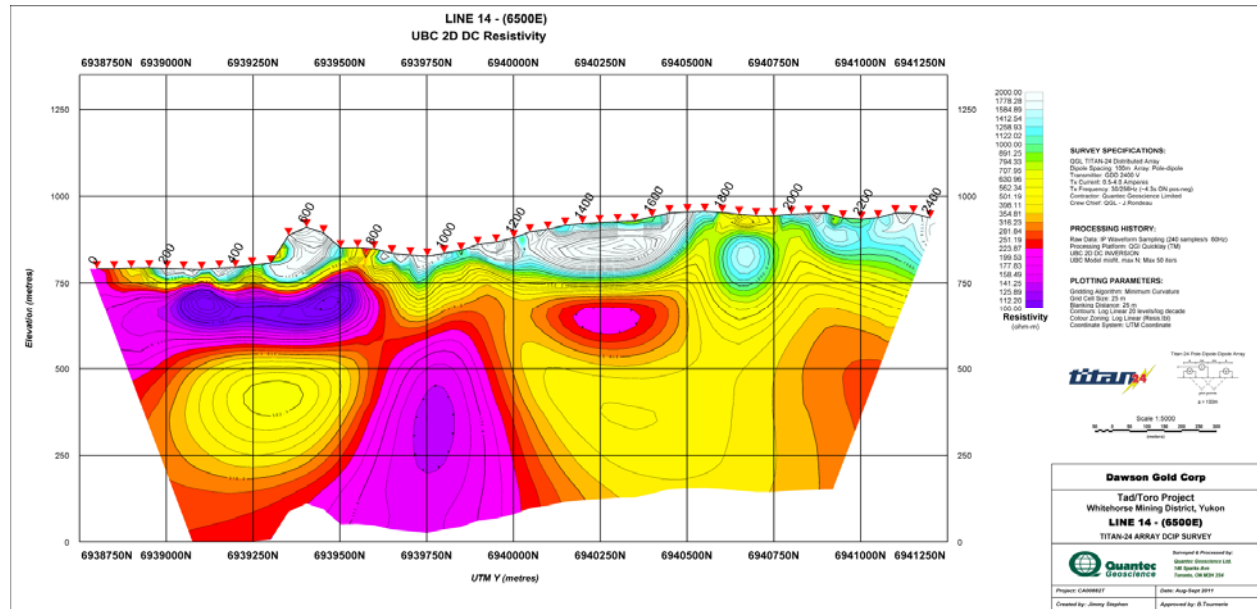


Line 13E –IP Chargeability 2D Model (using DC model as reference)

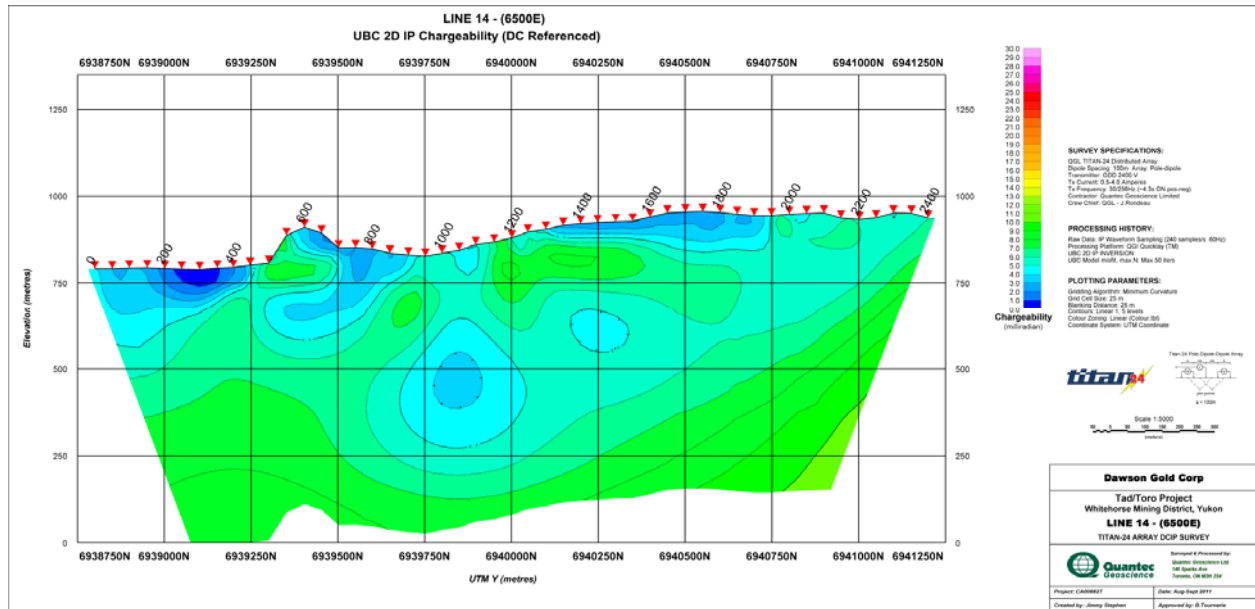


Line 13E –IP Chargeability 2D Model (using Half Space model as reference)

E.14 LINE 14E (6500E)

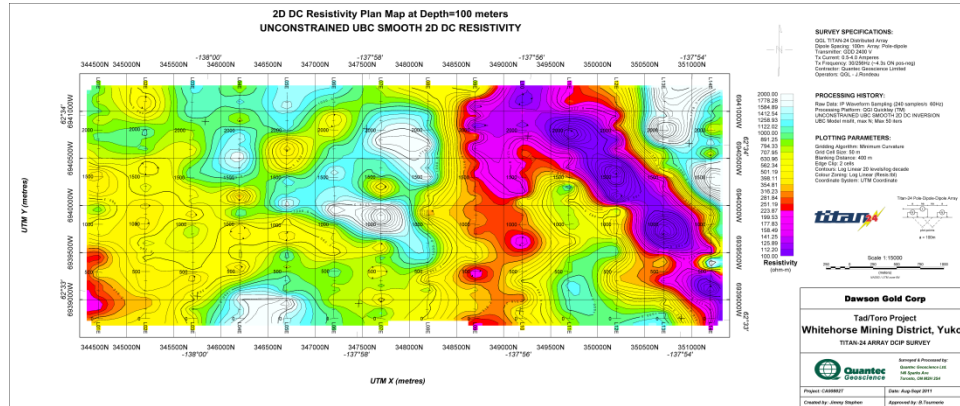


Line 14E –DC Resistivity 2D Model

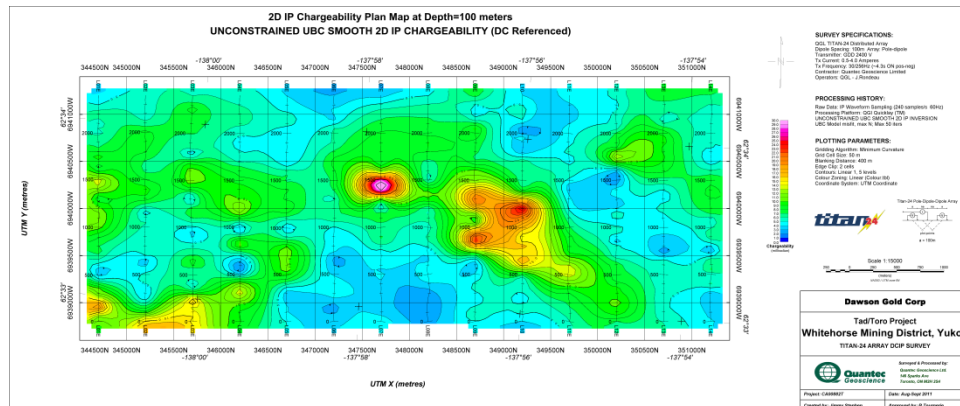


F GEOSOF PLAN MAPS OF THE 2D MODELS

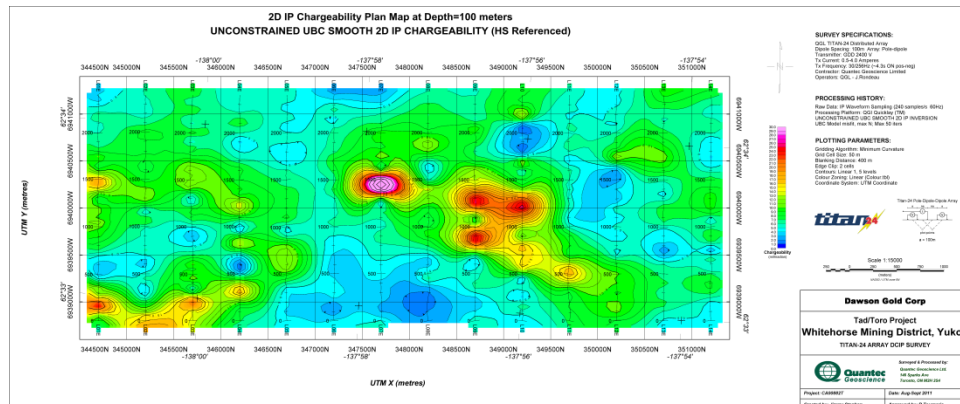
F.1 PLAN MAP AT 100M DEPTH



Plan Map at 100m Depth of DC Resistivity.

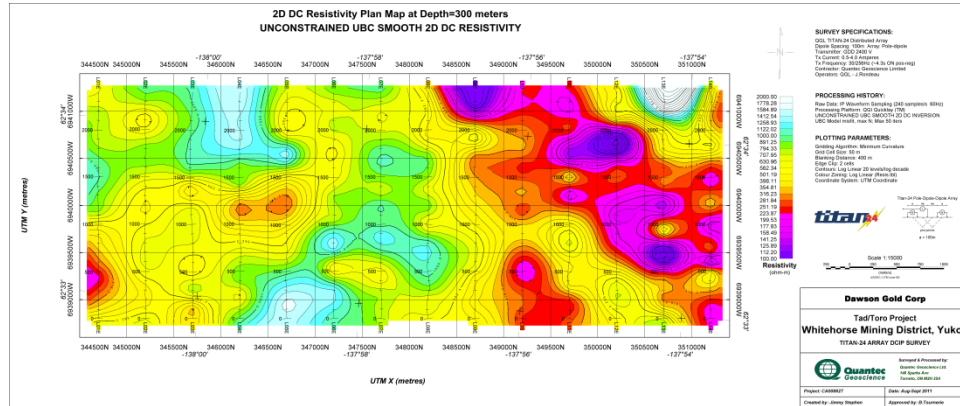


Plan Map at 100m Depth of IP Chargeability (use DC models as reference).

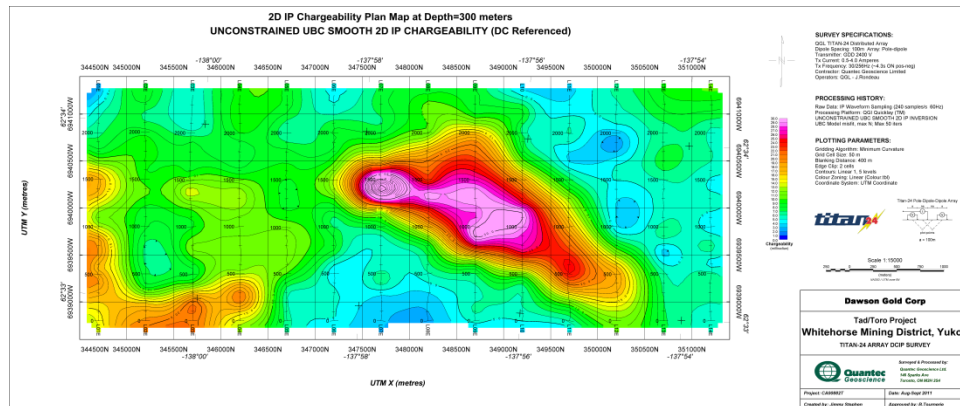


Plan Map at 100m Depth of IP Chargeability (use Half Space models as reference).

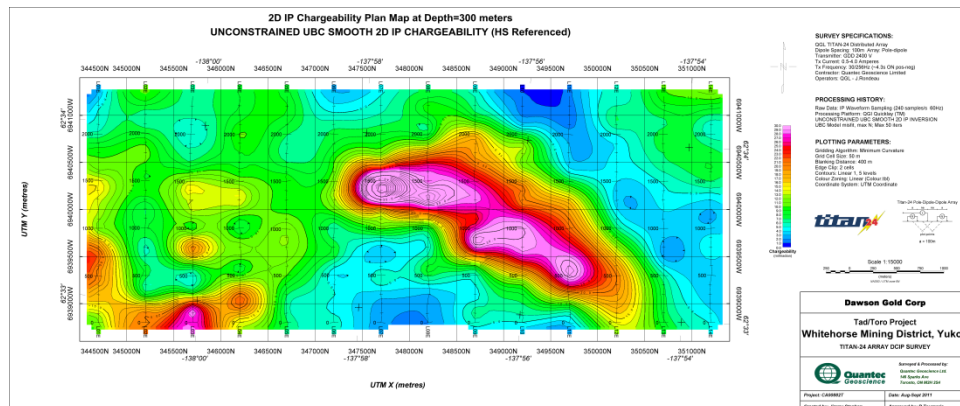
F.3 PLAN MAP AT 300M DEPTH



Plan Map at 300m Depth of DC Resistivity.

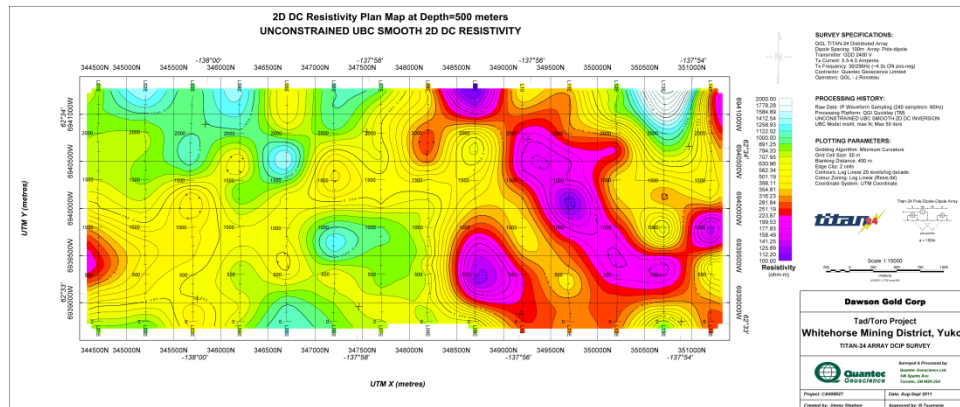


Plan Map at 300m Depth of IP Chargeability (use DC models as reference).

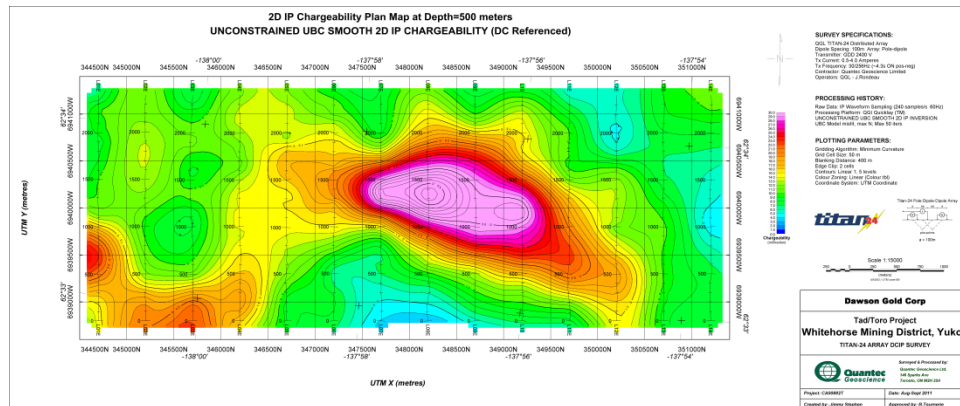


Plan Map at 300m Depth of IP Chargeability (use Half Space models as reference).

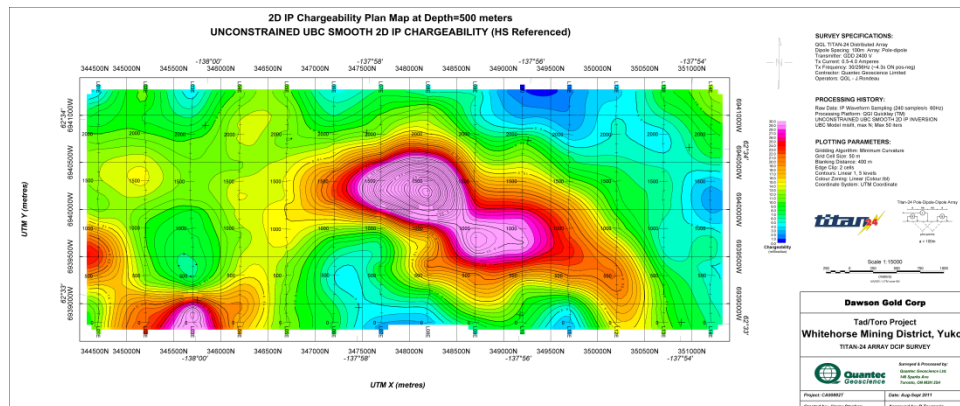
F.5 PLAN MAP AT 500M DEPTH



Plan Map at 500m Depth of DC Resistivity.

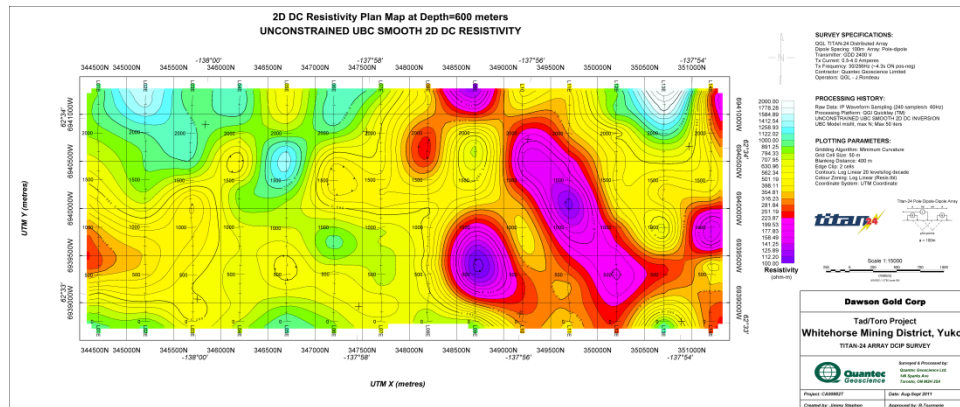


Plan Map at 500m Depth of IP Chargeability (use DC models as reference).

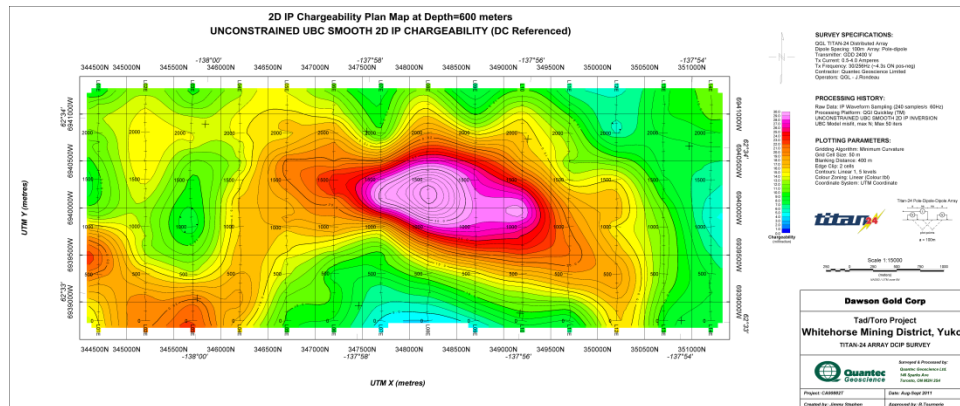


Plan Map at 500m Depth of IP Chargeability (use Half Space models as reference).

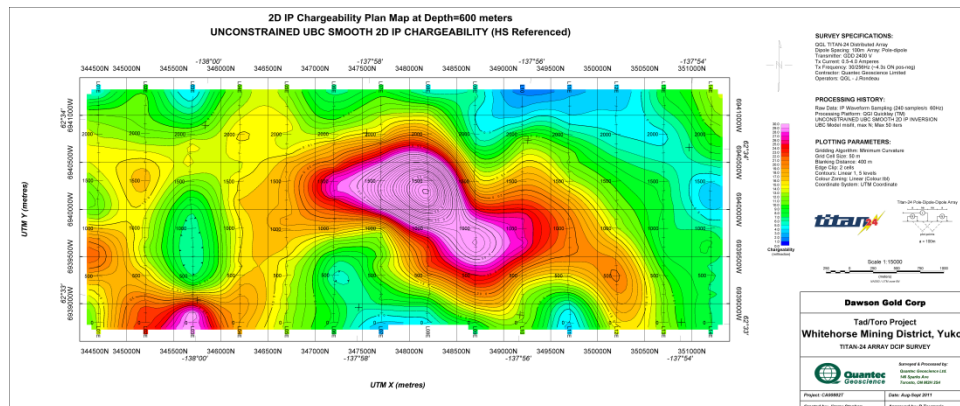
F.6 PLAN MAP AT 600M DEPTH



Plan Map at 600m Depth of DC Resistivity.



Plan Map at 600m Depth of IP Chargeability (use DC models as reference).



Plan Map at 600m Depth of IP Chargeability (use Half Space models as reference).

G AN INTRODUCTION TO TITAN-24 DIRECT CURRENT (DC) RESISTIVITY AND INDUCED POLARISATION (IP) METHODS

G.1 INTRODUCTION

Titan-24 is a 24-bit multi-channel, distributed acquisition system that allows for the collection of high quality Direct Current (DC) Resistivity and Induced Polarization (IP) data (Sheard 1998). The system provides high multiplicity data sets and records full-waveform time-series utilizing 24-bit Sigma Delta Analog to Digital (A/D) conversion. Like other conventional resistivity methods, acquisition is performed by the injection of an artificial controlled source of current, usually a series of full duty cycle¹² square pulses, into the ground through the transmitter electrode. The voltages, normalized by the injected current, are measured at the receiver electrodes as time series.

The use of 24-bit A/D converter allows the Titan-24 system to record the full waveform at the receivers, thus permitting the accurate removal or deconvolution of the source effects from the recorded time series. What is left of the time series after the deconvolution consist of mainly the responses of the ground and noise.

DC resistivity method is quite sensitive to small variations in resistivity near surface, and its effectiveness will be limited by high level of noise in the presence of a shallow conductive layer in the ground. On the other hand, in the desert or coarse-grained sandy environments, DC resistivity method can suffer from poor electrical contact with the ground. As a result, very little or no current can be injected into the ground, and no meaningful data can be collected.

The resistivity is among the most variable of all geophysical parameters, with a range exceeding 10^6 ohm-m. The resistivity of rocks depends primarily on their porosity, permeability and particularly the salinity of fluids contained, according to Archie's Law. Therefore, DC resistivity method can be utilized in a wide variety of applications in mineral exploration, mainly for mapping of resistivity structures and locating of conductive targets.

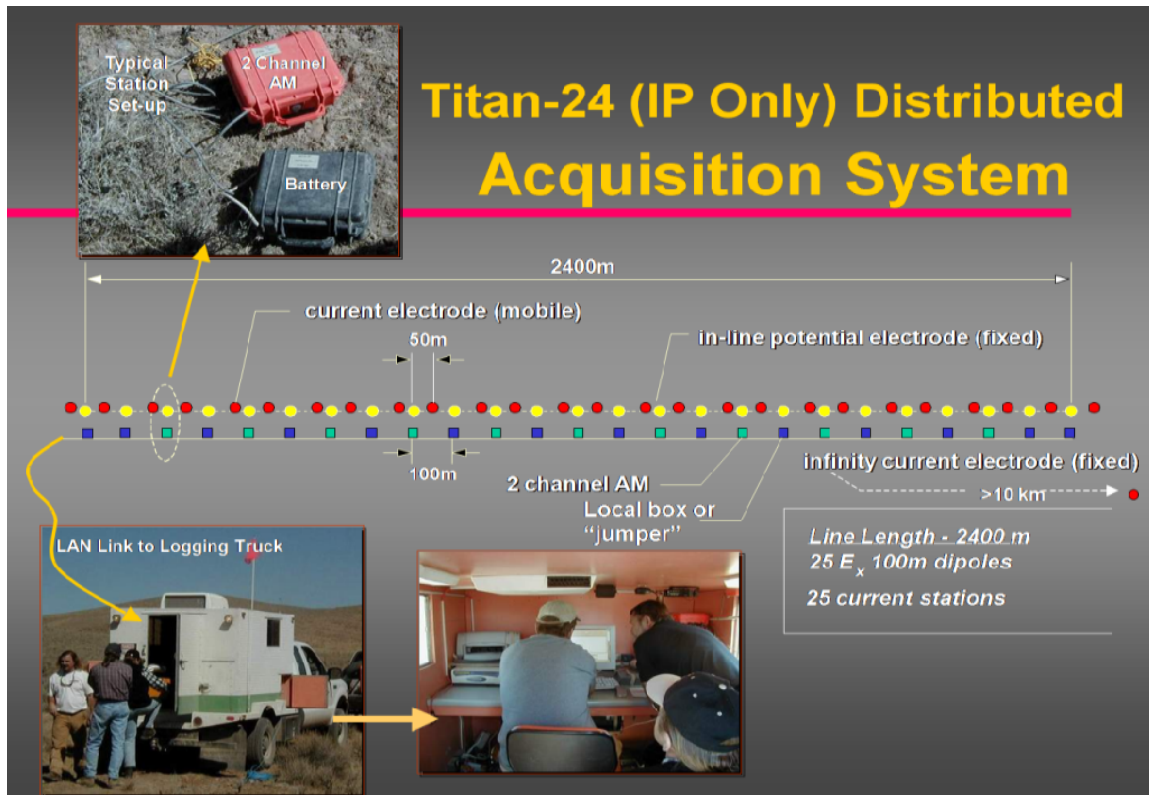
The chargeability responds to the presence of polarisable minerals (metals, sub-metallic sulphides and oxides, and graphite), in minute amounts. Both the quantity of individual chargeable grains present and their distributions within subsurface current flow paths are significant in controlling the level of response. The IP method can be used to directly detect disseminated to massive sulphides.

More detailed descriptions on the theory and application of the DCIP method can be found in Telford et al. (1976).

¹² Duty cycle is the ratio between the pulse duration and the period of a square waveform.

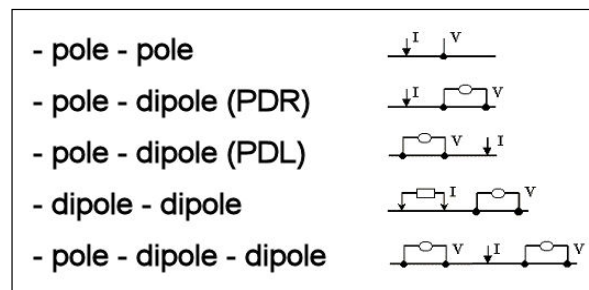
G.2 TITAN-24 DCIP SURVEY

Titan-24 is a distributed DCIP acquisition system. A typical survey layout, or spread, is 2400m long and has 25 inline (Ex) 100m potential dipoles and the current injections sites. With current extensions, a typical Titan-24 spread can be stretched to 3600m. If requested, the dipole length can be changed to 50m or 200m, and the resulting length Titan-24 spread will be 1200m or 4800m. Also, cross line dipoles (Ey) can be deployed as well.



Titan-24 Distributed Acquisition System (IP-only) layout.

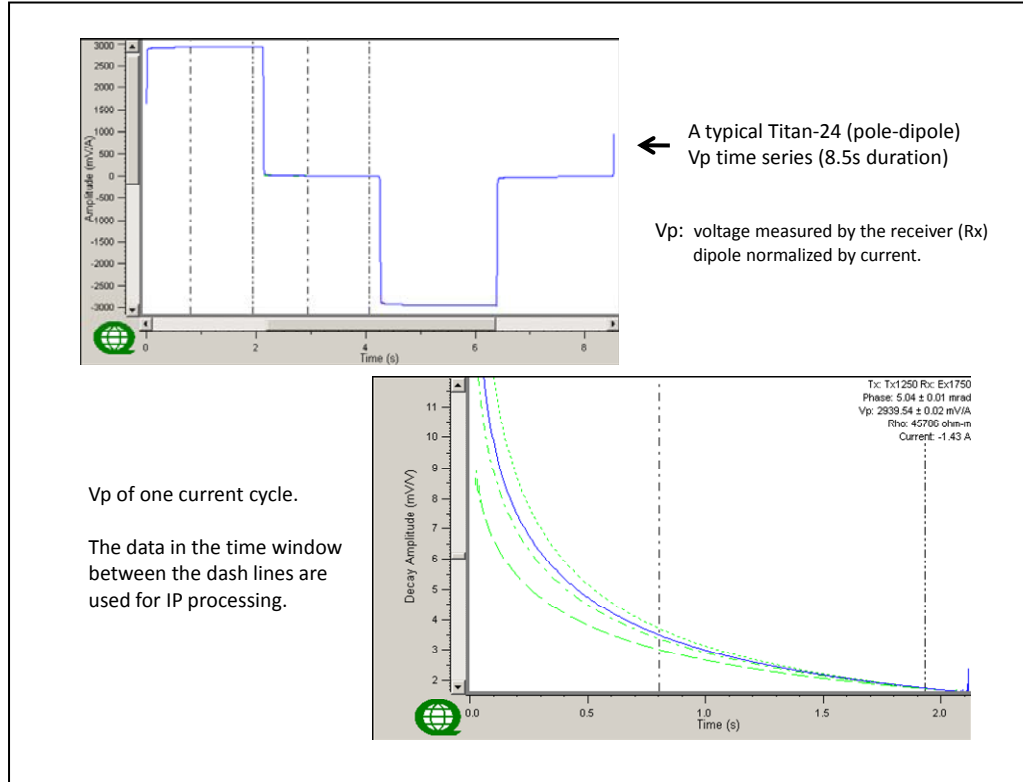
In a normal Titan-24 survey, the transmitter (Tx) and receiver (Rx) configuration is the pole-dipole-dipole array, combining pole-dipole right (PDR) and pole-dipole left (PDL). The current is injected at the mid-point between two potential electrodes. However, with special safety arrangements made to the system, the current can be injected at the potential electrode locations.



Titan-24 Transmitter (Tx) and Receivers (Rx) configurations.

G.3 TITAN-24 DCIP DATA PROCESSING

For one potential electrode pair, the data acquired with one current injection event is a time series of measured voltages at the electrodes normalized by the current, V_p in mV/A. A typical Titan-24 time series are shown below.



Typical Titan-24 DCIP time series.

A single injection event usually lasts approximately three minutes. The time series of an event are stacked twenty times per second in order to increase the signal to noise (S/N) ratio. The data processing is done in the frequency domain. Current waveform deconvolution and digital filtering of power line noise (60/50Hz, and their harmonics) are applied to the frequency domain data.

G.4 HALVERSON-WAIT CHARGEABILITY

Titan-24 IP chargeability are described using the Halverson-Wait spectral model (Halverson et al., 1981), which is not well known, but is similar to the Cole-Cole model proposed by Pelton et al. (1978) which is a simple relaxation model that fits complex (frequency-dependant) resistivity results.

The time domain chargeability, originally proposed by Siegel (1959), is defined (Telford et al., 1976) as:

$$M = \frac{1}{V_c} \int_{t_1}^{t_2} V(t) dt$$

where $V(t)$ is the residual or secondary voltage at a time t that is decaying after the current is cut off, between time t_1 and t_2 with the steady voltage V_c during the current flow interval. The ratio $V(t)/V_c$ is expressed in millivolts per volts (mV/V).

In the frequency domain, the “frequency effect” is defined as:

$$FE = \frac{(\rho_{DC} - \rho_{AC})}{\rho_{AC}}$$

where ρ_{DC} and ρ_{AC} are the apparent resistivity's measured at DC and “very high” frequency, usually in the 0.1 to 10 Hz range.

The Cole-Cole model for the chargeability m , as defined by Pelton et al. (1978) is given by the following:

$$Z(\omega) = R_0 \left[1 - m \left(1 - \frac{1}{1 + (i\omega\tau)^c} \right) \right]$$

where $Z(\omega)$ is the complex impedance with ω the angular frequency in Hz, R_0 the DC resistivity, m the chargeability in volts per volt, τ the time constant in seconds, and c is the frequency dependence (unit less). The latter two physical properties describe the shape of the decay curve in time domain or the phase spectrum in frequency domain, and commonly range between 0.01s to +100s and 0.1 to +0.5, respectively (Johnson, 1984).

The Halverson-Wait model was proposed by Halverson et al. (1981) as an extension to the Wait (1959) model of the impedance of “volume loading” of spheres, given by:

$$Z(\omega) = \frac{\rho}{G} \left[1 - 3\nu \left(1 - \frac{3\delta}{1 + 2\delta} \right) \right]$$

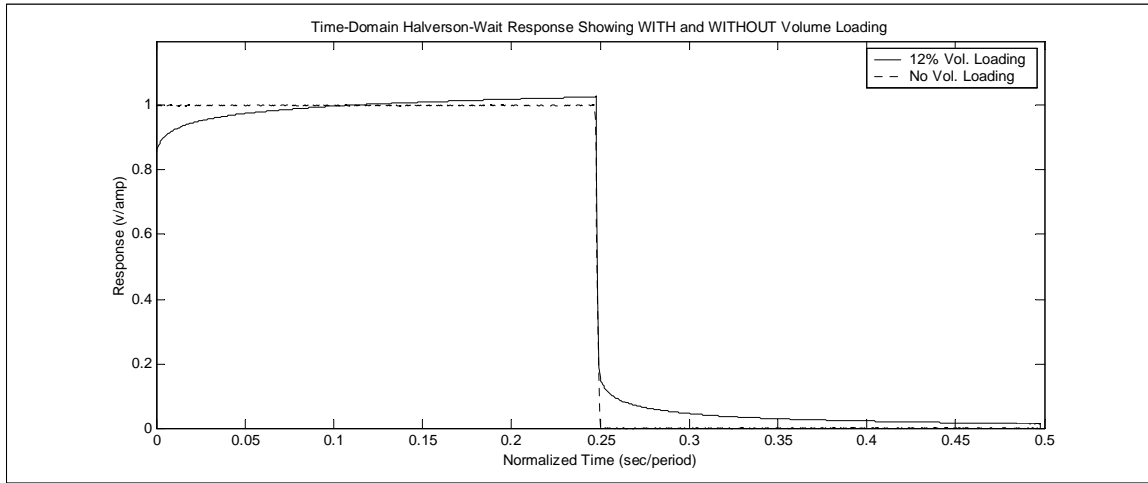
where G is a geometric factor, ρ the resistivity of the media, ν the volume loading (the volume fraction of chargeable “spheres”), δ the sphere surface impedance. The Wait model was designed to provide an explanation of the differences in the shape of decay curves from different polarisable targets, but does not describe very well the physical attributes of the rocks.

The Halverson-Wait model expands the Wait coated sphere IP model to include a new formulation of the sulphide-rock interface impedance, based on field studies and laboratory tests on samples. It is closely correlated to the Pelton et al. (1978) Cole-Cole model and is given by:

$$Z(\omega) = \frac{\rho}{G} \left[1 - 3\nu \left(1 - \frac{3/2}{1 + r[i\omega]^K} \right) \right]$$

where r is the sphere radius and is equivalent to τ - the Cole-Cole time constant ($r = \tau^K$). The volume loading ν compares well to m , the Cole-Cole chargeability (see equation below), and the exponent K is equal to c , the Cole-Cole frequency dependence (Halverson et al., 1981). For sulphide systems, the r -factor reflects the size or inter-connectedness of the sulphide grains and the K -factor reflects the electrical characteristics of the sulphide surfaces.

An example of time domain Halverson-Wait model responses is shown below:



Polarisable versus Non-Polarisable TD-IP response using Halverson-Wait Model.

In the Halverson-Wait model the theoretical Percentage Frequency Effect (PFE)¹³ (for infinite bandwidth), which equates to the theoretical chargeability in the Cole-Cole equation, is thereby defined by the volume loading:

$$\frac{PFE_0^\infty}{100} = m_0 = \frac{9\nu}{(2 + 3\nu)}$$

and m is output in units of milliradians (mrads).

G.5 TITAN-24 IP CHARGEABILITY DEFINITION (QTN001)

Quantec prefers to estimate IP responses using a time domain half-duty square-wave excitation standard, but convert those chargeability results to units of phase. The specific procedure and algorithm is as follows:

1. Determine the earliest time for which EM coupling has died out sufficiently. This time is called the averaging or integration *start time* t_0 . A typical value for t_0 is 0.8s;
2. Determine the latest charge/decay time that is minimally affected by sigma-delta and low-pass (usually Hanning window moving average) filtering, called the averaging or integration *end time* t_1 . A typical value for t_1 is 1.95s;
3. Adjust the *start time* (t_0) so that $t_1 - t_0$ (equated to number of samples) exactly spans an integer number of power-line signal periods. This can only be done for transmitted (fundamental) frequencies that are much lower than the power-line frequency;
4. Using the charge and decay sample numbers that equate to the averaging window¹⁴ defined by t_0 and t_1 , calculates the average charge and decay voltages. This average may

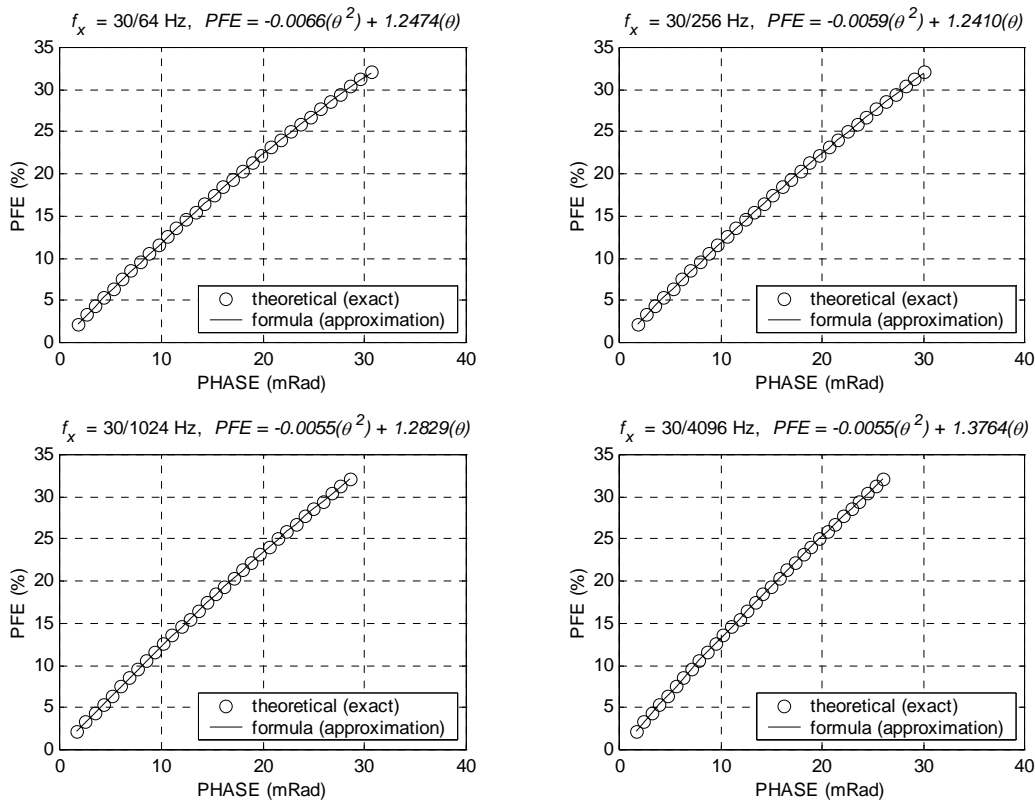
¹³ The classical definition of PFE is $100 \times (\rho_0 - \rho_\infty) / \rho_0$.

¹⁴ In practice this averaging window is tapered slightly to widen the stop-band notches and thereby provide enhanced power-line noise rejection.

involve a non-uniform weighting to further improve rejection of power-line noise;

5. Calculate the theoretical Halverson-Wait half-duty time-domain response using identical filtering to that applied to the measured data response estimate, and presuming the following spectral parameters:
 - a. volume loading: 0.125 (this value is not important)
 - b. r – value: 1.0
 - c. k – value: 0.2
6. For the standard Halverson-Wait spectral parameters mentioned, the synthesized time-domain response and the $t_1 - t_0$ averaging window, convert all estimated/measured charge and decay voltages (using the specified averaging window) to chargeability (millivolts/volt) and then to phase (milliradians).

This is the algorithm used in the Titan-24 data processing. The relationship between Titan-24 chargeability unit, phase in milliradians, and other frequency domain systems is straightforward – Quantec’s time-domain based phase equates to frequency domain based phase, see figures below.



Phase vs. PFE for various pulse lengths and presuming standard Halverson-Wait spectral parameters (r -value = 1.0 and k -value = 0.2).

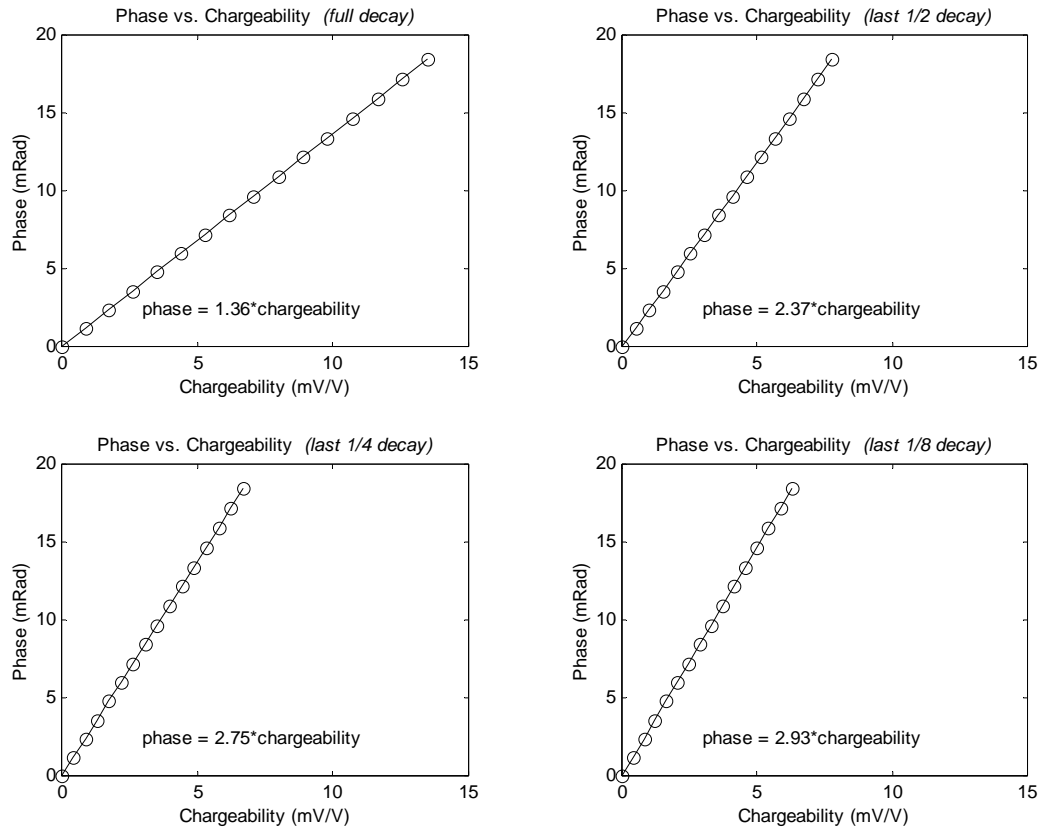


Illustration of the proportional relationship between phase (mrad) and chargeability (mV/V) for various charge/decay averaging windows

G.6 DCIP2D INVERSION

An excellent overview and introduction to both the theory and use of inversions in geophysics is available on the University of British Columbia (UBC) website (Oldenburg et al., 1998).

The DCIP2D inversion algorithms are developed by UBC-Geophysical Inversion Facility.

Mathematically, inversion is the process of fitting the observed data to a model through minimizing a function. The choice of which function to minimize ultimately defines the inversion model. In the inversion algorithm developed by UBC, this function is:

$$\phi = \phi_d + \beta \phi_m = (\text{misfit}) + \beta (\text{model norm})$$

$0 < \beta < \infty$ is a constant

The function to be minimized consists of a function, ϕ_d , that minimizes the data misfit, and a function ϕ_m that finds a “smooth” model. Beta, the regularization parameter, represents a relative weighting between fitting the data and smoothing the model.

Clearly, the data misfit function must be defined in more detail. One approach might be

$$\phi_d = \sum_{i=1}^N \left(\frac{F_i[m] - d_i^{obs}}{\varepsilon_i} \right)^2$$

This function defines the data misfit as the sum of the individual misfits squared (L2 norm), normalized by the errors associated with each data point. It is the least-squares definition of the data misfit.

The model misfit function must also be defined in more detail. One of the most flexible definitions is the one used by UBC

$$\phi_m(m, m_0) = \alpha_s \int_{vol} (m - m_0)^2 dv + \alpha_x \int_{vol} \left(\frac{\partial(m - m_0)}{\partial x} \right)^2 dv + \alpha_z \int_{vol} \left(\frac{\partial(m - m_0)}{\partial z} \right)^2 dv$$

In this definition there are three components to the “model norm” (or “smoothness” constraint, or “regularization”), each of which contains an α constant (α_s , α_x , α_z) that are commonly referred to as “alpha parameters”, and a fourth variable m_0 that refers to the starting or reference model – either a half-space or geophysical constraint – that also has a profound influence on the model-misfit.

The three “alpha” parameters represent a relative weighting of each component:

- the first component is simply an overall difference between the model and a “target” model;
- the second component is a horizontal smoothness;
- the third component is a vertical smoothness.

G.7 APPARENT RESISTIVITY OF UNIFORM HALF SPACE

From p.636, Telford et al. 1976, the apparent resistivity ρ_a is given as:

$$\rho_a = \frac{2\pi V_p}{G_f}$$

where G_f is the geometric factor defined as:

$$G_f = \left(\frac{1}{r_1} - \frac{1}{r_2} \right) - \left(\frac{1}{r_3} - \frac{1}{r_4} \right)$$

with:

r_1 the distance between current electrode P1 and potential electrode C1;

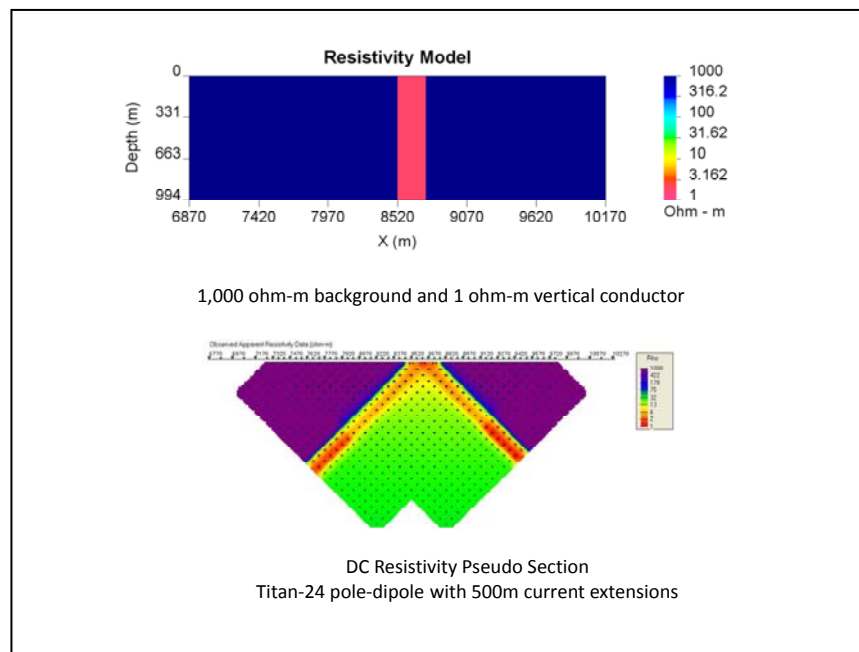
r_2 the distance between current electrode P1 and potential electrode C2;

r_3 the distance between current electrode P2 and potential electrode C1;

r_4 the distance between current electrode P2 and potential electrode C2;

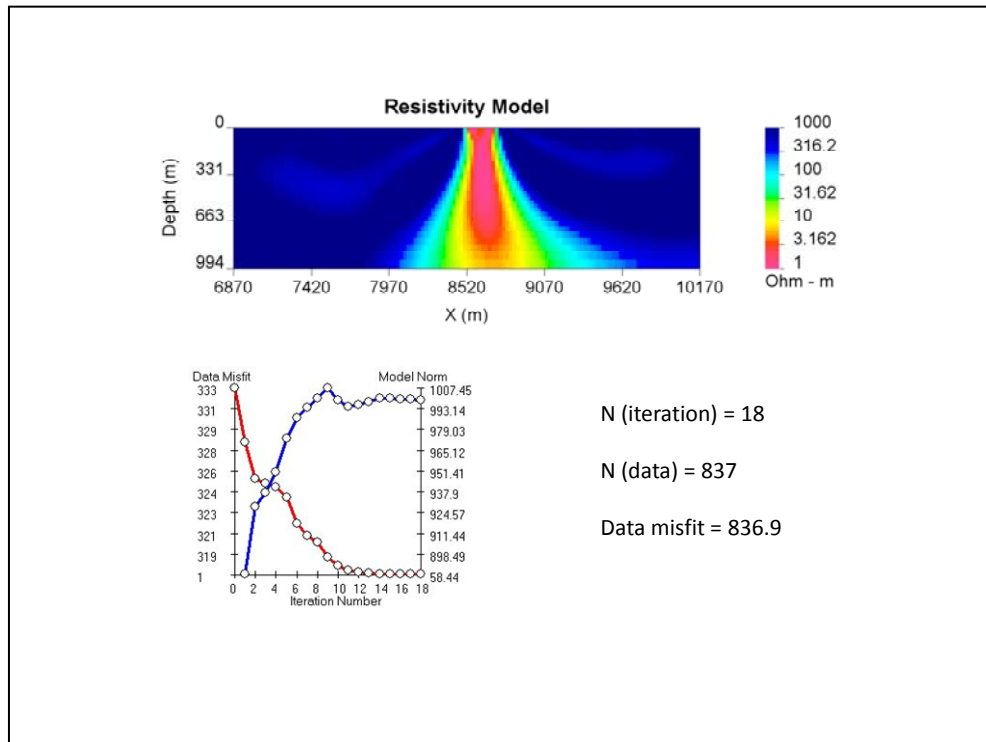
G.8 DC INVERSION USING A SYNTHETIC MODEL

A synthetic resistivity model and its apparent resistivity pseudo section based on Titan-24 configuration are shown here. The model consists of a background of 1,000 ohm-m and a vertical dyke of 1 ohm-m. The synthetic DC data, V_p 's, are computed using UBC's 2D forward modeling tool DCIPF2D



A synthetic model and its apparent resistivity pseudo section

The inverted resistivity model and the convergence curves are displayed below.



Inversion model, convergence curves and inversion statistics

G.9 IP INVERSIONS

For IP inversions, the apparent chargeability η is computed by carrying out two DC resistivity forward modeling with conductivity distributions $\sigma(x_i, z_j)$ and $(1 - \eta)\sigma(x_i, z_j)$ (Oldenburg and Li, 1994), where (x_i, z_j) specifies the location in a 2D mesh.

The conductivity distributions used in IP inversions can be the inverted DC model or a half space of uniform conductivity. The IP inversion, generated through the use of a half space, is called the "NullCon" or "HSref" IP model

H REFERENCES

H.1 TITAN-24 METHOD AND APPLICATION

- Donohue, J.G., and Sheard, S.N., 2001. Geophysics in North West Queensland – Improving the use of electrical geophysics. AIG Journal Paper 2001-01.
- Garner, S., and Webb, D., 2000. Broadband MT and IP electrical property mapping with MIMDAS. SEG Technical Program Expanded Abstracts, 1085-1088.
- Goldie, M., 2007. A comparison between conventional and distributed acquisition induced polarization surveys for gold exploration in Nevada. *The Leading Edge*, 26 (2), 180-183.
- Hollyer, G, and Hearst, R., 2009. Deep exploration technologies for discovery in the shadow of head frames. *First Break*, 27 (July), 99-105.
- Kingman, J., and Garner, S., 2003. Benefits of large channel capacity systems in electrical geophysics. ASEG 16th Geophysical Conference and Exhibition, Adelaide.
- Legault, J., Carriere, D., and Petrie, L., 2008. Synthetic model testing and distributed acquisition dc resistivity results over an unconformity uranium target from the Athabasca Basin, northern Saskatchewan. *The Leading Edge*, 27 (1), 46-51.
- Sheard, N., 1998. MIMDAS: A new direction in geophysics. Proceedings of the ASEG 13th International Conference, Hobart, Tasmania.
- White, M., and Gordon, R., 2003. Deep imaging: New technology lowers cost of discovery. *Canadian Mining Journal*, April, 27-28.

H.2 DIRECT CURRENT (DC) AND INDUCED POLARISATION (IP) METHODS

- Halverson, M.O., Zinn, W.G., McAlister, E.O., Ellis, R., and Yates, W.C., 1981. Assessment of results of broad-band spectral IP field test. In: *Advances in Induced Polarization and Complex Resistivity*, 295-346, University of Arizona.
- Johnson, I.M., 1984. Spectral induced polarization parameters as determined through time-domain measurements. *Geophysics*, v. 49, 1993-2003.
- Li, Y., and Oldenburg, W., 2000. 3-D inversion of induced polarization data. *Geophysics*, v 65 (6), 1931-1945.
- Loke, M.H., 2004. Tutorial: 2D and 3D electrical imaging surveys, Res2Dinv and Res3Dinv manual [www.geoelectrical.com].
- Oldenburg, D., and Li, Y., 1994. Inversion of induced polarization data. *Geophysics*, 59, 1327-1341.
- Oldenburg, D., Li, Y., and Jones, F., 1998. Tutorial: Inversion (Res/IP) Methodology. In: *The UBC-GIF Tutorials* [<http://www.geop.ubc.ca/ubcgif>].
- Oldenburg, D., and Li, Y., 1999. Estimating depth of investigation in DC and IP surveys. *Geophysics*, 64, 403-416.
- Pelton, W.H., Ward, S.H., Hallof, P.G., Sill, W.R. and Nelson, P.H., 1978. Mineral discrimination and removal of inductive coupling with multi-frequency IP. *Geophysics*, v.43, 588-609.

Quantec, 2009. Standard chargeability calculations in Titan-24 IP measurements. Quantec Technical Note 001.

Seigel, H., 1959. Mathematical formulation and type curves for induced polarization. *Geophysics*, 24, 547-565.

Telford., W.M., Geldart, L., Sheriff, R., and Keys, D., 1976. *Applied Geophysics*. Cambridge University Press, New York, NY.

Van Blaricom, R., 1992. *Practical Geophysics for the Exploration Geologist*. Northwest Mining Association, Spokane, WA.

Wait, J., 1959. *Overvoltage Research and Geophysical Applications*. Pergammon Press.

H.3 TECHNICAL REPORTS

Technical report (43-101) on the Tad/Toro Project, Whitehorse Mining District; by Jean Pautler, P.Geo., December, 20, 2009.

| Quantec Geoscience Ltd Summary Table | |
|--------------------------------------|--|
| CLIENT | |
| Client / Company Name | Dawson Gold Corp. |
| Client Main Location | (British Columbia, Canada) |
| Client Representative | Jason McLaughlin |
| Phone Number | (604) 687 2471 |
| Fax Number | (604) 687 2472 |
| Email Contact (if available) | Jason@dawsongold.com |
| PROJECT | |
| Project Grid Name | Tad/Toro Project |
| Project Grid Location | (Whitehorse Mining District, Yukon, Canada) |
| Survey Type | Titan-24 DC – IP |
| Survey Period (YY/MM/DD to YY/MM/DD) | 2011/08/18 to 2011/09/08 |
| Quantec Project Number | CA00882T |
| Responsible Geophysicist | Benoît Tournier Jimmy Stephen Kevin Killin |
| Data Processor | Darcy McGill |
| REPORT | |
| Report Date | 26/10/2011 |
| Quantec Template Version | 2011.2 |